



The synthesis and application of bulky *S*- stereogenic and *P*- stereogenic chiral ligands

Seán Doran

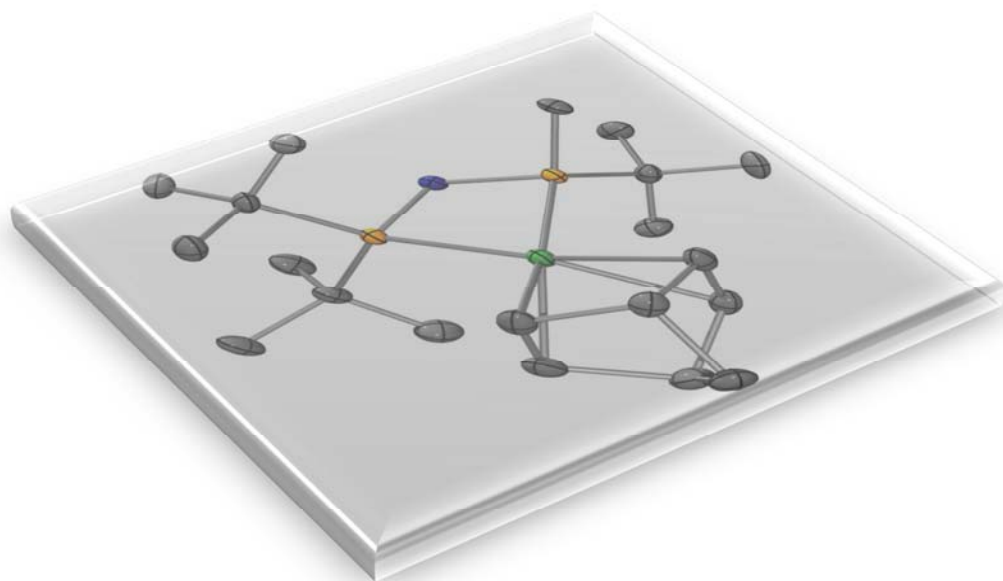
ADVERTIMENT. La consulta d'aquesta tesi queda condicionada a l'acceptació de les següents condicions d'ús: La difusió d'aquesta tesi per mitjà del servei TDX (www.tdx.cat) ha estat autoritzada pels titulars dels drets de propietat intel·lectual únicament per a usos privats emmarcats en activitats d'investigació i docència. No s'autoritza la seva reproducció amb finalitats de lucre ni la seva difusió i posada a disposició des d'un lloc aliè al servei TDX. No s'autoritza la presentació del seu contingut en una finestra o marc aliè a TDX (framing). Aquesta reserva de drets afecta tant al resum de presentació de la tesi com als seus continguts. En la utilització o cita de parts de la tesi és obligat indicar el nom de la persona autora.

ADVERTENCIA. La consulta de esta tesis queda condicionada a la aceptación de las siguientes condiciones de uso: La difusión de esta tesis por medio del servicio TDR (www.tdx.cat) ha sido autorizada por los titulares de los derechos de propiedad intelectual únicamente para usos privados enmarcados en actividades de investigación y docencia. No se autoriza su reproducción con finalidades de lucro ni su difusión y puesta a disposición desde un sitio ajeno al servicio TDR. No se autoriza la presentación de su contenido en una ventana o marco ajeno a TDR (framing). Esta reserva de derechos afecta tanto al resumen de presentación de la tesis como a sus contenidos. En la utilización o cita de partes de la tesis es obligado indicar el nombre de la persona autora.

WARNING. On having consulted this thesis you're accepting the following use conditions: Spreading this thesis by the TDX (www.tdx.cat) service has been authorized by the titular of the intellectual property rights only for private uses placed in investigation and teaching activities. Reproduction with lucrative aims is not authorized neither its spreading and availability from a site foreign to the TDX service. Introducing its content in a window or frame foreign to the TDX service is not authorized (framing). This rights affect to the presentation summary of the thesis as well as to its contents. In the using or citation of parts of the thesis it's obliged to indicate the name of the author.



**The synthesis and application of bulky
S- stereogenic and *P*- stereogenic chiral
ligands**



Seán Doran
Doctoral Thesis, Barcelona, 2012

The synthesis and application of bulky S- stereogenic and P- stereogenic chiral ligands

Seán Doran

Facultad de Química

Departamento de Química Orgánica

Programa de doctorado: Química Orgánica Bienio 2010-2012

Director de tesis: Xavier Verdaguer Espauella

Memoria presentada por Seán Doran para optar al grado de doctor por la Universitat de Barcelona.

Seán Doran

Revisada por:

Dr. Xavier Verdaguer Espauella

Barcelona, Octubre de 2012

Este trabajo se ha realizado con el soporte económico de la Obra Social “La Caixa” (becas pre-doctorales). El trabajo ha sido financiado mediante el proyecto de investigación MEC (CTQ 2008-00763), MICINN (CTQ2011-23620) y DGR (SGR-2009-00901).

El trabajo experimental se ha llevado a cabo en el laboratorio de la Unitat de Recerca en Síntesi Asimètrica (URSA) del Institut de Recerca Biomèdica de Barcelona (IRB Barcelona), ubicado en el Parc Científic de Barcelona.

Acknowledgements

First of all I would like to thank Prof. Antoni Riera for not only giving me the opportunity to carry out my doctoral thesis in his lab but also to completely transport my life from Ireland to beautiful Barcelona. Moving to Barcelona and Catalunya was the best decision I ever made in my life and it was your acceptance of me into the lab, Toni which made it possible so thank you so much. I want to of course thank my thesis supervisor Prof. Xavier Verdaguer for all the guidance, advice and help down through the years. You were available when I wasn't sure what to do or where to go next but I was always granted the freedom and independence to investigate and explore as I wished for which I was always very appreciative.

*I want to thank everyone in the lab whoever gave me a hand with whatever bit of chemistry I was carrying out or equally as important, whoever made the lab a bit more craic to work in. To start off with I'll have to thank (and of course I want to) the one and only Thierry Achard. You really helped me settle in at first, teaching me all about PNSO ligands, phosphines, rhodium and of course, for those first few nights out watching champions league with some Guinness in the Michael Collins before I knew anybody so thanks for that! I want to thank Marc Revés, you were always there to give a few pointers here and there especially in the beginning. I'll thank Pablo my personal Spanish teacher (*aunque mi español ha empeorado bastante ultimamente ya que lleva mil años en usa el muy berretes*). I'll thank Ana Vazquez, she was always there to give a hand, I might have only understood about half of what you were saying in the beginning (if that) but I loved hearing it! I'll say thanks to Núria for being the bestest hoodie ever! Thanks to Yi-Ning for your ever-present beaming shining positivity! Thanks to Thierry León (what do you think about my... yeah!) for making the lab a wee bit more interesting! Thanks to A.. A... Alex for keeping the line in such pristine crystal cleanliness at all times! And the dry-box! Thanks to Edgarrrr for all that awesome hydrogenation time! I want to thank Cati Ferrer, Jean-Claude and Agustí Lledó for all their help. Of course I can't forget in my thanks the frenchie Helea and hippie Silvia (hey soy Seán tio!). I'll give a nod and a wink to the big Dan man, otherwise known as Super-Dan, the best signing Toni ever made! And a big, big thanks to all you guys for helping me with the Spanish summary - Núria, Edgar, Silvia, Alex and Álvaro!!!*

I want to give special thanks to Clara Caminal for her kind attention and help, whenever it was needed throughout the whole process of the PhD. As well I would thank Patricia Nadal,

Maria Rovira and Silvia Aguadé for every bit of help and attention you gave through all the bureaucratic intricacies that needed to be solved.

I would thank the three members of my TAC committee Rodolfo Lavilla, Albert Moyano and Guillermo Müller for their help, advice and attention throughout the TAC proceedings. I would like to thank everybody from the Mass Spec facility for their work and contribution, past and present, Marta Vilaseca, Núria Omeñaca, Claudio Diema, Mar Vilanova and Marina Gay. I would give my thanks to everybody in the NMR unit in the Parc Científic and in UB for their help and contribution namely, Miguel Feliz, Maria Antònia Molins, Vicky Muñoz-Torero and Francisco Cárdenas. I would say thank you to Montse Alcón, Ester and Belen from Enantia for all their work on the chiral HPLC separations. Thanks should go Eduardo Carmelo Escudero for his work on the X-ray diffraction structures of the complexes shown here in this work.

I would say a big thanks to all the great friends I have made here in the IRB down throughout the short few years I've spent here, to Peter, to Andrey, to Michael, to Marta, Özgen, Arjen, Anna-Iris and Gonzalo (the beer festival organizer!) To every single Brutal/ Soft and fluffy Deluxer a heads up and a cheers.

A big special thank you and a kiss to Kader for all her love. A massive hug to my brothers Paddy and James who I miss so much and to all my friends who I wish I could spend more time with, Damian, Ross, Brendan, Jamie...and Tommy as well.

And of course to my lovely Mum and my dear old Dad, this thesis is dedicated to you and you alone for you are the main reason it has been possible. Thank you for all your support in every sense and all your patience. I owe you everything.

*All credibility,
all good conscience,
all evidence of truth come only from the senses.*

Friedrich Nietzsche (1844 – 1900).

Content

List of abbreviations

Chapter 1 Introduction and objectives	3
Chapter 2 Background	13
Chapter 3 <i>N</i> -Phosphino sulfinamide ligands	57
Chapter 4 P*-aminophosphine ligands	81
Chapter 5 MaxPHOS and asymmetric hydrogenation	115
Chapter 6 Conclusions	141
Chapter 7 Experimental	145
Chapter 8 ¹ H and ¹³ C NMR spectra	187
Chapter 9 Appendix I X-ray crystal structures & crystallographic data	225
Chapter 10 Appendix II Index of structures	237
Chapter 11 Appendix III Detailed Index	243
Chapter 12 Appendix IV Publications, Posters, Congresses	249
Chapter 13 Appendix V Summary in Spanish	255

Ac	acetyl	d.e.	diastereomeric excess
acac	acetylacetonate	descomp	descompuesto
<i>o</i> -An	ortho-anisyl	DIP	diisopropylamine
Å	Angstrom	DIPEA	diisopropylethylamine
°C	degree Celsius	DMSO	dimethylsulfoxide
δ	NMR chemical shift	DMF	N,N-dimethylformamide
λ	wavelength	dr	diastereomeric ratio
σ	sigma	dt	doublet of triplets
Bn	benzyl	EA	elemental analysis
Boc	<i>tert</i> -butoxycarbonyl	EDG	electron-donating group
br	broad	ee	enantiomeric excess
<i>n</i> -Bu	butyl	equiv.	equivalent
^t Bu	<i>tert</i> -butyl	er	enantiomeric ratio
cat.	catalyst	ESI	electrospray ionization
<i>c</i> / conc.	concentration	<i>et al.</i>	and others
conv.	conversion	EWG	electron-withdrawing group
COD/cod	1,5-cyclooctadiene	FT	fourier-transform
d	doublet	GC	gas chromatography
DABCO	1,4-diazabicyclo[2.2.2]octane	HPLC	High-Performance Liquid Chromatography
DBU	1,8-diazabicyclo[5.4.0.]undec-7-ene	HRMS	High Resolution Mass Spectrometry
DCM	dichloromethane	IR	infrared (spectroscopy or spectrum)
dd	doublet of doublets	<i>J</i>	coupling constant

kcal mol ⁻¹	kilocalories per mole	T	temperature
LDA	lithium diisopropylamide	t.a.	temperatura ambiente
m	multiplet	TBA	<i>tert</i> -butylamine
MAC	methylacetamido cinnamate	TBAF	tetrabutylammonium fluoride
recrys.	recrystallized/recrystallization	TBDPS	<i>tert</i> -butyldiphenylsilyl
RF	retention factor	TCFP	trichickenfootphos
mol %	mole percent	TEA	triethylamine
m.p.	melting point	TFA	trifluoroacetic acid
Ms	mesylate	Tf	trifluoromethanesulfonyl
m/z	mass to charge ratio	TFE	trifluoroethanol
NBD	norbornadiene	THF	tetrahydrofuran
NMR	nuclear magnetic resonance	TLC	thin layer chromatography
PNSO	<i>N</i> -phosphino sulfinamide ligands	TMEDA	tetramethylethylenediamine
ppm	parts per million	TMS	trimethylsilyl
p.p.	producto de partida	TOF	turn-over frequency
q	quartet	TON	turn-over number
quant.	quantitative	Ts	tosylate
RMN	resonancia magnetica nuclear	TsOH	toluenesulfonic acid
rt/r.t.	room temperature	vs.	versus
s	singlet	w.r.t	with respect to
S/C	substrate/catalyst ratio		
t	triplet		

Introduction and Objectives

1

Introduction

Enantioselective hydrogenation is one of the most widely utilized asymmetric transformations in industry today. Rhodium catalyzed enantioselective hydrogenation has gained huge importance commercially due in no small part to the demand on a global scale of naturally and unnaturally occurring amino acids. Rather than isolating them from natural sources, it can often make more economic sense to synthesize expensive, naturally occurring amino acids. Phenyl alanine is an example of an industrially synthesized, naturally occurring amino acid of economic importance which is a key component in the synthesis of the artificial sweetener, aspartame. One of the foremost syntheses employed industrially to achieve enantiopure L-phenylalanine uses an asymmetric rhodium catalyzed hydrogenation.

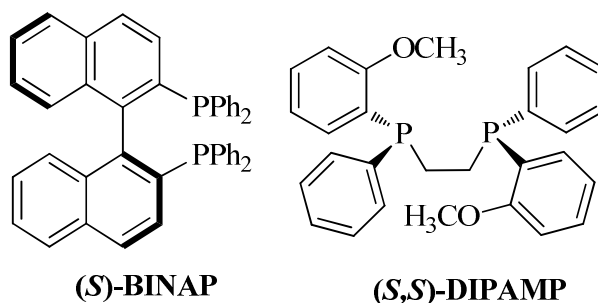
Asymmetric hydrogenation is an atom efficient way of accessing chiral products with excellent yield and enantioselectivity possible with as little as 100 ppm or less of catalyst loading¹. Almost invariably a chiral, chelating diphosphine ligand is employed to coordinate to the metal center to induce reactivity and infer chirality to the reaction. These chiral diphosphines are usually synthetically made, giving equal access to either one enantiomer or the other and thus bestowing this freedom of enantioselection to the given asymmetric hydrogenation in which it is utilized; one simply has to choose which enantiomer of ligand to use in order to obtain the desired product.

The first asymmetric hydrogenation was reported in 1968 by Knowles *et al.* from the Monsanto Company where they used a chiral tertiary phosphine ligated to a rhodium (III) complex to hydrogenate α -phenylacrylic acid to optically active hydratropic acid with an enantiomeric excess of 15 % *ee*.² Since then the investigation into different chiral ligands has exploded and has led to the development of catalysts that provide near perfect enantioselectivities, as well as huge turn over numbers (TONs) and turn over frequencies (TOFs).

The chiral diphosphine motif as a ligand in asymmetric catalysis has been vastly successful and is commonplace. Two of such ligands which are of such renown, they could almost be considered “household names” are BINAP and DIPAMP. BINAP is a chiral diphosphine ligand where chirality is derived from the axially chiral backbone of the ligand and is applied in a host of asymmetric transformations using a variety of different catalytic metal centers including but not restricted to palladium, rhodium and ruthenium. DIPAMP is a diphosphine which was again developed by the Monsanto Company in the 1970s in the search for an

efficient, optically pure synthesis of the rare amino acid L -DOPA, used in the treatment of Parkinson's disease.³ DIPAMP is an example of the class of diphosphines where the chirality of the ligand is derived from the chiral centres at phosphorous.

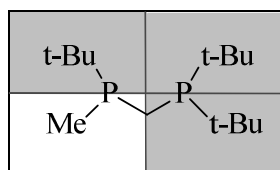
Figure 1.1. Examples of landmark chiral phosphines.



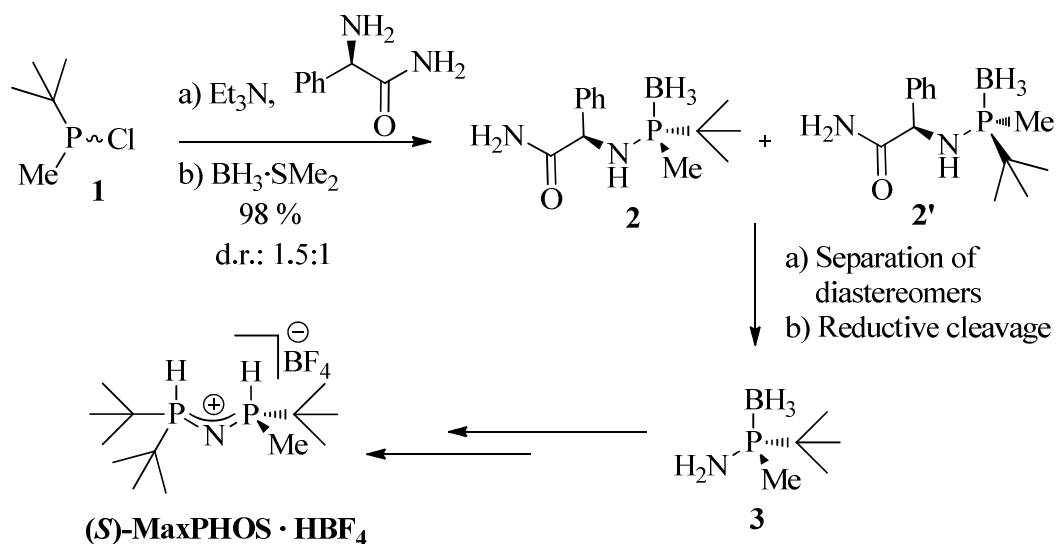
Other stand out work as regards P-stereogenic diphosphines was pioneered by Evans and co-workers in the 1990s with the development of enantioselective deprotonation of dimethyl aryl phosphines in the presence of (-)-sparteine.⁴ This work laid the foundation for the synthesis of such C_2 -symmetric ligands as the very effective BisP*⁵ and QuinoxP*⁶ developed by Inamoto *et al.*

The synthesis of this P-stereogenic class of ligand can often be complex and difficult and perhaps for this reason the development of these types of ligand has been largely placed on the backburner in recent times while research into diphosphines with chirality residing on the backbone of the ligand has taken centre stage. More recently however diphosphines with chirality residing on phosphorous has undergone resurgence.

In 2004 Hoge *et al.* published their findings⁷ on their trichickenfootphos (TCFP) ligand, a C_1 -symmetric, P-stereogenic diphosphine ligand. It proved highly effective at catalysing the asymmetric hydrogenation of a host of α -acetamido dehydroamino acids. They highlighted the usefulness of the “quadrant diagram” paradigm while designing new ligands, revealing the three hindered quadrant ligand design to be an attractive design even though up until then the two non-adjacent hindered quadrants design was more prevalent. Since this time a handful of C_1 -symmetric, three hindered quadrant diphosphines have been developed and have proved highly successful.⁸

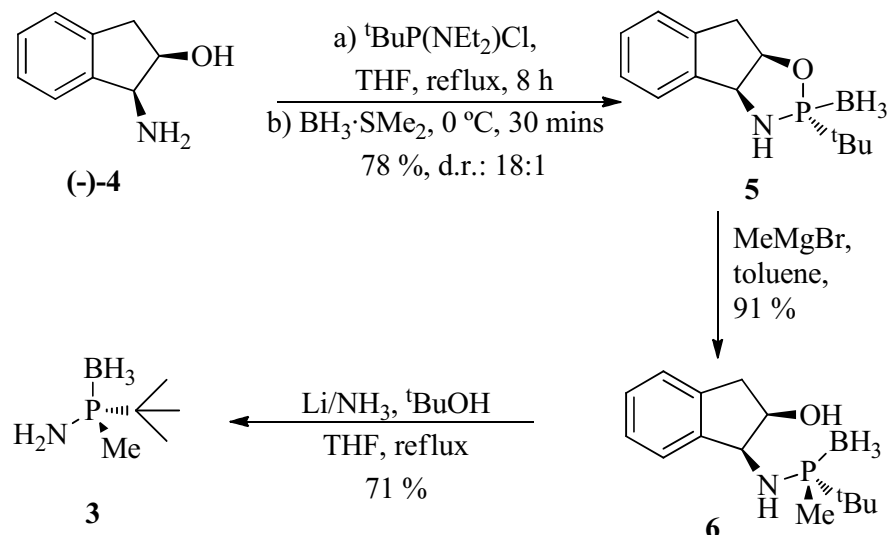
Figure 1.2. Trichickenfootphos, a 3-hindered quadrant diposphine.

One such ligand which has been developed within our research group and which has proven very successful in asymmetric hydrogenation has been the MaxPHOS ligand.⁹ The synthesis of the MaxPHOS ligand was first achieved during the thesis of M. Revés. A method was devised to form primary aminophosphines in enantioselectively pure form by building on the work of Kolodiazhnyi *et al.*¹⁰ First a dynamic kinetic resolution of racemic chloro phosphines with chiral amines as resolving agents was employed to form a diastereomerically enriched secondary aminophosphine borane, then separation of diastereomers to achieve diastereomerically pure same and lastly a reductive cleavage *via* lithium in liquid ammonia. The primary aminophosphines were then ready to be used as building blocks in the preparation of the family of PnP diposphine ligands which included MaxPHOS.

Scheme 1.1: The synthesis of the MaxPHOS·HBF₄ salt *via* dynamic kinetic resolution.

During the Thesis of T. León the optimized synthesis of the MaxPHOS ligand was accomplished. The previous synthesis had relied on the separation of a 1:1.5 mix of diastereomers but it was found that enantiomerically pure primary amino phosphine **3** could be obtained from the condensation of a chloro phosphine with *cis*-1-amino-2-indanol **4** yielding two diastereomeric ring closed condensation products in high diastereoselectivity, with the major diastereomer easily isolated from crystallization. The ring closed product **5** could be opened in excellent yield with complete selectivity using various Grignard reagents, MeMgBr in the case of the MaxPHOS ligand to give **6**, and enantiopure aminophosphine **3** was obtained after reductive cleavage with lithium in liquid ammonia as before.¹¹ In this way the aminophosphine key intermediate in the synthesis of pure MaxPHOS ligand could be obtained efficiently, in high yield and in enantiopure form.

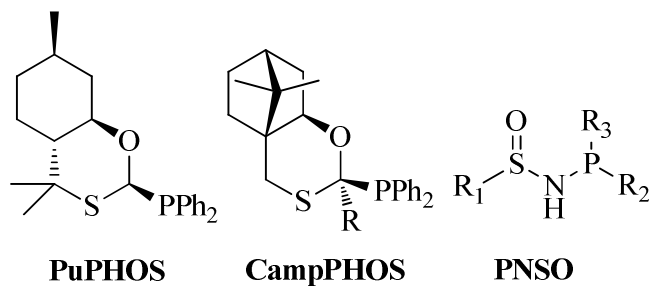
Scheme 1.2: The synthesis of aminophosphines *via* a heterocyclic intermediate.



Our research group has also had much experience with S-stereogenic and C-stereogenic chiral ligands such as the CamPHOS, PuPHOS and the PNSO family of ligands. These ligands were applied successfully to the asymmetric Pauson-Khand reaction.¹² They were coupled with carbonyl dicobalt-alkyne complexes and tested in the intermolecular PK

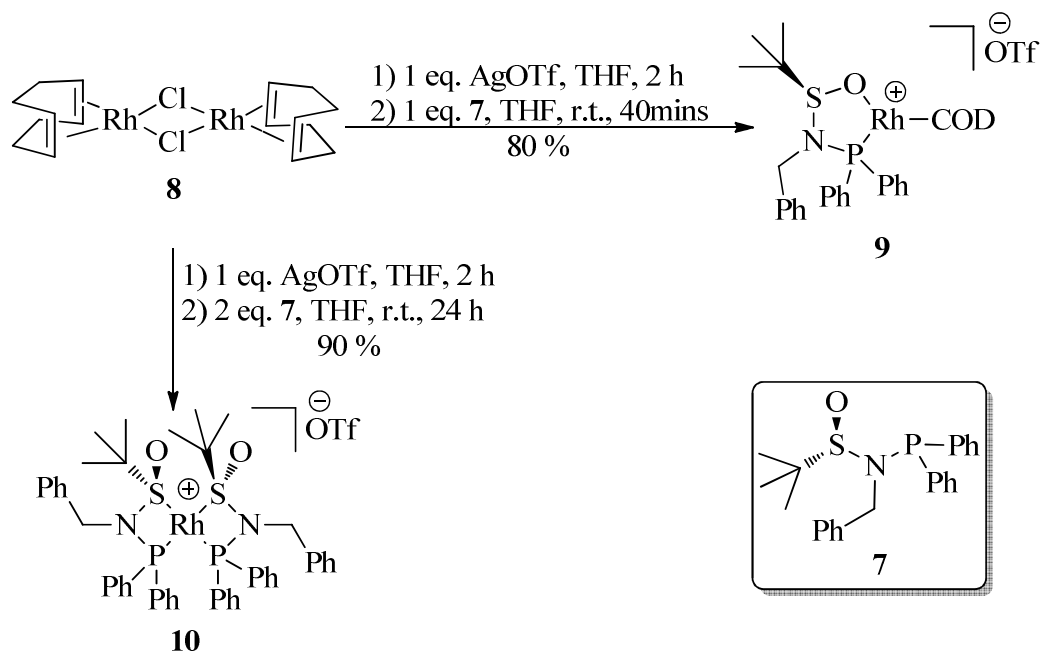
reaction with norbornadiene to form substituted cyclopentenones in high yield and high enantioselectivity.

Figure 1.3: S-stereogenic and C-stereogenic sulphur containing phosphine ligands.



It was later shown that PNSO ligands coordinate readily to rhodium.¹³

Scheme 1.3: The preparation of PNSO-Rh complexes.



1. Introduction and Objectives

The ligand coordinates strongly through phosphorous as would be expected but due to the sulfoxide moiety of the PNSO ligand either O-Rh or S-Rh coordination can be seen. It was observed as a very general rule, PNSO-Rh complexes, monomeric of ligand to metal mainly exhibit oxygen to rhodium coordination behaviour affording a five-membered ring around the metal center. While PNSO-Rh-PNSO complexes, dimeric of ligand to metal, exhibit sulphur to rhodium ligation, affording 4-membered rings around the metal centre. Although this coordination behaviour has been in general observed, due to the hemi-labile nature of the sulfoxide moiety, it is surely subject to other factors besides ligand to metal stoichiometry.

Objectives

1. The development and synthesis of new *N*-phosphino ligands with application in asymmetric metal catalysis.
2. The fine-tuning of reaction conditions and the expansion of substrate scope as regards the MaxPHOS ligand and its application in the rhodium catalyzed asymmetric hydrogenation reaction.
3. To study in-depth the MaxPHOS ligand and discover its full potential as regards its electronic nature, structural derivitization and complexation with metal species to form new complexes.

-
- ¹ Busacca, C. A.; Fandrick, D. R.; Song, J. J.; Senanayake, C. H. *Adv. Synth. Catal.* **2011**, *353*, 1825.
- ² Knowles, W. S.; Sabacky, M. J. *Chem. Commun.* **1968**, 1445.
- ³ Knowles, W. S. *J. Chem. Educ.* **1986**, *63*, 222.
- ⁴ Muci, A. R.; Campos, K. R.; Evans, D. A. *J. Am. Chem. Soc.* **1995**, *117*, 9075.
- ⁵ Imamoto, T.; Watanabe, J.; Wada, Y.; Masuda, H.; Yamada, H.; Tsuruta, H.; Matsukawa, S.; Yamaguchi, K. *J. Am. Chem. Soc.* **1998**, *120*, 1635.
- ⁶ Imamoto, T.; Sugita, K.; Yoshida, K. *J. Am. Chem. Soc.* **2005**, *127*, 11934.
- ⁷ Hoge, G.; Wu, H. P.; Kissel, W. S.; Pflum, D. A.; Greene, D. J.; Bao, J. *J. Am. Chem. Soc.* **2004**, *126*, 5966.
- ⁸ (a) Zhang, Z.; Tamura, K.; Mayama, D.; Sugiya, M.; Imamoto, T. *J. Org. Chem.* **2012**, *77*, 4184. (b) Tang, W.; Capacci, A. G.; White, A.; Ma, S.; Rodriguez, S.; Qu, B.; Savoie, J.; Patel, N. D.; Wei, X.; Haddad, N.; Grinberg, N.; Yee, N. K.; Krishnamurthy, D.; Senanayake, C. H. *Org. Lett.* **2010**, *12*, 1104. (c) Huang, K.; Zhang, X.; Emge, T. J.; Hou, G.; Cao, B.; Zhang, X. *Chem. Commun.* **2010**, *46*, 8555.
- ⁹ Reves, M.; Ferrer, C.; Leon, T.; Doran, S.; Etayo, P.; Vidal-Ferran, A.; Riera, A.; Verdaguer, X. *Angew. Chem., Int. Ed.* **2010**, *49*, 9452-9455.
- ¹⁰ Kolodiazhnyi, O. I.; Gryshkun, E. V.; Andrushko, N. V.; Freytag, M.; Jones, P. G.; Schmutzler, R. *Tetrahedron-Asymmetry* **2003**, *14*, 181.
- ¹¹ Leon, T.; Riera, A.; Verdaguer, X. *J. Am. Chem. Soc.* **2011**, *133*, 5740.
- ¹² (a) Verdaguer, X.; Moyano, A.; Pericas, M. A.; Riera, A.; Maestro, M. A.; Mahia, J. *J. Am. Chem. Soc.* **2000**, *122*, 10242. (b) Verdaguer, X.; Pericas, M. A.; Riera, A.; Maestro, M. A.; Mahia, J. *Organometallics* **2003**, *22*, 1868. (c) Sola, J.; Reves, M.; Riera, A.; Verdaguer, X. *Angew. Chem., Int. Ed.* **2007**, *46*, 5020. (d) Reves, M.; Achard, T.; Sola, J.; Riera, A.; Verdaguer, X. *J. Org. Chem.* **2008**, *73*, 7080.
- ¹³ Achard, T.; Benet-Buchholz, J.; Riera, A.; Verdaguer, X. *Organometallics* **2009**, *28*, 480.

Background

2

2.1	Chiral Phosphorus and Asymmetric Hydrogenation	13
2.2	Asymmetric Hydrogenation	17
2.3	Strategies employed in the synthesis of chiral phosphorus	26
2.4	The development of MaxPHOS	36
2.5	The optimized route to MaxPHOS	41
2.6	P, S ligands with chirality on sulphur	44

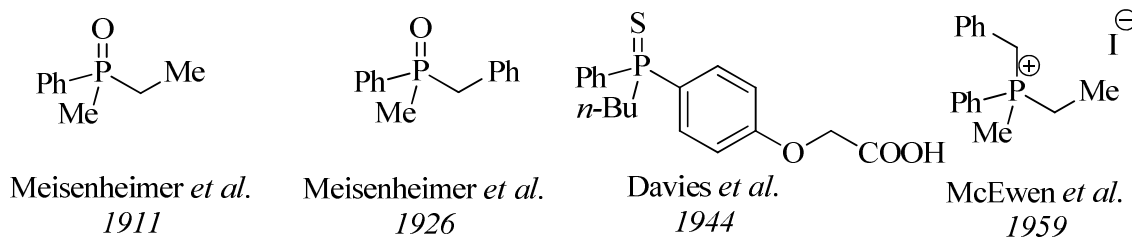
2 Background

2.1 Chiral Phosphorus and Asymmetric Hydrogenation

Molecular chirality was discovered over a century and a half ago by the French chemist and later microbiologist, Louis Pasteur in 1848.¹ The first asymmetric transformation was published in the literature in 1889/1890 by the German organic chemist Emil Fischer while he worked on verifying the molecular structure and synthesis of glucose, fructose and other sugars.² It was some time after when the first chiral phosphine was identified. In 1911 Meisenheimer and Lichtenstadt discovered that phosphorus could be substituted by 4 different functional groups forming a stereogenic centre.³ The history of chiral and asymmetric synthetic organic chemistry indeed stretches back a long time but its awakening was slow. It would not be until more modern times i.e., the 1960s and 1970s spring boarding from the pioneering work of Wilkinson, Nozaki, Horner and Knowles that asymmetric catalysis employing chiral phosphines would really take off.

In its beginning the interest in chiral phosphorous was small and growing very slowly. It would be 15 years after the first was discovered, in 1926, when only the second racemic mixture ever of a phosphine oxide would be resolved again by Meisenheimer *et al.*⁴ In 1944 Davies and Mann would resolve the first racemic mixture of a thiophosphine⁵ and in 1959 the first racemic mixture of an acyclic phosphonium salt was resolved.⁶ Not long after this through the work of Horner *et al.* the first optically pure trivalent phosphorous species were isolated.⁷

Figure 2.1: Examples of the first optically active phosphines.

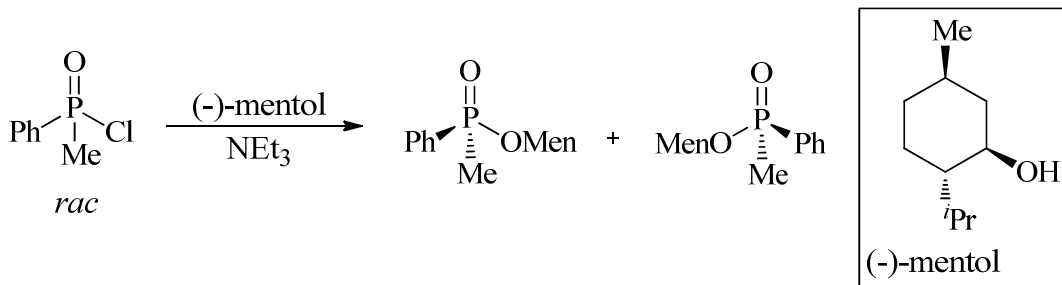


In 1968 a new synthesis of pure optically active phosphine oxides appeared in the literature making use of (-)-mentol. Korpiun *et al.* demonstrated that by reacting (-)-mentol with a

2. Background

racemic chlorophosphine, separating the resulting diastereomeric mixture and reducing they could ultimately arrive at pure optically active phosphine oxides.⁸

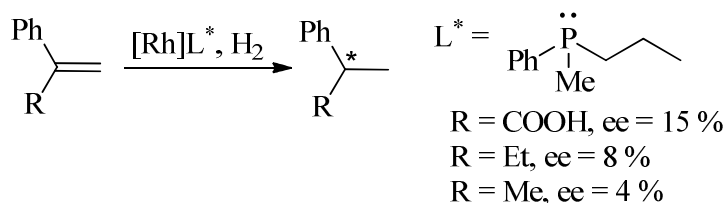
Scheme 2.1: Mentol derived route to chiral phosphines.



At the same time those of the Wilkinson group were discovering the ability of a homogenous triphenylphosphine aided rhodium catalyst $[\text{RhCl}(\text{PPh}_3)_3]$ to successfully hydrogenate substituted olefins.⁹

It was these two new methodologies which would be combined independently by the groups of Horner¹⁰ and Knowles¹¹ to carry out the first catalytic asymmetric hydrogenation by replacing the triphenylphosphine ligand of Wilkinson's catalyst with optically enriched chiral phosphines. The enantiomeric excesses obtained were low but it demonstrated the feasibility of enantioselective hydrogenation.

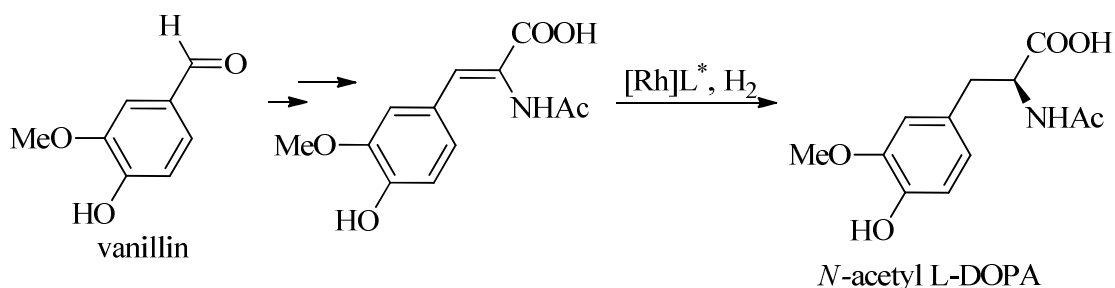
Scheme 2.2: First asymmetric hydrogenations carried out.



The discovery of the medicinal effects of L-DOPA (L-3,4-dihydroxyphenylalanine) in the treatment of the symptoms of Parkinson's disease led directly to the explosion in demand for this naturally occurring, non-standard amino acid. There was a gaping niche in the pharmaceutical industry for an effective enantioselective synthesis of this psychoactive drug and this was a driving force behind the research into the synthesis of new chiral ligands for catalytic asymmetric hydrogenation. Knowles and collaborators were the first to devise an enantiospecific route to the amino acid in question.¹² The last step and the key transformation was an asymmetric reduction and they opted of course to use a rhodium catalysed

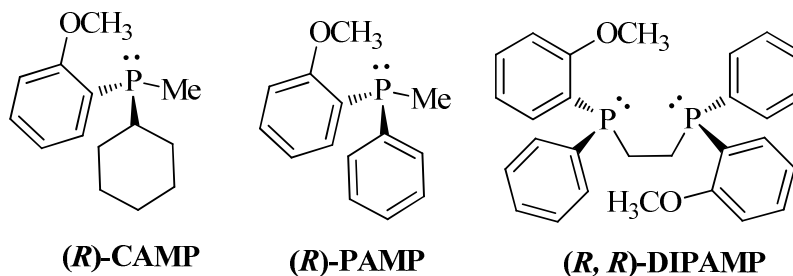
hydrogenation employing a chiral phosphine. They tested various chiral monophosphines and discovered the CAMP¹³ phosphine could carry out the transformation with an ee of 85 %, a very impressive enrichment of enantiopurity for that era. This outcome was considered to be so effective and efficient that it was scaled up and utilized industrially.

Scheme 2.3: The Monsanto L-DOPA process.



The success of monophosphines such as CAMP was limited and so attentions shifted to bi-dentate ligands to constrain and limit the degrees of freedom at the catalyst centre, and therefore increase enantioselectivity. Shortly after Knowles and co-workers developed the DIPAMP diphosphine¹⁴ which succeeded in enantioselectively hydrogenating various α -acetamidoacrylic acids with enantiomeric excesses of up to 96 %. DIPAMP was brought about through the dimerization of the PAMP monophosphine. These results confirmed the advantageousness of bi-denticity around the metal center from the coordinating phosphine ligands. In the end the DIPAMP ligand became key to the synthesis of the highly important anti-Parkinsons drug L-DOPA and also of the amino acid (*S*)-phenylalanine, one of the two components that make up the artificial sweetener aspartame.

Figure 2.2: Monsanto Industrial Chemicals Company's CAMP, PAMP and DIPAMP ligands.



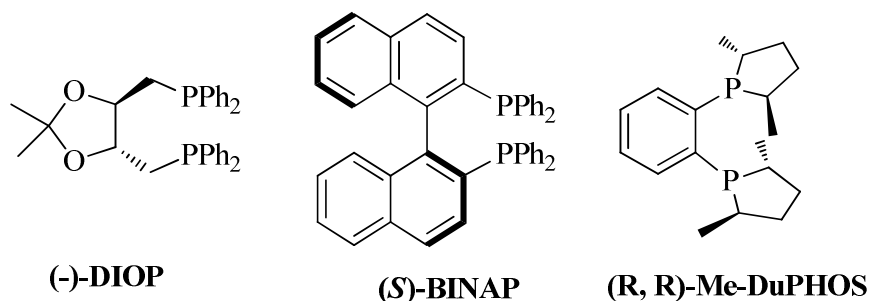
Concurrently while those of the Monsanto Company were developing their *P*-stereogenic mono and diphosphine ligands, the researchers of Dang and Kagan were bringing about the

2. Background

development of the DIOP chiral diphosphine.¹⁵ The DIOP ligand provided enantioselectivities in the rhodium catalysed asymmetric hydrogenation comparable to those of CAMP. The results obtained utilizing the DIOP ligand served to underline the validity of the bi-dentate ligand paradigm but more importantly it demonstrated that chirality need not reside on the coordinating atom but indeed can lie on the skeletal back-bone of the ligand and still infer desirable enantio-induction.

Upon the emergence of the axially chiral BINAP ligand¹⁶, developed in the Noyori group, the versatility and the scope of reaction of rhodium catalyzed asymmetric hydrogenation was augmented greatly. It was applied in the synthesis of the phenylalanine derivative en route to aspartame with near perfect enantioselectivity. A BINAP rhodium complex was employed in a key transformation in the synthesis of the clinically important HIV protease inhibitor indinavir providing high enantioselectivities.¹⁷ Some ten years later from the group of Burk the DuPHOS ligand was introduced, again with its chirality lying on the skeletal backbone.¹⁸ It has proved even to this date to have one of the largest scopes of substrates seen from any of the hundreds of chiral phosphine ligands developed for rhodium catalyzed asymmetric reductions. Later on researchers began to replace rhodium catalysts with ruthenium ones and saw substrate scopes expand further including asymmetric carbonyl reductions.¹⁹ One-pot Rh/Ru/BINAP mixtures were even employed to asymmetrically reduce carbon-carbon double bonds simultaneously as carbon-oxygen double bonds en route to a synthesis of statine analogues, components of HIV protease inhibitors.²⁰

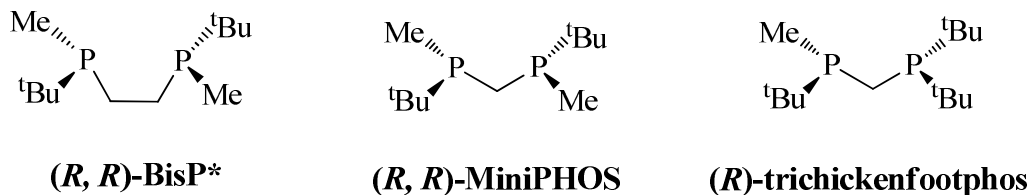
Figure 2.3: Highly effective non *P*-stereogenic chiral phosphines.



With the runaway success of diphosphines with chirality residing on the backbone of the ligand, the interest in *P*-stereogenic diphosphine chiral ligands largely died away for the greater part of two decades but has undergone resurgence of late, through the work of

Imamoto²¹ and Hoge²² among others, with the emergence of BisP*, MiniPHOS and trichickenfootphos coming out of each group respectively.

Figure 2.4: Highly effective *P*-stereogenic chiral phosphines.



These ligands provided excellent enantioselectivities in asymmetric hydrogenation of a host of α -acetamidocinnamic acids. In this field of research the standard has been set high, many research groups compete against each other to develop new ligands and catalysts to broaden substrate scopes even further, while increasing resulting enantioselectivities to near perfection which must be combined with low catalyst loading and high turn-over frequencies. It is a veritable arms race with no let-up in sight.

2.2 Asymmetric Hydrogenation: Catalytic cycle, mechanism, origin of enantioselectivity

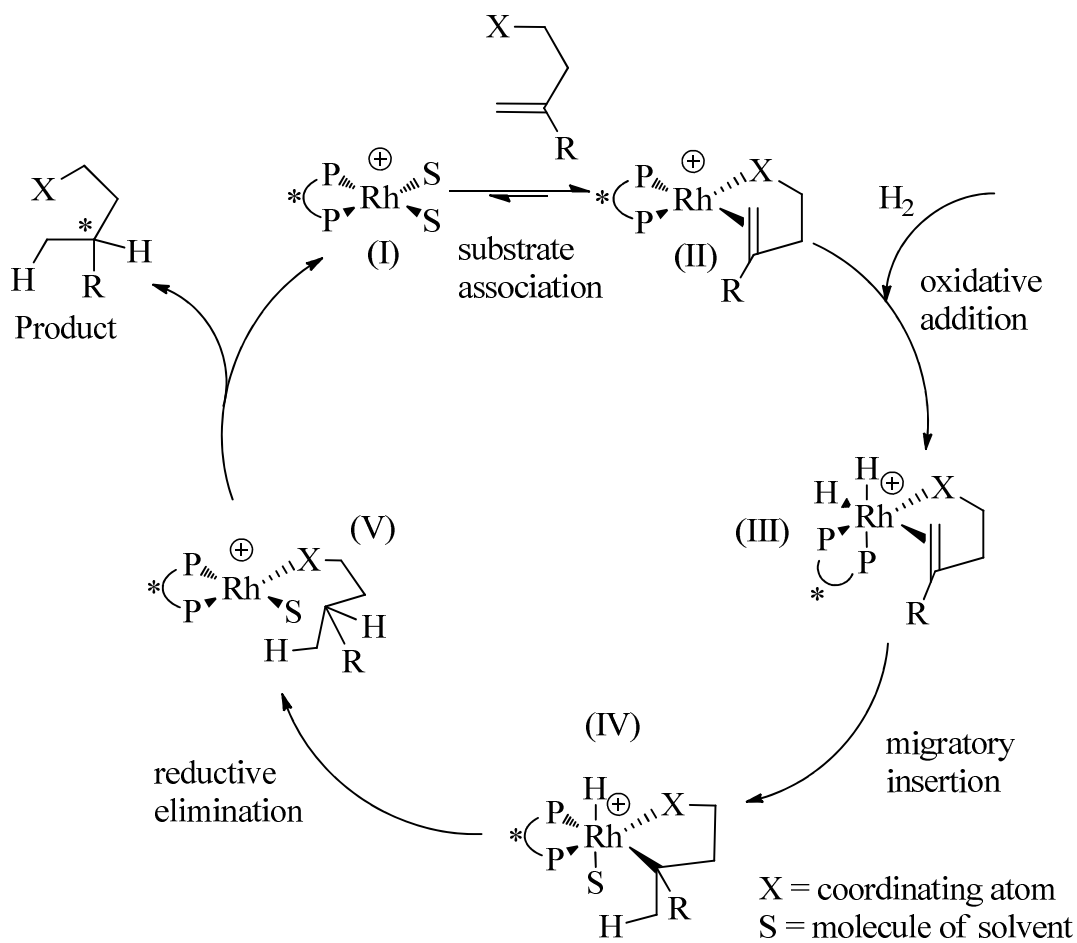
Since its inception the mechanism of the rhodium catalyzed asymmetric hydrogenation has been studied widely. The sheer quantity of computational and experimental information is enormous. Investigation and research into this topic began shortly after the first diphosphine rhodium complexes were characterized. Because it was known the Wilkinson's catalyst formed a stable dihydride complex²³, it was expected similar complexes would be observed and would play a key role in the mechanism of the asymmetric rhodium catalyzed hydrogenation using diphosphine ligands but to some surprise no hydride complexes were observed, it was sure they were present but they remained elusive.²⁴ What were observed were solvated diphosphine-Rh complexes (scheme 2.4, I) bearing two molecules of solvent and two formally vacant coordination sites around the metal centre, these were characterized both in solution and in solid state.²⁵

Upon the addition of a prochiral substrate to these solvated ones as expected, two diastereomeric substrate-catalyst complexes emerged (scheme 2.4, IIa and IIb), in the case of the C_2 symmetric diphosphines. In general these two diastereomers would be present in very un-equal quantities with diastereomeric ratios between 5:1 and 100:1 being observed at first.²⁶ Because of the stability of the substrate-catalyst complexes in comparison with the

2. Background

dihydride complexes which could not be even characterized, for a long period of time, some three decades, what is called the “unsaturated mechanism” was accepted as *the* mechanism of asymmetric hydrogenation.

Scheme 2.4: Proposed “unsaturated” pathway of asymmetric hydrogenation.



The unsaturated mechanism tells that the enantioselection of the reaction occurs before an oxidative addition step when the substrate is coordinating to the complex. It was shown that the substrate can chelate to the metal reversibly, that is to say the chelate can open, only coordinating by one atom as a molecule of solvent occupies the vacant site and can re-coordinate perhaps giving the other complex diastereomer.²⁷ It was noted also in the beginning of these studies that the major diastereomer would most usually *not* be the source of stereospecificity of the resulting hydrogenated substrate.²⁸ It would be the minor

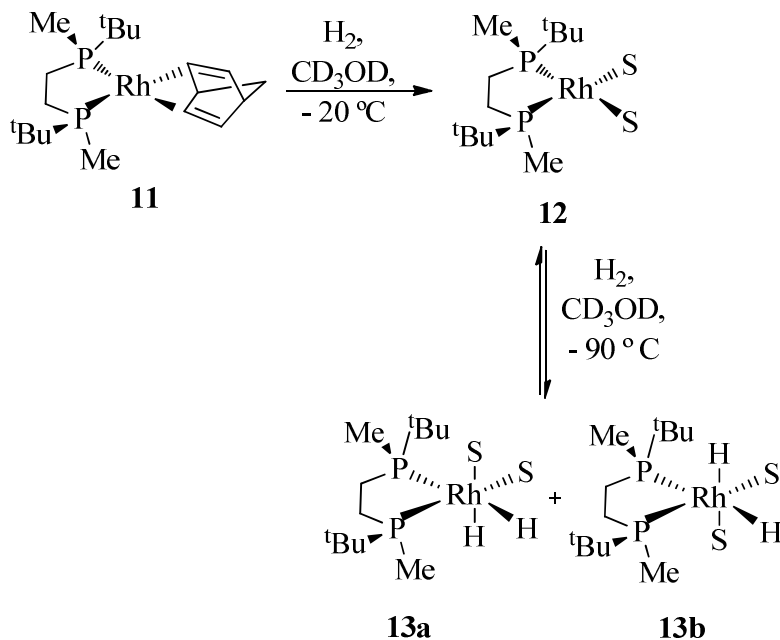
diastereoisomer which would correspond to the absolute configuration of the product. And since it was shown that the minor diastereomer was consumed faster in low temperature experiments,²⁹ it was thought enantioselectivity of the asymmetric hydrogenation could be explained purely by considering the difference in reactivity of the two square planar diastereomeric substrate-catalyst complexes.

Some criteria would need to be true for this reaction pathway to feasibly give the enantioselectivities the reactions were yielding, such as: the rate of reaction of the hydrogenation of the less reactive diastereomer should be considerably slower than the rate of conversion in between the two diastereomers and this was proved to be the case.³⁰ Also further evidence to prove the credibility of the unsaturated mechanism was presented when it was observed that at lower temperatures, poorer enantioselectivities were observed, this fit nicely into the hypothesis as lower temperature would mean less inter-conversion between the substrate-catalyst diastereomers.³¹

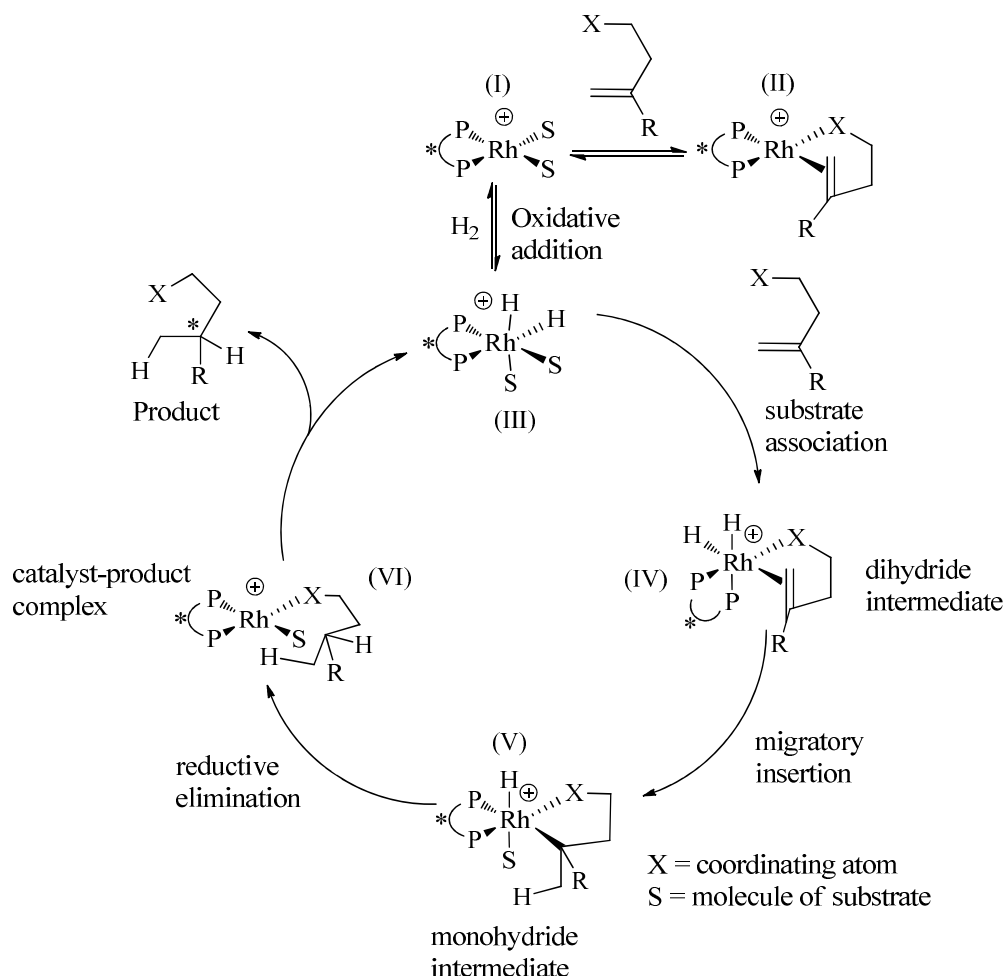
More recently through the outstanding work of Gridnev and Imamoto new ideas about the mechanism of asymmetric hydrogenation have arisen, especially as regards those of *P*-stereogenic ligands with bulky electron rich substituents. They demonstrated the previously elusive dihydride complexes.³² At first it was found with the complex they were working, [(NBD)Rh(BisP*)]BF₄ (Scheme 2.5, **11**) could not be cleanly hydrogenated to the solvated complex at room temperature, dark coloured solutions resulted with incomprehensible NMR spectra. By reducing the temperature to – 20 °C they managed to observe the formation of the solvated complex but also some impurities. By reducing the temperature even further to – 90 °C to circumvent the appearance of impurities, they were surprised to observe and be able to characterize the solvated dihydride complexes.

It was observed these complexes formed reversibly unlike other similar complexes such as the dihydride complexes of benzylic type BisP* which, formed irreversibly, it was found they were stable up to 0 °C and their reactions which occurred at higher temperatures were not accompanied by hydrogen loss.³³ This showed that the substituents on the phosphorous influence very much the stability of the hydride complexes where electron donating substituents increase affinity for the rhodium complex to dihydrogen.

Scheme 2.5: Formation of solvated dihydride complexes of rhodium and BisP* diphosphine ligand.



Having found a methodology to observe and characterize the hydride complexes they then set about testing these complexes in hydrogenations of *Z*-MAC at near stoichiometric amounts to gauge the plausibility of the “dihydride mechanism”, as outlined in scheme 2.6. Carrying the reactions out at $-100\text{ }^\circ\text{C}$ with 50 mol % of dihydride solvated catalyst (scheme 2.6, III) they found the hydrogenations proceeded with enantioselectivities the same as the catalytic reaction, 99 % ee and only one diastereomer of mono-hydride intermediate (scheme 2.6, V) was observed. This meant the substrate association and subsequent migratory insertion step proceeded almost instantly and with near complete selectivity. Other α -dehydroaminoacids,³⁴ enamides³⁵ and (*E*)- β -dehydroaminoacids³⁶ were tested in this simulation of the dihydride pathway and all yielded enantioselectivities identical to their respective catalytic reactions and were all above 98 % ee, this proved that the dihydride pathway was a viable mechanistic pathway.

Scheme 2.6: Proposed “dihydride” pathway of asymmetric hydrogenation.

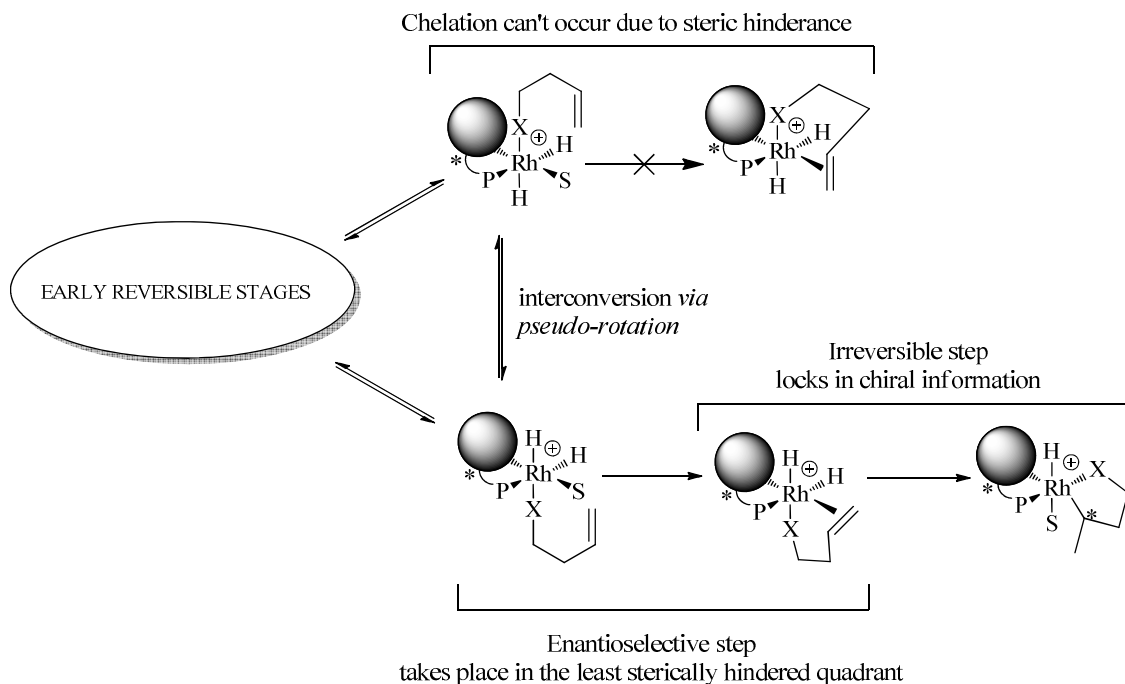
It was also attempted to hydrogenate the pre-formed substrate-catalyst square planar complexes (scheme 2.6, II) at low temperatures. Loosely bound $[(\text{BisP}^*)\text{Rh}(\text{substrate})]\text{BF}_4$ complexes with enamides^{35b} and β -dehydroaminoacids³⁶ could both be hydrogenated at the same temperature as when the solvated dihydride complexes were used to hydrogenate, at $-100\text{ }^\circ\text{C}$. However, more tightly bound substrate-catalyst complexes such as when the substrate was dimethyl 1-benzoyloxyethene phosphonate could not be hydrogenated at $-100\text{ }^\circ\text{C}$. The temperature had to be risen to $-30\text{ }^\circ\text{C}$ before hydrogenation would take place and then enantioselectivity of just 75 % ee would be obtained, when previously the same substrate was hydrogenated simulating the hydride pathway at $-100\text{ }^\circ\text{C}$ and gave an excess of 97 % ee. This was explained as the loosely bound substrate-catalyst square planar complexes could open its' chelate, reforming the solvate-catalyst complex which could re-enter the dihydride pathway while the more tightly bound substrate-catalyst complexes could not open its' chelate, and was forced to react *via* the “unsaturated pathway”. All this mechanistic data

2. Background

proved that more than likely when considering hydrogenations using bulky, electron rich *P*-stereogenic ligands the dihydride pathway is the mechanism which is providing the high enantioselectivities.

It was later shown that there need not be such debate between “unsaturated pathway” and “dihydride pathway”. All of the reaction intermediates are in equilibrium with each other and all reaction steps are reversible up until the migratory insertion or even in some cases until the reductive elimination step.³⁷ The two pathways outlined above are competing reversible pathways in equilibrium which convene on a single decisive irreversible step. It was found that enantioselection actually occurs at the point of the double bond associating with the metal. The substrate goes from singly bonding to the metal through a carbonyl for example, as it displaces a solvent molecule to form a chelate. This is also a process which is in fast equilibrium and is reversible and so acts as a “trial and error” method for determining the ultimate stereoselectivity, which is fixed when the irreversible migratory insertion/reductive elimination step occurs.

Scheme 2.7: Origin of enantioselection for C_1 and C_2 symmetric chiral diphosphine catalysed asymmetric hydrogenation.

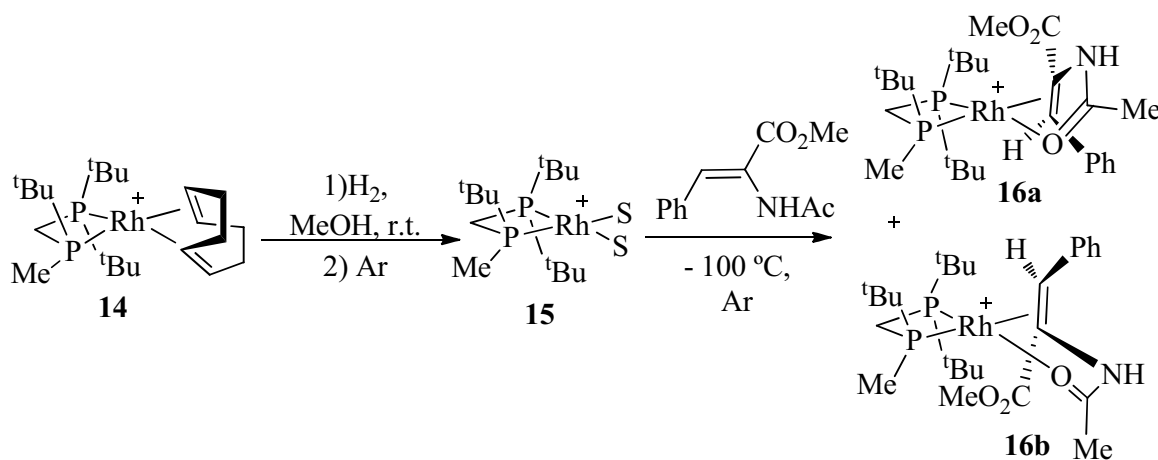


In scheme 2.7 it is shown how the enantioselective olefin association step occurs in the least hindered quadrant of a C_1 symmetric diphosphine such as (di-*tert*-butylphosphino)(methyl-

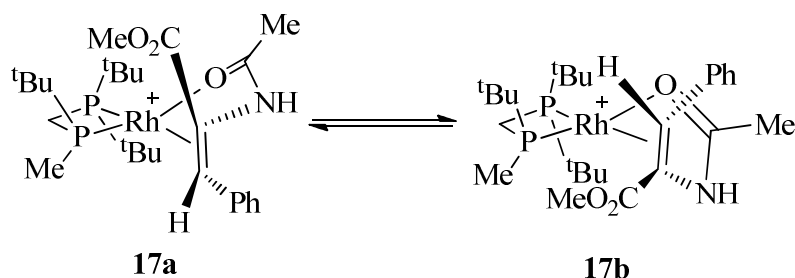
tert-butylphosphino)methane (trichickenfootphos) and then the enantioselection is trapped by the very fast migratory insertion step. In the case of C_2 symmetric diphosphines the process behaves in exactly the same way but in the other side of the complex as well.

In 2008 Gridnev, Imamoto and Hoge published their findings on the in-depth mechanistic studies of the asymmetric hydrogenation of the *Z*-MAC dehydroaminoacid by the just previously mentioned C_1 symmetric *P*-stereogenic diphosphine trichickenfootphos.³⁸ Through low temperature ^1H , ^{13}C and ^{31}P NMR studies coupled with computational calculations they were able to build a very detailed description of the different mechanistic pathways which are present and why such high enantioselectivity is achieved. Through the combination of these experiments they were able to observe when H_2 was applied to the trichickenfootphos precatalyst at room temperature the cyclooctadiene ligand is hydrogenated and is freed from the complex to yield the solvated catalyst. Hydrogen gas was then replaced with argon gas and the substrate *Z*-MAC was mixed with the solvate complex at $-100\text{ }^\circ\text{C}$ to form a set of two coordination isomers of the substrate-catalyst chelate.

Scheme 2.8: Initial approach of substrate to catalyst.



The oxygen of the acetate group is the first to coordinate to the catalyst and it approaches from the side of the least hindered quadrant. The chelate is closed when the double bond then coordinates to the metal to form a mixture of two kinetic products, neither one overly favoured above the other. These products are stable at $-100\text{ }^\circ\text{C}$ but as the temperature is raised to $-80\text{ }^\circ\text{C}$ a reorganization takes place to form a more thermodynamically favoured set of products as the double bond is moved to the other side of the catalyst alongside the less hindered, stereogenic phosphorus.

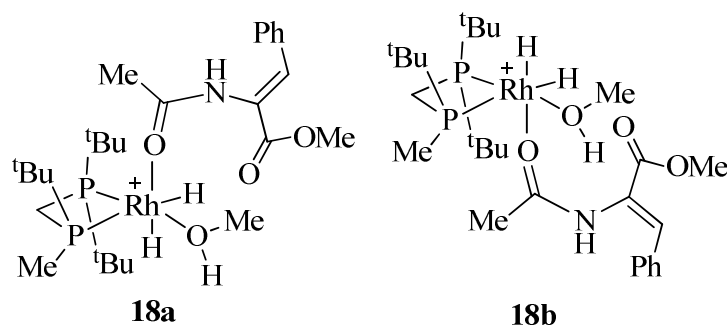
Figure 2.5: The most stable square planar catalyst-substrate chelates.

At room temperature it could be seen that the two isomers **17a** and **17b** are in a fast equilibrium with each other, fast with respect to for example, the equilibrium between the chelated complex and complete dissociation. Computationally neither one structure nor the other is more thermodynamically stable than the other however. At lower temperatures i.e., between $-80\text{ }^{\circ}\text{C}$ and $-100\text{ }^{\circ}\text{C}$ the equilibrium between **17a** and **17b** is halted. It was shown by NMR at this temperature that **17b** is in equilibrium with a partially dissociated complex where a molecule of MeOH occupies the vacant coordination site while **17a** was stable. It was discovered the reason for this was most probably that to facilitate this equilibrium each complex must go through a partially dissociated complex where one molecule of MeOH coordinates to the metal, in the case of **17b** the molecule of MeOH approaches from the bottom through the least hindered quadrant, hydrogen bonding with the oxygen of the ester. This process is made more difficult in the case of **17a** as the molecule of MeOH must approach sideways, closer to the hindered quadrant while hydrogen bonding with the oxygen of the ester to push out the associated double bond. The effects of this equilibrium or lack of it at low temperature were observed when low temperature hydrogenations were carried out. Hydrogenating for 30 minutes at $-100\text{ }^{\circ}\text{C}$ only provided starting material but hydrogenating at $-78\text{ }^{\circ}\text{C}$ for 30 minutes provided hydrogenated product with 40 % conversion and a 97 % ee, complex **17a** still remained in solution but **17b** had been consumed. Leaving the reaction for 5h longer gave complete conversion, **17a** had been completely consumed from the reaction but the overall enantiomeric excess remained the same at 97 % ee. What this meant was the coordination face of the double bond to rhodium did not matter, be it to the *Re* or *Si* face, enantioselectivity was occurring in a later step and opening of the chelate and formation of partially dissociated complex was essential for hydrogenation. This can be understood

perfectly when thinking that it would be difficult for dihydrogen to coordinate to such a sterically hindered square planar substrate-catalyst chelate, it would much easier coordinate to an open partially dissociated complex.

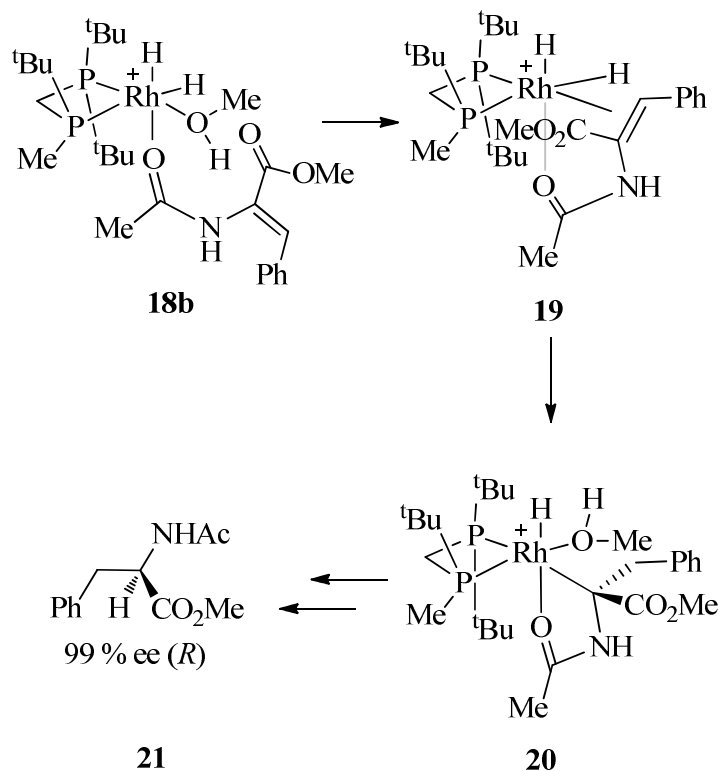
And so it was discovered in the case of the *trichickenfootphos* complex and the Z-MAC substrate, hydrogenation took place on the partially dissociated substrate-catalyst complex (**18a** and **18b**). As dihydrogen coordinates to the complex it can create numerous dihydride octahedral isomers but the secret to enantioselectivity was narrowed down to the difference between just two different paths involving two isomers.

Figure 2.6: Most relevant dihydride substrate-catalyst complexes.



Computational studies found that both complexes **18a** and **18b** could pass through several transition states for the association of the double bond to rhodium step to occur but one in particular involving complex **18b** had a particularly lower energy than all the rest. This association step involves much activity in the least hindered quadrant of the catalyst where the orbital lobe of oxygen coordinates to rhodium while simultaneously pushing out the molecule of methanol. The activation barrier for this event when it occurs in the case of **18a** is 6.9 kcal/mol higher than that of **18b** and herein it is believed lays the reason behind the high selectivity while hydrogenating this substrate. Subsequently the β -carbon is first hydrogenated as the very fast migratory insertion step occurs to give complex **20**, and as the substrate is released upon reductive elimination to give enantioselectively hydrogenated substrate **21**, the catalyst is solvated and entered back into the catalytic cycle.

Scheme 2.9: Enantioselective double bond association followed by migratory insertion.



2.3 Strategies employed in the synthesis of chiral phosphorus.

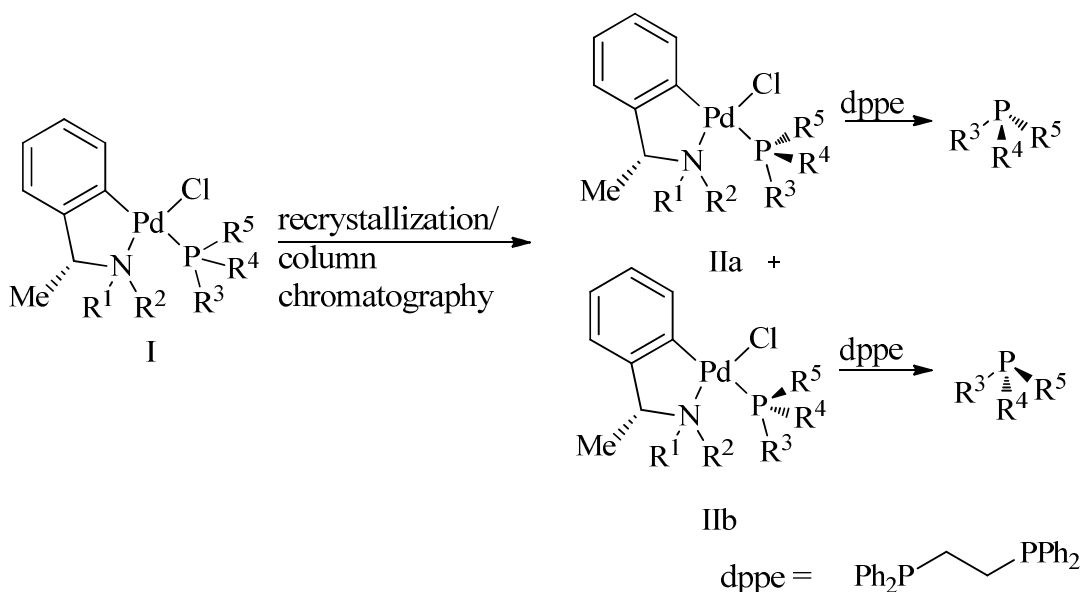
Separation of a racemic mixture.

The first recognized and characterized optically active organophosphorus compound recorded was ethylmethylphenylphosphine oxide which was resolved by protonation by (+)-bromocamphorsulfonic acid and then separation of the resulting diastereomeric salts. This separation was carried out some 15 years after the synthesis of the racemic mixture and was finally separated by fractional crystallization from ethyl acetate and ethyl acetate/diethyl ether mixtures.^{3,4} It was the same method used to separate the comparable compound benzylmethylphenylphosphine in the same laboratory. Apart from these two compounds there are no more recorded instances in the literature of a comparable methodology of separation of diastereomers brought about from protonation of the weakly basic phosphoryl oxide and subsequent chiral salt formation being successfully used in the separation of a mixture of

enantiomeric phosphines. However the method has been shown to aid in the separation of some *P*-diastereomeric mixtures³⁹ and also in the resolution of some chiral backbone phosphine compounds such as BINAP and NORPHOS.⁴⁰

Most of the first methods to be employed in the preparation of optically pure chiral phosphines involved the synthesis of the desired compound in racemic form with an ultimate separation of the racemic mixture with the aid of a chiral auxiliary *via* recrystallization or by column chromatography. The major drawbacks of this methodology lie in that chromatographic separation and recrystallizations can often be tedious and difficult accompanied with low yields. Also the choice of chiral auxiliary can constrain the variety of substituting groups on the phosphorus atom due to incompatibility. That being said, the approach has still been used in recent times as shown by Imamoto *et al.* in 2004 when they prepared a very strained *P*-stereogenic diphosphine by racemic means and then resolved with (+)-dibenzoyl-D-tartaric acid.⁴¹ Hoge *et al.* also made use of this strategy during the synthesis of the aforementioned trichickenfootphos ligand when they synthesized the compound racemically and subsequently carried out a separation of enantiomers *via* preparatory chiral HPLC.

One of the most successful and widely used methods of preparing chiral phosphines through the resolution of racemic mixtures exploits palladium (II) complexes of enantiomerically pure orthometallated 1-phenylethylamine or 1-naphthylethylamine as a chiral auxiliary.⁴² The phosphine racemic mixture is coordinated to the dinuclear metallocycle which forms two equivalents of a mononuclear species in a 1:1 ratio. Also it was shown to be possible to only use a half equivalent of the resolving agent whereby one enantiomer of the phosphine racemic mixture would react while the other would remain in solution. Separation of the diastereomers was then made possible as would be expected using column chromatography or recrystallization. The desired optically pure phosphine could then be liberated from the auxiliary by the use of the strongly binding coordinating agent dppe.

Scheme 2.10: Resolution of a racemic mixture by palladium (II) metallocycle.Preparation by stereoselective synthesis.

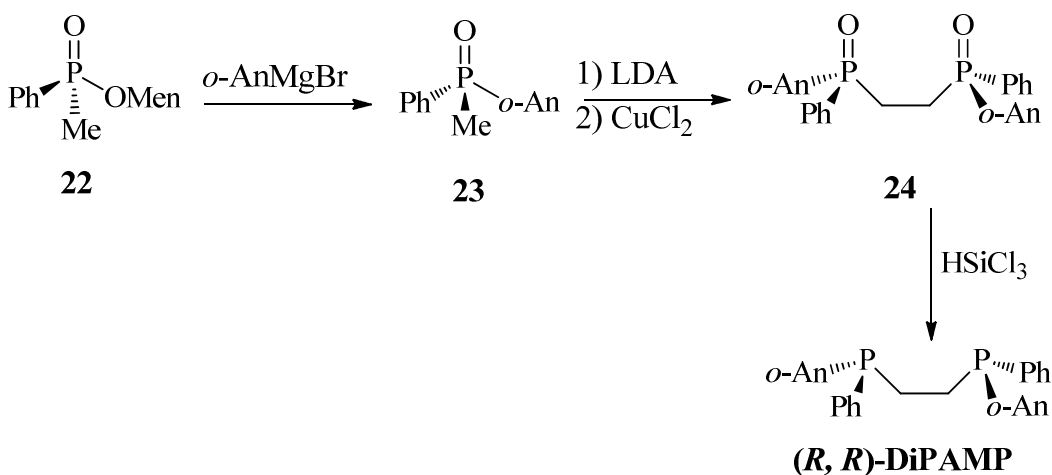
This strategy relies on the use of a stoichiometric amount of a chiral auxiliary during the synthetic process to deliver a *P*-resolved precursor which can undergo stereoselective substitutions forming new C-P bonds towards the desired phosphine. Among the most widely used systems which have been put to successful use include menthol/dihalophosphine, sparteine/dimethylphosphine-borane, sparteine/racemic secondary phosphine-borane and ephedrine/diaminophosphine. One of the most notable discoveries of the research in this field has been the phosphine-boranes, with their easy manageability being often crystalline compounds and their stability under non-inert reaction conditions compared with phosphine-chalcogen compounds, especially phosphine oxide.

Use of menthol as a chiral auxiliary.

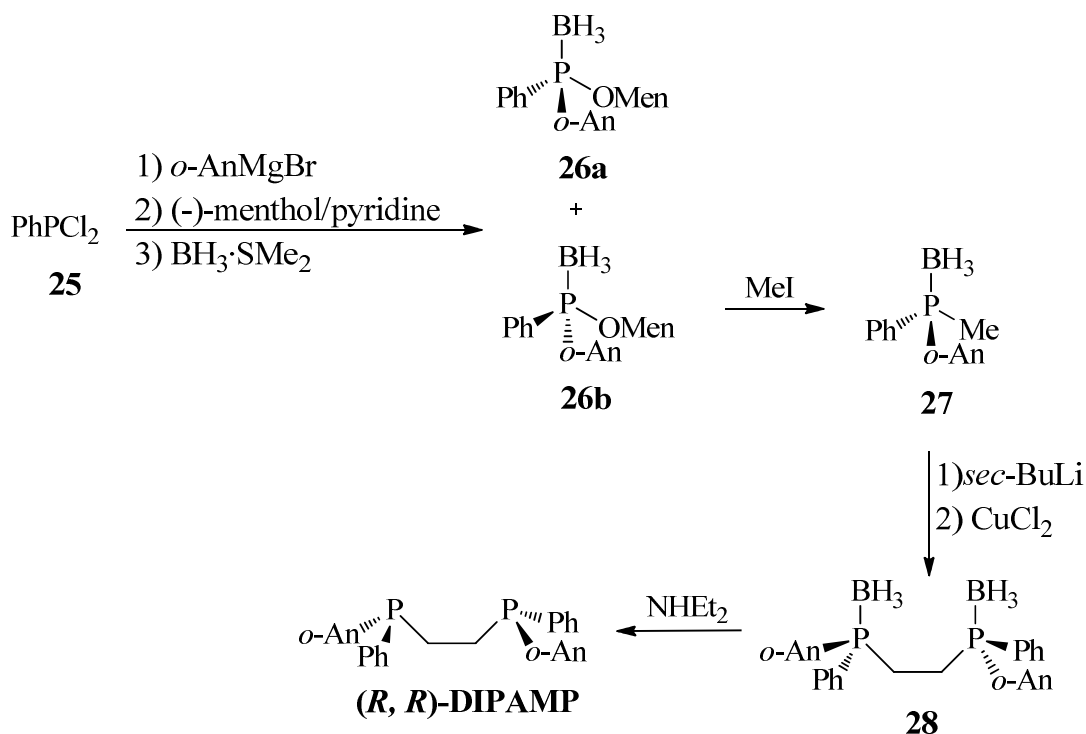
The idea that non-symmetrically substituted menthyl phosphinates could be separated into their diastereomerically pure forms by crystallization was first explored by Nudelman and Cram⁴³ and also by the group of Mislow.⁴⁴ By recrystallization they found they could isolate one diastereomer while the other remained in the mother liquor. Once having obtained the pure diastereomer they were able to react the same with a Grignard reagent yielding a tertiary phosphine oxide with complete inversion of stereochemistry at the phosphorus centre.

It was this exact reaction pathway which was utilized in the very first synthesis by Knowles and co. of the very successful and effective C_2 symmetric diphosphine ligand, DIPAMP.⁴⁵ Drawbacks of this method were that very harsh conditions were required to force the reaction to proceed such as an excess of Grignard reagent. Also a successful reaction very much depended on the substituents on the phosphorus centre however high selectivity could be obtained.

Scheme 2.11: First synthesis of DIPAMP.

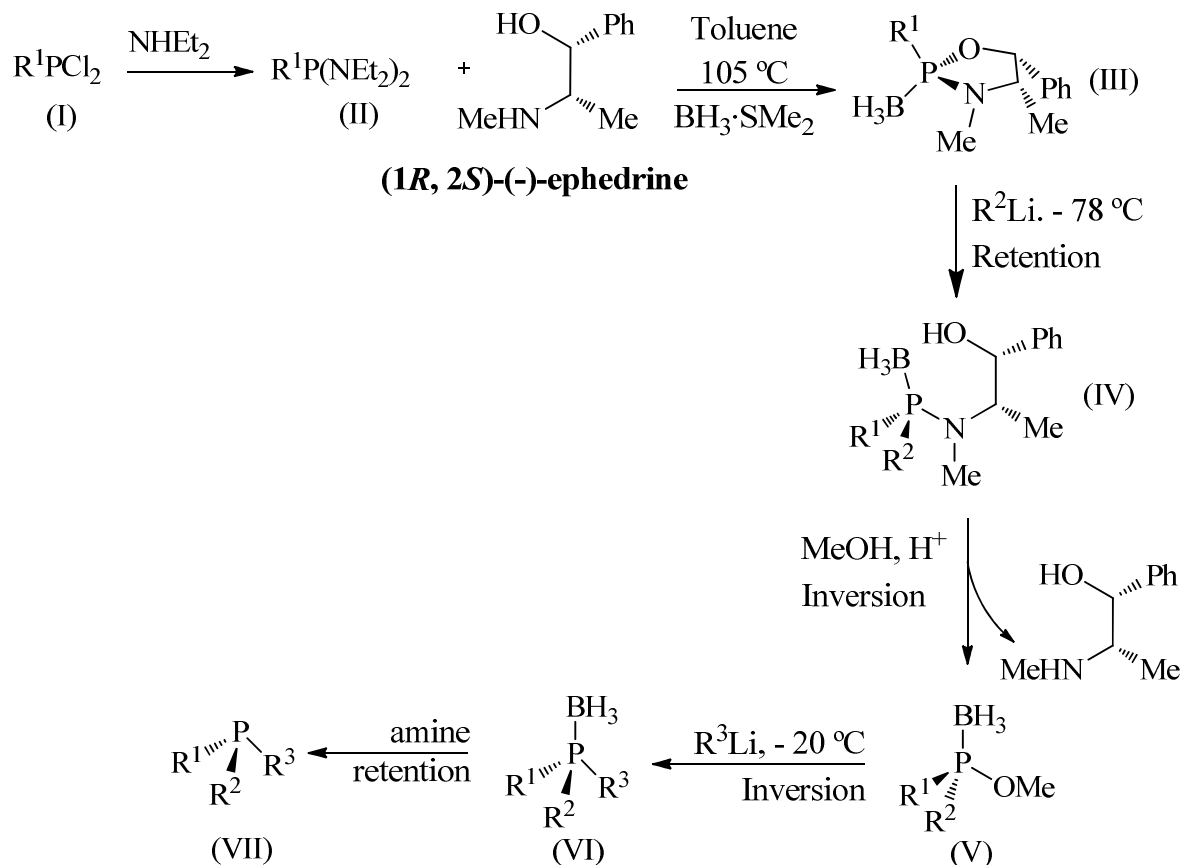


In his landmark paper published in 1990 Imamoto divulged the work his group had developed on the use of phosphine-boranes instead of phosphine oxides towards the synthesis of optically pure DIPAMP.⁴⁶ This was seminal work as the use of phosphine-boranes allows for more facile recrystallization and column chromatography of phosphine intermediates which might not be possible with the equivalent phosphine oxides or free phosphines and also limits the use and handling of corrosive and odorous, free phosphines until absolutely necessary. It was observed that the boranato groups could be removed by stirring the phosphine in an excess of base such as DABCO, diethylamine or morpholine or in the case of very basic phosphine-boranes, strong acids.

Scheme 2.12: Imamoto's synthesis of DIPAMP using phosphine-boranes.Use of heterobifunctional chiral auxiliaries.

Due to the discovery that nucleophilic substitutions on stereogenic phosphorus centres proceed with high stereoselectivity both in the case of phosphinates as well as phosphinate-boranes with complete inversion of stereochemistry, it was considered two successive substitutions should proceed with equal selectivity. For this approach to be viable it was expected that *P*-resolved compounds unsymmetrically substituted by two unequal but both good leaving groups would be necessary. This system took form when heterocyclic phospholidines were introduced and put to this purpose. Heterobifunctional chiral auxiliaries were used to form these phospholidines in high diastereomeric ratio and purity. The diastereomerically pure phospholidines would then be able to be consecutively subjected to nucleophilic substitutions which would be highly selective in manner, leading to enantiomerically pure tertiary phosphines. One application which took very good advantage of this strategy and proved to be one of the most reproduced and used was the system developed by Jugé *et al.* employing (1*R*, 2*S*)-(-)-ephedrine as the heterobifunctional chiral auxiliary.⁴⁷

Scheme 2.13: The method developed by Jugé *et al.* using heterocyclic phospholidines to prepare enantiopure tertiary phosphines.



The powerful method described in scheme 2.13 developed by the group of Jugé first employed a phenyl group in the R^1 position and in most instances of its application R^1 was phenyl but there are examples of other functional groups being used.⁴⁸ The key intermediate is the oxazaphospholidine brought about from the condensation of bis(diethylamino)phenylphosphine with (1R, 2S)-(-)-ephedrine in toluene at $105\text{ }^\circ\text{C}$ (scheme 2.13, III) which proceeds with high diastereoselectivity. It is thought the high selectivity is achieved from the steric need for the phenyl group on phosphorus to be on the opposite side to the ephedrine substituents. Alkyl and aryl organolithium reagents cleanly open the oxazaphospholidine heterocycle in a completely regioselective manner breaking the P-O bond with retention of configuration and a d.e. of greater than 85 % to give IV (scheme 2.13). The observed unexpected retention of configuration during this substitutional reaction was

2. Background

explained mechanistically through the initial attack of the organolithium nucleophile on phosphorus by the least hindered side of the P-O bond, forming a trigonal pyramidal transition state which undergoes stereopermutation in equilibrium before breaking the P-O bond while it is in an apical position giving rise to the resulting stereochemical product.⁴⁹

Some drawbacks of this method arose when highly sterically hindered nucleophiles proved to provide poor diastereoselectivities upon the ring-opening of the oxazaphospholidine ring such as with 1,1'-dilithioferrocene⁵⁰ most likely due to the high temperatures required to force reactivity which hindered stereoselection. Also it was shown there was no reactivity whatsoever with *o,o'*-aryllithium nucleophiles.⁵¹

The following methanolysis reaction to give compounds of type V (scheme 2.13) proceeded in high yields generally with complete inversion of stereochemistry probably due to an S_N2 reaction pathway which takes place and allows for the recuperation of the (1*R*, 2*S*)-(-)-ephedrine chiral auxiliary. It was found when R² was a *tert*-butyl group it made the methanolysis step impossible more than likely due to its steric hindrance and basicity.⁵²

The substitution reaction with phosphinite-boranes again proceeded with complete inversion of stereochemistry, proceeded well with alkyl and aryl organolithium nucleophiles but provided no reactivity with the of *o,o'*-disubstituted aryllithium once again.

To circumvent unreactive methanolysis steps and unreactive resulting phosphinite-boranes in this methodology, acidolysis to chlorophosphine-boranes was investigated as a possible reaction pathway detour to the tertiary phosphines desired.⁵³ It was found the chlorophosphine-boranes were somewhat attractive synthons if used *in-situ* whereas otherwise their instability compared with phosphinite-boranes meant their isolation is difficult and problematic. Also they were more likely to undergo racemization if trace amounts of HCl were present. Generally their use lead to lower enantiomeric excess in their relevant transformations in comparison with phosphinite-boranes if very cautious control of reaction conditions was not maintained and therefore there have been very few applications of chiral chlorophosphine-boranes in the literature.

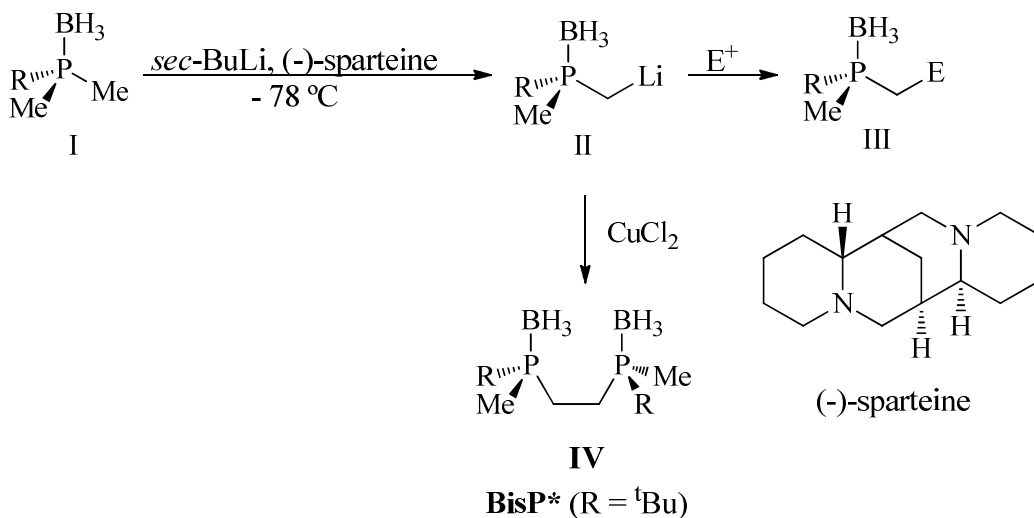
Stereoselective deprotonation of enantiotopic methyl groups.

Methyl groups substituted on phosphine-oxides and phosphine-boranes contain C-H bonds sufficiently acidic to be deprotonated by organolithium bases such as *sec*-butyllithium and *n*-butyllithium. This reactivity has been put to good use towards the preparation of very useful

and efficacious diphosphines as the so-called DIPAMP and trichickenfootphos diphosphine ligands, ligands which have been shown previously in this section. The acidity of the C-H bond is due to the electron withdrawing nature of the P-O and P-B bonds and also it has been known for some time that these deprotonations occur maintaining the integrity of the stereochemistry on the phosphorous chiral center.⁵⁴ The highly nucleophilic carbanions which are thusly generated open access to a veritable gamut of α -functionalized products and can also be oxidatively coupled by copper.

In order to arrive at optically pure α -functionalized *P*-stereogenic products *via* deprotonation, optically pure *P*-stereogenic methylphosphine intermediates must be used *unless* differentiation between two enantiotopical methyl groups residing on a prochiral phosphorus can be made. It was just this strategy which was employed by the group of Evans when they employed (-)-sparteine as a chiral auxiliary in the deprotonation of an achiral dimethylphosphine.⁵⁵ It is thought (-)-sparteine coordinates the lithium atom and so creates a chiral environment as the alkyl anion deprotonates the methyl group which exerts an influence over which one is deprotonated. This approach was used to prepare a small family of diphosphines with good enantiomeric excess and diastereomeric excess in the Evans group before other groups such as those of Imamoto, Jugé, and Mezzetti took up and carried on the strategy, diversifying it.

Scheme 2.14: The strategy developed by Evans *et al.* of enantioselective deprotonation.

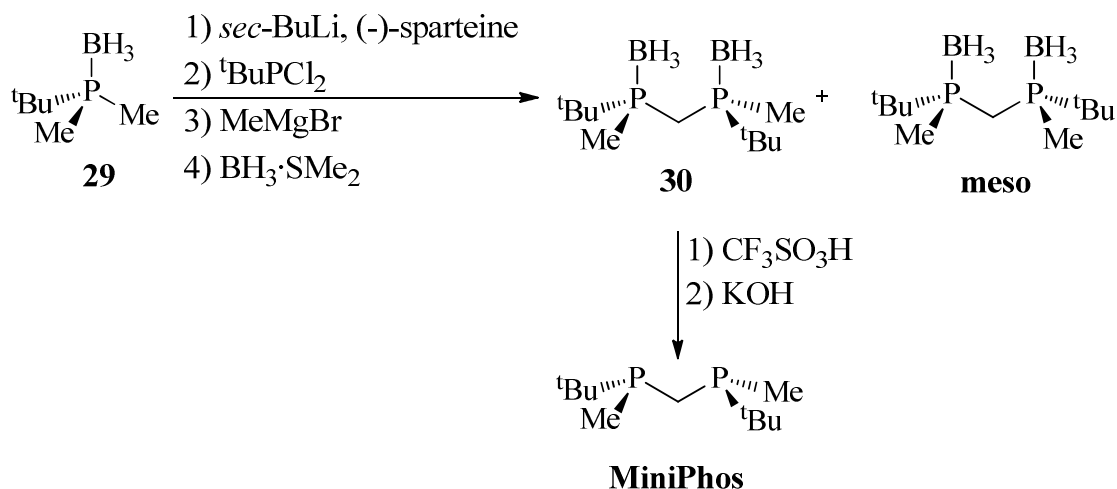


The group of Imamoto succeeded in preparing the MiniPhos ligand in this fashion, a ligand which proved successful when implemented in asymmetric hydrogenations as well as

2. Background

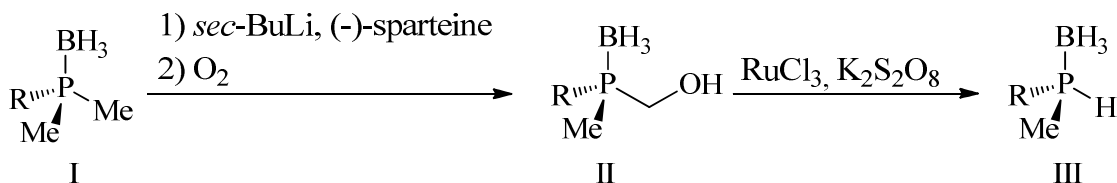
hydrosilylations and Michael additions. From the given dimethylphosphine-borane **29** shown in scheme 2.15 a 1:1 mixture of isomers was obtained containing the desired phosphine and its meso isomer. The desired phosphine was isolated by recrystallization and liberated from the borane moieties using an acidic procedure as the phosphine proved to be too basic to be deprotected by the more conventional amine method.

Scheme 2.15: Enantiotopical deprotonation employed by Imamoto to prepare MiniPhos.

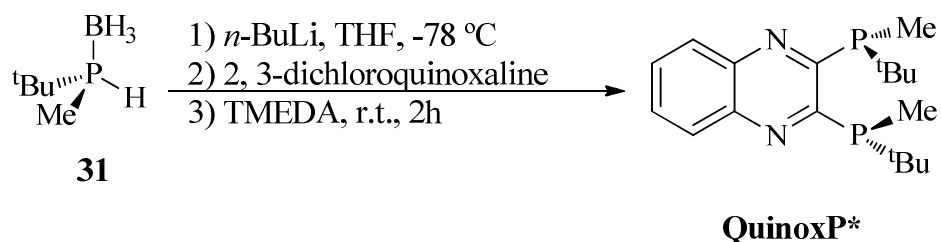


Other processes involving enantiotopical deprotonation developed by Imamoto *et al.* permitted access to phosphine-boranes containing good β -positioned leaving groups and also secondary phosphine-boranes which led ultimately to the preparation of the C₂ symmetrical BisP* and the QuinoxP* ligands.⁵⁶ Selectively deprotonating the dimethylphosphine-borane and then reacting with molecular oxygen allows for the formation of the primary alcohols which can then be oxidatively degraded to the secondary phosphine-boranes as shown in scheme 2.16.

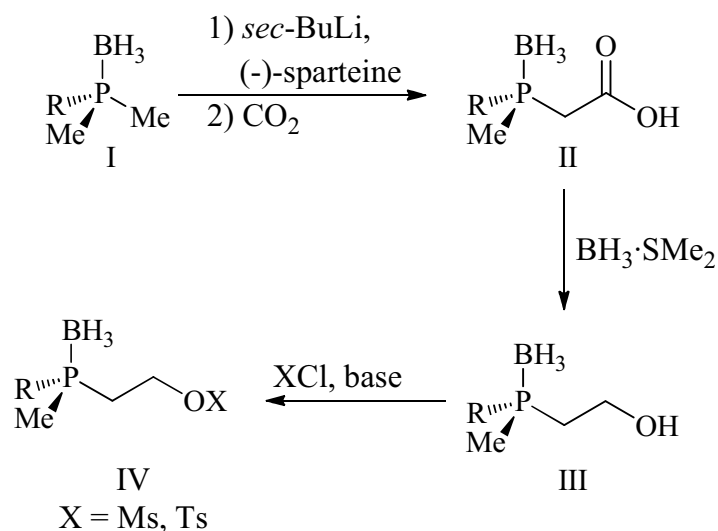
Scheme 2.16: Preparation of secondary phosphine-boranes.



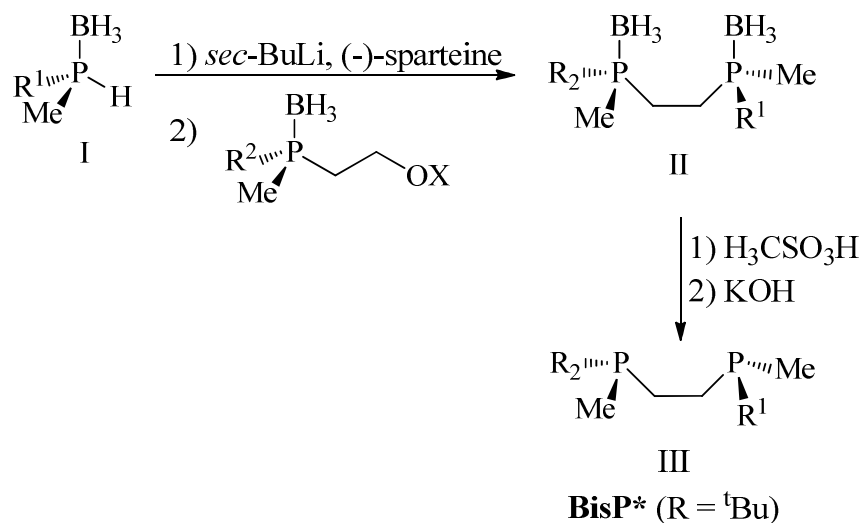
The secondary phosphine-borane **31** was used as a chiral building block towards the preparation of the QuinoxP* ligand.

Scheme 2.17: Preparation of QuinoxP* ligand.

The selective deprotonation of dimethylphosphine-boranes with *sec*-BuLi/(-)-sparteine followed by the reaction of the resulting α -carbanion with CO₂ gave rise to phosphinoacetic-borane acids. These could be reduced with BH₃·SMe₂ to the corresponding alcohol which could be used to introduce good leaving groups such as mesylates and tosylates.

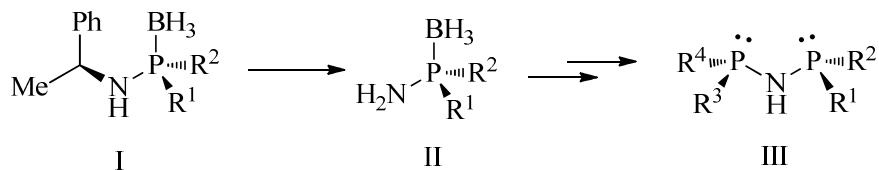
Scheme 2.18: Phosphine-boranes with leaving groups in the β position.

The good leaving group containing phosphine-boranes were then reacted with the secondary phosphine-boranes to form a family of unsymmetrical BisP* ligands proven successful in the rhodium catalyzed asymmetric hydrogenation of various substrates.

Scheme 2.19: A route to unsymmetrical BisP* ligands.

2.4 The development of MaxPHOS

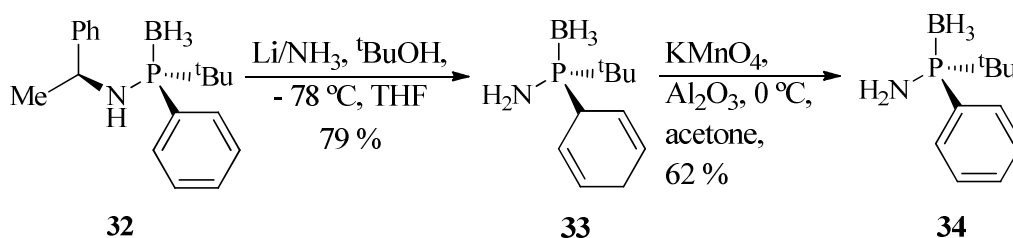
P-stereogenic chiral diphosphines such as trichickenfootphos and MiniPhos have shown to be very successful in their application. They also show a high degree of similarity being made up of two phosphines joined by a carbon bridge. In the literature previously a successfully applicable chiral *P*-stereogenic diphosphine with a heteroatom bonding to phosphorous had never been seen. P* aminophosphines in general were very rare as free primary amino phosphines tend to form dimers with the evolution of ammonia. But it was reported by Kolodiaznyi⁵⁷ that borane amino phosphines such as I (scheme 2.20) are stable and can be obtained in diastereomerically pure form using phenyl-ethylamine as a chiral amine.

Scheme 2.20: Potential utility of borane-aminophosphines.

These compounds had never been applied in catalysis before nor had their hydrogenolysis been described. In our group it was hypothesized that with reductive cleavage of the aryethyl fragment it would be possible to arrive at P* aminophosphines that could be used as useful chiral building blocks in the synthesis of catalytically active chiral diphosphines.⁵⁸

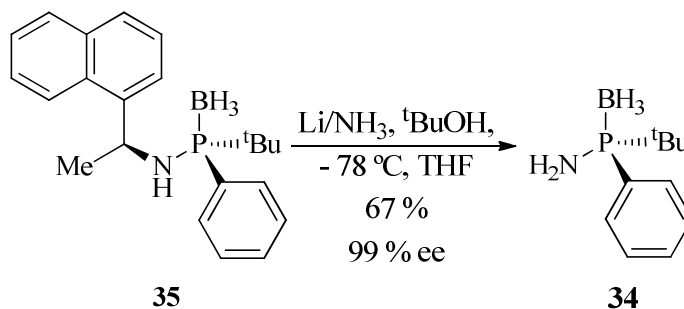
The first port of call to test out this hypothesis consisted of attempting the reductive cleavage of known compound **32**. All initial attempts at hydrogenolysis of the compounds failed. It was eventually successfully reductively cleaved by reacting with lithium in liquid ammonia. However at this time an unexpected side reaction occurred when it was observed that concomitant Birch-type reduction occurred to form the phosphinodiene. Compound **33** could then be oxidized using KMnO_4 on alumina to form new chiral aminophosphine **34**.

Scheme 2.21: First synthesis of primary aminophosphine-borane.



To circumvent the Birch style reduction and subsequent required oxidation step the naphthyl derivative **35** was prepared. Compound **35** underwent reductive cleavage in liquid ammonia with lithium as before but no Birch reduction occurred on the phenyl group. It was also observed that no racemization of the phosphorus chiral center occurred under these conditions.

Scheme 2.22: Circumvention of oxidation step.



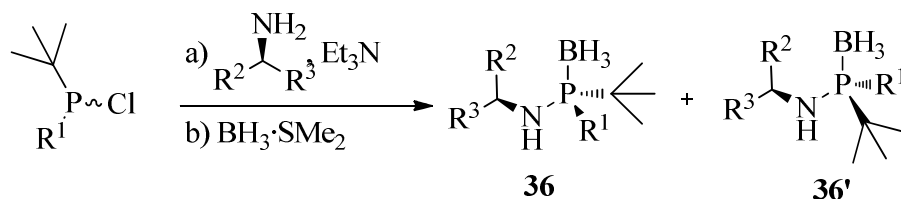
The optimization of reaction conditions for the reductive cleavage was the first step on the road to the synthesis of chiral aminophosphines. The next would be the development of a diastereoselective methodology to form the aminophosphines required for the hydrogenolysis step. It was known at the time that substitution reactions of chiral alcohols with chlorophosphines undergo dynamic kinetic resolutions and so provide diastereomerically

2. Background

enriched mixtures. With this in mind a screening of chiral amines in the substitution reaction with $(\pm)^t\text{Bu}(\text{Ph})\text{PCl}$ and $(\pm)^t\text{Bu}(\text{Me})\text{PCl}$ was carried out.

The chiral amine which was found to provide highest diastereoselectivity in the reaction was the 1-naphtylethylamine for both chloro-phosphines as seen in entries 2 and 8 of table 2.1. However the phenyl-glycinamide was found also to be a very favourable resolving agent (entries 6 and 9). It was found to provide lower diastereoselectivities than the naphthyl chiral amine but the amino phosphines it formed were easily separable by column chromatography and also highly crystalline which aided their isolation. At this point it was decided to make the phenyl substituted amino phosphines using 1-naphtylethylamine and the methyl substituted amino phosphines using phenyl-glycinamide. Multigram quantities were obtained of product **36i**. After exhaustive methylation and then reductive cleavage, a secondary amino phosphine was obtained in 99 % ee which could be used as a building block in the formation of a series of *N*-methyl diphosphines.

Table 2.1: Screening of chiral amines for diastereoselectively biased substitution.



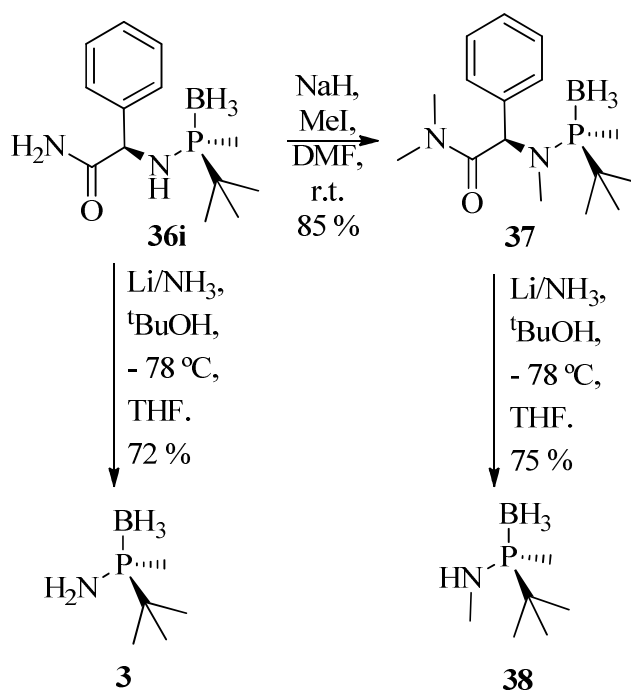
Entry	R ¹	R ² , R ³	Yield [%]	d.r.	Product
1	Ph	Ph, Me	87	5:1	36a, 36a'
2	Ph	1-naph, Me	91	6:1	36b, 36b'
3	Ph	<i>p</i> -tol, Me	88	4:1	36c, 36c'
4	Ph	<i>p</i> -MeOC ₆ H ₄ , Me	90	4:1	36d, 36d'
5	Ph	<i>p</i> -ClC ₆ H ₄ , Me	88	4,5:1	36e, 36e'
6	Ph	Ph, CONH ₂	95	1:1	36f, 36f'
7	Me	Ph, Me	91	1:2	36g, 36g'
8	Me	1-naph, Me	90	1:3	36h, 36h'
9	Me	Ph, CONH ₂	98	1,5:1	36i, 36i'

[a] Yields corresponds to product mixtures purified by flash column chromatography.

[b] Diastereomeric excesses determined by ¹H NMR spectroscopy.

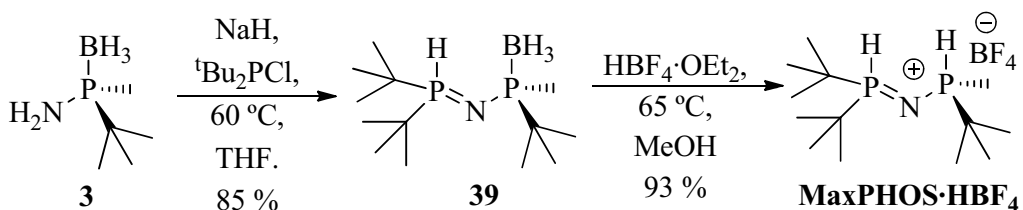
Skipping the methylation step and proceeding directly with reductive cleavage of the chiral secondary amino phosphine **36i** gave rise to the primary amino phosphine **3** in 72 % yield and also perfect enantioselectivity which then could be used as a chiral building block in the synthesis of the MaxPHOS ligand.

Scheme 2.23: Primary and secondary amino phosphine synthesis.



Reaction of optically pure amino phosphine **3** with ^tBu₂P₂Cl formed the bisphosphinamine **39**. This compound was serendipitously found to exist exclusively as its P-H tautomer which serves to protect the phosphine moiety from oxidation. Reacting bisphosphinamine **39** in the presence of tetrafluoroboric acid at 65 °C successfully removed the borane group and concurrently formed the phosphonium salt **MaxPHOS·HBF₄** which resulted to be an air-stable, crystalline solid.

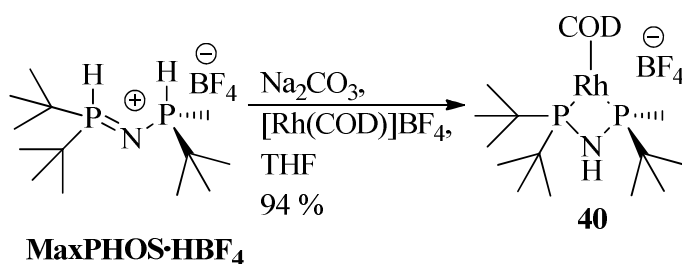
Scheme 2.24: The synthesis of MaxPHOS from the primary aminophosphine-borane.



2. Background

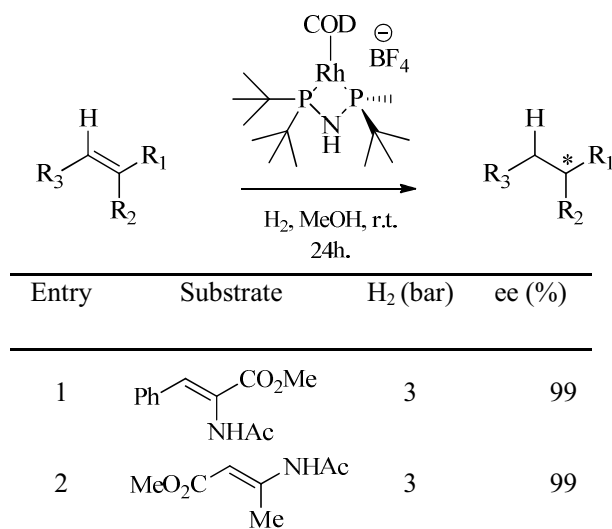
The phosphonium salt **MaxPHOS**·**HBF₄** was then reacted in the presence of the inorganic base **Na₂CO₃** and **[Rh(COD)₂]**BF₄** in THF to form the MaxPHOS-Rh complex. The complex is, in fact, a nitrogen containing analogue of the trichickenfootphos rhodium precatalyst, which already had been proven to be one of the most effective asymmetric hydrogenation catalysts ever invented. To test the efficacy of the analogue and the hypothesis that a bisphosphinoamine ligand coordinated to rhodium could be an effective hydrogenation pre-catalyst the complex was tested against olefinic substrates in asymmetric hydrogenation of 2 different olefins.**

Scheme 2.25: The synthesis of the MaxPHOS rhodium catalyst.



This preliminary study was very promising as the MaxPHOS rhodium complex had hydrogenated the chosen substrates with almost complete enantioselectivity. This had proved the hypothesis that aminodiphosphines could be successfully applied as ligands in asymmetric catalysis even though they had not been up until then and that *P*-stereogenic aminophosphines were indeed useful chiral building blocks.

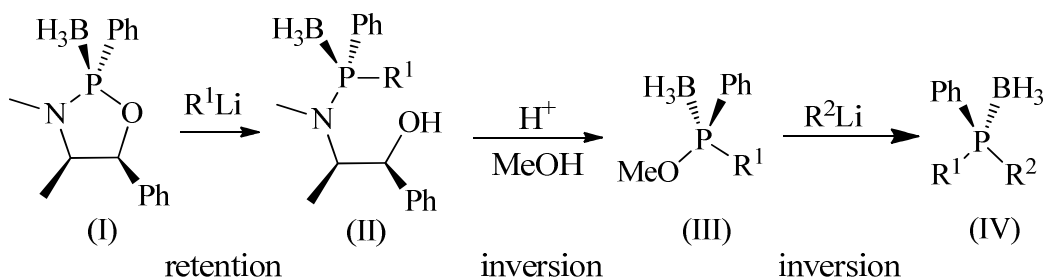
Table 2.2: Initial testing of MaxPHOS-Rh-COD as hydrogenation pre-catalyst.



2.5 The optimized route to MaxPHOS

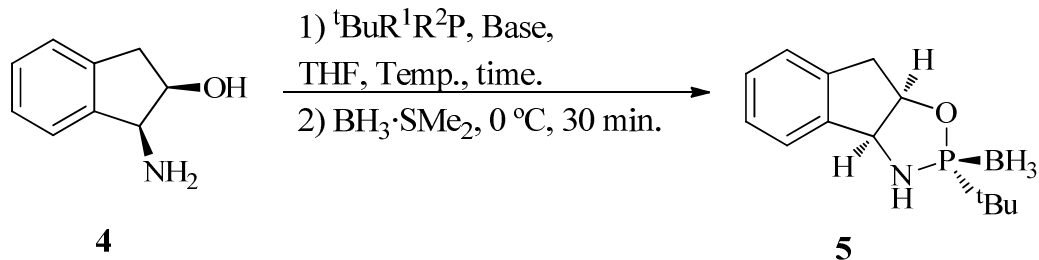
The synthetic path just outlined previously to arrive at enantiomerically pure MaxPHOS ligand was hindered by a dynamic kinetic resolution step which was only mildly diastereoselective. Because of this, a new more optimal preparation was developed to arrive at optically pure amino phosphines.⁵⁹ It was decided to turn to oxazaphospholidine chemistry in response, the brand of chemistry pioneered by Jugé *et al.* when he showed it was possible to condense bis(dialkylamino) phenylphosphine with (-)-ephedrine and subsequently ring open with alkyl lithium reagents in a very diastereomerically biased fashion as described earlier.⁶⁰

Scheme 2.26: The Jugé strategy to P-stereogenic tertiary phosphines.



Upon deciding which reagent to use to employ this strategy in the synthesis of MaxPHOS it was known it should be a β -amino alcohol where the amine moiety lies in a benzylic position. With this in mind *cis*-1-amino-2-indanol **4** was chosen to begin the study, as well as possessing the necessary features just described it was also commercially available in both enantiomers, in bulk quantity and it had also been previously reported in the literature having been used in the preparation of chiral sulfoxides and sulfinamides.⁶¹ Once the decision of which β -amino alcohol to use in the condensation reaction had been made, a screening was carried out to discover which *tert*-butyl phosphine reagent would be best to condense with the *cis*-1-amino-2-indanol **4**.

As seen in entry 4 of table 2.3 it was shown that racemic chloro-*tert*-butyl(diethylamino)-phosphine proved to be the most effective reagent with a high yield of 78 % and a very high diastereoselectivity of 18:1. The major diastereomer could be isolated in diastereomerically pure form after recrystallization. Crystals of the condensation product were obtained and X-ray analysis demonstrated that the bulky *tert*-butyl fragment was positioned *trans* to the indane fragment to avoid steric hindrance.

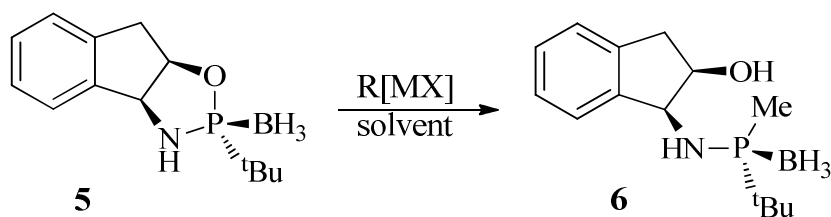
Table 2.3: Screening of *tert*-butyl phosphines for condensation reaction.

Entry	R ¹	R ²	Base	Temp (°C)	Time (h)	Yield (%) ^a	d.r.(R _p /S _p)
1	Cl	Cl	NEt ₃	r.t.	5	22	10:1
2	NEt ₂	NEt ₂	-	60	4	18	11:1
3	Cl	NEt ₂	-	r.t.	7	0	n.a.
4	Cl	NEt ₂	-	reflux	8	78	18:1

^a Yields correspond to a mixture of diastereomers. ^b Diastereomeric mixtures were determined by ³¹P NMR.

Having an efficient methodology in place to prepare the ring-closed condensation product, a screening of how best to form the ring-opened product was undertaken. Various organolithium and Grignard reagents were tested as well as some aluminium reagents with varying reaction conditions, those relative to the preparation of MaxPHOS are shown in table 2.4.

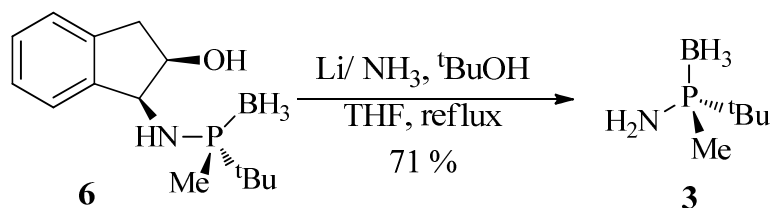
It was found that by reacting the oxazaphospholidine **5** with the Grignard reagent at 100 °C the ring-opened product was provided with outstanding yield and complete selectivity. A curiosity arose when X-ray analysis of the compound **6** confirmed that the phosphorus center had opposite configuration to that of the starting material **5**. The literature precedent up until this point had been that retention of stereo configuration in this process was expected.⁶² Jugé *et al.* had postulated that this expected stereochemical outcome was probably due to coordination of the organometallic reagent to the oxygen of the heterocyclic ring, forming a pentacoordinate phosphorus centre which eventually forces out the oxygen leaving group. In our group it was suggested that perhaps the presence of the secondary amine moiety affected this process.

Table 2.4: Screening of reagents and reaction conditions towards the ring-opened product.

Entry	R[MX]	Solvent	Temp. (°C)	Yield (%) ^a	d.r. ^b
1	MeLi	Et ₂ O	-78	0	n.a.
2	MeLi	THF	40	47	>96:4
3	MeLi	Toluene	40	76	>96:4
4	MeMgBr	Toluene	100	91	>99:1

^a Yield given as mixture of diastereoisomers. ^b Determined by ¹H NMR.

To test the hypothesis that the NH functional group affected the Grignard reagent attack, the *N*-methyl analogue of **6** was prepared and subjected to the same transformation. The organometallic reagents used were MeLi, MeMgBr, and AlMe₃ which had all worked to some extent at certain conditions in the previous case. It was observed that there was no reactivity in the case of the *N*-methyl analogue. So it was confirmed the NH group was essential for reactivity. It was also noted that to induce a ring opening of compound **5**, an excess of equal or greater to two equivalents of MeMgBr was necessary. This was interpreted as first the NH moiety was perhaps deprotonated forming an N⁻, and so it was thought the nitrogen anion coordinates to the second equivalent of Grignard reagent to direct its attack on the phosphorus center in order to bring about the ring opening. With compound **6** at hand it was subjected to the same reductive cleavage methodology as before with success.

Scheme 2.27: Solvated lithium in ammonia reductive cleavage.

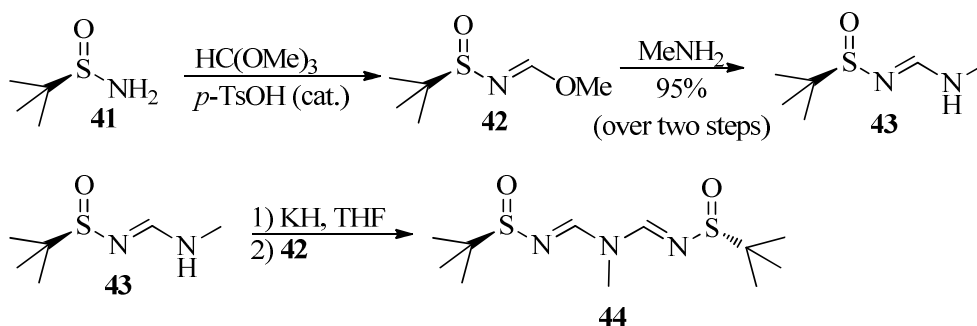
2. Background

Using this dissolved metal reduction procedure the amino phosphine **3**, key intermediate in the preparation of the MaxPHOS ligand was prepared in a 71 % yield with complete selectivity, 99 % ee as judged by chiral GC. This compound was then ready to be coupled to the di-*tert*-butylphosphine fragment and subsequently deprotected of the protecting borane group using tetrafluoroboric acid to form the phosphonium MaxPHOS salt as described before. Thus far this constitutes the optimized synthesis of the MaxPHOS ligand.

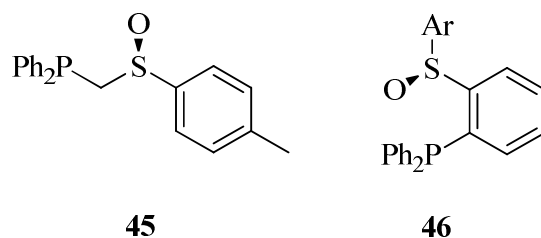
2.6 P,S ligands with chirality on sulphur

The synthesis of chiral sulphur compounds is convenient and facile, especially in comparison with stereogenic phosphorus containing compounds. Many chiral sulfoxides and sulfinamides are commercially available and in bulk quantity.⁶³ Often they are used as sacrificial chiral auxiliaries in a multitude of synthetic transformations.⁶⁴ However they had been rarely used in the building of chiral ligands; one noteworthy example was the siam **44** ligand which was used to confer stereoselectivity to the Lewis acid catalyzed asymmetric Diels-Alder reaction by copper.⁶⁵

Scheme 2.28: Synthesis of the Siam ligand from commercially available *tert*-butyl sulfinamide.

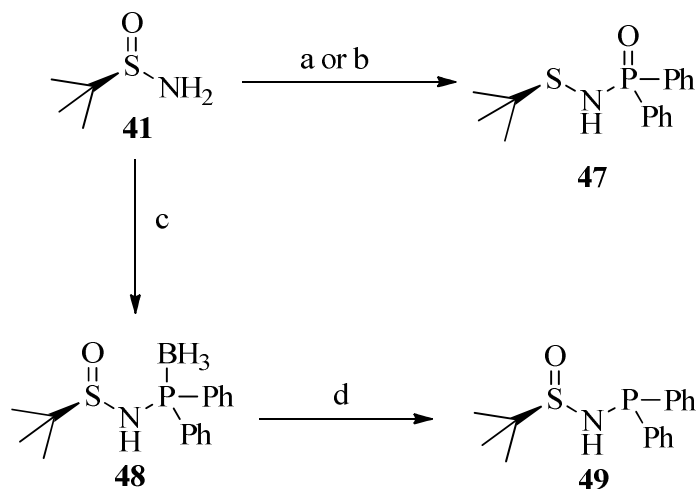


The poorer metal coordination capabilities of sulfoxides in comparison with phosphines, presents a real drawback towards the use of chiral sulphur ligands in efficient asymmetric transformations. However, by binding the chiral sulfoxide moiety to a phosphine moiety one obtains a ligand where the phosphine fragment provides strong ligand to catalyst coordination while the sulfoxide group supplies a source of chiral information.

Figure 2.7: P, S=O ligands.

Ligands **45** and **46** appeared in the literature previously but both were structurally unstable as they underwent sulphur to phosphorus, oxygen migration.⁶⁶ In our group a family of *N*-phosphino sulfinamide chiral ligands were assembled which were structurally stable towards oxygen migration. These ligands were successfully applied to the asymmetric intermolecular Pauson-Khand reaction and were dubbed “PNSO” ligands.⁶⁷

Scheme 2.29: The circumvention of the inhibitory sulphur to phosphorus, oxygen migration.



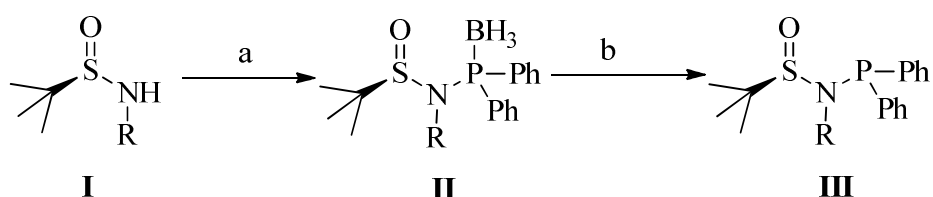
a) Ph_2PCl , NEt_3 , THF, 99%. b) *n*-BuLi, Et_2O , -78°C , then Ph_2PCl , reflux; c) *n*-BuLi, THF, -78°C , Ph_2PCl , $\text{BH}_3\cdot\text{SMe}_2$ at -30°C , 66 %. d) DABCO, toluene, r.t., 83 %.

The coupling reaction of the *tert*-butyl sulfinamide with a chlorophosphine at first also gave sulphur to phosphorus migration to yield compound **47** as shown in scheme 2.29 however, quenching with $\text{BH}_3\cdot\text{SMe}_2$ closely after the phosphine coupling step gave rise to the stable BH_3 protected *N*-phosphino ligand **48**. The BH_3 group was then removed by the base 1,4-

2. Background

diazabicyclo octane (DABCO) which gave the “free” ligand **49** which was stable towards the oxygen migration process which jeopardized the stability of those similar ligands previously in the past. This methodology was used to build a set of ligands using the *tert*-butyl sulfinamide as a chiral building block. The stereochemical purity of this family of PNSO ligands was examined by HPLC and pleasantly it was found no racemization had taken place and the ligands were indeed enantiomerically pure.

Table 2.5: The synthesis of a family of chiral PNSO ligands.



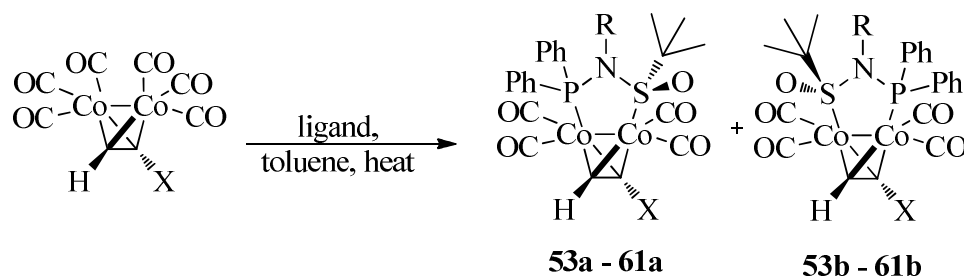
Entry	R	Yield of II	Yield of III	Ligand
1	H	66	83	49
2	CH ₃	83	96	50
3	Bn	86	95	7
4	<i>p</i> -F-C ₆ H ₄ CH ₂	88	88	51
5	<i>p</i> -MeO-C ₆ H ₄ CH ₂	81	90	52

a) *n*-BuLi, THF, -78 °C, Ph₂PCl, BH₃·SMe₂ at -30 °C. b) DABCO, toluene, r.t. c) Yields of isolated product after flash column chromatography.

In our group there is much experience working with P,S ligands applied to the intermolecular Pauson-Khand reaction.⁶⁸ For this reason the coordination behaviour towards dicobalt-alkyne complexes of these PNSO ligands were first investigated. It was found they readily bind through phosphorus and sulphur to the cobalt cluster forming a bridged complex upon heating of the ligand with dicobalthexacarbonyl complex in toluene at 65-70 °C. They were found to form diastereomeric mixtures with diastereomeric ratios of as high as >20:1 in one case. It was observed that the benzylic group residing on nitrogen was an important influencing factor for the formation of biased diastereomeric mixtures as the conformation it takes up conveys well the chiral information into the complexation process. The complexes

formed were highly crystalline, facilitating the purification and separation of diastereomers by recrystallization.

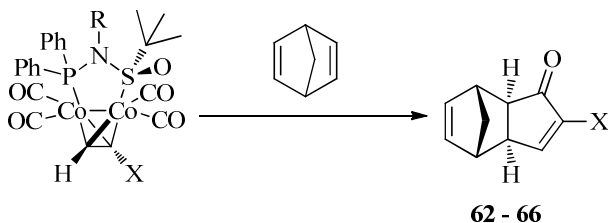
Table 2.6: Coordination of PNSO ligand to terminal alkyne dicobalt complexes.



Entry	X	L	R	Conditions	Yield [%] ^a	d.r. ^b	Complex
1	C(CH ₃) ₂ OH	49	H	70 °C, 10 h	20 ^c	1:1	53a/53b
2	C(CH ₃) ₂ OH	50	Me	65 °C, 16 h	92	1.5:1	54a/54b
3	C(CH ₃) ₂ OH	7	Bn	65 °C, 16 h	95	7:1	55a/55b
4	TMS	7	Bn	70 °C, 16 h	78	12:1	56a/56b
5	Ph	7	Bn	65 °C, 5 h	81	8:1	57a/57b
6	CH ₂ OTBDPS	7	Bn	65 °C, 6 h	85	10:1	58a/58b
7	CH ₂ OH	7	Bn	65 °C, 5h	50	>20:1	59a/59b
8	TMS	51	<i>p</i> -F-C ₆ H ₄ CH ₂	65 °C, 40 h	99	10:1	60a/60b
9	TMS	52	<i>p</i> -MeO-C ₆ H ₄ CH ₂	65 °C, 24h	75	12:1	61a/61b

a) Diastereomeric mixture, yield isolated product after purification by flash column chromatography. b) Diastereomeric ratio determined by ¹H NMR analysis. c) Yield estimated by ¹H NMR analysis of resulting mixture.

The ligand-cobalt-alkyne complexes once isolated to enantiopure form from their diastereomeric mixtures *via* crystallization were applied in the intermolecular Pauson-Khand reaction with norbornadiene. In general yields were excellent and enantiomeric excesses of the Pauson-Khand adduct obtained were unprecedented. These adducts undergo a retro Diels-Alder reaction to form substituted cyclopentenones which can serve as very interesting natural product building blocks.

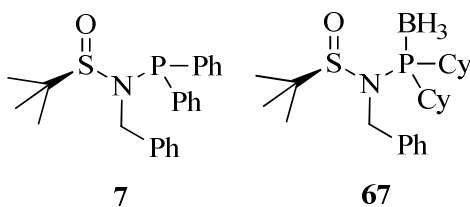
Table 2.7: PNSO cobalt complexes applied in the intermolecular Pauson-Khand with norbornadiene.

Entry	Complex	R	X	Conditions ^a	Yield [%] ^b	ee [%] ^c	Product
1	55a	Bn	C(CH ₃) ₂ OH	A, 1 h	95	92	62
2	55a	Bn	C(CH ₃) ₂ OH	B, 16 h	87	93	62
3	56a	Bn	TMS	B, 16 h	99	97	63
4	57a	Bn	Ph	C, 4h	99	99	64
5	58a	Bn	CH ₂ OTBDPS	C, 5h	99	92	65
6	59a/59b^d	Bn	CH ₂ OH	B, 16 h	65	73	66
7	61	<i>p</i> -MeO-C ₆ H ₄ CH ₂	TMS	B, 40 h	99	>99	63
8	60a	<i>p</i> -F-C ₆ H ₄ CH ₂	TMS	B, 48h	99	78	63

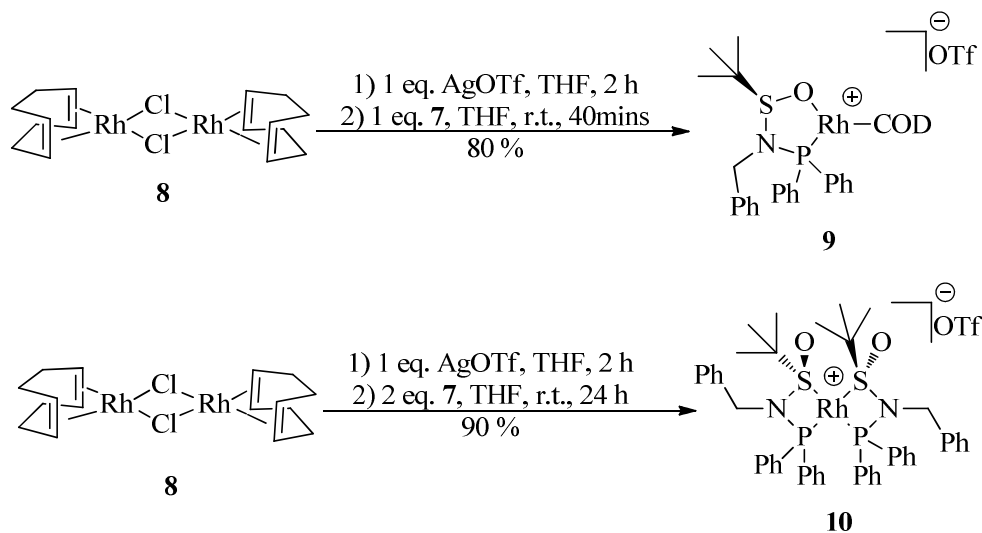
a) A: Toluene, 70 °C; B: 6 equiv. *N*-methylmorpholine *N*-oxide, CH₂Cl₂, r.t.; C: toluene, r.t. b) Yield of isolated product after flash column chromatography. c) Enantiomeric excess determined by either chiral HPLC or GC. d) > 20:1 (¹H NMR) Diastereomeric mixture of isomers was used.

These ligands constituted the first examples of a chiral sulfur atom coordinating to cobalt. Taking advantage of the phosphorous' coordinative strengths and the chirality supplied by the chiral *tert*-butylsulfonamide they provided excellent enantioselectivities in an asymmetric transformation. The short synthetic pathway of the PNSO ligands made them a very attractive prospect for perhaps opening the scope of their application in asymmetric catalysis.

Later our group reported on the coordination behavior of the PNSO ligand **7** and also the related ligand **67** to monometallic systems, initially Rh(I) but later extending to Ir(I), Cu(I), Pd(II) and Pt(II).⁶⁹

Figure 2.8: The *N*-benzyl PNSO ligands whose coordination to rhodium was investigated.

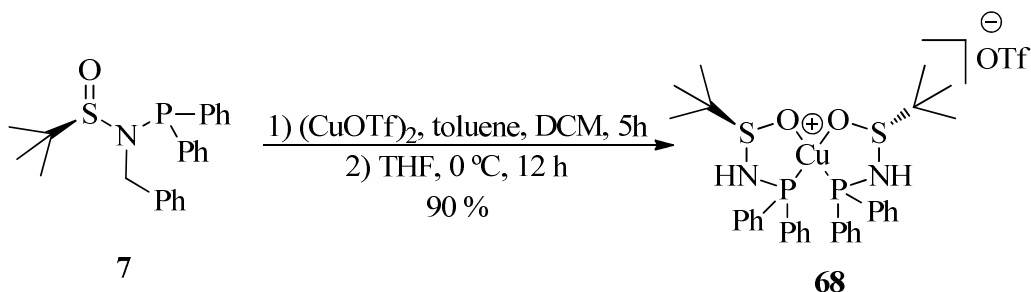
Depending on the equivalents of ligand added with respect to metal and time reacted, complexations of ligands to metal could give rise to complexes monomeric of ligand or dimeric of ligand. Also the nature of the metal seemed to influence the coordination mode of the ligand as PNSO ligands can coordinate to the metal *via* oxygen or sulphur as well as phosphorus. When **7** was reacted with a Rh(I) using $[\text{Rh}(\text{COD})_2\text{Cl}_2]$ and AgOTf as the source of rhodium, over a short space of time it formed a complex monomeric of ligand to metal, with oxygen to metal coordination closing the chelate. When the time allowed to react was increased to overnight for example, a complex dimeric of ligand to metal atom would present itself however the coordination mode would change, presenting sulphur to metal coordination.

Scheme 2.30: PNSO-Rh complexes.

2. Background

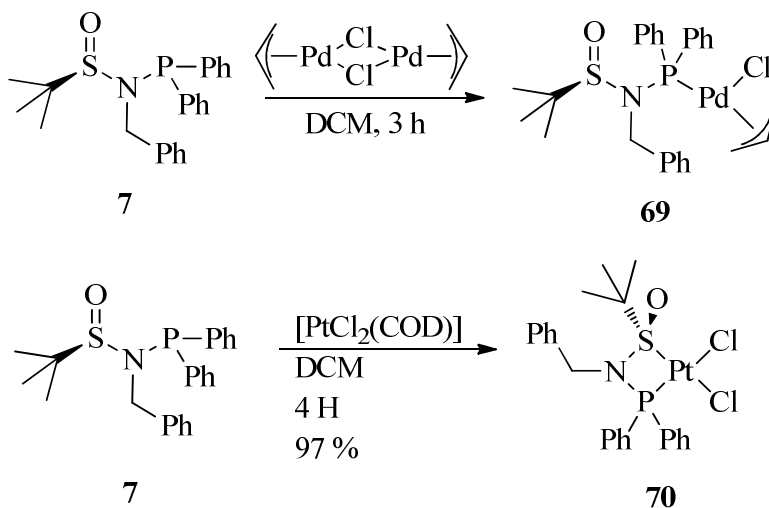
The same ligand behaved almost identically when complexed to iridium. When complexation of **7** to copper was attempted using $(\text{CuOTf})_2$ a complex dimeric of ligand to metal was obtained but consisting of oxygen to copper coordination.

Scheme 2.31: PNSO-Cu complex.



Also observed were complexes of **7** coordinating to Pd(II) by reacting the ligand with $[(\eta^3\text{-allyl})\text{PdCl}]_2$ in the presence NH_4PF_6 , in this instance a lack of sulfoxide coordination was discovered as the ligand was bound to the palladium metal solely through phosphorus. The ligand was found to complex also to Pt(II) forming a dichloride species when reacted with $\text{PtCl}_2(\text{COD})$ or $\text{PtCl}_2(\text{CH}_3\text{CN})$. Overall, it was shown that the coordination behaviour of PNSO ligands to various metals is diverse and rich.

Scheme 2.32: Palladium and platinum PNSO complexes.



-
- ¹ Pasteur, L. *C R Seances Acad Sci*, **1848**,26, 538–538.
- ² a) Fischer, E.;Passmore, F. *Ber. Dtsch. Chem. Ges.* **1889**, 22, 2728–2736. b) Fischer, E. *Ber. Dtsch. Chem. Ges.* **1890**, 23, 2611–2624.
- ³ Meisenheimer, J.; Lichtenstadt, L. *Ber. Dtsch. Chem. Ges.* **1911**, 44, 356.
- ⁴ Meisenheimer, J.; Casper, J.; Horing, M.; Lauter, W.; Lichtenstadt, L.; Samuel, W. *Liebigs Ann.* **1926**, 449, 213
- ⁵ Davies, W. C.; Mann, F. C. *J. Chem. Soc.* **1944**, 276.
- ⁶ Kumli, K. F.; McEwen, W. E.; Vanderwerf, C. A. *J. Am. Chem. Soc.* **1959**, 81, 248.
- ⁷ a) Horner, L.; Winkler, H.; Rapp, A.; Mentrup, A.; Hoffmann, H.; Beck, P. *Tetrahedron Lett.* **1961**, 2, 161. b) Horner, L. *Pure Appl. Chem.*, **1964**, 9, 225. c) Horner, L.; Schedlbauer, F.; Beck, P. *Tetrahedron Lett.* **1964**, 5, 1421. c) Horner, L.; Winkler, H. *Tetrahedron Lett.* **1964**, 5, 175. d) Horner, L.; Balzer, W.D. *Tetrahedron Lett.* **1965**, 6, 1157. f) Horner, L.; Balzer, W.D.; Peterson, D.J. *Tetrahedron Lett.* **1966**, 7, 3315.
- ⁸ a) Korpiun, O.; Lewis, R. A.; Chickos, J.; Mislow, K. *J. Am. Chem. Soc.* **1968**, 90, 4842. b) Lewis, R. A.; Korpiun, O.; Mislow, K. *J. Am. Chem. Soc.* **1968**, 90, 4847.
- ⁹ a) Young, J. F.; Osborn, J. A.; Jardine, F. H.; Wilkinso.G *Chem. Commun.* **1965**, 131. b) Osborn, J. A.; Jardine, F. H.; Young, J. F.; Wilkinso.G *J. Chem. Soc. A* **1966**, 1711.
- ¹⁰ Horner, L.; Siegel, H.; Buthe, H. *Angew. Chem., Int. Ed.* **1968**, 7, 942.
- ¹¹ Knowles, W. S.; Sabacky, M. J. *Chem. Commun.* **1968**, 1445.
- ¹² Knowles, W. S. *Adv. Synth. Catal.* **2003**, 345, 3.
- ¹³ Knowles, W. S.; Vineyard, B. D.; Sabacky, M. J. *J. Chem. Soc., Chem. Commun.* **1972**, 10.
- ¹⁴ Knowles, W. S.; Sabacky, M. J.; Vineyard, B. D.; Weinkauff, D. J. *J. Am. Chem. Soc.* **1975**, 97, 2567.
- ¹⁵ a) Dang, T. P.; Kagan, H. B. *Journal of the Chemical Society D-Chemical Communications* **1971**, 481. b) Kagan, H. B.; Dang, T. P. *J. Am. Chem. Soc.* **1972**, 94, 6429.
- ¹⁶ a) Miyashita, A.; Yasuda, A.; Takaya, H.; Toriumi, K.; Ito, T.; Souchi, T.; Noyori, R. *J. Am. Chem. Soc.* **1980**, 102, 7932. b) Noyori, R. *Adv. Synth. Catal.* **2003**, 345, 15.
- ¹⁷ Askin, D. *Curr. Opin. Drug Discovery Dev.* **1998**, 1, 338.
- ¹⁸ a) Burk, M. J.; Calabrese, J. C.; Davidson, F.; Harlow, R. L.; Roe, D. C. *J. Am. Chem. Soc.* **1991**, 113, 2209. b) Burk, M. J.; Feaster, J. E.; Nugent, W. A.; Harlow, R. L. *J. Am. Chem. Soc.* **1993**, 115, 10125. c) Burk, M. J.; Bienewald, F.; Challenger, S.; Derrick, A.; Ramsden, J. A. *J. Org. Chem.* **1999**, 64, 3290.
- ¹⁹ a) Noyori, R. *Science* **1990**, 248, 1194. b) Kitamura, M.; Hsiao, Y.; Ohta, M.; Tsukamoto, M.; Ohta, T.; Takaya, H.; Noyori, R. *J. Org. Chem.* **1994**, 59, 297. c) Noyori, R.; Takaya, H. *Acc. Chem. Res.* **1990**, 23, 345.
- ²⁰ Doi, T.; Kokubo, M.; Yamamoto, K.; Takahashi, T. *J. Org. Chem.* **1998**, 63, 428.
- ²¹ Imamoto, T.; Watanabe, J.; Wada, Y.; Masuda, H.; Yamada, H.; Tsuruta, H.; Matsukawa, S.; Yamaguchi, K. *J. Am. Chem. Soc.* **1998**, 120, 1635.
- ²² Hoge, G.; Wu, H. P.; Kissel, W. S.; Pflum, D. A.; Greene, D. J.; Bao, J. *J. Am. Chem. Soc.* **2004**, 126, 5966.
- ²³ Young, J.F.; Osborn, F. H.; Jardine, F. H.; Wilkinson, G. *Chem. Comm. (London)*, **1965**, 131.

2. Background

-
- ²⁴ Halpern, J.; Riley, D. P.; Chan, A. S. C.; Pluth, J. J. *J. Am. Chem. Soc.* **1977**, *99*, 8055
- ²⁵ a) Brown, J. M.; Chaloner, P. A. *Tetrahedron Lett.* **1978**, 1877. b) Slack, D. A.; Greveling, I.; Baird, M. C. *Inorg. Chem.* **1979**, *18*, 3125. c) Chan, A. S. C.; Pluth, J. J.; Halpern, J. *J. Am. Chem. Soc.* **1980**, *102*, 5952. d) Brown, J. M.; Chaloner, P. A. *J. Am. Chem. Soc.* **1980**, *102*, 3040. e) Ojima, I.; Kogure, T.; Yoda, N. *J. Org. Chem.* **1980**, *45*, 4728. f) Miyashita, A.; Takaya, H.; Souchi, T.; Noyori, R. *Tetrahedron* **1984**, *40*, 1245. g) Allen, D. G.; Wild, S. B.; Wood, D. L. *Organometallics* **1986**, *5*, 1009.
- ²⁶ a) Brown, J. M.; Chaloner, P. A. *Tetrahedron Lett.* **1978**, 1877. b) Chan, A. S. C.; Halpern, J. *J. Am. Chem. Soc.* **1980**, *102*, 838. c) Chan, A. S. C.; Pluth, J. J.; Halpern, J. *Inorg. Chim. Acta* **1979**, *37*, L477. d) Brown, J. M.; Parker, D. *J. Org. Chem.* **1982**, *47*, 2722. e) Giovannetti, J. S.; Kelly, C. M.; Landis, C. R. *J. Am. Chem. Soc.* **1993**, *115*, 4040. f) Bender, B. R.; Koller, M.; Nanz, D.; Vonphilipsborn, W. *J. Am. Chem. Soc.* **1993**, *115*, 5889.
- ²⁷ a) Brown, J. M.; Chaloner, P. A.; Morris, G. A. *J. Chem. Soc., Chem. Commun.* **1983**, 664. b) Brown, J. M.; Chaloner, P. A.; Morris, G. A. *J. Chem. Soc., Perkin Trans. 2* **1987**, 1583. c) Landis, C. R.; Halpern, J. *J. Am. Chem. Soc.* **1987**, *109*, 1746. d) Bircher, H.; Bender, B. R.; Vonphilipsborn, W. *Magn. Reson. Chem.* **1993**, *31*, 293. e) Kadyrov, R.; Freier, T.; Heller, D.; Michalik, M.; Selke, R. *J. Chem. Soc., Chem. Commun.* **1995**, 1745.
- ²⁸ Chua, P. S.; Roberts, N. K.; Bosnich, B.; Okrasinski, S. J.; Halpern, J. *J. Chem. Soc., Chem. Commun.* **1981**, 1278.
- ²⁹ Brown, J. M.; Parker, D. *J. Chem. Soc., Chem. Commun.* **1980**, 342.
- ³⁰ Landis, C. R.; Halpern, J. *J. Am. Chem. Soc.* **1987**, *109*, 1746.
- ³¹ Halpern, J. *Science* **1982**, *217*, 401.
- ³² Gridnev, I. D.; Imamoto, T. *Acc. Chem. Res.* **2004**, *37*, 633.
- ³³ Gridnev, I. D.; Higashi, N.; Imamoto, T. *Organometallics* **2001**, *20*, 4542.
- ³⁴ Gridnev, I. D.; Yamanoi, Y.; Higashi, N.; Tsuruta, H.; Yasutake, M.; Imamoto, T. *Adv. Synth. Catal.* **2001**, *343*, 118.
- ³⁵ a) Gridnev, I. D.; Higashi, N.; Imamoto, T. *J. Am. Chem. Soc.* **2000**, *122*, 10486. b) Gridnev, I. D.; Yasutake, M.; Higashi, N.; Imamoto, T. *J. Am. Chem. Soc.* **2001**, *123*, 5268.
- ³⁶ Yasutake, M.; Gridnev, I. D.; Higashi, N.; Imamoto, T. *Org. Lett.* **2001**, *3*, 1701.
- ³⁷ Gridnev, I. D.; Imamoto, T. *Chem. Commun.* **2009**, 7447.
- ³⁸ Gridnev, I. D.; Imamoto, T.; Hoge, G.; Kouchi, M.; Takahashi, H. *J. Am. Chem. Soc.* **2008**, *130*, 2560.
- ³⁹ a) Horner, L.; Simons, G. *Phosphorus, Sulfur Silicon Relat. Elem.* **1984**, *19*, 65. b) Yamamoto, K.; Tomita, A.; Tsuji, J. *Chem. Lett.* **1978**, 3.
- ⁴⁰ a) Takaya, H.; Akutagawa, S.; Noyori, R. *Org. Synth.* **1989**, *67*, 20. b) Toda, F.; Mori, K.; Stein, Z.; Goldberg, I. *J. Org. Chem.* **1988**, *53*, 308.
- ⁴¹ Imamoto, T.; Crepy, K. V. L.; Katagiri, K. *Tetrahedron-Asymmetry* **2004**, *15*, 2213.
- ⁴² a) Otsuka, S.; Nakamura, A.; Kano, T.; Tani, K. *J. Am. Chem. Soc.* **1971**, *93*, 4301. b) Tani, K.; Brown, L. D.; Ahmed, J.; Ibers, J. A.; Yokota, M.; Nakamura, A.; Otsuka, S. *J. Am. Chem. Soc.* **1977**, *99*, 7876.
- ⁴³ Nudelman, A.; Cram, D. J. *J. Am. Chem. Soc.* **1968**, *90*, 3869.

-
- ⁴⁴ a) Korpiun, O.; Mislow, K. *J. Am. Chem. Soc.* **1967**, *89*, 4784. b) Korpiun, O.; Lewis, R. A.; Chickos, J.; Mislow, K. *J. Am. Chem. Soc.* **1968**, *90*, 4842.
- ⁴⁵ Vineyard, B. D.; Knowles, W. S.; Sabacky, M. J.; Bachman, G. L.; Weinkauff, D. J. *J. Am. Chem. Soc.* **1977**, *99*, 5946.
- ⁴⁶ Imamoto, T.; Oshiki, T.; Onozawa, T.; Kusumoto, T.; Sato, K. *J. Am. Chem. Soc.* **1990**, *112*, 5244.
- ⁴⁷ Juge, S.; Stephan, M.; Laffitte, J. A.; Genet, J. P. *Tetrahedron Lett.* **1990**, *31*, 6357.
- ⁴⁸ a) Maienza, F.; Spindler, F.; Thommen, M.; Pugin, B.; Malan, C.; Mezzetti, A. *J. Org. Chem.* **2002**, *67*, 5239. b) Nettekoven, U.; Kamer, P. C. J.; Widhalm, M.; van Leeuwen, P. *Organometallics* **2000**, *19*, 4596.
- ⁴⁹ Juge, S.; Stephan, M.; Merdes, R.; Genet, J. P.; Halutdesportes, S. *J. Chem. Soc., Chem. Commun.* **1993**, 531.
- ⁵⁰ a) Nettekoven, U.; Kamer, P. C. J.; van Leeuwen, P.; Widhalm, M.; Spek, A. L.; Lutz, M. *J. Org. Chem.* **1999**, *64*, 3996. b) Kaloun, E. B.; Merdes, R.; Genet, J. P.; Uziel, J.; Juge, S. *J. Organomet. Chem.* **1997**, *529*, 455.
- ⁵¹ Maienza, F.; Spindler, F.; Thommen, M.; Pugin, B.; Malan, C.; Mezzetti, A. *J. Org. Chem.* **2002**, *67*, 5239.
- ⁵² Rippert, A. J.; Linden, A.; Hansen, H. J. *Helv. Chim. Acta* **2000**, *83*, 311.
- ⁵³ a) Moulin, D.; Darcel, C.; Juge, S. *Tetrahedron-Asymmetry* **1999**, *10*, 4729. b) Moulin, D.; Bago, S.; Bauduin, C.; Darcel, C.; Juge, S. *Tetrahedron-Asymmetry* **2000**, *11*, 3939. c) Humbel, S.; Bertrand, C.; Darcel, C.; Bauduin, C.; Juge, S. *Inorg. Chem.* **2003**, *42*, 420. d) Bauduin, C.; Moulin, D.; Kaloun, E. B.; Darcel, C.; Juge, S. *J. Org. Chem.* **2003**, *68*, 4293.
- ⁵⁴ Korpiun, O.; Lewis, R. A.; Chickos, J.; Mislow, K. *J. Am. Chem. Soc.* **1968**, *90*, 4842.
- ⁵⁵ Muci, A. R.; Campos, K. R.; Evans, D. A. *J. Am. Chem. Soc.* **1995**, *117*, 9075.
- ⁵⁶ a) Ohashi, A.; Kikuchi, S.; Yasutake, M.; Imamoto, T. *Eur. J. Org. Chem.* **2002**, 2535. b) Ohashi, A.; Imamoto, T. *Tetrahedron Lett.* **2001**, *42*, 1099. c) Imamoto, T.; Sugita, K.; Yoshida, K. *J. Am. Chem. Soc.* **2005**, *127*, 11934.
- ⁵⁷ Kolodiaznyhny, O. I.; Gryshkun, E. V.; Andrushko, N. V.; Freytag, M.; Jones, P. G.; Schmutzler, R. *Tetrahedron-Asymmetry* **2003**, *14*, 181.
- ⁵⁸ Revés, M.; Ferrer, C.; León, T.; Doran, S.; Etayo, P.; Vidal-Ferran, A.; Riera, A.; Verdaguer, X. *Angew. Chem. Int. Ed.* **2011**, *50*, 8776.
- ⁵⁹ Leon, T.; Riera, A.; Verdaguer, X. *J. Am. Chem. Soc.* **2011**, *133*, 5740.
- ⁶⁰ a) Juge, S.; Genet, J. P. *Tetrahedron Lett.* **1989**, *30*, 2783. b) Kaloun, E. B.; Merdes, R.; Genet, J. P.; Uziel, J.; Juge, S. *J. Organomet. Chem.* **1997**, *529*, 455. c) Bauduin, C.; Moulin, D.; Kaloun, E. B.; Darcel, C.; Juge, S. *J. Org. Chem.* **2003**, *68*, 4293.
- ⁶¹ a) Han, Z. X.; Krishnamurthy, D.; Grover, P.; Fang, Q. K.; Senanayake, C. H. *J. Am. Chem. Soc.* **2002**, *124*, 7880. b) Han, Z. X.; Krishnamurthy, D.; Grover, P.; Wilkinson, H. S.; Fang, Q. K.; Su, X. P.; Lu, Z. H.; Magiera, D.; Senanayake, C. H. *Angew. Chem., Int. Ed.* **2003**, *42*, 2032.
- ⁶² a) Juge, S.; Genet, J. P. *Tetrahedron Lett.* **1989**, *30*, 2783. b) Kaloun, E. B.; Merdes, R.; Genet, J. P.; Uziel, J.; Juge, S. *J. Organomet. Chem.* **1997**, *529*, 455. c) Bauduin, C.; Moulin, D.; Kaloun, E. B.; Darcel, C.; Juge, S. *J. Org. Chem.* **2003**, *68*, 4293. d) Leyris, A.; Nuel, D.; Giordano, L.; Achard, M.; Buono, G. *Tetrahedron Lett.* **2005**, *46*, 8677. e) den Heeten, R.; Swennenhuis, B. H. G.; van Leeuwen, P. W. N. M.; de Vries, J. G.;

2. Background

Kamer, P. C. J. *Angew. Chem., Int. Ed.* **2008**, *47*, 6602. f) Zupancic, B.; Mohar, B.; Stephan, M. *Org. Lett.* **2010**, *12*, 3022.

⁶³ Fernandez, I.; Khair, N. *Chem. Rev.* **2003**, *103*, 3651.

⁶⁴ Ellman, J. A. *Pure Appl. Chem.* **2003**, *75*, 39.

⁶⁵ Owens, T. D.; Hollander, F. J.; Oliver, A. G.; Ellman, J. A. *J. Am. Chem. Soc.* **2001**, *123*, 1539.

⁶⁶ a) Alcock, N. W.; Brown, J. M.; Evans, P. L. *J. Organomet. Chem.* **1988**, *356*, 233. b) Hiroi, K.; Suzuki, Y.; Kawagishi, R. *Tetrahedron Lett.* **1999**, *40*, 715.

⁶⁷ a) Sola, J.; Reves, M.; Riera, A.; Verdaguer, X. *Angew. Chem., Int. Ed.* **2007**, *46*, 5020. b) Reves, M.; Achard, T.; Sola, J.; Riera, A.; Verdaguer, X. *J. Org. Chem.* **2008**, *73*, 7080. c) Ji, Y.; Riera, A.; Verdaguer, X. *Org. Lett.* **2009**, *11*, 4346.

⁶⁸ a) Verdaguer, X.; Moyano, A.; Pericas, M. A.; Riera, A.; Maestro, M. A.; Mahia, J. *J. Am. Chem. Soc.* **2000**, *122*, 10242. b) Verdaguer, X.; Lledo, A.; Lopez-Mosquera, C.; Maestro, M. A.; Pericas, M. A.; Riera, A. *J. Org. Chem.* **2004**, *69*, 8053. c) Verdaguer, X.; Pericas, M. A.; Riera, A.; Maestro, M. A.; Mahia, J. *Organometallics* **2003**, *22*, 1868.

⁶⁹ Achard, T.; Benet-Buchholz, J.; Riera, A.; Verdaguer, X. *Organometallics* **2009**, *28*, 480. b) Achard, T.; Benet-Buchholz, J.; Escudero-Adan, E. C.; Riera, A.; Verdaguer, X. *Organometallics* **2011**, *30*, 3119.

***N*-Phosphino Sulfinamide**

3

ligands

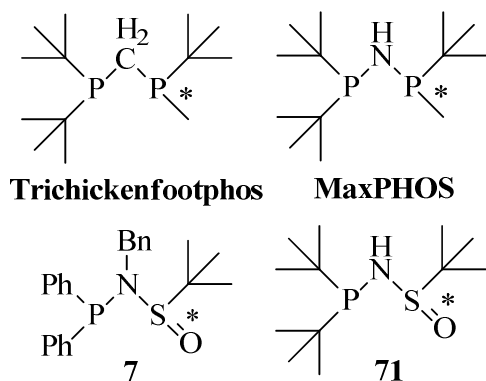
3.1	The <i>tert</i>-butyl and <i>p</i>-tolyl sulfinamide derived ligands	57
3.1.1	The synthesis and examination of the ligands and their complexes	58
3.1.2	Hydrogenations of <i>Z</i> -MAC catalysed by the PNSO-Rh complexes	63
3.2	Attempts towards the synthesis of PNSO analogues	66
3.2.1	The <i>N</i> -methyl PNSO ligand	67
3.2.2	The PNNSO ligand	69
3.2.3	The attempt to introduce a carbon atom into the PNSO scaffold	74
3.3	Conclusions	77

3 *N*-Phosphino Sulfinamide ligands

3.1 The *tert*-butyl and *p*-tolyl sulfinamide derived ligands:

As stressed repeatedly thus far chiral bi-dentate ligands have become highly relevant in the field of asymmetric catalysis. These compounds not only increase reactivity but more importantly, they induce the high enantioselectivities currently demanded by the pharmaceutical industry.¹ One approach of effectively transferring chirality from ligand to the relevant asymmetric transformations involved is to move the chiral information of the ligand as close as possible to the catalysing metal center. This can be achieved by conferring chirality to the metal-coordinating atom. Despite the great efficiency of the P-stereogenic diphosphine set of ligands, their synthesis remains generally somewhat laborious. The synthesis of the TCFP ligand was uncomplicated but not without drawbacks as it involves a racemic procedure followed by separation of enantiomers by chiral preparative HPLC, which could be considered disadvantageous on a larger scale. There have been other preparations of TCFP relying on asymmetric synthesis.² In this respect, here we addressed the preparation of other cost-effective 3-hindered quadrant ligands that can be readily assembled from commercially available materials.

Figure 3.1: Structural similarity between C_1 symmetric P-stereogenic phosphines and PNSO ligands.



We previously showed that the PNSO family of ligands, those containing a sulfinamide moiety bound to a phosphine group through the nitrogen atom where chirality resides on sulphur, can be highly efficient when applied to the intermolecular asymmetric Pauson-

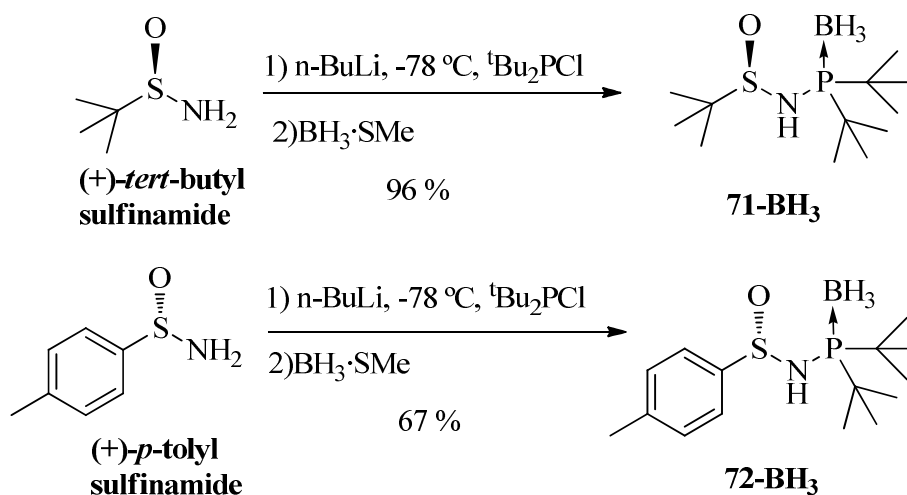
3. *N*-Phosphino sulfinamide ligands

Khand reaction.³ These ligands can be obtained in a very straightforward manner, often involving a one-step, one-pot synthesis using chiral sulfinamides that are commercially available in large amounts.⁴ Also, we demonstrated that ligands such as **7** and similar analogues coordinate readily to rhodium and other metals to give either P,O or P,S bidentate coordination.⁵ The positive results with these ligands in the Pauson-Khand reaction led us to test their efficacy in rhodium-catalyzed asymmetric hydrogenation of dehydroamino acids. We were willing to test whether the *N*-di-*tert*-butylphosphino-*tert*-butylsulfinamide ligand (PNSO) (**71**) could be another example of the 3-hindered quadrant chiral ligand template, such as the TCFP and MaxPHOS ligands.⁶

3.1.1 The synthesis and examination of the ligands and their complexes

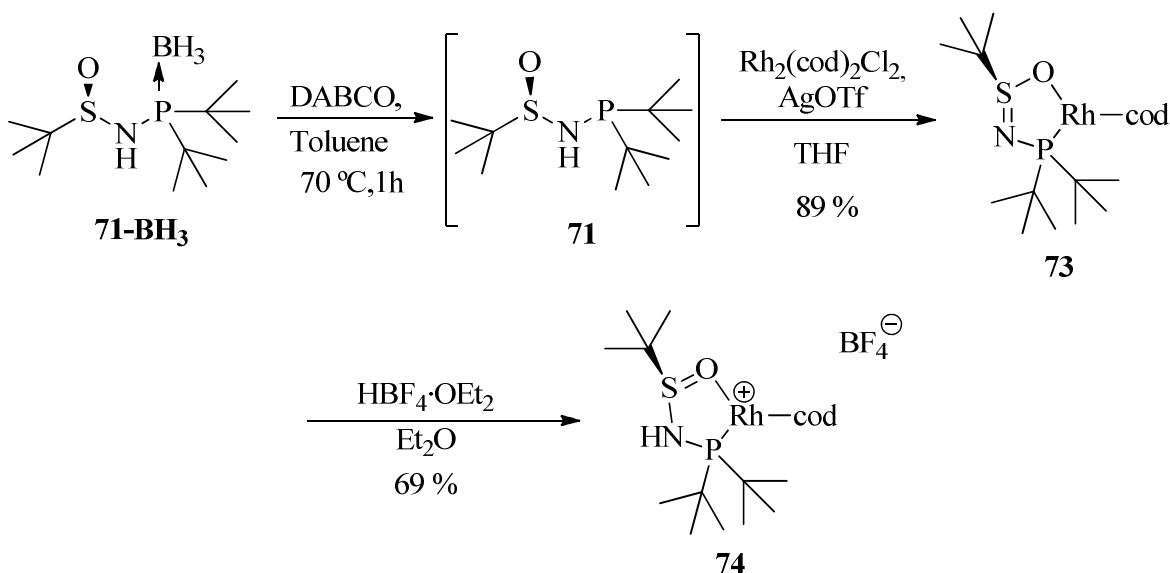
The boron-protected chiral PNSO ligand **71** was synthesized from the commercially available (+)-*tert*-butylsulfinamide in a one-pot reaction (Scheme 3.1). The anion of the sulfinamide was formed at low temperature with *n*-BuLi. Addition of the ^tBu₂PCl electrophile, which was allowed to react to completion at room temperature after warming up from -78 °C, led to total consumption of the sulfinamide starting material (easily monitored by TLC). Finally, the phosphine was protected with borane by addition of the BH₃·SMe₂ complex. Borane-protected **71** was isolated in an excellent 96 % yield after flash chromatography on SiO₂. The analogue **72-BH₃** was synthesized in exactly the same manner from the commercially available dextrorotatory *p*-tolylsulfinamide. The ligands were not isolated in their borane-free form due to expected oxidation of the phosphine.

Scheme 3.1: Synthesis of bulky BH₃-protected PNSO ligands.



The compound **71-BH₃** was heated to 70 °C in toluene with an excess of DABCO to release the ligand from the boron protecting group (Scheme 3.2), a process which was easily monitored by TLC. When no protected form remained, the reaction was removed from the heat and allowed to cool. The source of rhodium Rh₂(cod)₂Cl₂/AgOTf (first filtered over celite and concentrated in *vacuo*) was then added to the reaction, dissolved in THF. The resulting rhodium complex derived from ligand **71** was very apolar, running high on the TLC plate in a 9:1 hexane:ethyl acetate mobile phase and also passing easily through a silica column. This behaviour was not expected from a cationic complex. After stirring and later evaporation of solvents, the complex was then purified by column chromatography to give pure complex **73** as an orange oil, which slowly solidified.

Scheme 3.2: Synthesis of neutral and cationic rhodium complexes **73** and **74** derived from (+)-*tert*-butylsulfinamide.

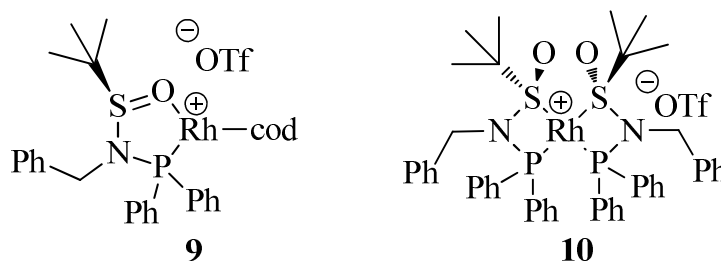


¹H NMR analysis of complex **73** revealed a lone signal for the sulfinyl *tert*-butyl group at 1.1 ppm, a pair of overlapping doublets between 1.22-1.26 ppm corresponding to the phosphino *tert*-butyl groups, and a set of olefinic proton signals residing between 3.97 ppm and 5.25 ppm. These results led us to believe we had synthesized a monomeric PNSO-Rh complex that probably displayed oxygen to rhodium coordination reminiscent of complex **9**, previously synthesized by our group. The sulfinyl *tert*-butyl ¹H NMR peak of **73** appeared

3. N-Phosphino sulfinamide ligands

much further upfield than those of the previously reported complexes **9** and **10**, where their sulfinyl *tert*-butyl peaks lay at 1.54 ppm and 1.47 ppm, respectively.⁷ The ¹H NMR spectrum could not confirm the ligand-metal coordination mode. A reliable structural elucidation was sought by X-Ray analysis; however, due to the apolar nature of **73** and its high solubility in a range of solvents from hexane to methanol, our attempts to form crystals suitable for X-ray crystallography failed time and again.

Figure 3.2: PNSO-Rh complexes previously prepared in the group.

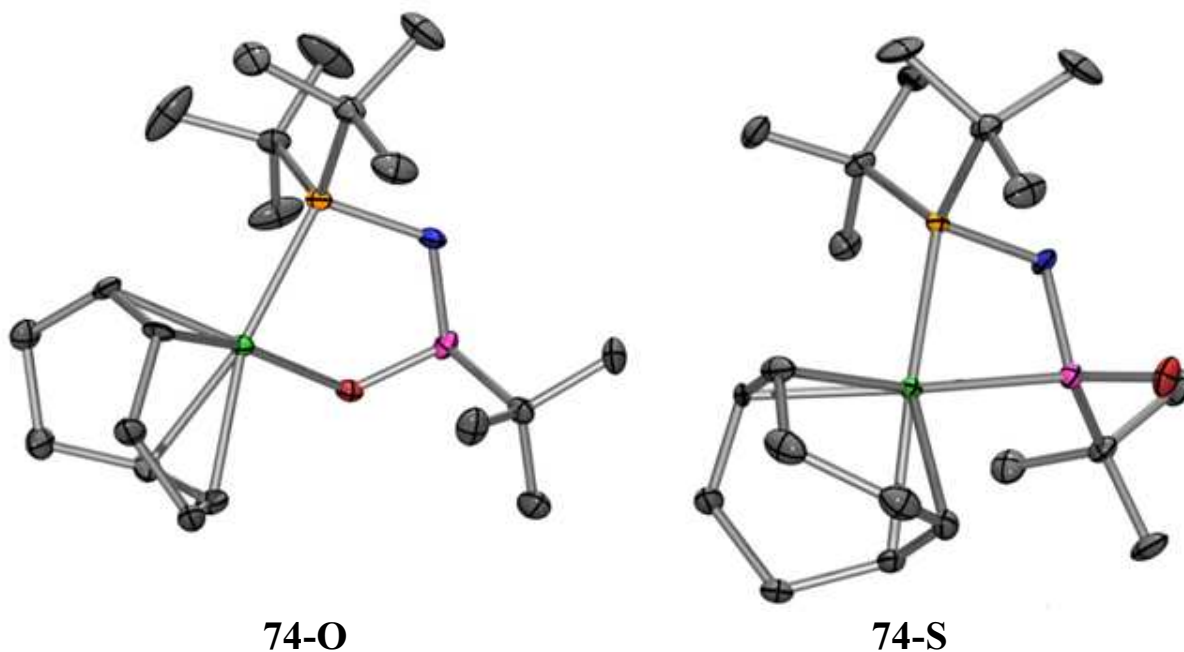


In an attempt to explain the chromatographic behaviour of complex **73**, we postulated that it was not a salt but a neutral complex that resulted from deprotonation of the NH functionality in the presence of excess DABCO in the reaction mixture, structurally related neutral Rh complexes have been reported.⁸ We hypothesized that by adding 1 eq. of acid to the complex stirring in an apolar solvent we could achieve a complex from which crystals suitable for X-ray crystallography could be formed. This hypothesis was confirmed experimentally; addition of 1 eq. of HBF₄·OEt₂ to the dissolved complex in Et₂O yielded a bright yellow precipitate. This precipitate was the protonated cationic complex **74** (Scheme 3.2).

Crystals suitable for X-ray crystallography were formed by dissolution of the salt complex **74** in a small amount of DCM followed by the layering of an excess of Et₂O. Surprisingly, in one unit cell of the crystal (Figure 3.3) we detected two distinct structures showing both sulphur coordination (P,S) and at the same time oxygen coordination (P,O) to the metal center. This finding led us to assume that in complex **74** neither O- or S- to metal coordination was greatly favoured over the other. Despite this, the crystallographic data of complex **74** gave us a unique opportunity to compare the effect of the different coordination modes on the bond lengths and bond angles of the molecule and also to analyse them with respect to comparable complexes such as **9** and **10**, previously synthesized by our group. The O-coordinated complex **74-O** showed a significant *trans* effect, whereby the olefinic-rhodium bonds were shortened when *trans* to oxygen, from 2.21 Å in the S- coordinated complex to

2.13 Å, comparable with those of the monomeric complex **9** which has an olefinic-rhodium bond of 2.10 Å. The sulfoxide bond also lengthened from 1.46 Å to 1.52 Å when going from S- to O- coordination. S- coordination clearly contracted the S-N-P bond angle from 120 ° to 104 °, showing more similarity to the S-N-P bond angle of the dimeric complex **10** of 102 °. We observed that the Rh-O bond had a length of 2.12 Å while that of the Rh-S bond was of 2.32 Å. Also, the Rh-P bond was 2.31 Å in coordination modes **74-O** and **74-S** and clearly longer than the Rh-P bonds of complexes **9** and **10**, which were both 2.25 Å.

Figure 3.3: Ortep drawing for crystal structure of complex **74-O** and **74-S** with 50% probability of ellipsoids. The two different structures coexist in a single unit cell showing P,O and P,S coordinated ligand.

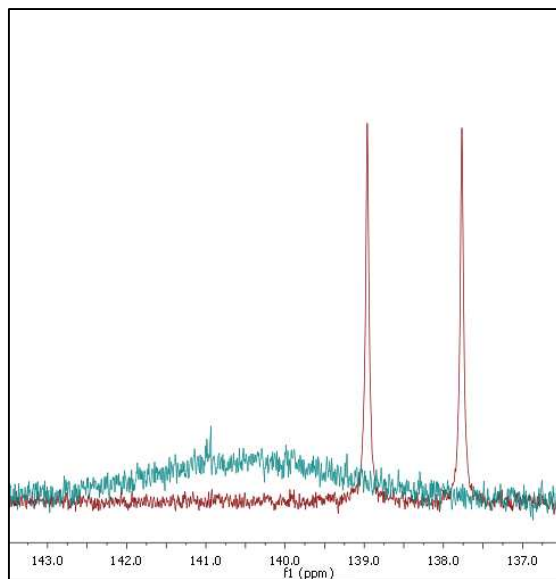


The ^{31}P NMR spectrum of the neutral compound **73** showed a very well defined doublet at 138 ppm while the cationic species **74** showed a broad signal pushed slightly downfield at 141 ppm. The morphology of the ^{31}P NMR signals of the neutral complex **73** versus those of the salt complex **74** suggests that **73** has a more stable, steady structure in CDCl_3 solution and favours one of the two possible coordination modes (P,O or P,S) while a fluxional process occurs for the cationic complex **74**. The equilibrium of coordination modes from chalcogen to

3. *N*-Phosphino sulfinamide ligands

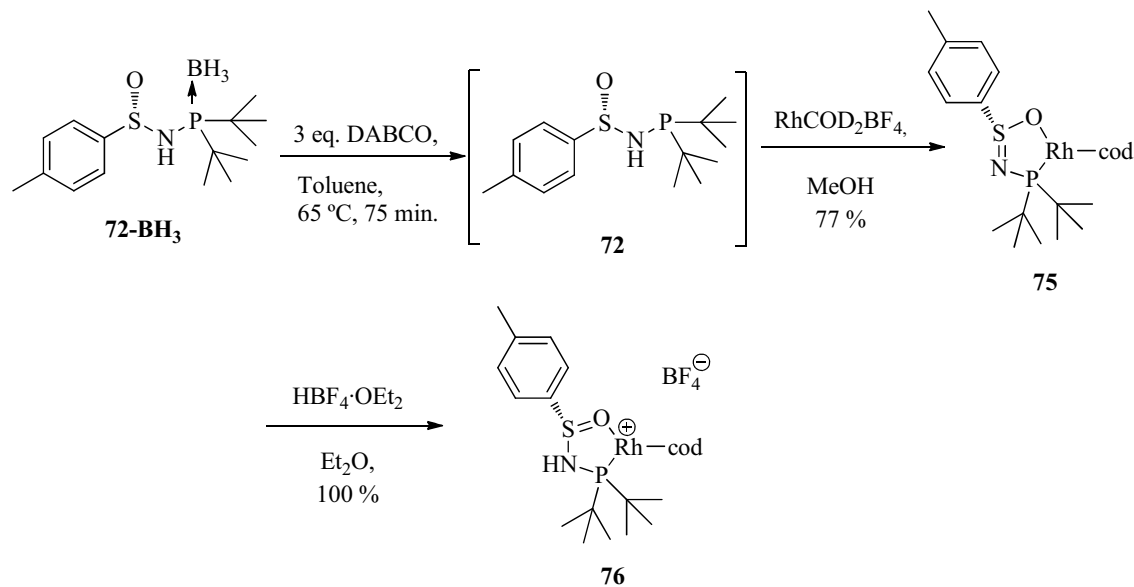
the rhodium center, which favours neither sulphur coordination nor oxygen coordination, could be responsible for the fluxional behaviour of complex **74** in solution.

Figure 3.4: Overlapping of ^{31}P NMR spectra of complexes **73** (red) and **74** (green).



The syntheses of the *p*-tolyl-substituted sulfinamide-derived complexes **75** and **76** are described in Scheme 3.3. In analogous fashion with its *tert*-butyl analogue, coordination to rhodium in the presence of a base (DABCO) provided the neutral complex **75**, which was easily purified by flash chromatography on silica gel. Addition of $\text{HBF}_4\text{-OEt}_2$ over the neutral complex afforded the more conventional cationic species **76** as a yellow solid. Analysis of the ^{31}P NMR showed that the neutral complex **75** had a well-defined doublet at 149 ppm while the cationic complex **76** showed a slightly less well defined doublet pushed upfield to 140 ppm. Although the difference in morphology of the peaks was not as apparent as in the previous case, again it suggests that the coordination mode of the cationic species is more fluxional in nature than that of the neutral complex.

Scheme 3.3: Synthesis of neutral and cationic rhodium complexes **75** and **76** derived from (+)-*p*-tolylsulfonamide.



3.1.2 Hydrogenations of *Z*-MAC catalysed by the PNSO-Rh complexes

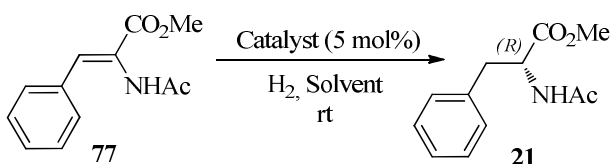
Hydrogenations of *N*-acetamido phenylalanine dehydroamino acid (*Z*-MAC) **77** were attempted using the given complexes under varying pressures of hydrogen and various solvents (Table 3.1). The *p*-tolyl complexes **75** and **76** failed to provide any hydrogenation product (Table 3.1, entries 1 and 2). In contrast, the *tert*-butylsulfonamide-derived complexes **73** and **74** gave hydrogenations with complete conversion as determined by ¹H NMR (Table 3.1, entries 3-6). The best selectivity was observed for the neutral complex **73** at room temperature with a 38% enantiomeric excess, yielding the *R* enantiomer of **21** when the reaction was run in dichloromethane with 4 bar of H₂ (Table 3.1, entry 7). The selectivity was improved to 42 % enantiomeric excess by running the hydrogenation at 0 °C in methanol (Table 3.1, entry 8). Most interestingly, the more conventional cationic Rh complex **74** consistently yielded lower enantioselectivities. This observation again suggested that the neutral species in solution is more tightly coordinated than the cationic one, thereby resulting in higher selectivity during the hydrogenation.

To test whether a specific solvent or an additive could be used to induce a more selective coordination mode and thereby give a better enantiomeric excess, we applied various solvents. The results obtained varied greatly, THF for example, slowed the reaction dramatically and gave no selectivity. We thought that the addition of a base would give

3. *N*-Phosphino sulfinamide ligands

favourable results; however, addition of Et₃N or *tert*-butylamine only impaired the enantiomeric excesses obtained (Table 3.1, entries 13 and 14). The pressure of hydrogen had a key effect on the reaction outcome. We found high pressures gave poor excesses while the lower the pressure the better the performance. However, reducing the pressure to 1-2 bars of H₂ led to no conversion while 3 bars could not give full conversion. The optimum pressure was found to be 4-5 bars.

Table 3.1: Hydrogenation of dehydroamino acid *Z*-MAC using PNSO-Rh complexes.

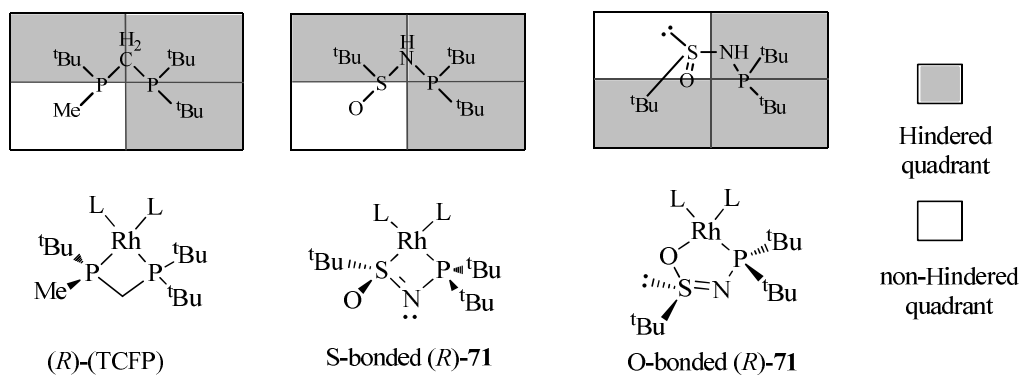


Entry	Catalyst	Solvent	Bar (H ₂)	Conversion (%) ^a	ee (%) ^b
1	75	MeOH	3	0	0
2	76	MeOH	3	0	0
3	74	MeOH	3	100	11
4	74	CH ₂ Cl ₂	4	100	12
5	73	MeOH	5	100	35
6	73	CH ₂ Cl ₂	4	100	38
7	73	CH ₂ Cl ₂	3	45	0
8 ^c	73	MeOH	4	100	42
9	73	MeOH	30	100	8
10	73	CH ₂ Cl ₂	25	100	6
11	73	THF	5	90	0
12	73	TFE	5	100	13
13 ^d	73	MeOH	5	100	32
14 ^e	73	MeOH	5	100	11

a) Conversions to hydrogenated product determined by ¹H NMR. b) Enantiomeric excess determined by chiral HPLC. c) Reaction was carried out at 0 °C. d) 10 mol % of Et₃N were added. e) 10 mol % of *tert*-butylamine were added.

The quadrant diagram method has been widely applied to correlate the steric demand surrounding the metal center and the absolute configuration of hydrogenation products.⁹ In this respect, Hoge and co-workers demonstrated that the (*R*)-(TCFP) ligand hydrogenates phenylalanine dehydroamino acid (*Z*-MAC) **77** to give the product (*R*) enantiomer with 99 % enantiomeric excess. According to the quadrant-analysis method, in complexes **73** and **74**, switching from an S- to O-coordination modifies the non-hindered quadrant available for the substrate coordination (Figure 3.5). This phenomenon can be clearly observed in the X-ray structures of **74-O** and **74-S** (Figure 3.3). The predomination of O- or S-coordination should ultimately determine the absolute configuration of the final hydrogenation product. Thus, for both the (*R*)-TCFP ligand and our S- bonded ligand (*R*)-**71**, the lower-left quadrant is the non-hindered one, and therefore, these compounds should provide the same hydrogenated enantiomer. In contrast, the O-bonded ligand (*R*)-**71** should provide the opposite enantiomer, since now the free quadrant is the upper-left one. Since the major enantiomer found in the hydrogenation using **73** as catalyst had the *R* configuration, we assumed that the S-coordination mode was the most abundant for the neutral complex during hydrogenation. Of course it must be taken into account that the two isomers could exist in any ratio of abundance while the S- bonded complex is simply more reactive than the O- bonded complex. However, the low enantiomeric bias observed during the hydrogenation indicates that the hemi-labile nature of the S-Rh linkage is detrimental to attain high selectivity in the hydrogenation catalysis.

Figure 3.5: Quadrant analysis for S- and O-bonded ligand (*R*)-**71**, and comparison with (*R*)-TCFP ligand. Absolute configurations refer to the free ligand.



3. *N*-Phosphino sulfinamide ligands

Thus far the synthesis of two new di-*tert*-butyl-phosphino PNSO ligands and their subsequent coordination to a rhodium(I) center has been described. The secondary amine nature of these ligands together with the basic nature of their borane deprotection before metal coordination gave rise to neutral rhodium complexes with more interesting properties than their more normal cationic rhodium species. These complexes are apolar and soluble in solvents such as hexane and diethyl ether as well as in more polar solvents such as methanol. The neutral complexes can be easily protonated to form their more standard salt counterparts. NMR and X-ray studies have shown that the coordination mode of ligand **71** to rhodium *via* either sulphur or oxygen is ill-defined for the cationic species, where there is an equally balanced equilibrium between the two possible coordination modes. In contrast, the neutral complexes display a more stable coordination mode to the metal center. In this respect, the absolute configuration of the hydrogenation products along with the quadrant analysis method indicates that the sulphur coordination is preferred for the neutral complex **73**. Although the neutral complex **73** is active as a hydrogenation catalyst, the hemi-labile nature of the S–Rh is detrimental to attain high enantiomeric excess.

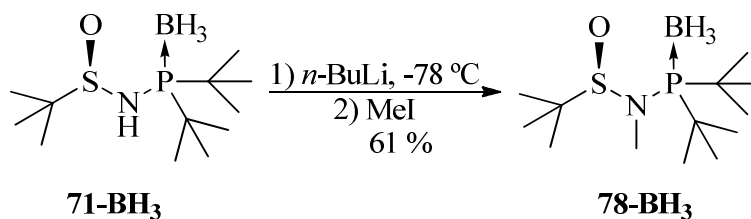
3.2 Attempts towards the synthesis of PNSO analogues

Although poor enantiomeric excesses were obtained while carrying out asymmetric hydrogenation on the *Z*-MAC dehydroamino acid substrate with our new rhodium complexes **73** and **74** we were encouraged all the same. The complex **73** first prepared during this work was the first PNSO-Rh complex developed in our group which could successfully catalyse asymmetric hydrogenation with any significant enantiomeric excess. Monochelated cationic complex **9**, previously reported by our group, provided full conversion to the hydrogenated compound **21** but with 0 % enantiomeric excess (5 mol% of **9**, CH₂Cl₂, 20 bar of H₂, rt, 22h). The dichelated PNSO-Rh-PNSO complex **10** already described here and also the rhodium complex of dicyclohexyl-substituted PNSO **67** had shown no reactivity as regards asymmetric hydrogenation. We felt progress had been made, the complexes **73** and **74** were active and perhaps with only fine-tuning of the ligand enantiomeric excess could be increased.

3.2.1 The *N*-methyl PNSO ligand

With ligand **71-BH₃** at hand we were curious as to what behaviour its *N*-methylated analogue might exhibit. Perhaps with even more steric bulk on the ligand and around the metal center the coordination mode of the sulfoxide to the metal could be influenced. Also with the introduction of a methyl group, the basicity of the amine could be affected perhaps giving different sulfoxide coordination behaviour. Perhaps the equilibrium between O-Rh and S-Rh coordination could be shifted to reside entirely on one side and not the other and therefore improving stereoselectivity in the asymmetric hydrogenation of the *Z*-MAC substrate. The *N*-methylated ligand **78-BH₃** was easily prepared.

Scheme 3.4: Methylation of the di-*tert*-butyl(1,1-dimethylethylsulfinamido)phosphine-BH₃.



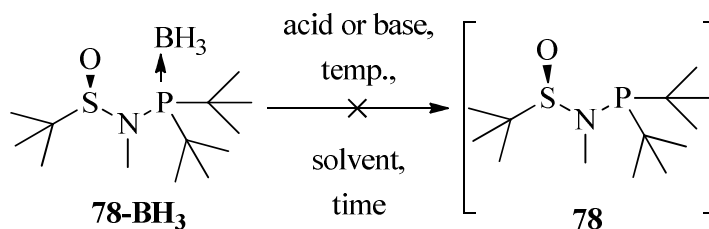
Some difficulties were encountered at first while carrying out this reaction whereby very low yields were obtained while employing one to one stoichiometry of reactants but acceptable yields were obtained when an excess of iodomethane was used. Upon obtaining the *N*-methylated ligand the next step required as before was its deprotection of BH₃ before it could be coordinated with rhodium.

As it turned out, it was observed that the introduction of a methyl group affected the basicity of the phosphine-borane to quite some degree. The quick deprotection of the ligand of BH₃ by stirring and heating of the phosphine in the presence of DABCO while monitoring by TLC, as in the case of ligand **71-BH₃**, was no longer applicable. Bases such as morpholine and diethylamine were also tested in the deprotection process by their addition in excess but only ever yielded starting material (Table 3.2, entries 5, 6) as confirmed by TLC and ³¹P NMR. As shown by Livinghouse *et al.* published in 1994¹⁰ and also proven through the work of our

3. *N*-Phosphino sulfinamide ligands

group as published during the development of the MaxPHOS ligand¹¹, particularly basic phosphine-boranes can be decomplexed of BH₃ with the use of certain acids. It was attempted to liberate **78-BH₃** of borane using TFA and HBF₄·OEt₂ using various conditions (Table 3.2, entries 2-4) and the removal of BH₃ was sometimes observed but usually accompanied by decomposition of the ligand as confirmed by ¹H and ³¹P NMR.

Table 3.2: BH₃ deprotection of *N*-methylated PNSO ligand.



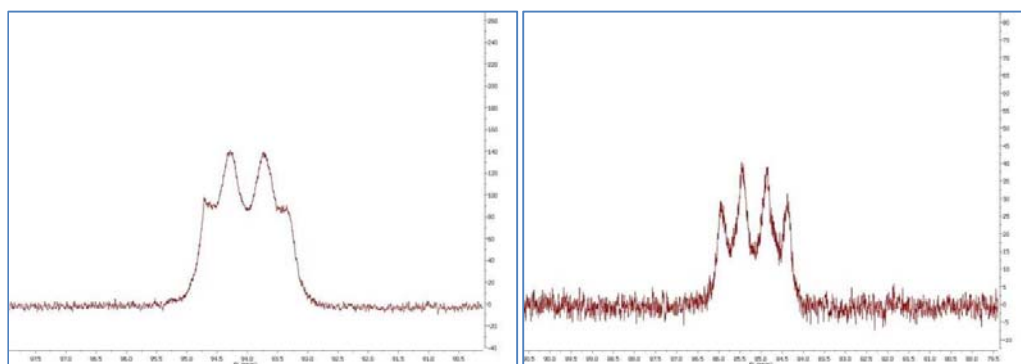
Entry	Acid or Base	Solvent	Temp. (°C)	Time (h)	Yield ^a
1	DABCO	Toluene	80	22	s.m.
2	TFA	-- ^b	r.t.	18	decomp.
3	TFA	-- ^b	r.t.	1	decomp.
4	HBF ₄ ·OEt ₂	CH ₂ Cl ₂	r.t.	19	decomp.
5	Morpholine	CH ₂ Cl ₂	r.t.	18	s.m.
6	NHEt ₂	-- ^b	45	41	s.m.

^a As judged by a combination of ³¹P, ¹H NMR and TLC. ^b Reagent used as solvent.

It is interesting to note the comparable ³¹P NMR spectrums of ligands **71-BH₃** and **78-BH₃**. First of all the morphology of the peaks can shed light on the nature of the bonding between phosphorus and the borane group. It has been observed that a well-defined quartet signal tells of a phosphorus-borane bond which is highly basic and strong, more likely to prove difficult to deprotect in basic conditions in comparison with a phosphorus peak which is more rounded, this phenomenon will be confirmed later on with further examples. This is the case when comparing the ³¹P NMR spectrums of **71-BH₃** and **78-BH₃** and also it is observed that

the phosphorus peak of the latter is pushed upfield from 94 ppm to 85 ppm, hinting at a more electron rich and basic phosphine. So it seemed the introduction of the methyl group had served to strengthen the phosphorus-borane bonding to the point where such harsh conditions were needed to liberate it of BH_3 which the stability of the ligand could not withstand.

Figure 3.6: The comparable ^{31}P NMR spectra of **71-BH₃** on the left and **78-BH₃** on the right. Although the signal to noise ratio in the spectrum of **78-BH₃** on the right is smaller, its more defined quartet signal can still be appreciated.



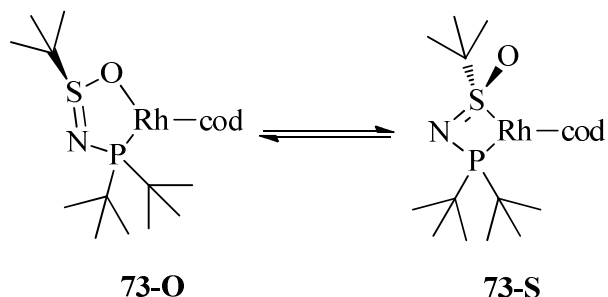
3.2.2 The PNNSO ligand

In our group T. Achard had postulated previously that S-Rh coordination was preferred in PNSO-Rh complex **10**, a complex dimeric of ligand to metal, probably due to the electronically rich nature of the rhodium atom not bearing an olefinic cyclooctadiene ligand preferring the soft coordinating mode of the sulphur. Perhaps this was also the case in complexes **73** and **74** where the highly electron donating *tert*-butyl groups residing on phosphorus resulted in more electron density being donated into the metal's d orbitals through phosphorus making a richer rhodium centre favouring S-Rh coordination. However it can be observed from X-ray structure of complex **74** that the steric hindrance present on the ligand creates a very small S-Rh-P bite angle of only 70.7 ° when coordinated through sulphur. This is smaller than the S-Rh-P bite angle of dimeric complex **10** which was described as 71.2 °. It is even smaller than the P-Rh-P bite angle of the trichickenfootphos ligand when coordinated to rhodium, which was described as 72.6 ° and only slightly larger than that of the MaxPHOS-rhodium complex which has been described at 70 ° for the P-Rh-P

3. *N*-Phosphino sulfinamide ligands

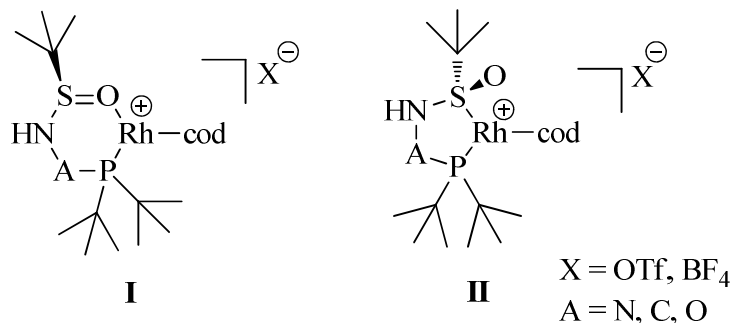
angle. It is obvious to see there must be much ring strain when a 4-membered ring structure is taken up around the metal centre in complexes **73** and **74** and considering the sulfoxide-metal coordination mode is hemi-labile in nature it is clear why an equilibrium might exist where the sulphur closed chelate might flick open to provide oxygen to rhodium coordination.

Figure 3.7: O- versus S- coordination.



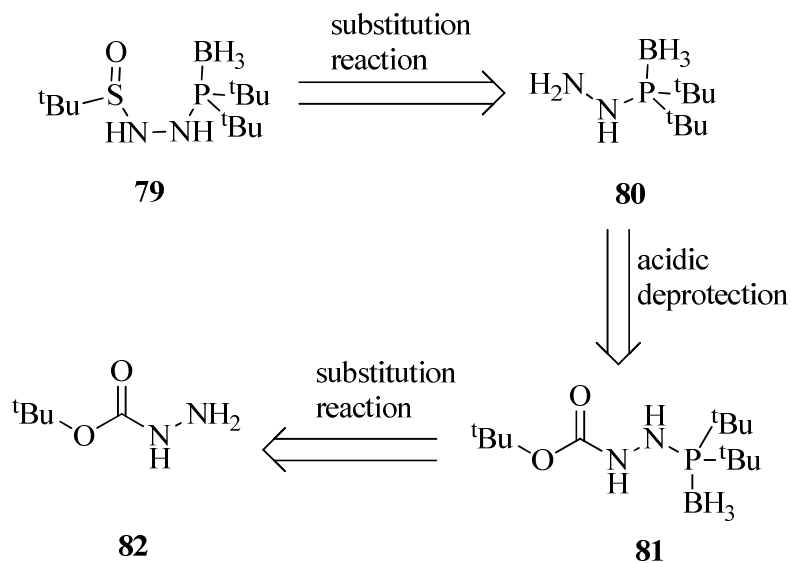
It was speculated that the bite angle of complexes **73** and **74** was too small and the 4-membered ring that sulphur to rhodium coordination brought about was too strained for the hemi-labile nature of the PNSO ligand to provide a stable chiral environment around the catalytic centre. It was thought interesting to modify the ligand in such a way that it would have an extra atom in between the two metal coordinating phosphorus and sulphur atoms. It was surmised that perhaps if there were an extra atom between sulphur and phosphorus that there would be less ring strain present in the 5-membered ring formed while, the electron density donated to the rhodium centre derived from the *tert*-butyl substituted phosphine would provide a complex where S-Rh coordination was preferred. It was also taken into consideration that the same case as before could arise where neither S-Rh coordination nor O-Rh coordination would be favoured but it was thought with less strain present in the ring around the metal centre that a more coordinationally stable catalyst would emerge and it was considered interesting to investigate this uncertainty.

Figure 3.8: Adding a “spacer” atom into the PNSO ligand.



First of all it was thought to insert another nitrogen atom in between the sulfoxide and phosphine moieties would be most desirable. The retrosynthetic analysis shown in scheme 3.5 was considered.

Scheme 3.5: Retrosynthetic analysis for proposed PNNSO ligand.



To arrive at the proposed “PNNSO” compound **79** it was acknowledged that it would be difficult to induce the formation of a hydrazine, building off the *tert*-butyl sulfinamide so it could be coupled with di-*tert*-butylphosphine as in the preparation of PNSO ligand **71-BH₃**. It was considered most wise to begin with a commercially available hydrazine rather than to try to form one ‘from scratch’. We decided to employ *tert*-butyl carbazate **82** as it provided the necessary hydrazine fragment while also served to protect one side of it to the proposed first substitution reaction. The other side would be made available later by acidic deprotection of the amine-protecting Boc group for the preceding second substitution reaction step.

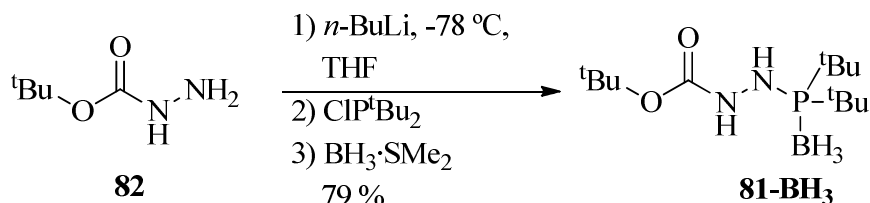
After deciding which reactant the ligand should be built off from it was simply a matter of choosing in which order each fragment should be coupled to it. In the end it was opted to couple first the phosphine fragment, then the Boc-deprotection step would follow and finally the sulfoxide fragment would be added. The reasoning behind this order was that we had seen previously and it has been described here already that *N*-phosphino-boranes were stable functional groups and we believed it would have a greater chance of surviving the Boc group removal conditions. Also it made more logical sense to reserve the enantiomeric

3. *N*-Phosphino sulfinamide ligands

transformation until last to avoid any racemization which might occur during said protecting group removal conditions.

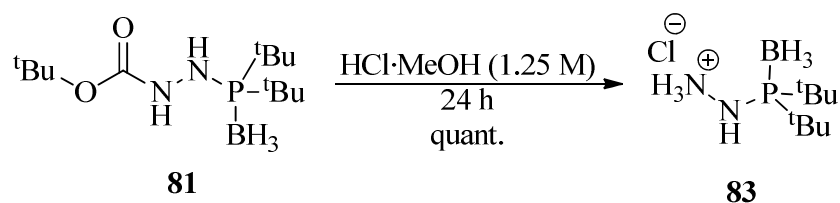
To begin this short synthetic pathway the coupling of the *tert*-butyl carbazate **82** was reacted with di-*tert*-butylchlorophosphine at room temperature in the presence of Et₃N, to neutralize the evolution of HCl. Monitoring by TLC it became apparent the hydrazine was not a strong enough nucleophile to react well with the phosphine electrophile. It was necessary to raise the temperature to induce reactivity and many side products formed within the reaction and very poor yield resulted. Through prior formation of an anion on the hydrazine through the addition of *n*-butyllithium with the phosphine electrophile added later and directly, it yielded a much more desirable reaction with good yield and negligible side-product formation.

Scheme 3.6: Preparation of the Boc-protected hydrazine phosphine-borane.



The next step required in the preparation of the proposed PNNSO ligand **79** would be the removal of the Boc protecting group. This was induced by reacting in a 1.25M HCl in methanol solution. Upon removal of the solvent in *vacuo*, ¹H NMR confirmed the removal of the Boc group and through examination using thin layer chromatography it was obvious a salt species had formed. No form of purification was carried out on the product and it was used in its crude form in the next reaction.

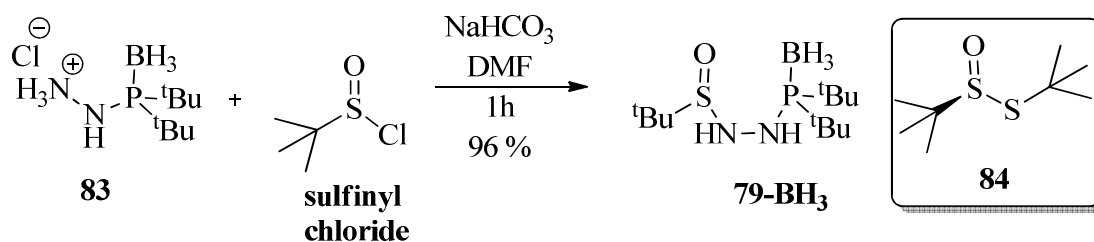
Scheme 3.7: Boc protecting group removal.



Upon obtaining the phosphine salt **83** it was then reacted with racemic sulfinyl chloride in DMF in the presence of an inorganic base to form the racemic compound **79-BH₃** in excellent

yield at the first attempt. A simple aqueous work-up was sufficient to purify the compound to acceptable and desirable purity judging by ^1H NMR. The reaction was carried out with racemic sulfinyl chloride in this manner as it was thought the racemic compound would just as well serve to examine the stability, physical properties and coordination capabilities of the compound and if these were proven to be attractive the final step could be carried out with an enantiopure source of the *tert*-butyl sulfinyl group at a later time, such as with enantiomerically pure compound **84**¹² which is now available from commercial sources.

Scheme 3.8: Preparation of racemic PNNSO phosphine-borane.

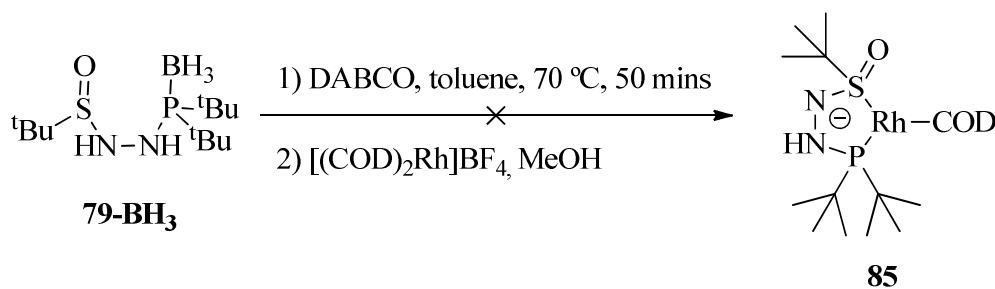


With the racemic *N*-phosphino sulfinyl compound **79-BH₃** at hand its coordinative capability to rhodium was investigated. Removal of the borane protecting group was procured by reacting **79-BH₃** in the presence of DABCO at 70 °C for 50 minutes in toluene monitoring by thin layer chromatography, completion of borane removal could be seen by the appearance of a more apolar spot as the starting material spot disappeared. Once no more starting material remained [(1, 5-cyclooctadiene)₂Rh]BF₄ complex was added to the reaction mixture with the addition of MeOH to aid solubility. After stirring for as little as 30 minutes a bright yellow spot could be seen rising high on the TLC plate upon monitoring by thin layer chromatography. Stirring of the reaction was stopped at this point, the solvent was removed and the yellow residue was purified by flash column chromatography. The complex that was obtained was indeed a rhodium complex but it was clear, observing by ^1H NMR that there was no *tert*-butylsulfinyl moiety present. A doublet could be observed at 1.45 ppm clearly representing the *tert*-butyl peaks on phosphorus. Examining the ^{31}P NMR spectrum it was noted that a well-defined doublet appeared at 72.8 ppm. The observed signal clearly denoted a complex composed of a phosphine coordinating to rhodium with rhodium's nucleus and its

3. *N*-Phosphino sulfinamide ligands

spin of $\frac{1}{2}$ coupling to the nucleus of phosphorus to produce a doublet. The chemical shift of the phosphorus signal was interesting as it appeared much further upfield at 72.8 ppm in comparison with complexes **73-76** which all appear around the 140 ppm region. A phosphorus chemical shift of 72.8 ppm would be in accordance with the chemical shift of the phosphorus signal observed for the complex **10** synthesized previously which appeared at 69.5 ppm. This would suggest that instead of forming the desired PNNSO-Rh-COD complex it seemed the sulfinamide S-N bond was broken and what was formed was a complex dimeric of phosphine-hydrazine to rhodium however, the exact structure could not be determined as HRMS and ^1H NMR was inconclusive but it was certain the desired complex **85** had not formed.

Scheme 3.9: Loss of integrity of PNNSO structure.

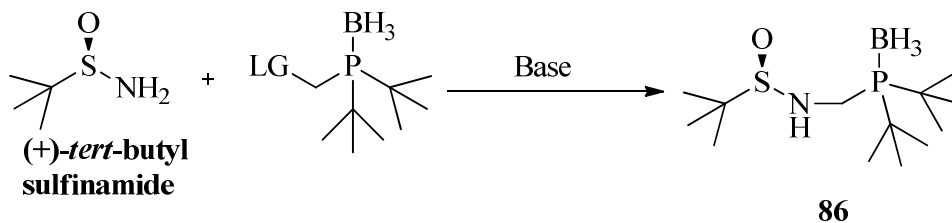


It was thought that perhaps the high temperature coupled with the basic conditions compromised the structure of the ligand and perhaps by carrying out the complexation at room temperature a positive outcome could be brought about. The PNNSO compound **79-BH₃** was reacted with both DABCO and [(1, 5-cyclooctadiene)₂Rh]BF₄ in THF with the hope that as the ligand was slowly deprotected of borane it could immediately coordinate to rhodium and slowly form complex. Unfortunately what resulted was a reaction mixture which contained many different side-products, judging by TLC. It had become evident that the PNNSO ligand motif was not viable due to its instability.

3.2.3 The attempt to introduce a carbon atom into the PNSO scaffold

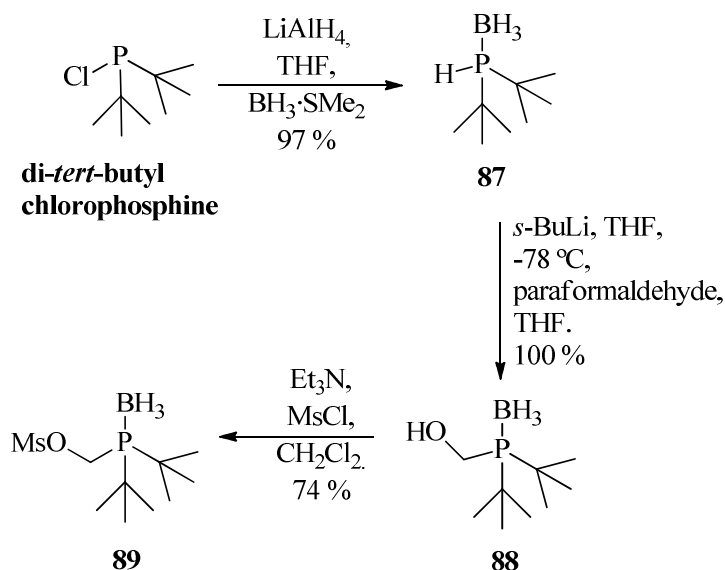
It was attempted to add an extra “spacer” atom as per figure 3.8 by other means. It was thought the di-*tert*-butylchlorophosphine could be modified so as to introduce to it a carbon electrophile with a leaving group such as a mesylate or a tosylate so the *tert*-butylsulfinamide could attack the electrophile and kick out the leaving group in an S_N2 manner to give compound **86**.

Scheme 3.10: Alternative strategy to introduce an extra spacer atom in the PNSO ligand motif.



It was thought it would be possible to synthesize compound **86** by preparing the di-*tert*-butylphosphane-borane compound **87** from di-*tert*-butylchlorophosphine and LiAlH₄. Later an anion could be formed on phosphorus before reacting it with paraformaldehyde to form the alcohol compound **88** which could be mesylated to provide compound **89** which bears a good leaving group, a method developed and published by Hoge *et. al.* in 2003.¹³ Compound **89** could then be reacted with a sulfinamide anion as shown in scheme 3.10 to hopefully form a 3-hindered quadrant phosphino-sulfinamide ligand such as **86**. The phosphine **89** was prepared as described in scheme 3.11.

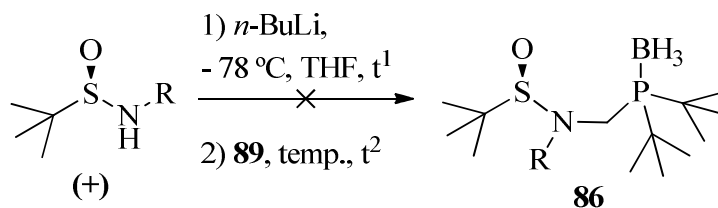
Scheme 3.11: Preparation of ‘leaving group’-containing bulky, tertiary phosphine-boranes developed by Hoge *et al.*



3. *N*-Phosphino sulfinamide ligands

Following a procedure similar to that of the preparation of PNSO ligand **71-BH₃**, *tert*-butylsulfonamide was reacted with *n*-BuLi in THF at low temperature and left sufficient time stirring to form an anion before the electrophile **89**, also dissolved in THF, was added to the reaction mixture. This was allowed to warm up to room temperature and left to react overnight while stirring but this did not yield desired product only starting materials (entry 1, table 3.3). It was also attempted after addition of the electrophile to the sulfonamide anion at low temperature, to allow to warm up to room temperature while stirring with subsequent heating to 60 °C, stirring at said temperature overnight to try to force the progression of the reaction to no avail, only unwanted side-products were obtained (entry 2, table 3.3). Also the benzyl substituted sulfonamide (table 3.3, entry 3) was prepared by the method described by T. Achard,¹³ previously of our group and was reacted in a similar manner with the tertiary phosphine-borane **89** but only starting materials were obtained.

Table 3.3: The reaction of the *tert*-butylsulfonamides with di-*tert*-butylphosphinomesylate-borane.



Entry	R	<i>n</i> -BuLi (eq.)	<i>t</i> ¹ (h)	temp. (°C)	<i>t</i> ² (h)	yield ^a
1	H	1,2	0,8	- 78 °C to r.t.	19	s.m.
2	H	1,1	1,3	- 78 °C to 60 °C	25	decomp.
3	Bn	1,2	1	- 78 °C to r.t.	18	s.m.

^a Judging by TLC of reaction mixture and ¹H NMR of the isolated residue after an aqueous work-up.

It was concluded at this point that the nucleophilic reactivity of an anion residing on the *tert*-butylsulfonamide and the benzylic *tert*-butylsulfonamide resulted incompatible with this particular electrophile, this tertiary phosphine-borane **89** and this line of research was not pursued further.

3.3 Conclusions

During this work novel *N*-phosphino sulfinamide compounds have been prepared such as **71**, **72**, **78** and **79**. Their preparation has been outlined. Their potential for use as chiral ligands in asymmetric metal catalysis and more specifically the asymmetric hydrogenation reaction has been investigated. The ligand **71** hinted at potential for success within the ligand class as it was applied in the asymmetric hydrogenation of the *Z*-MAC hydrogenation substrate **77** and provided hydrogenation with a best enantiomeric excess recorded of 42 % ee. Difficulties were encountered while trying to expand the ligand class to provide ligands of different size bearing additional atoms between the separate metal-coordinating sulphinyl and phosphine moieties but the introduction of an extra nitrogen atom into the PNSO ligand scaffold was achieved with the preparation of the compound **79-BH₃**. Unfortunately the poor stability and coordinating nature of the compound **79-BH₃** to rhodium suggested this compound did not have potential application in asymmetric catalysis. It was these results that lead us to believe that the line of research of *N*-phosphino sulfinamide ligands applied towards asymmetric catalysis and especially the asymmetric hydrogenation reaction was not as viable as was initially hoped and the direction of research should change. It was decided to turn focus towards P*-stereogenic diphosphine ligands and especially the MaxPHOS ligand. The MaxPHOS ligand had recently been prepared within the group and had shown great promise. It was thought to focus attention more closely on this ligand in particular and to investigate fully its potential.

¹ a) *Phosphorous Ligands in Asymmetric Catalysis*; Börner, A., Ed.; Wiley-WCH: Weinheim, 2008; Vol. I-III. b) Nugent, T. C.; El-Shazly, M. *Adv. Synt. Catal.* **2010**, *352*, 753-819. c) Xie, J.; Zhu, S.; Zhou, Q. *Chem. Rev.* **2011**, *111*, 1713-1760. d) Gómez, A. R.; Adrio, J.; Carretero, J. C. *Angew. Chem. Int. Ed.* **2006**, *45*, 7674-7715.

² a) Imamoto, T.; Tamura, K.; Ogura, T.; Ikematsu, Y.; Mayama, D.; Sugiya, M. *Tetrahedron: Asymmetry* **2010**, *21*, 1522-1528. b) Granander, J.; Secci, F.; Canipa, S. J.; O'Brien, P.; Kelly, B. *J. Org. Chem.* **2011**, *76*, 4794-4799.

³ a) Verdaguer, X.; Moyano, A.; Pericas, M. A.; Riera, A.; Maestro, M. A.; Mahia, J. *J. Am. Chem. Soc.* **2000**, *122*, 10242. b) Verdaguer, X.; Lledo, A.; Lopez-Mosquera, C.; Maestro, M. A.; Pericas, M. A.; Riera, A. *J. Org. Chem.* **2004**, *69*, 8053. c) Verdaguer, X.; Pericas, M. A.; Riera, A.; Maestro, M. A.; Mahia, J. *Organometallics* **2003**, *22*, 1868.

⁴ a) Robak, M. T.; Herbage, M. A.; Ellman, J. A. *Chem. Rev.* **2010**, *110*, 3600-3740. b) Cogan, D. A.; Liu, G.; Kim, K.; Backes, B. J.; Ellman, J. A. *J. Am. Chem. Soc.* **1998**, *120*, 8011-8019. c) Fernandez, I.; Khair, N. *Chem. Rev.* **2003**, *103*, 3651-3706. d) Zhang, Y.; Chitale, S.; Goyal, N.; Li, G.; Han, Z. S.; Shen, S.; Ma, S.; Grinberg, N.; Lee, H.; Lu, B. Z.; Senanayake, C. H. *J. Org. Chem.* **2012**, *77*, 690-695.

3. N-Phosphino sulfinamide ligands

- ⁵ Achard, T.; Benet-Buchholz, J.; Riera, A.; Verdaguer, X. *Organometallics* **2009**, *28*, 480. b) Achard, T.; Benet-Buchholz, J.; Escudero-Adan, E. C.; Riera, A.; Verdaguer, X. *Organometallics* **2011**, *30*, 3119.
- ⁶ Evans, D. A.; Michael, F. E.; Tedrow, J. S.; Campos, K. R. *J. Am. Chem. Soc.* **2003**, *125*, 3534.
- ⁷ Achard, T.; Benet-Buchholz, J.; Riera, A.; Verdaguer, X. *Organometallics* **2009**, *28*, 480.
- ⁸ a) Chatziapostolou, K. A.; Vallianatou, K. A.; Grigoropoulos, A.; Raptopoulou, C. P.; Terzis, A.; Kostas, I. D.; Kyritsis, P.; Pneumatikakis, G. *J. Organomet. Chem.* **2007**, *692*, 4129-4138. b) Slawin, A. M. Z.; Smith, M. B.; Woollins, J. D. *J. Chem. Soc., Dalton Trans.* **1996**, , 4575-4581.
- ⁹ Knowles, W. S. *Acc. Chem. Res.* **1983**, *16*, 106-112.
- ¹⁰ McKinstry, L.; Livinghouse, T. *Tetrahedron Letters* **1994**, *35*, 9319.
- ¹¹ Reves, M.; Ferrer, C.; Leon, T.; Doran, S.; Etayo, P.; Vidal-Ferran, A.; Riera, A.; Verdaguer, X. *Angew. Chem., Int. Ed.* **2010**, *49*, 9452-9455.
- ¹² a) Kagan, H. B.; Dunach, E.; Nemecek, C.; Pitchen, P.; Samuel, O.; Zhao, S. H. *Pure Appl. Chem.* **1985**, *57*, 1911. b) Kagan, H. B.; Dunach, E.; Nemecek, C.; Pitchen, P.; Samuel, O.; Zhao, S. H. *Pure Appl. Chem.* **1985**, *57*, 1911. c) Weix, D. J.; Ellman, J. A. *Org. Lett.* **2003**, *5*, 1317.
- ¹³ Hoge, G. S., II; Goel, O. P. 2003.

P-stereogenic aminophosphine ligands

4

4.1	New MaxPHOS complexes	81
4.1.1	Coordinating MaxPHOS to palladium, copper and nickel	82
4.1.2	Coordinating MaxPHOS to cobalt and rhodium	84
4.2	Examining the electronic nature of the MaxPHOS ligand	89
4.2.1	Examination of carbonyl stretching frequencies	89
4.2.2	Examination of $J(^{31}\text{P}-^{77}\text{Se})$ coupling frequencies	91
4.3	Derivatives of MaxPHOS-BH₃ as ligands	94
4.3.1	The preparation of the mono-chalcogenated MaxPHOS derivatives	94
4.3.2	The mono-chalcogenated MaxPHOS derivative metal complexes	98
4.4	Towards the synthesis of C₁/C₂ P*-stereogenic amidine ligands	107
4.5	Conclusions	110

4 P-stereogenic aminophosphine ligands.

It has been described already the enantioselective preparation of the MaxPHOS·HBF₄ phosphonium salt and its subsequent coordination to rhodium and thereafter its effective application in asymmetric catalysis, namely the asymmetric hydrogenation reaction. In a later chapter the efficacy and scope of the MaxPHOS rhodium catalyst as applied to asymmetric hydrogenation will be explored more in depth but in this chapter other aspects of the ligand shall be discussed, such as its coordination behaviour towards other metals other than rhodium and the application of those complexes. The electronic nature of the MaxPHOS ligand shall be discussed with special focus on its phosphine electronic character. The preparation of new MaxPHOS derivatives shall be described. Also it shall be described the use of MaxPHOS preparation key intermediates to form new *P*-stereogenic ligands with new ligand-metal complexes. Also the application of these new complexes in asymmetric catalysis shall be revealed.

4.1 New MaxPHOS complexes

The efficacy of such ligands as BINAP and DuPhos in asymmetric hydrogenation has been stressed several times up until now however they have also shown a plethora of applicability in other asymmetric transformations catalysed by metals besides rhodium.¹ BINAP and its derivatives have been successfully employed with good enantioselectivities in palladium catalysed asymmetric allylations², palladium catalysed asymmetric allylic alkylations³, the ruthenium catalysed cyanosilylation of ketones⁴, ruthenium catalysed asymmetric hydrogenation of keto-acids, iridium catalysed asymmetric ring opening reactions⁵ and even iridium catalysed Pauson-Khand like reactions.⁶

DuPhos has been successfully employed delivering enantiomeric excess in such asymmetric transformations as, but not restricted to, the palladium catalysed enantioselective conjugate addition of arylboronic acids,⁷ palladium catalysed asymmetric allylic alkylations,⁸ palladium catalysed asymmetric hydrogenation of functionally substituted ketones⁹ and the nickel catalysed asymmetric arylation of benzaldehyde derivatives¹⁰ as well as many more asymmetric transformations.¹¹

The examples of smaller *P*-stereogenic diphosphine ligands being successfully employed in asymmetric transformations away from the rhodium catalysed asymmetric hydrogenation reaction are less common but do exist such as when the *P*-stereogenic diphosphine MiniPhos

4. *P*-stereogenic aminophosphine ligands

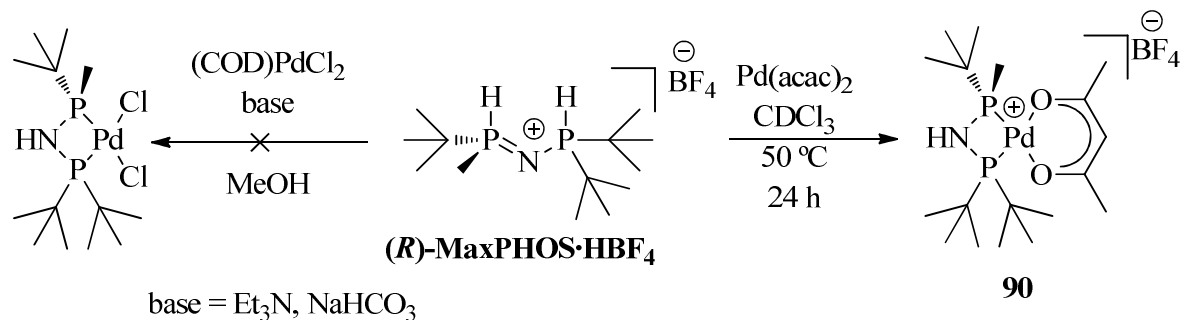
developed by Imamoto *et al.* was utilized to form a dinuclear palladium species which successfully catalysed alkylative ring-opening reactions of azabenzonorbornadienes with complete enantioselectivity.¹²

4.1.1 Coordinating MaxPHOS to palladium, copper and nickel

It was our desire to begin an investigation into the versatility of the MaxPHOS ligand. It would be necessary first to research its coordination capabilities to other metals, a screening of reaction conditions to form complexes with metals such as palladium, copper, nickel and cobalt would be carried out.

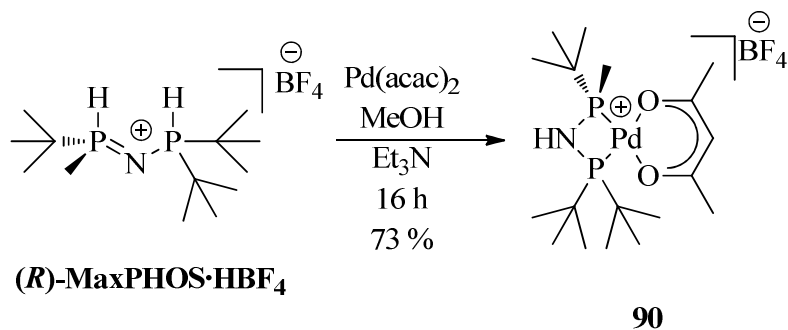
At first it was attempted to coordinate the MaxPHOS ligand to palladium *via* the dichloro(1,5-cyclooctadiene)palladium(II) complex. Stirring MaxPHOS and Pd(COD)Cl₂ in the presence of NaHCO₃ in MeOH and later MaxPHOS, Pd(COD)Cl₂ and Et₃N in MeOH provided unfavourable results judging by ¹H NMR after attempting to remove unwanted salts by filtration over a small pad of silica. Next Pd(acac)₂ was employed to try to invoke complexation of MaxPHOS ligand to palladium. A test was carried out in CDCl₃ in an NMR tube with one equivalent of Pd(acac)₂ and one equivalent of MaxPHOS ligand, following its coordination progress by ³¹P NMR.

Scheme 4.1: The attempts to complex the MaxPHOS ligand to palladium.



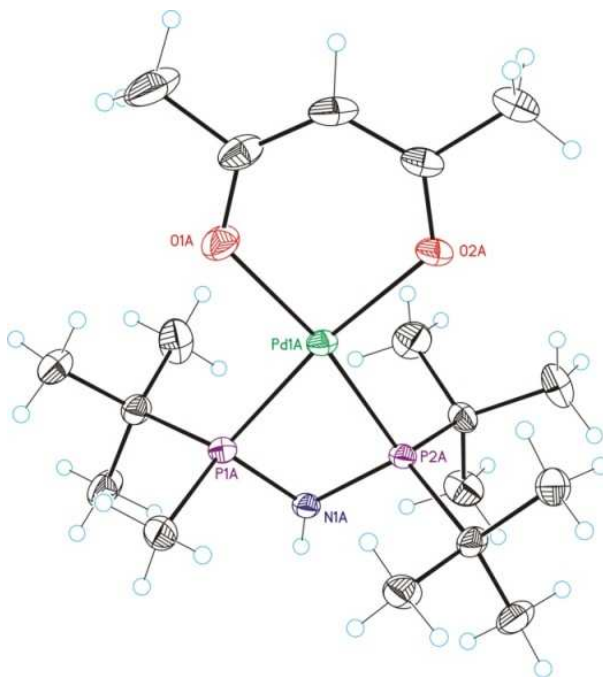
The reaction was monitored intermittently by ³¹P NMR and it was found after 24 hours heating negligible starting material remained. However it was found with the addition of one equivalent of Et₃N the reaction proceeded quicker, with less formation of side products and could complex stirring at room temperature.

Scheme 4.2: A [(MaxPHOS)Pd(acac)]BF₄ complex was formed.



The complex was purified by recrystallization from a layering process of diethyl ether over methylene chloride by which crystals for X-ray crystallography were obtained. The crystals obtained provided a clear crystallographic view of the complex. The complex obviously showed great similarity in structure to the [(MaxPHOS)Rh(COD)]BF₄ complex. The P-Pd bond was slightly shorter than that of P-Rh at 2.24 Å instead of 2.34 Å and the P-Pd-P bite angle was ever so slightly larger than that of P-Rh-P at 71.6 ° rather than 70 °.

Figure 4.1: ORTEP drawing of the [(MaxPHOS)Pd(acac)]BF₄ complex **90** where the counterion is omitted.



It must be noted that the P-Pd-P bite angle is much smaller at 71.6 ° than the bite angle calculated for BINAP-Pd (99 °) and DuPhos (85 °) which could pose as a hindrance to the

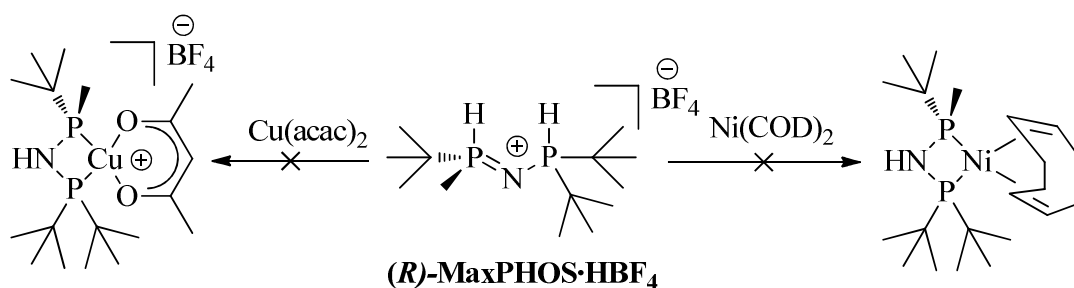
4. *P*-stereogenic aminophosphine ligands

success of a MaxPHOS-palladium catalyst system in asymmetric transformations such as asymmetric allylic alkylations however this was not tested during this work.

It was attempted to coordinate the MaxPHOS ligand to Ni(0) using [Ni(COD)₂] as the source of metal by testing in a method similar to that laid out in scheme 4.1, the ligand and the metal were mixed in an NMR tube in CDCl₃ and heated to 50 °C and the reaction was monitored by ³¹P NMR however in this instance only starting material was observed and no coordination could be seen to take place.

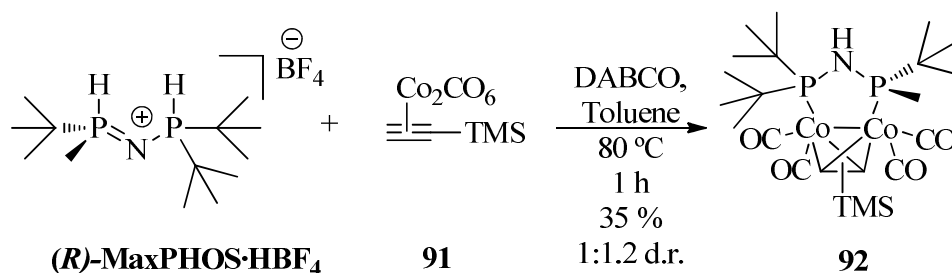
Similar coordination tests were carried out with the MaxPHOS ligand in the attempt to coordinate it to copper. [Cu(acac)₂] was used as the source of copper and it was heated in an NMR tube in CDCl₃ at 60 °C monitoring by ³¹P NMR for 4 hours by which point only starting material was present. The experiment was repeated with one equivalent of MaxPHOS, one equivalent of [Cu(acac)₂] with also one equivalent of Et₃N, heating at 60 °C in CDCl₃ for 6 hours after which a ³¹P NMR showed much starting material remained while also a multitude of other peaks had formed.

Scheme 4.3: Attempts to coordinate MaxPHOS to nickel and copper were unsatisfactory.



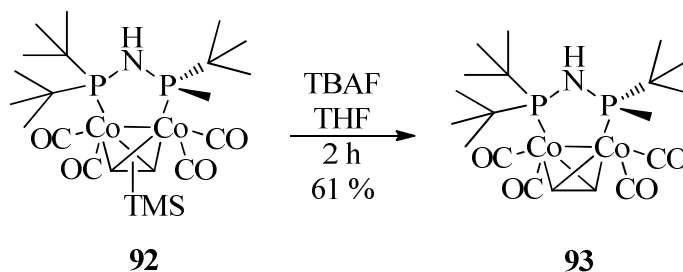
4.1.2 The coordination of MaxPHOS to cobalt and rhodium

It was next attempted to form a MaxPHOS-cobalt complex. There is much experience with ligand bound carbonyl cobalt complexes in our group through many years of work with the asymmetric Pauson-Khand reaction and this lead us to attempt a complexation of the MaxPHOS ligand to the trimethylsilane-substituted terminal alkyne-cobalt hexacarbonyl complex **91**.

Scheme 4.4: The preparation of a MaxPHOS dicobalt complex.

The reaction was carried out according to scheme 4.4 and after an hour no more starting material remained. By thin layer chromatography the formation of two diastereomers could be seen to form which would be inseparable by flash column chromatography. ^1H NMR confirmed a 1:1.2 mixture of diastereomers. For the complex to have utility in the asymmetric Pauson-Khand reaction a clear diastereoselectivity in the complex formation is preferable. It was thought however the complex could be applied in the catalytic Pauson-Khand reaction if the TMS group of the complex could be removed which would therefore remove the question of diastereoselectivity as the complex would no longer be a mixture of diastereomers.

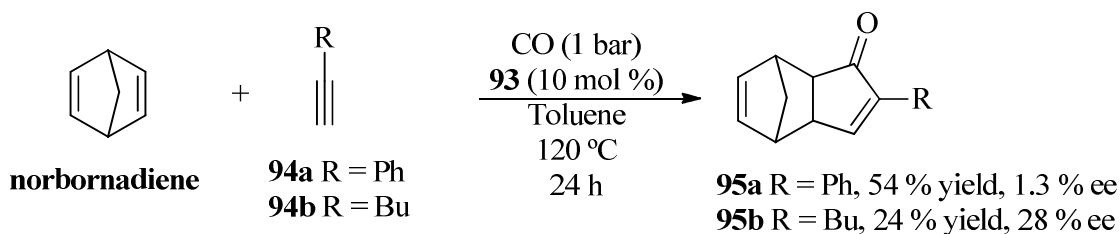
To remove the TMS group, one equivalent of tetrabutylammoniumfluoride (TBAF) stirring in THF was employed. After stirring for a little under 2 hours (1.6 h), monitoring the reaction by TLC by which two spots on the TLC plate could be observed to give way to a single spot with a similar RF and after removing solvent under *vacuo*, pure complex **93** was obtained after flash column chromatography.

Scheme 4.5: Removing the TMS group of the MaxPHOS-dicobalt complex mixture to form a singular complex.

The complex **93** was tested in the catalytic asymmetric intermolecular Pauson-Khand reaction with norbornadiene.

4. *P*-stereogenic aminophosphine ligands

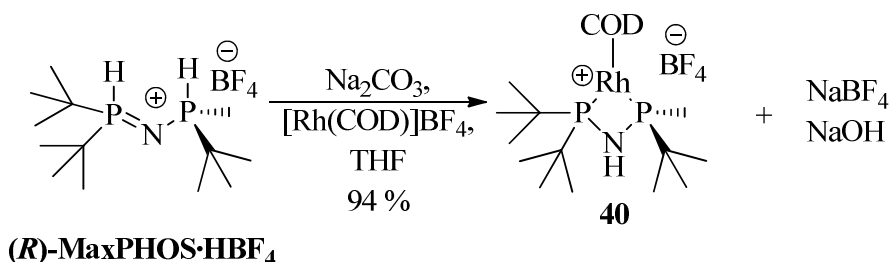
Scheme 4.6: The utility of the MaxPHOS-dicobalt complex **93** in the asymmetric catalytic intermolecular Pauson-Khand reaction:



The MaxPHOS-dicobalt carbonyl cluster provided the Pauson-Khand adducts **95a** and **95b** from norbornadiene and substituted alkynes **94a** and **94b** with the given reaction conditions showed in scheme 4.6. The adduct **95a** was provided in moderate yield and poor enantioselectivity while the adduct **95b** was provided with a reasonable enantiomeric excess for the *catalytic* intermolecular PKR of 28 % ee, albeit with poor yield. A proposed explanation for this poor activity observed could be that such an electron rich diphosphine as MaxPHOS provided a very electron rich dicobalt nucleus which in turn makes for very strong CO-Co binding. Although not the rate-determining step, it has been shown that the release of CO from the cobalt cluster is a very important step in the reaction mechanism of the PKR and if the energy barrier is too great, activity is negatively affected.¹³

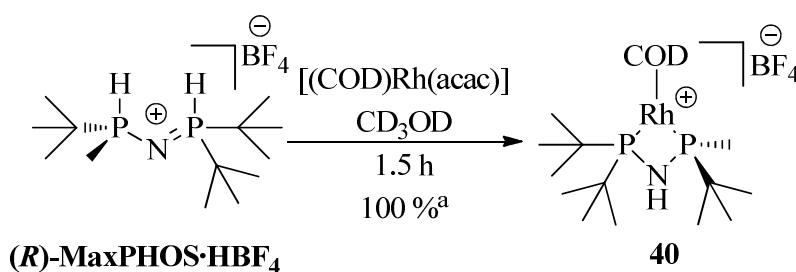
In chapter 2 titled background (page 40, scheme 2.25), the method of preparing the [(MaxPHOS)Rh(COD)]BF₄ complex **40** was outlined. It involved stirring the MaxPHOS·HBF₄ phosphonium salt, one equivalent of [Rh(COD)₂]BF₄ with one equivalent of Na₂CO₃ in THF. The THF was removed in *vacuo* after stirring overnight, the resulting residue was suspended in DCM and filtered to remove the insoluble salts which had formed. The filtrate was then reduced in *vacuo* once again and the orange residue was recrystallized. A cleaner and more efficient preparation of the MaxPHOS-rhodium catalyst was desired.

Scheme 4.7: The method developed by M. Revés to prepare MaxPHOS-rhodium catalyst complex.



A complexation test was carried out by shaking one equivalent of MaxPHOS·HBF₄ salt and one equivalent of [(COD)Rh(acac)] dissolved in deuterated methanol in an NMR tube and intermittently performing ³¹P NMR experiments to monitor the reaction. It was found that within 1.5 hours of the two components of the reaction having been added together in CD₃OD that no more starting material remained and complex had cleanly formed.

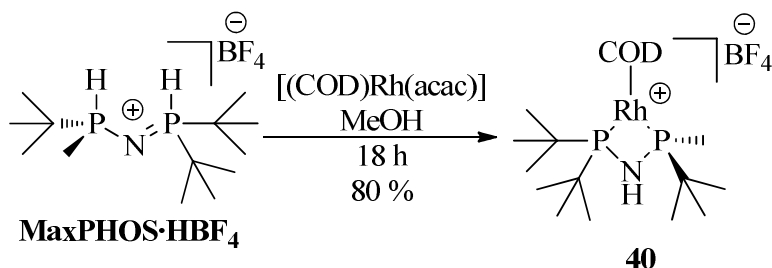
Scheme 4.8: A ³¹P NMR monitored complexation test to form [(MaxPHOS)Rh(COD)]BF₄ complex *via* [(COD)Rh(acac)].



^a 100 % conversion was confirmed by ³¹P NMR by complete absence of characteristic starting material peaks.

And so it was discovered that using commercially available [(COD)Rh(acac)] as the source of rhodium provided a faster and cleaner complexation of MaxPHOS ligand to rhodium metal. Using [(COD)Rh(acac)] negates the need for base be it organic or inorganic as in essence the displaced acetylacetonate ligand serves as a base to deprotonate the phosphonium salt and the BF₄ counterion is already conveniently present as part of the MaxPHOS salt which can be transferred to the resulting MaxPHOS-Rh complex.

Scheme 4.9: An optimised route to the [(MaxPHOS)Rh(COD)]BF₄ hydrogenation catalyst.

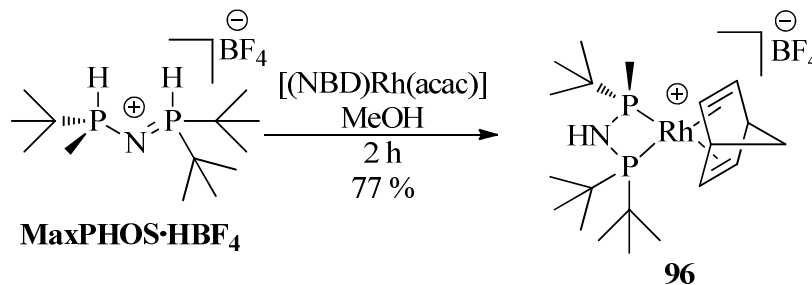


4. *P*-stereogenic aminophosphine ligands

An advantage to the use of [(COD)Rh(acac)] as the source of rhodium for the formation of the complex was that without the addition of an inorganic base such as Na₂CO₃ which was used previously to form the pre-formed MaxPHOS-Rh catalyst complex, the inorganic salts NaBF₄ and NaOH did not form as side products and so they did not need to be filtered from the catalyst complex. The reaction could be let stir overnight, the following morning solvents were removed in *vacuo*, recrystallization by means of a layering process between CH₂Cl₂ and diethyl ether was carried out and pure crystals of MaxPHOS rhodium catalyst were obtained in good yield as shown in scheme 4.9.

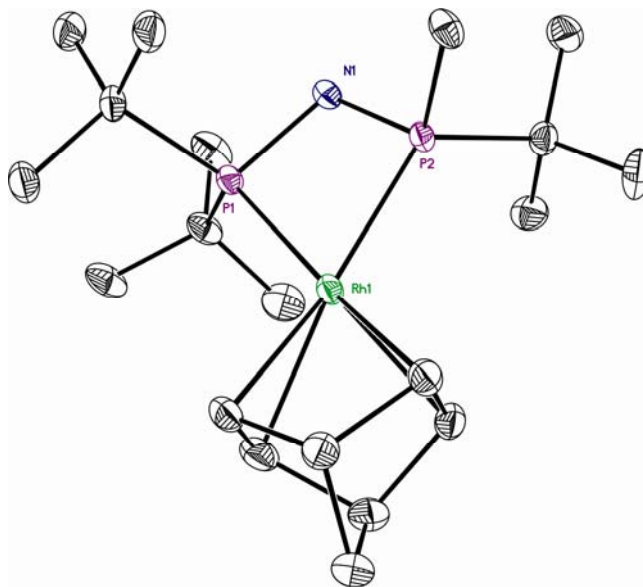
The [(MaxPHOS)Rh(NBD)]BF₄ was prepared in a similar fashion. The MaxPHOS·HBF₄ phosphonium salt was stirred overnight with [(NBD)Rh(acac)] in MeOH however upon the removal of MeOH after 18 hours stirring and an ¹H NMR experiment only degradation could be appreciated. It was noted that the reaction was very fast and could not be allowed to stir for excessive time without decomposition.

Scheme 4.10: The preparation of the [(MaxPHOS)Rh(NBD)]BF₄ catalyst complex.



Upon removal of the MeOH under *vacuo* after 2 hours stirring a recrystallization was carried out whereby it was dissolved in minimum dichloromethane in a schlenk tube, which was frozen at − 90 °C, excess Et₂O was layered on top and the schlenk was placed in the fridge to slowly warm up and slowly form crystals. Crystals suitable for X-ray crystallography were obtained.

Figure 4.2: ORTEP drawing of [(NBD)Rh(MaxPHOS)]BF₄ complex **96**. Protons are omitted for clarity. Purple phosphorus, blue nitrogen, green rhodium.



The crystallographic data provided no surprises and showed the complex as exactly it would have been expected. Little to no difference was noted between the MaxPHOS-Rh-COD and the MaxPHOS-Rh-NBD complexes as the change in ligand made virtually no change to P-Rh bond lengths or the P-Rh-P bite angle.

The norbornadiene ligand did however burden the MaxPHOS rhodium complex with instability more than likely due to its poor coordinating nature in comparison with 1,5-cyclooctadiene and so the complex is poorly bench stable and if left in open air for several hours, quickly decomposes. For the complex to be stored without decomposition it needed to be stored under inert atmosphere at low temperature.

4.2 Examining the electronic nature of the MaxPHOS ligand

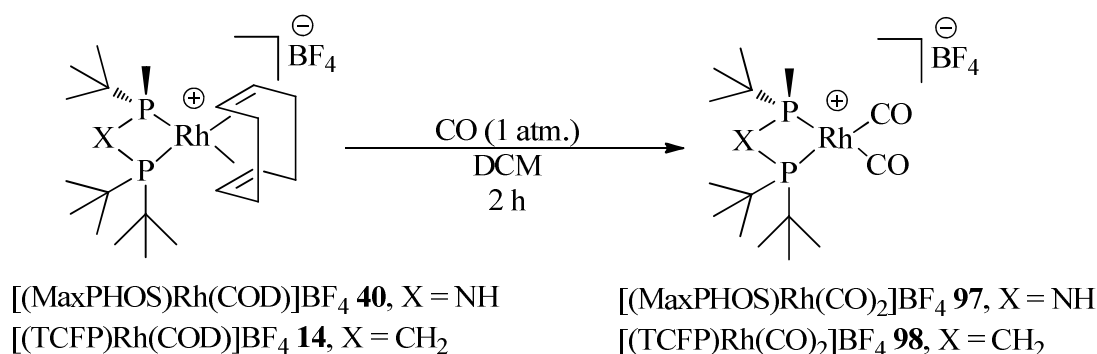
4.2.1 Examination of carbonyl stretching frequencies

To obtain an understanding of the electronic nature of the phosphine moieties of the MaxPHOS ligand and their electron donating character we wished to form the [(MaxPHOS)Rh(CO)₂]BF₄ complex and observe the carbonyl stretching frequencies by IR spectroscopy. This was carried out by stirring the [(MaxPHOS)Rh(COD)]BF₄ complex **40** for 2 hours in dichloromethane while bubbling CO through the round bottom flask *via* a CO filled balloon, an immediate colour change from orange to yellow was appreciated. After

4. *P*-stereogenic aminophosphine ligands

removal of solvents in *vacuo* and washing of the obtained residue with diethyl ether the complex was examined by IR. The same procedure was followed to examine the carbonyl stretching of the trichickenfootphos (TCFP) ligand by bubbling CO through the commercially available [(TCFP)Rh(COD)]BF₄ complex stirred in DCM. This was intended to act as a yardstick from which to compare our MaxPHOS ligand. Table 4.1 shows the recorded CO stretching frequencies for the MaxPHOS and TCFP rhodium complexes while also including those of MeDuPHOS, BINAP and DIOP as reported.¹⁴

Table 4.1: Displacement of cyclooctadiene and insertion of carbon monoxide into MaxPHOS and TCFP rhodium complexes.



Complex	ν_{CO} symmetric (cm ⁻¹)	ν_{CO} antisymmetric (cm ⁻¹)
$[(\text{R-MaxPHOS})\text{Rh}(\text{CO})_2]\text{BF}_4$	2091	2046
$[(\text{TCFP})\text{Rh}(\text{CO})_2]\text{BF}_4$	2085	2040
$[(\text{R,R})\text{-MeDuPHOS})\text{Rh}(\text{CO})_2]$	2089	2045
$[(\text{R})\text{-BINAP})\text{Rh}(\text{CO})_2]$	2097	2051
$[(\text{S,S})\text{-DIOP})\text{Rh}(\text{CO})_2]$	2102	2046

The carbonyl stretching was obtained immediately after complex formation by FT-IR using KBr disc method.

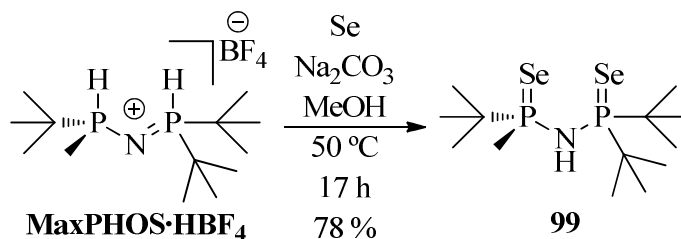
The carbonyl stretching frequencies noted for the MaxPHOS complex **97** were observed to be only slightly higher than the TCFP complex **98**, with as little as 6 cm⁻¹ in the difference. This could be reasoned intuitively as changing a CH₂ group for a more electron withdrawing NH group would serve to inductively withdraw electron density from the phosphine moieties resulting in less electron donation from the phosphine sp³ lone pairs into the metal centre, reducing the metal back-bonding into CO anti-bonding orbitals providing carbon monoxide

groups with higher stretching frequencies.¹⁵ It is interesting to note the similarity of the CO stretching of the MaxPHOS and MeDuPHOS Rh complexes.

4.2.2 Examination of $J(^{31}\text{P}-^{77}\text{Se})$ coupling frequencies

Another accepted method to quantify and compare the σ -donating capacity of the phosphine lone pair is by the preparation of the seleniated analogue and examination of the $J(^{31}\text{P}-^{77}\text{Se})$ coupling present in the ^{31}P NMR spectra.¹⁶ It is known that the phenomenon of J coupling observed in NMR spectra is brought about by the Fermi-contact interaction of nuclear moments and electron spins in s orbitals.¹⁷ It has been described that the phosphorus-selenide bond shows very little $\text{P}_{3d\pi}\text{-Se}_{4d\pi}$ character¹⁸ and so nearby electronegative groups according to Bent's Law¹⁹, lower the energy of the phosphine lone pair and increase the probability of the electron density residing in the $3s$ orbital, showing more s character and in turn influencing the $J(^{31}\text{P}-^{77}\text{Se})$ coupling values. Because ^{77}Se is only 7.63 % abundant and is the only selenium isotope observable by NMR the $J(^{31}\text{P}-^{77}\text{Se})$ coupling constants are ascertained from the satellite peaks produced on the phosphorus peaks in the ^{31}P NMR. The preparation of the MaxPHOS diselenide was facile and was prepared from the MaxPHOS· HBF_4 phosphonium salt.

Scheme 4.11: The MaxPHOS· HBF_4 phosphonium salt was seleniated through reaction of an excess of inorganic base (5 eq.) and elemental selenium (5 eq.), with heating in methanol.

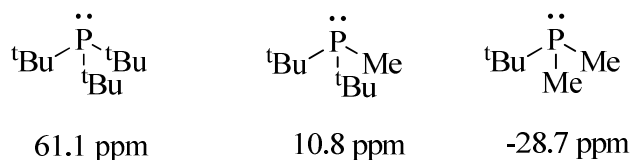


The preparation outlined in scheme 4.11 converted the MaxPHOS· HBF_4 phosphonium salt into the highly apolar and UV active diselenide **99**. The ^{31}P NMR was

4. *P*-stereogenic aminophosphine ligands

examined and the $J(^{31}\text{P}-^{77}\text{Se})$ values were obtained. The TCFP diselenide was also prepared by first following the racemic procedure outlined by Hoge *et al.* to prepare and isolate TCFP-BH₃ which was later simultaneously deprotected of BH₃ and seleniated in a one-pot reaction to form the diselenide **100**.²⁰ The $J(^{31}\text{P}-^{77}\text{Se})$ coupling of diselenide TCFP **100** was observed from its ³¹P NMR spectra and is annotated in table 4.2 (page 93). The $J(^{31}\text{P}-^{77}\text{Se})$ value obtained for the BINAP diselenide was taken from the literature and was included out of interest.²¹ The ³¹P NMR spectrum of compound **99** shows two doublets, one at 99.25 ppm which would correspond to the di-*tert*-butyl phosphorus and another at 84.12 ppm which would correspond to the methyl-*tert*-butyl phosphorus, if the trend of alkyl phosphines applies by which increasingly bulky groups increase the chemical shift in the ³¹P NMR spectra.²²

Figure 4.3: ³¹P NMR trend for alkyl phosphines.

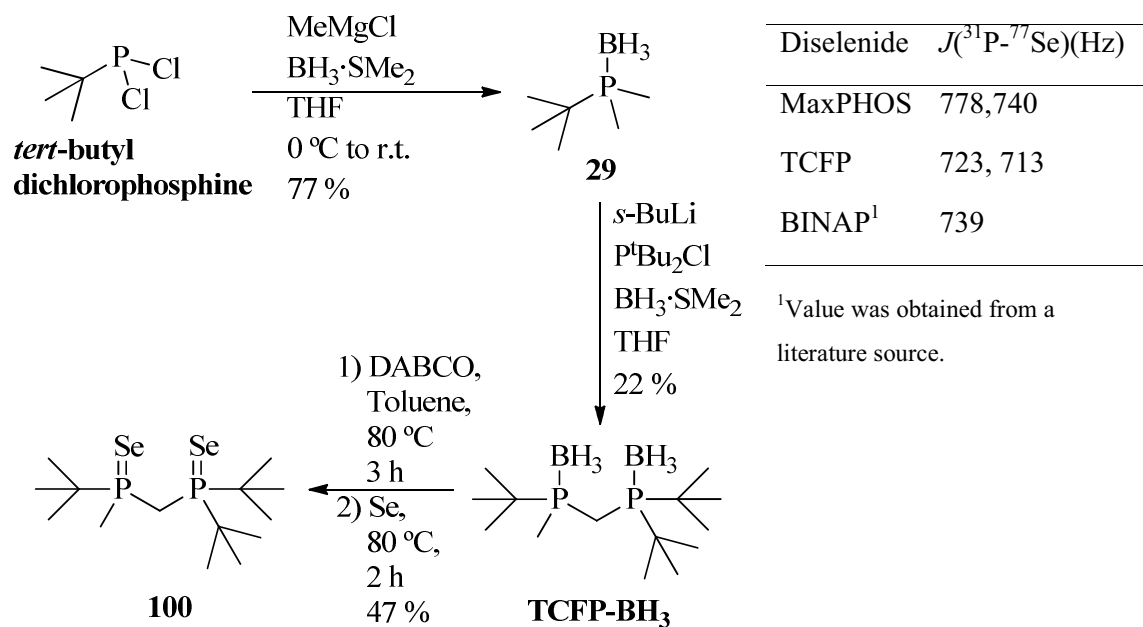


The peaks appear as doublets because each phosphine nucleus couples to the other. Each doublet has a set of ³¹P-⁷⁷Se satellite peaks and it is from these that we examine the $J(^{31}\text{P}-^{77}\text{Se})$ coupling peaks to infer information of the σ -donating character of the phosphorus atom. The satellite peaks corresponding to the phosphorus atom represented by the doublet at 99.25 ppm show a $J(^{31}\text{P}-^{77}\text{Se})$ coupling value of 778 Hz whereas the satellite peaks corresponding to the phosphorus represented by the peaks at 84.12 ppm show a $J(^{31}\text{P}-^{77}\text{Se})$ coupling value of 740 Hz, in the case of the MaxPHOS diselenide **99**.

The same trends could be seen emerging when the ³¹P NMR spectrum of the TCFP diselenide compound **100** was observed. Two doublets were observed, one at 72.24 ppm and another at 47.37 ppm corresponding to the di-*tert*-butyl phosphorus and the methyl-*tert*-butyl phosphorus respectively, pushed more upfield than their MaxPHOS counterparts due to the change of NH for CH₂. It was observed that the di-*tert*-butyl phosphorus peak at 72.24 ppm showed a $J(^{31}\text{P}-^{77}\text{Se})$ coupling of 723 Hz in its ³¹P-⁷⁷Se satellite peaks eluding to a

phosphorus atom which is considerably more σ electron donating than its MaxPHOS counterpart. The methyl-*tert*-butyl phosphorus peak at 47.37 ppm provided ^{31}P - ^{77}Se satellite peaks of 713 Hz of $J(^{31}\text{P}$ - $^{77}\text{Se})$ coupling energy again describing a phosphorus more σ donating than its MaxPHOS counterpart although though the disparity between the values was not as large as before

Table 4.2: The preparation of the TCFP diselenide and the values obtained for the $J(^{31}\text{P}$ - $^{77}\text{Se})$ coupling of the MaxPHOS diselenide and the TCFP diselenide . Values obtained of same for the BINAP diselenide are also included as a point of reference.²³

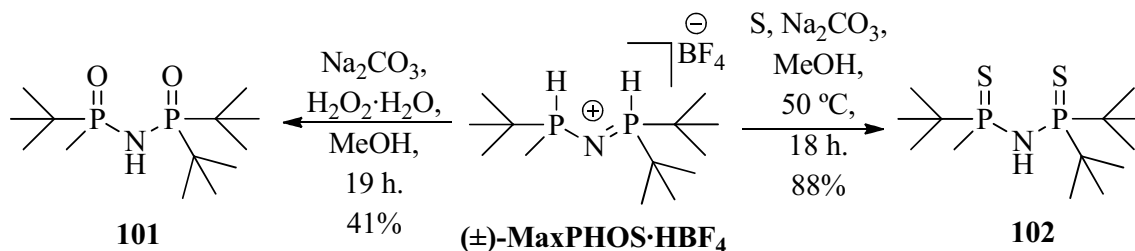


The MaxPHOS ligand is synthesized in its phosphonium salt form²⁴, a fact which prevents satisfactory analysis of the enantiomeric purity of the ligand by HPLC. Also up until this point, the isolation of the MaxPHOS ligand in its neutral state has not yet been achieved. Because of this it was thought that a chalcogenated derivative of the ligand such as **99** which can be prepared from the ligand by one simple step and is a neutral species could be in fact used to analyse the enantiomeric purity of the ligand by HPLC. To this end racemic

4. *P*-stereogenic aminophosphine ligands

diselenide MaxPHOS **99** was prepared and was analysed by HPLC but it was not possible to find suitable conditions to effectively separate the two enantiomers. The disulphide and the dioxide MaxPHOS derivatives were also prepared.

Scheme 4.12: The preparations of the racemic dioxide MaxPHOS derivative **101** and the racemic disulphide MaxPHOS derivative **102** are shown.



To prepare the dioxide MaxPHOS derivative **101**, MaxPHOS·HBF₄ phosphonium salt was reacted with an excess of Na₂CO₃ (3 eq.) and an excess of hydrogen peroxide (3 eq.) in MeOH overnight to provide the product as a clear oil after aqueous workup and flash column chromatography. The disulphide MaxPHOS derivative **102** was prepared in much the same manner however it was necessary to heat the reaction to 50 °C. The preparations of the neutral chalcogenated MaxPHOS derivatives were straight forward however their analysis by HPLC was not. For suitable HPLC separating conditions could be found for neither the dioxide derivative **101** nor the disulphide derivative **102**.

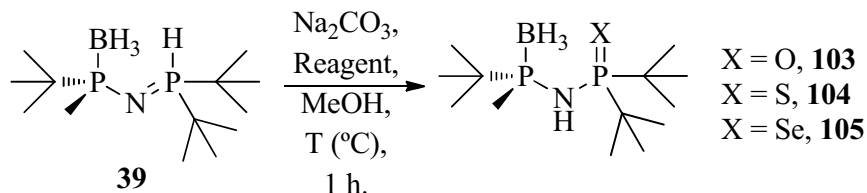
4.3 Derivatives of MaxPHOS-BH₃ as ligands

4.3.1 The preparation of the mono-chalcogenated MaxPHOS derivatives

It was proposed to form new chiral ligands for asymmetric metal catalysis by the derivitization of the borane protected MaxPHOS ligand intermediate, MaxPHOS-BH₃ **39**. It was thought that by subjecting MaxPHOS-BH₃ **39** to the same conditions as were applied to the MaxPHOS ligand to form its diselenide as described in scheme 4.11 (page 91), a single

chalcogen atom could be introduced onto the phosphorus atom free of borane while the borane protected phosphorus would remain just so, protected. This was proven to be the case as outlined in table 4.3.

Table 4.3: “Chalcogenization” of MaxPHOS-BH₃.



Entry	Reagent ^a	T. (°C)	X	Yield (%) ^b	Product
1	H ₂ O ₂ ·H ₂ O	r.t.	O	62	103
2	S	50	S	85	104
3	Se	50	Se	85	105^c

^a 3 equivalents of the reagent were used. ^b After flash column chromatography. ^c The opposite configuration of **39** to that described was used (*S*-(+)-MaxPHOS-BH₃).

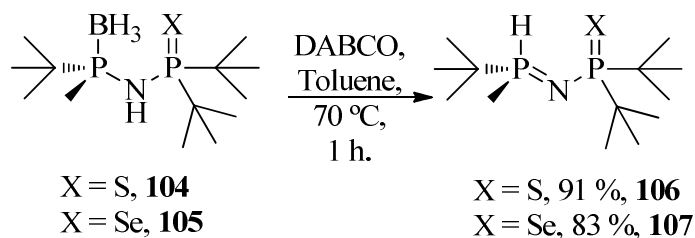
Reacting MaxPHOS-BH₃ in the presence of Na₂CO₃ to ensure deprotonation of the hydrogen protecting the phosphorus atom with subsequent addition of H₂O₂·H₂O provided oxidation of the phosphorus to give compound **103** after a filtration over a short pad of silica in a 62 % yield. MaxPHOS-BH₃ was reacted similarly with Na₂CO₃ and elemental sulphur and also with Na₂CO₃ and elemental selenium at 50 °C to form compounds **104** and **105** respectively as seen in entries 2 and 3 of table 4.3, both in yields of 85 % obtained after flash column chromatography. It could be appreciated from ¹H NMR upon examination of the three mono-chalcogenated compounds **103**, **104**, and **105** that the introduction of the chalcogen atom onto the phosphorus served to push the ¹H signals of the *tert*-butyl groups and the methyl group further downfield in comparison with MaxPHOS-BH₃ **39**. It was noted that selenium displaced the ¹H signals further downfield than did sulphur, which in turn pushed the ¹H signals further downfield than did oxygen. This alludes to a trend which could perhaps be considered counter-intuitive as it goes against the trend of electronegativity but it is a trend which has been noted elsewhere in the literature with similar species.²⁵

To test the removal of the borane moiety the first option to try was the base DABCO. It was found that compounds **104** and **105** could both easily be freed from borane under standard reaction conditions. Stirring the phosphine with 3 equivalents of the base DABCO at 70 °C in

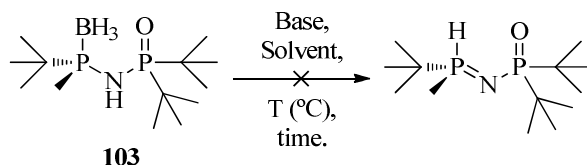
4. *P*-stereogenic aminophosphine ligands

toluene under inert conditions for an hour would reveal by TLC the absence of starting material.

Scheme 4.12: The deprotection of the diphosphines **104** and **105** of borane *via* the base DABCO.



Upon the confirmation by TLC that no starting material remained, the solvent was removed *in vacuo* and the products **106** and **107** were obtained in excellent yield after flash column chromatography. Once the products were isolated ^1H NMR confirmed the obtained phosphines existed in their tautomeric state whereby the methyl-*tert*-butyl phosphine was protonated, this could be understood in the case of **106** from the presence of a doublet signal in the 6.6 ppm region of the ^1H NMR spectrum with a large $J(^{31}\text{P}-^1\text{H})$ coupling constant of 442.4 Hz, with each peak of the doublet existing as an apparent quintet due to the proximity of a methyl group and another phosphorus a nitrogen atom away to which it also coupled to. It was judged to exist mainly in this tautomeric state at room temperature as the existence of an NH group could not be appreciated by ^1H NMR. The same was observed by ^1H NMR when the compound **107** was examined whereas its $J(^{31}\text{P}-^1\text{H})$ coupling constant value was ever so slightly larger at 446.3 Hz. It is thought it is the tautomeric nature of these compounds **106** and **107** which makes them bench-stable solids where degradation or oxidation is not appreciated by ^1H or ^{31}P NMR when they are left stored in a sample vial under air for large periods of time, just as the MaxPHOS $\cdot\text{HBF}_4$ phosphonium salt.

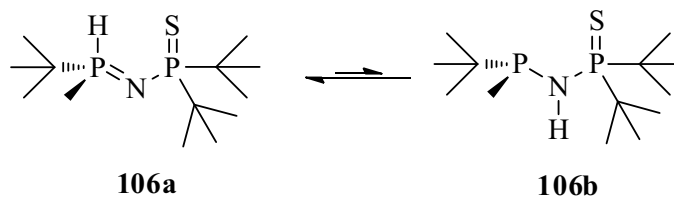
Table 4.4: The attempts made to deprotect the compound **97** of borane are shown.

Entry	Base	Solvent	T (°C)	Time (h)	Result ^a
1	DABCO ^b	Toluene	70	1	unable to isolate
2	NHEt ₂ ^c	THF	60	17	starting material

^aJudged by ¹H NMR. ^b 3 equivalents were used. ^c 10 equivalents were used.

It was found similarly that when the oxidized diphosphine **103** was subjected to the same procedure, namely stirring in toluene with 3 equivalents of DABCO base in inert atmosphere for an hour, deprotection of borane could be deduced to occur through observation by TLC. However unlike compounds **106** and **107** whose retention factors had been moderate, rising half way up the TLC plate in a solvent system of 8:2 (hexane: ethyl acetate), compound **103** deprotected of borane had a much more polar RF. which co-eluted with borane-bound DABCO on the TLC plate and in the column which made its purification extremely difficult.

The tautomerization of the compound **106** was examined by temperature dependent ¹H and ³¹P NMR whereby spectra were taken at room temperature, then at 40 °C and later at – 20 °C. No shift in equilibrium of the tautomerization could be observed, at high temperature the peaks simply appeared broader and at low temperature the peaks appeared more defined such as the P-H doublet of apparent quintets. Especially in the low temperature ¹H NMR experiment in the 2.12 ppm region, extra *tert*-butyl peaks could be appreciated to some degree suggesting the presence of a small amount of the **106b** tautomer.

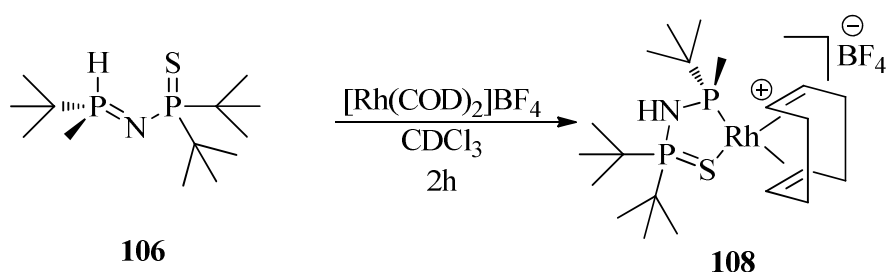
Figure 4.4: Tautomerization of the sulphide-MaxPHOS compound **98**.

4. *P*-stereogenic aminophosphine ligands

4.3.2 The mono-chalcogenated MaxPHOS derivative metal complexes

Upon the isolation of the mono-chalcogenated MaxPHOS derivatives **106** and **107** it was considered interesting to investigate their coordination behaviour towards certain metal atoms such as rhodium, palladium and cobalt. As before coordination tests were carried out by mixing the reactants in an NMR tube and following the complexation process by ^1H and ^{31}P NMR.

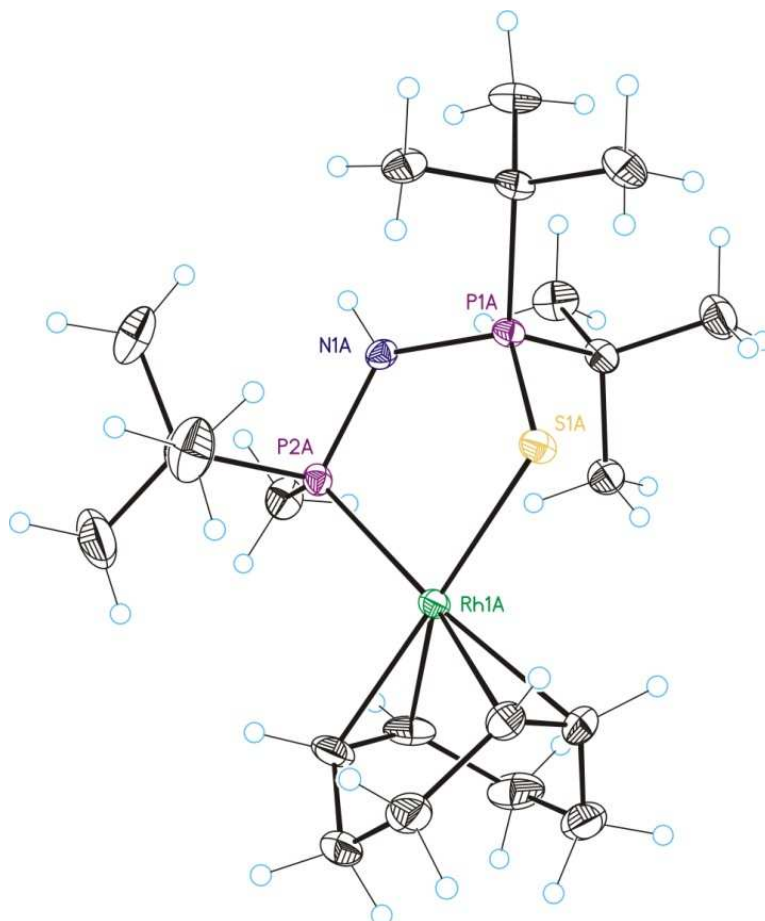
Scheme 4.13: The mono-sulphide MaxPHOS compound **106** was coordinated to rhodium.



Two hours after the rhodium complex and the ligand had been mixed in deuterated chloroform, it could clearly be appreciated by ^{31}P NMR that a clean complexation process had taken place. The two peaks, one lying at 86.54 ppm corresponding to the methyl-*tert*-butyl phosphine bearing hydrogen and further upfield at 27.40 ppm for the sulphide bearing di-*tert*-butyl phosphine of the starting material **106** had given away to reveal a new set of peaks downfield in the spectrum. The free phosphine as a result of being bound to rhodium formed a double-doublet and was pushed downfield, now residing at 113.04 ppm (dd, $J = 153.1, 21.0$ Hz). The sulphide-phosphine was pushed even further downfield, moving from 27.40 ppm in the starting material to form a double-doublet at 115.80 ppm (dd, $J = 21.0, 3.2$ Hz), being split much less than the directly metal-bound phosphine due to the metal now being one atom away. The *tert*-butyl groups of the ^1H NMR were also observed to have shifted downfield, revealing a doublet at 1.64 ppm (d, $J = 7.1$ Hz, 3H), a double-doublet at 1.49 ppm (dd, $J = 16.8, 3.3$ Hz, 18H) and another doublet at 1.27 ppm (d, $J = 15.6$ Hz, 9H), corresponding to the methyl group, and the three *tert*-butyl groups respectively.

The complex was purified by removal of solvents in *vacuo*, washing with hexane, removal of supernatant and once again drying in *vacuo*. Crystals suitable for X-ray crystallography were formed by layering Et_2O over the complex dissolved in minimum dichloromethane.

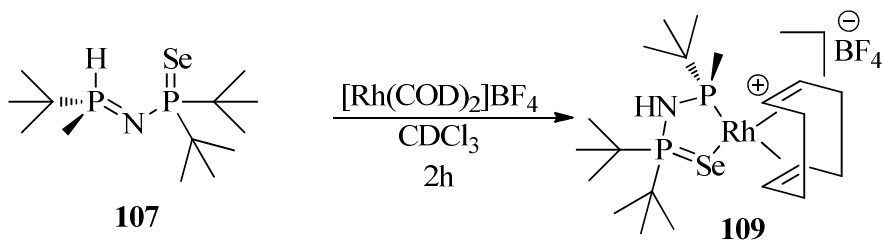
Figure 4.5: ORTEP drawing of the rhodium complex **108**. The counterion was omitted for clarity.



The X-ray data of the complex **108** unveiled a crystallographic structure bearing a 5-membered ring around the metal centre mimicking an envelope type conformation with a dihedral angle of -22.390° with rhodium sticking out of the plane. The P-Rh bond was shown to be 2.28 \AA , significantly shorter than the equivalent bond in the $[(\text{MaxPHOS})\text{Rh}(\text{COD})]\text{BF}_4$ complex which was 2.34 \AA . The S-Rh bond length was 2.39 \AA , the P-S bond was 2.01 \AA , it made a bite angle around the metal of course much larger than the MaxPHOS complex at 87.5° as opposed to the 70° bite angle observed in $[(\text{MaxPHOS})\text{Rh}(\text{COD})]\text{BF}_4$. It made a P-N-P bond angle of 121° , again as would be expected, significantly larger than that of the MaxPHOS complex mentioned earlier which bore a P-N-P bond angle of 103° .

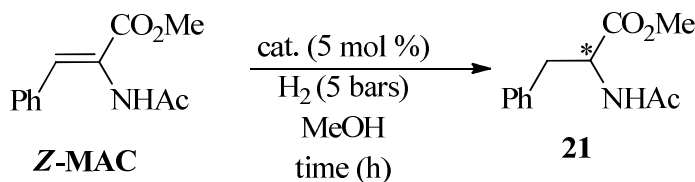
4. *P*-stereogenic aminophosphine ligands

Scheme 4.14: The coordination of the Seleniated MaxPHOS derivative **107** to rhodium.



The seleniated MaxPHOS derivative **107**'s coordination to rhodium was also tested and was shown to coordinate just as readily as the sulphide-MaxPHOS derivative **106**. An observation of note from the ^{31}P NMR of the complex **109** was that the rhodium bound phosphorus peaks appeared pushed further downfield at 115.68 (dd, $J = 154.1, 25.0$ Hz) than the selenide phosphine which appeared at 110.69 (dd, $J = 24.9, 3.4$ Hz), being somewhat opposite in nature to what was observed for complex **108** where the phosphorus-sulphide appeared further downfield.

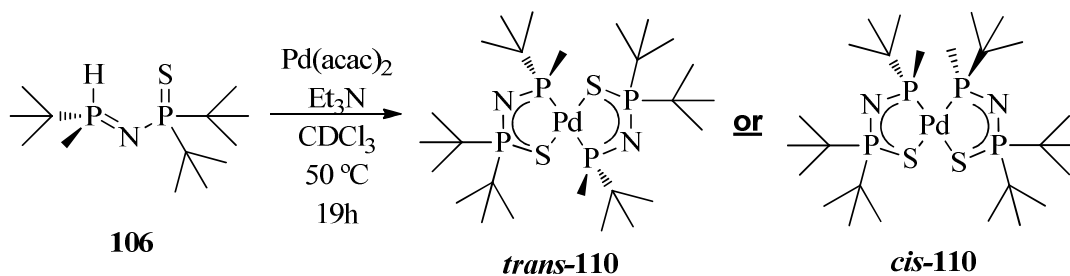
The rhodium complexes **108** and **109** were applied as chiral catalysts in the asymmetric hydrogenation of the dehydroamino acid *Z*-MAC under standard reaction conditions at first. At 5 bars of H_2 pressure the complex **108** could only catalyse the asymmetric hydrogenation of the *Z*-MAC substrate to a conversion of 20 % after 24 hours stirring. When the pressure was raised to 20 bars of hydrogen pressure full conversion to hydrogenated product was obtained but gave rise to an enantiomeric excess of only 21 %. The selenide complex **109** achieved almost the same result under the same conditions yielding a low 21 % enantiomeric excess.

Table 4.5: The hydrogenation of the substrate Z-MAC by the complexes **106** and **109**.

Entry	cat.	P. (bars H ₂)	t (h)	conversion (%) ¹	ee (%)
1	106	5	24	20	--
2	106	8	74	75	19
3	106	20	18	100	21
4	109	20	18	100	23

¹Judged by ¹H NMR. ² Judged by chiral HPLC.

The MaxPHOS-sulphide compound **106**'s capacity for coordination to palladium was tested just as before by mixing in an NMR tube in CDCl₃ and following the reaction by ¹H and ³¹P NMR and it was quickly noticed that at room temperature without additives, no reaction would occur. The absence of starting material peaks in the ³¹P NMR spectrum was finally noticed after the addition of Et₃N with heating overnight. It was also noted that a complex dimeric of ligand to metal had formed as the absence of metal coordinated acac ligand was noted in the ¹H NMR spectrum and also the peaks present in the ³¹P NMR exhibited a triplet signal at 124.63 ppm (t, *J* = 26.6 Hz) and another at 117.95 ppm (t, *J* = 27.3 Hz).

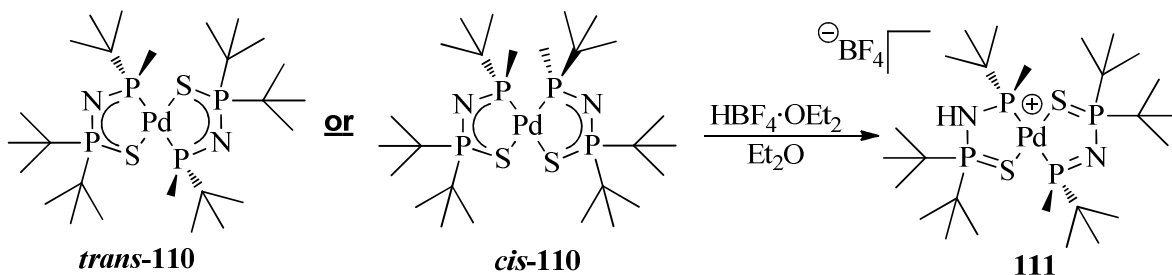
Scheme 4.15: The result of compound **106**'s coordination to palladium.

The triplet peak morphology observed in the ³¹P NMR spectrum suggested the phosphorus atoms were coupling to two distinct phosphorus atoms which could only be brought about by the formation of a mono nuclear complex bearing two ligands. The complex **110** obtained as described in scheme 4.15 exhibited an apolar nature similar to that of the PNSO-Rh-COD

4. *P*-stereogenic aminophosphine ligands

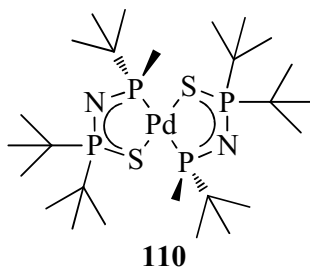
complex **73** (section 3.1), rising high up the TLC plate during thin layer chromatography with an RF of 0.7 in a mobile phase solvent system of 8:2 (hexane: ethyl acetate) and so it was assumed as before that it was a neutral complex. It was decided to protonate as before with $\text{HBF}_4 \cdot \text{OEt}_2$ to form a salt species from which X-ray crystallographic crystals could be grown to confirm absolutely the ligands' coordination mode to the metal centre.

Scheme 4.16: The complex **110** was protonated to form a cationic species.



The palladium complex **110** was stirred in Et_2O and to it was added drop wise $\text{HBF}_4 \cdot \text{OEt}_2$. Upon the addition of 1 equivalent of the acid a precipitate immediately formed and was isolated. Crystals were grown for X-ray analysis once again by dissolution in minimum methylene chloride with the slow layering on top of Et_2O . The crystallographic data confirmed it was the complex **111** which had formed which in turn implied it was in fact the *trans* C_2 symmetric complex **110** which had formed in the process outlined in scheme 4.15. It should be noted that upon protonation of the complex **110** only one nitrogen atom was protonated before its precipitation, breaking its symmetry and rendering it a C_1 symmetric complex.

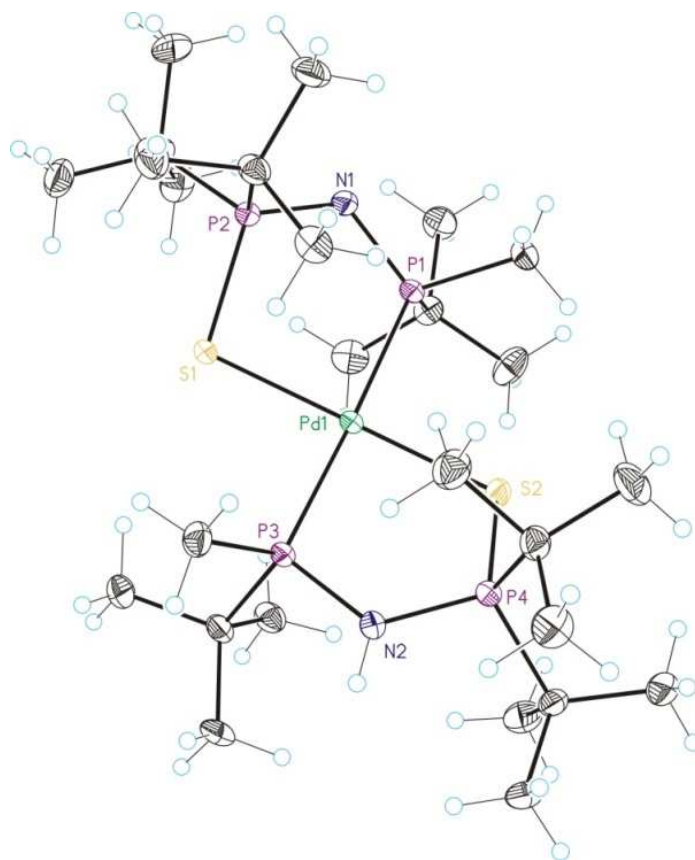
Figure 4.4: The *trans* arrangement was determined to be the true structure of the neutral bis-S-MaxPHOS-Pd complex **110**.



What was presented in the crystallographic data was that the ligands had taken up a *trans* conformation around the square planar Pd (II) core. Two 5-membered rings were closed

around the metal centre, taking up once again envelope conformations, the ring bearing the NH group possessing a torsion angle of -18.4° while the other exhibited a torsion angle of -20.9° . The crystal structure showed Pd-P bonds which were not entirely symmetrical, the phosphine bonded to Pd and NH showed a Pd-P bond length of 2.31 \AA while the other was 2.33 \AA in length, the NH perhaps releasing more electron density to strengthen and shorten the nearby P-Pd bond. Also it was noted that these bonds were clearly longer than the P-Pd bond lengths of the $[(\text{MaxPHOS})\text{Pd}(\text{acac})]\text{BF}_4$ complex which were recorded at 2.23 and 2.24 \AA . The P-Pd-S bite angles were recorded at 90.6° on the side bearing NH and slightly smaller on the other side at 88.3° . The average P-NH bond length was 1.68 \AA whereas the average P-N bond length 1.61 \AA indicating its greater double bond character.

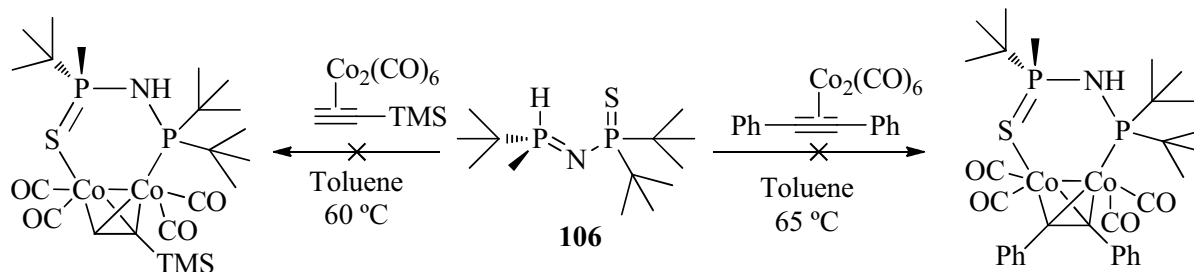
Figure 4.5: The ORTEP drawing of the palladium complex **111**.



It was also attempted to coordinate the sulphide-MaxPHOS derivative **106** to cobalt carbonyl-alkyne cluster for potential application in the asymmetric Pauson-Khand reaction but the attempts were unsuccessful.

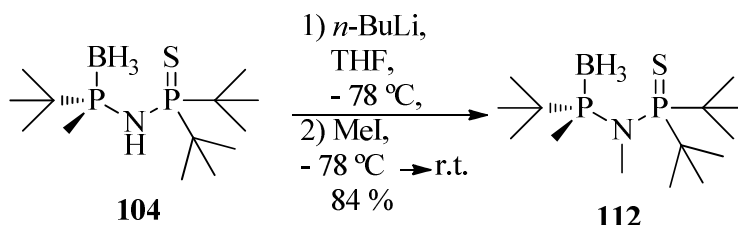
4. *P*-stereogenic aminophosphine ligands

Scheme 4.17: Attempts to coordinate the sulphide-MaxPHOS **106** to a cobalt-alkyne cluster were unsatisfactory.



When the attempted coordination of the ligand **106** to the cobalt clusters were carried out, examination of the reactions by TLC disappointingly gave a very complicated mixture of products with starting material remaining also. An assumption was made relying on prior experience in the laboratory of these types of coordination reactions that perhaps the secondary amine functionality of the ligand was detrimental to the reaction. It was proposed to remove that functionality by methylating the NH functional group of the borane protected sulphide-MaxPHOS precursor **104** and subsequently deprotecting of borane to form the methylated sulphide-MaxPHOS derivative.

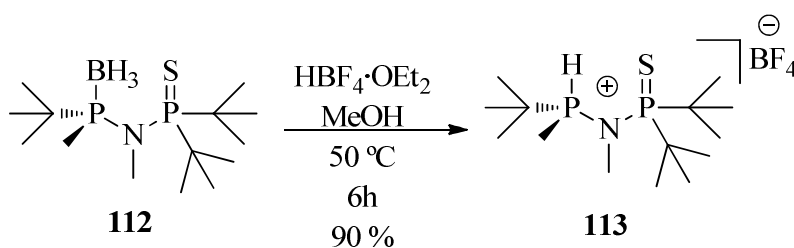
Scheme 4.18: The borane-protected sulphide-MaxPHOS derivative **104** was methylated on nitrogen in good yield.



The methylation reaction proceeded in good yield and was monitored by TLC, observing the disappearance of starting material and the appearance of a spot on the TLC plate of ever so slightly higher *R_F*. Pure compound **112** was isolated after aqueous work-up and flash column chromatography. The extra methyl group could be appreciated in the ¹H NMR of the product **112** hidden amongst the signal of the twin *tert*-butyl groups of the sulphide-phosphine at 1.36 (dd, *J* = 16.3, 6.9 Hz, 21 H). The introduction of the methyl group served to push the signals in the ³¹P NMR from 98.05 ppm (d, *J* = 41.3 Hz) and 85.85 – 83.03 ppm (m) further upfield to 59.24 ppm (d, *J* = 24.0 Hz) and 58.74 – 56.06 ppm (m) respectively.

The deprotection of the borane moiety from the compound **112** was initially tested using the DABCO base (3 equivalents) once again, carrying the reaction out in an NMR tube and following its progression by ^{31}P NMR. The reaction did not progress after heating at 65 °C in CDCl_3 for 19 hours, only starting material could be appreciated by examination of the ^{31}P NMR spectrum. Solvents were removed in *vacuo* and the reaction was carried out in toluene so it could be heated at higher temperature. No deprotection of the borane group was observed by monitoring of the reaction by TLC while heating at 80 °C. It was obvious once again, just as in the case of similar *N*-Me containing molecule **78-BH₃** (section 3.2), that deprotection of the borane moiety was not possible using the DABCO reagent. The nearby methyl group makes the phosphine-borane bond too basic to be removed by this reagent.

Scheme 4.19: The removal of the borane moiety from the *N*-methylated sulphide-MaxPHOS derivative **112** by the acid $\text{HBF}_4\cdot\text{OEt}_2$.



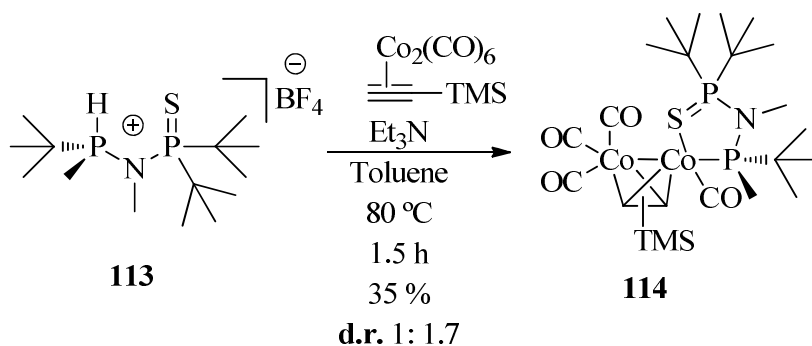
It was decided to attempt the removal of the borane group of the compound **112** by the acid $\text{HBF}_4\cdot\text{OEt}_2$. It was clear from examination by TLC that after 6 hours of stirring compound **112** in MeOH at 50 °C with 5 equivalents of the $\text{HBF}_4\cdot\text{OEt}_2$ acid that no starting material remained. After a basic work up and extraction, pure product could be isolated as a white solid. The ^{31}P NMR confirmed the removal of the borane group as the four spread out peaks of the phosphine-borane signal at 58.74 – 56.06 ppm in the spectrum of the starting material **112** had given away to reveal a very well-defined doublet pushed downfield at 73.42 ppm (d, $J = 35.0$ Hz). The sulphide-phosphine signal was also a well-defined doublet pushed much farther upfield at 27.38 ppm (d, $J = 35.1$ Hz). From the ^1H NMR it was clear the deprotected phosphine had been protonated as a double-doublet appeared downfield at 7.22 (dd, $J = 490.8, 4.2$ Hz, 1H), with a very large J coupling constant characteristic of a protonated phosphonium cation. The ^{19}F NMR spectrum confirmed the presence of a BF_4 counterion and the retention factor under TLC scrutiny proved the phosphonium salt nature of the compound.

4. *P*-stereogenic aminophosphine ligands

The coordination of the *N*-methylated sulphide-MaxPHOS derivative **113** to a cobaltcarbonyl-alkyne cluster was attempted anew. Monitoring by TLC it became apparent the reaction proceeded more cleanly and satisfactorily using the *N*-methylated ligand **113**. After stirring and heating for 1.5 hours, the solvent was removed in *vacuo* and the product was obtained as a 1:1.7 mixture of diastereomers as confirmed by ^1H NMR. It was FT-IR spectroscopy which was used to confirm the coordination mode of the ligand to the cobalt cluster as it became apparent from the aspect of the carbonyl peaks observed that the ligand was in fact coupling through phosphorus and sulphur to a single cobalt atom. A small peak was observed at 1943 cm^{-1} , a large peak at 1983 cm^{-1} with a medium sized peak at 2044 cm^{-1} .

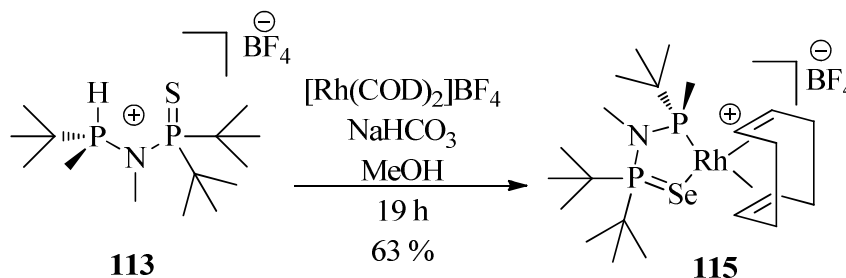
It was known from experience in the group and also when held in comparison with the MaxPHOS-cobalt carbonyl complexes **90** and **91** that cobalt carbonyl alkyne complexes bearing bidentate ligands bound to the cluster through each cobalt atom show FT-IR spectrums where four separate signals for each CO can be appreciated in the $1900\text{-}2020\text{ cm}^{-1}$ region. Through the experience gained in our group with regards to these types of complexes as applied to the asymmetric Pauson-Khand reaction it was considered that alkyne cobalt cluster-ligand complexes bearing the mode of coordination exhibited by **114** are not preferable especially considering the low diastereoselectivity in the ligand's coordination to the cluster.

Scheme 4.20: The *N*-methylated sulphide-MaxPHOS derivative **113** was coordinated to the trimethylsilane substituted alkyne cobalt carbonyl cluster.



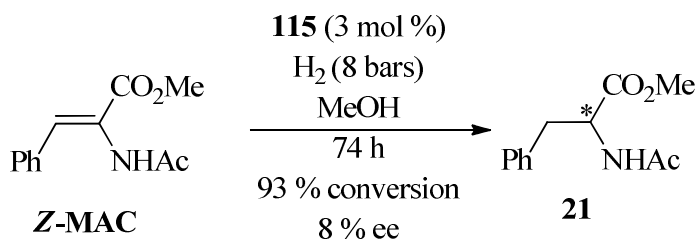
The phosphonium salt ligand **113** was also coordinated to rhodium. It was reacted with NaHCO_3 and $[\text{Rh}(\text{COD})]\text{BF}_4$ overnight in MeOH to give the expected complex as an orange solid upon isolation after a filtration of the inorganic salts and recrystallization.

Scheme 4.21: The *N*-methylated sulphide-MaxPHOS derivative **113** was complexed with rhodium.



The rhodium complex **115** was applied as catalyst in the asymmetric hydrogenation of the *Z*-MAC substrate. The rhodium complex **115** was found to give very poor enantiomeric excess at the first attempt failing even to give full conversion to hydrogenated product at 3 mol % of catalyst loading with 8 bars of hydrogen pressure and so was not tested further as catalyst in the asymmetric hydrogenation reaction.

Scheme 4.22: Complex **115** was used as the catalyst in the asymmetric hydrogenation of the *Z*-MAC substrate.

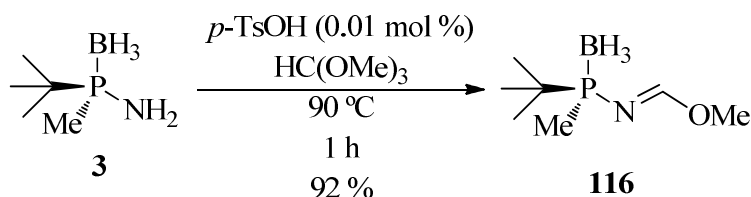


4.4 Towards the synthesis of C_1/C_2 P*-stereogenic amidine ligands

It was considered interesting to prepare chiral diphosphine ligands originating from another one of the key precursors in the preparation of the MaxPHOS ligand namely in this instance the aminophosphine **3**. It was proposed to use the methodology developed by Evans *et al.* as outlined in scheme 2.28 of chapter 2: background (page 44), to introduce an imidate group at the amine position, which would harbour an electrophilic centre with a good -OMe leaving group on which to hook another phosphine moiety yielding a preparation for another chiral diphosphine ligand.

4. *P*-stereogenic aminophosphine ligands

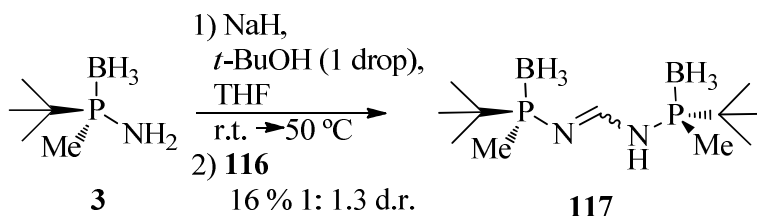
Scheme 4.23: The formation of an electrophilic imidate group on the amine functionality of the aminophosphine **3**.



The formation of the imidate group proceeded exceedingly well with almost quantitative yield and almost no need for purification with a clean and satisfactory ¹H NMR spectrum upon removal of the solvent/reagent in *vacuo*.

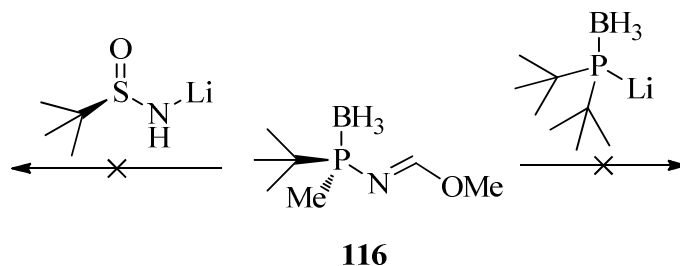
The phosphine **116** was reacted with another moiety of the aminophosphine **3** in an attempt to form a *C*₂ symmetric chiral diphosphine.

Scheme 4.24: The preparation of a *C*₂-symmetric diphosphine compound derived from the aminophosphine **3**.



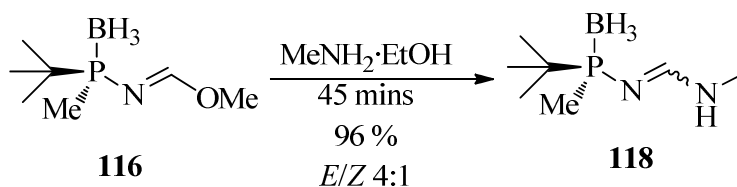
The anion formed on the aminophosphine **3** did not react satisfactorily well with the imidophosphine **116**. After acidic work up and purification by flash column chromatography a 16% overall yield as a 1:1.3 mixture of *Z/E* isomers were obtained where separation of the different isomers on the column was extremely difficult.

Scheme 4.25: Other attempts to react the imidophosphine **116** with a nucleophile were unsuccessful.



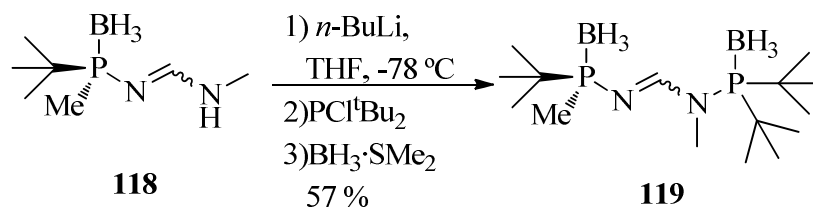
The imidophosphine **116** showed no reactivity towards the attack by a sulphinamide anion nor a phosphane anion but as described by Evans *et al.* the imidate moiety was reactive towards attack by methylamine yielding the amidine-phosphine **118** after an aqueous work-up in a *cis/trans* ratio of 1:4 as judged by ^1H NMR.²⁶

Scheme 4.26: The imidophosphine **116** readily reacted with the nucleophilic methylamine in a very clean and fast reaction to displace the methoxy group and replace it with the methylamine group.



The imidamide-phosphine **118** was then deprotonated at nitrogen to form a lithium coordinated anion by *n*-BuLi in the following reaction to add a di-*tert*-butyl phosphine moiety.

Scheme 4.27: A new borane protected diphosphine compound was prepared by coupling the amine moiety to di-*tert*-butyl phosphine.



4. *P*-stereogenic aminophosphine ligands

The diphosphine compound **119** was achieved in moderate yield after flash column chromatography. Subsequent reactions attempting to reduce the double bond of **119** using NaBH₄ and LiAlH₄ were never satisfactory nor were the attempts to reduce the double bond of **118** by NaBH₄ and so this line of research was left at this position.

4.5 Conclusions

In this chapter it has been described the coordination of the MaxPHOS ligand to form MaxPHOS-palladium **90** and MaxPHOS-cobalt **92** and **93** complexes. The MaxPHOS-cobalt complex **93** was tested in the catalytic asymmetric Pauson-Khand reaction with norbornadiene and two separate terminal alkynes, namely the phenyl substituted alkyne **94a** and the butyl substituted alkyne **94b** where the reaction with norbornadiene and **94b** yielded a reasonably noteworthy 28 % ee. It has been described the discovery of a new optimal preparation of the MaxPHOS-rhodium complex **40** taking advantage of [Rh(acac)COD] as the source of rhodium. The preparation of a new [(MaxPHOS)Rh(NBD)]BF₄ complex **96** has been outlined. The [(MaxPHOS)Rh(CO)₂]BF₄ complex **97** has been prepared and used along with the diselenide MaxPHOS **99** to describe the electronic nature of the ligand. The preparation of a series of mono and di-chalcogenated MaxPHOS derivatives has been shown and their coordination to rhodium, palladium and cobalt has successfully been achieved and is described along with their respective X-ray crystallographic structures. The application of the rhodium complexes of the mono-chalcogenated MaxPHOS derivatives in the asymmetric hydrogenation has been presented. Also the attempts to prepare new P*-stereogenic phosphine ligands derived from the aminophosphine **3** using methodology developed by Evans *et al.* has been described and although new diphosphine species such as **117** and **119** were prepared they proved inapplicable in asymmetric catalysis.

In the next chapter it shall be discussed, the further investigation as regards the MaxPHOS ligand and its rhodium complex as it is applied to the asymmetric hydrogenation reaction. Particular focus will be given to the expansion of its substrate scope, its asymmetric hydrogenation of the *Z*-MAC substrate involving *in-situ* formation of the catalyst with also an investigation into the speed of its catalysis.

-
- ¹ Ohkuma, T.; Kurono, N. In *Privileged Chiral Ligands and Catalysts*; Wiley-VCH Verlag GmbH & Co. KGaA: 2011, p 1.
- ² Ogasawara, M.; Ngo, H. L.; Sakamoto, T.; Takahashi, T.; Lin, W. *Org. Lett.* **2005**, *7*, 2881.
- ³ Yamaguchi, M.; Shima, T.; Yamagishi, T.; Hida, M. *Tetrahedron Lett.* **1990**, *31*, 5049.
- ⁴ Uemura, M.; Kurono, N.; Sakai, Y.; Ohkuma, T. *Adv. Synth. Catal.* **2012**, *354*, 2023.
- ⁵ Yang, D.; Long, Y.; Zhang, J.; Zeng, H.; Wang, S.; Li, C. *Organometallics* **2010**, *29*, 3477.
- ⁶ Shibata, T.; Takagi, K. *J. Am. Chem. Soc.* **2000**, *122*, 9852.
- ⁷ Gini, F.; Hessen, B.; Minnaard, A. J. *Org. Lett.* **2005**, *7*, 5309.
- ⁸ Marinho, V. R.; Ramalho, J. P. P.; Rodrigues, A. I.; Burke, A. J. *Eur. J. Org. Chem.* **2009**, 6311.
- ⁹ Wang, Y.-Q.; Lu, S.-M.; Zhou, Y.-G. *Org. Lett.* **2005**, *7*, 3235.
- ¹⁰ Sakurai, F.; Kondo, K.; Aoyama, T. *Tetrahedron Lett.* **2009**, *50*, 6001.
- ¹¹ Zhang, W.; Zhang, X. In *Privileged Chiral Ligands and Catalysts*; Wiley-VCH Verlag GmbH & Co. KGaA: 2011, p 55.
- ¹² gura, T.; Yoshida, K.; Yanagisawa, A.; Imamoto, T. *Org. Lett.* **2009**, *11*, 2245.
- ¹³ a) Lledo, A.; Sola, J.; Verdaguer, X.; Riera, A.; Maestro, M. A. *Adv. Synth. Catal.* **2007**, *349*, 2121. b) Cabot, R.; Lledó, A.; Revés, M.; Riera, A.; Verdaguer, X. *Organometallics* **2007**, *26*, 1134.
- ¹⁴ Fabrello, A.; Dinoi, C.; Perrin, L.; Kalck, P.; Maron, L.; Urrutigoity, M.; Dechy-Cabaret, O. *Magn. Reson. Chem.* **2010**, *48*, 848.
- ¹⁵ Cotton, F. A.; Kraihanzel, C. S. *J. Am. Chem. Soc.* **1962**, *84*, 4432.
- ¹⁶ Allen, D. W.; Taylor, B. F. *J. Chem. Soc., Dalton Trans. (1972-2002)* **1982**, 51.
- ¹⁷ Pople, J. A.; Santry, D. P. *Mol. Phys.* **1964**, *8*, 1.
- ¹⁸ McFarlane, W.; Rycroft, D. S. *Dalton Trans. (1972-2002)*, **1973**, 2162.
- ¹⁹ Bent, H. A. *Chem. Rev.* **1961**, *61*, 275.
- ²⁰ Hoge, G.; Wu, H. P.; Kissel, W. S.; Pflum, D. A.; Greene, D. J.; Bao, J. *J. Am. Chem. Soc.* **2004**, *126*, 5966.
- ²¹ Adams, D. J.; Bennett, J. A.; Duncan, D.; Hope, E. G.; Hopewell, J.; Stuart, A. M.; West, A. J. *Polyhedron* **2007**, *26*, 1505.
- ²² Tong, J.; Liu, S.; Zhang, S.; Li, S. Z. *Spectrochim. Acta, Part A.* **2007**, *67*, 837.
- ²³ Adams, D. J.; Bennett, J. A.; Duncan, D.; Hope, E. G.; Hopewell, J.; Stuart, A. M.; West, A. J. *Polyhedron* **2007**, *26*, 1505.
- ²⁴ Revés, M.; Ferrer, C.; León, T.; Doran, S.; Etayo, P.; Vidal-Ferran, A.; Riera, A.; Verdaguer, X. *Angew. Chem. Int. Ed.* **2011**, *50*, 8776.
- ²⁵ Ritch, J. S.; Chivers, T.; Eisler, D. J.; Tuononen, H. M. *Chem. Eur. J.* **2007**, *13*, 4643.
- ²⁶ Owens, T. D.; Hollander, F. J.; Oliver, A. G.; Ellman, J. A. *J. Am. Chem. Soc.* **2001**, *123*, 1539.

MaxPHOS and Asymmetric Hydrogenation

5

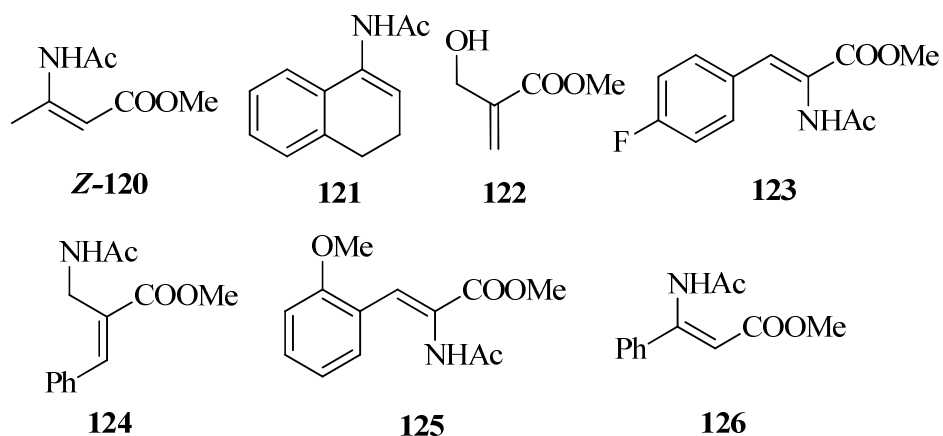
5.1	Exploring the substrate scope of the MaxPHOS-Rh catalyst	115
5.1.1	The choice of substrates	115
5.1.2	The methodologies employed to prepare the new substrate set	118
5.2	The application of the MaxPHOS-Rh catalyst in the asymmetric hydrogenation of the Z-MAC substrate	127
5.2.1	Hydrogenating Z-MAC with <i>in-situ</i> formation of the catalyst	128
5.2.2	Reduction of catalyst loading	131
5.2.3	The low enantiomeric excess dilemma	132
5.2.4	Speed of reaction and TOF of the MaxPHOS catalyst	134
5.3	Conclusions	137

5 MaxPHOS and Asymmetric Hydrogenation

5.1 Exploring the substrate scope of the MaxPHOS-Rh catalyst

Our group has reported as also it has already been described in a previous section, the application of the MaxPHOS ligand in the rhodium catalysed asymmetric hydrogenation as applied to the reduction of two prochiral substrates which provided very high enantioselectivities (Chapter 2, Table 2.2, page 40). It was decided that as part of *this* work the substrate scope of the MaxPHOS ligand should be investigated and if possible expanded. A list of prochiral olefins with coordinating functional substituents was drawn up and was to constitute a small library of substrates to further test the enantioselectivity and reactivity of the MaxPHOS ligand when applied in the rhodium catalysed asymmetric hydrogenation.

Figure 5.1: The proposed small library of asymmetric hydrogenation substrates to be tested.



5.1.1 The choice of substrates

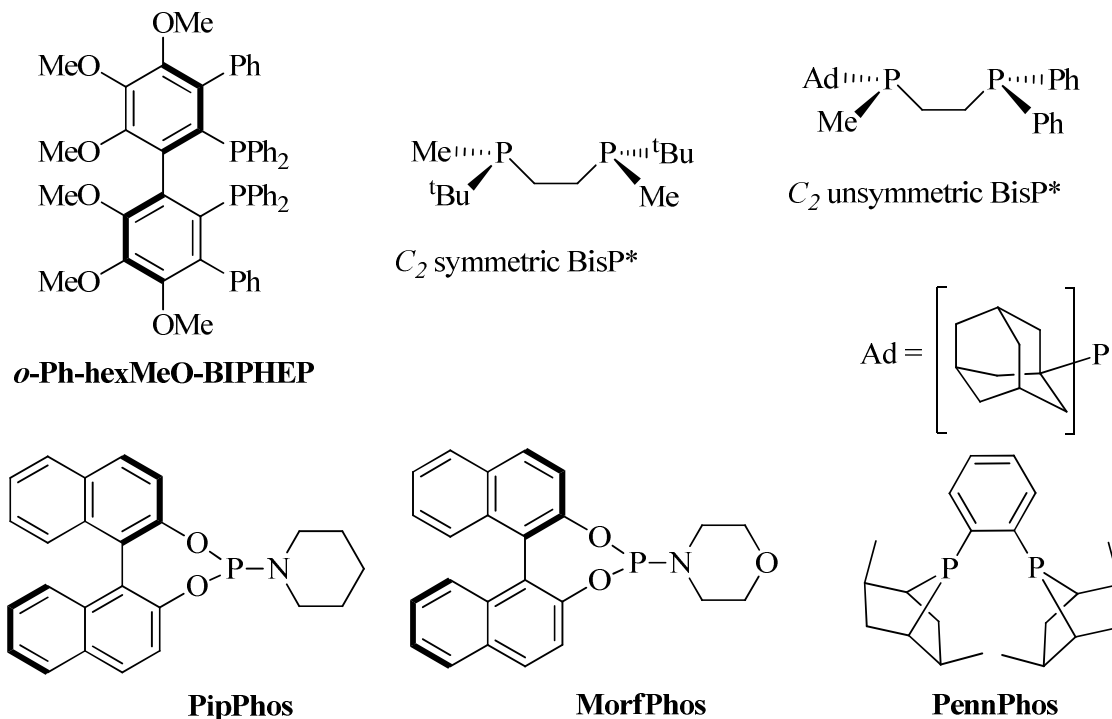
It was considered interesting to test the reactivity and enantioselectivity of the MaxPHOS ligand in the asymmetric hydrogenation of the β^2 -dehydroamino acid **120** as it was reported the trichickenfootphos ligand hydrogenated this substrate with only 96 % ee unlike the greater than 99 % ee reported for many other substrates under optimized conditions which they reported as being 1 bar of H₂ stirring in MeOH with complete conversion obtained after 15 minutes.¹

Compound **121** was considered interesting as a substrate to gauge the reactivity and applicability of MaxPHOS towards the asymmetric reduction of a cyclic enamide where many catalysts only provided poor or moderate enantioselectivities such as with BINAP,

5. MaxPHOS and Asymmetric Hydrogenation

DIOP and DuPHOS which were reported as only providing 24 %, 10 % and 1 % ee with 2.7 bars of H₂ in MeOH over 20 hours.² The C₂ symmetric *tert*-butyl substituted BisP* phosphine asymmetrically reduced cyclic enamide **121** with an enantiomeric excess of just 8.5 % with 20.2 bars of H₂ in MeOH over 12 hours however the C₁ symmetric (methyladamantylphosphino)(diphenylphosphino)ethane BisP* ligand managed to asymmetrically hydrogenate with 89.9 % ee under the same conditions.³ The BINOL/piperidine derived and the BINOL/morpholine derived mono-phosphine ligands PipPhos and MorfPhos selectively hydrogenated this substrate with 98 % ee and 94 % ee respectively however only when the reaction was carried out at – 20 °C under 55 bars of H₂ and 8 hours of stirring.⁴ The ligand PennPHOS provided a best enantiomeric excess of 98 % when carried out in CH₂Cl₂ at 1.7 bars of H₂ also at – 20 °C.⁵ The *o*-Ph-hexMeO-BIPHEP ligand hydrogenated **121** with 98 % ee in CH₂Cl₂ and 1.7 bars of H₂ again only at – 20 °C.⁶

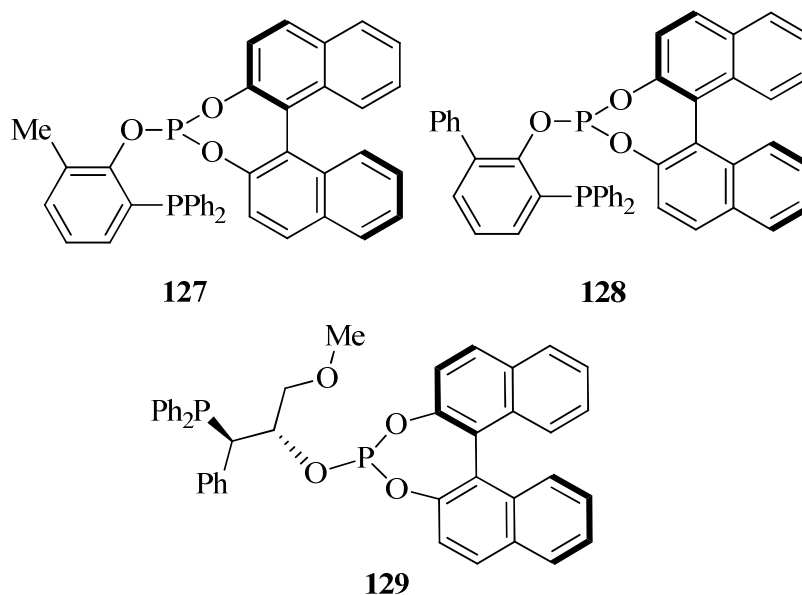
Figure 5.2: Just some of the phosphine ligands cited in the literature as being used in the asymmetric hydrogenation of the cyclic enamide N-(3,4-dihydronaphthalen-1-yl) acetamide **121**.



The acrylic ester **122** is a precursor *via* asymmetric hydrogenation of 3-hydroxy-2-methylpropionic acid methyl ester also known as the Roche ester, a compound with significant synthetic interest.⁷ It is present as a building block in the preparation of natural

products and synthetic compounds with biologically active properties, such as Discodermolide, a cytotoxic polyketide with potent anti-cancer activity.⁸ Up until recently the enantioselective hydrogenation of this substrate **122** had been reported scarcely. Saito and co-workers reported in 2002⁹ that a DuPHOS-Rh catalyst hydrogenated this substrate with near perfect yield and with a good enantiomeric excess of 90 % but the benzophospholane rhodium catalysts they prepared and reported in that communication all gave very low enantioselectivities. More recently some phosphine-phosphite ligands have been described which catalyse the hydrogenation of this substrate in high yields and enantioselectivity such as compounds **127** and **128** developed by the group of Reek and **129** developed by the group of Anton Vidal-Ferran.¹⁰

Figure 5.3: The phosphine-phosphite ligands proven very effective in the asymmetric hydrogenation of the Roche ester precursor.

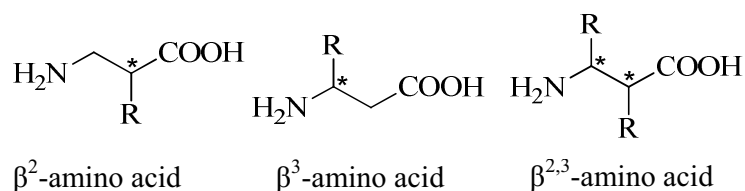


The *para*-fluoro *Z*-MAC substrate **123** was chosen to be part of the substrate set to confirm the efficacy of The MaxPHOS ligand in catalysing the asymmetric hydrogenation of electron withdrawing group containing α -dehydroamino acids as there was some doubt within the group as to its proficiency with such substrates. The first reported instance of this substrate being subjected to an asymmetric hydrogenation occurred in the literature in 1993 when Burk and co-workers published their seminal work on the ligand DuPhos which gave outstanding enantiomeric excess of greater than 99 % ee.¹¹

5. MaxPHOS and Asymmetric Hydrogenation

Compounds **120**, **124**, and **126** are precursors of β -amino acids which are the building blocks of β -peptides. β -peptides have garnered some interest in recent history due to their attractive physical properties such as their tendency for predictable folding in solutions to form secondary structures, their higher resistance to peptidases and metabolic pathways which induce their degradation and their propensity to mimic α -peptides in protein-protein or peptide-protein interactions.¹² β -amino acids can be subdivided into different categories.

Figure 5.4: β -amino acids.



β -amino acids with the side chain bonded to the α -carbon are known as β^2 -amino acids, those with the side chain bonded to the β -carbon are known as β^3 -amino acids and those with a side chain on both the α -carbon as well as the β -carbon, they are known as $\beta^{2,3}$ -amino acids. Methods to obtain enantiomerically pure β -amino acids have been mainly focused on obtaining β^3 -amino acids and methods to obtain enantiomerically pure β^2 -amino acids have been less common and it is this group which compound **124** belongs to as it is a precursor for a β^2 -amino acid, making it an interesting substrate.

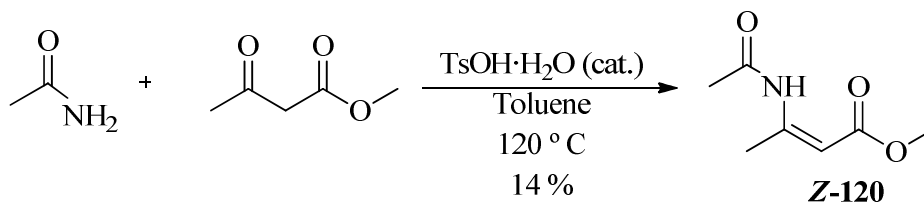
The *o*-MeO-*Z*-MAC compound **125** is another substrate occasionally employed in recent times to gauge the efficiency and efficacy of chiral phosphine ligands in rhodium catalysed asymmetric hydrogenation whether they be mono or bidentate¹³, being interesting as a tool to ensure that the electronic and the steric effects of the methoxy group lying so close to the olefin in the ortho position on the phenyl ring does not interfere with the enantioselection process once good enantioselectivity has already been observed in the asymmetric hydrogenation of the more commonly used *Z*-MAC substrate.

5.1.2 The methodologies employed to prepare the new substrate set

The synthetic reaction pathways and procedures followed to prepare the desired hydrogenation substrates in multigram quantities were obtained from the literature and were as follows: The *N*-acylated, α -unsaturated 3-carboxylic ester compound **120** was prepared according to a procedure found in an American patent filed by Jaekel *et al.* in 2009.¹⁴ The

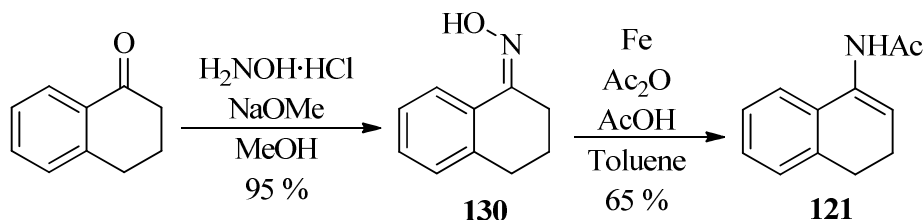
reaction components were heated at 120 °C while stirring in toluene in a round bottom flask with a dean-stark apparatus attached for 23 hours, yielded 3.07g of pure product (*Z*) in a 14 % yield after work up and distillation under vacuum.

Scheme 5.1: Preparation of (*Z*)-methyl 3-acetamidobut-2-enoate.



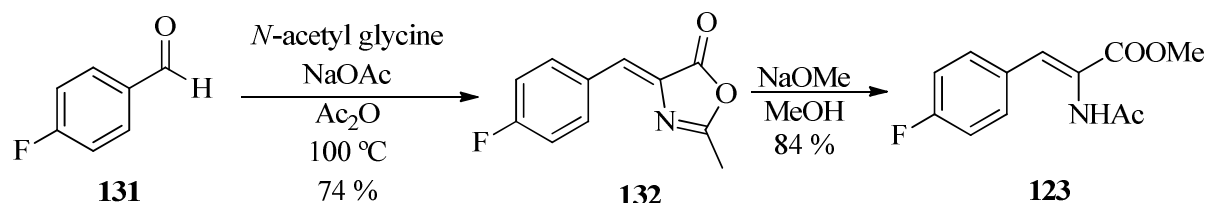
The *N*-(3,4-dihydronaphthalen-1-yl)acetamide **121** was prepared *via* the synthesis outlined by the group of Burk and co-workers while they published their work on the efficient syntheses of substrates for asymmetric hydrogenation by their effective Me-DuPhos-Rh and Me-BPE-Rh catalysts.¹⁵

Scheme 5.2: Preparation of the α -tetralone derived enamide **121**.

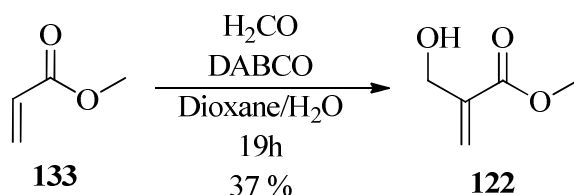


In this way, 7.2 g of the desired cyclical enamide **121** was prepared in a two-step procedure beginning with the α -tetralone starting material, forming the oxime **130** in excellent yield and after reduction of the oxime **130** by iron powder in the presence of Ac₂O gave the desired product with an overall yield of 80 %.

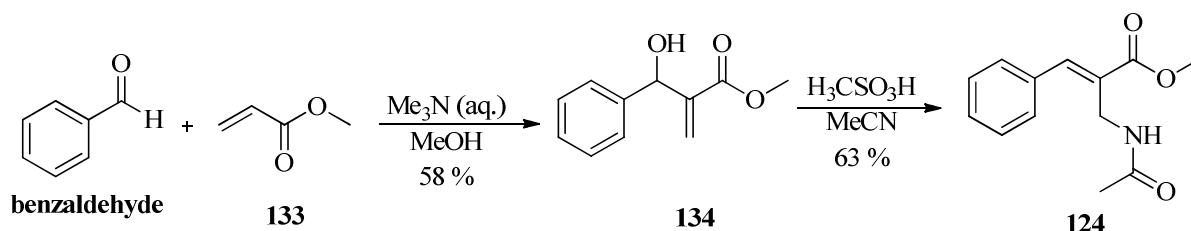
To prepare the *para*-flouro *Z*-MAC olefin **123** a combination of two procedures was followed.¹⁶ The first, outlined in scheme 5.3 consisted of cyclization of the *N*-protected glycine and condensation with the aldehyde **131** affording the preparation of 12.2 g of the *para*-flourobenzo oxazolone **132** in 74 % yield. The oxazolone was then ring opened with NaOMe in MeOH to yield 1.9 g of the desired product **123** in 84 % yield.

Scheme 5.3: Preparation of the *para*-fluoro Z-MAC.

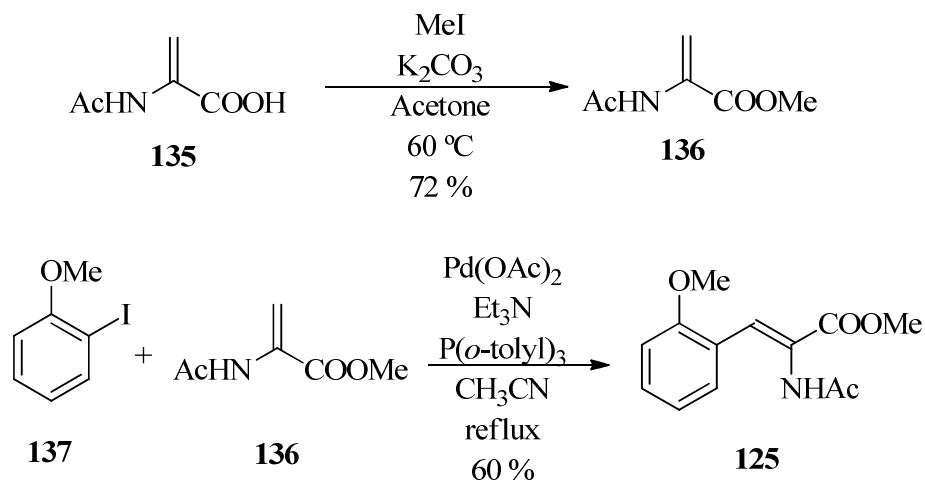
To prepare the Roche ester precursor **122** a published Baylis-Hillsman reaction using a stoichiometric amount of DABCO in aqueous conditions was employed.¹⁷ The reaction components were stirred overnight at room temperature and afforded 5.9 g of desired product **122** after aqueous work-up and flash column chromatography in a yield of 37 %, a lower yield than reported possibly due to a lesser excess of 2 equivalents of methyl acrylate **133** being used instead of 3 equivalents.

Scheme 5.4: Baylis-Hillsman reaction employed to afford the Roche ester precursor **122**.

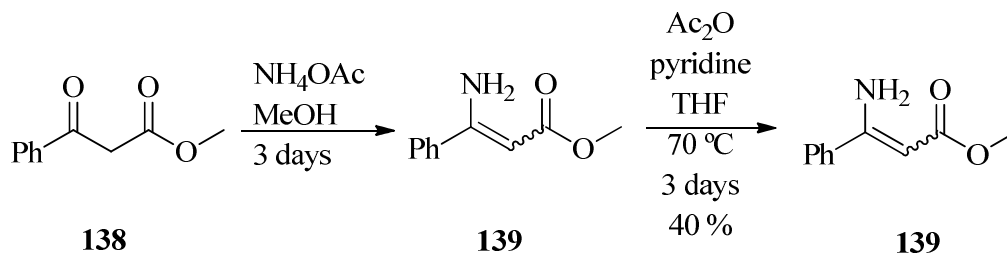
The β^2 -dehydroamino acid **124** was obtained *via* a Baylis-Hillman reaction followed by a Ritter reaction,¹⁸ to provide 3.1 g of the desired product in a 63 % yield in the final step.

Scheme 5.5: A Baylis-Hillman reaction followed by a Ritter reaction is shown to obtain a desired β^2 -amino acid precursor.

The *ortho*-methoxy substituted Z-MAC **125** was prepared by first methylation of 2-acetamido acrylic acid **135**,¹⁹ and subsequently reacting the product in a palladium catalysed Heck reaction with *ortho*-methoxy-iodobenzene **137**.

Scheme 5.6: Preparation of the *o*-MeO-Z-MAC **125**.

In preparation of the β^3 -dehydroamino acid **126**, methyl 3-oxo-3-phenylpropanoate **138** was reacted with ammonium acetate in MeOH for 3 days in accordance with literature precedent.²⁰ After 3 days solvents were removed, the residue was added to CH_2Cl_2 which formed a precipitate, which was isolated and washed with further CH_2Cl_2 before being reacted in the following step to acetylate the free amine. It was stirred in THF with acetic anhydride and pyridine for 3 days at reflux temperature. A residue was obtained after an acidic work-up which was distilled. It was found only acetic anhydride had distilled and what remained was the free enamine **139**. It was decided that **139** which was an un-protected enamine was also an interesting substrate with which to test the efficacy of the MaxPHOS-Rh catalyst as such substrates have been reported in the literature to be able to be asymmetrically reduced using rhodium catalysts,²¹ and so **139** replaced **126** in our new substrate set.

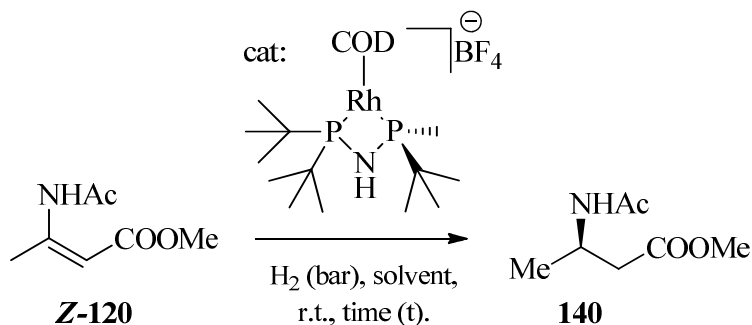
Scheme 5.7: The procedure followed in the attempt to obtain β^2 -dehydroamino acid **126**.

5. MaxPHOS and Asymmetric Hydrogenation

5.1.3 Testing the MaxPHOS-Rh catalyst against the new substrate set

The screening and optimisation of reaction conditions of the different substrates began once their preparation had been completed.

Table 5.1: The screening of reaction conditions for (Z) β^2 -dehydroamino acid **120**.



Entry	solvent	P. (bars)	cat. (mol%)	t (hours)	conversion (%) ^a	ee (%) ^b
1	MeOH	3	1	20	100	86
2	MeOH	3	1	2	100	89
3	MeOH	2	1	2	100	82
4	MeOH	2	1	1	100	85
5	THF	3	1	2	100	96
6	THF	3	1	1	90	94
7	THF	1	1	20	12	-

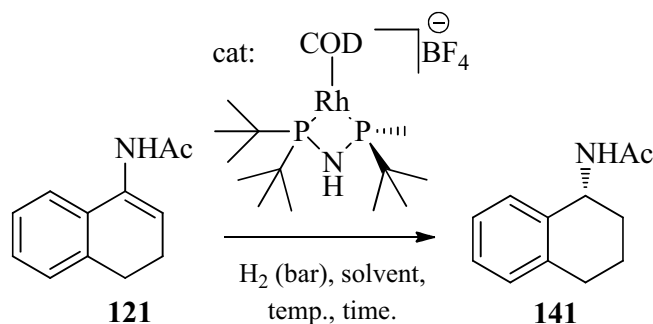
^a Determined by ¹H NMR. ^b Determined by chiral GC (Beta-DEX 30m column).

The trends found while exploring the reaction conditions for the reaction outlined in table 5.1 found that THF instead of MeOH gave preferable enantiomeric excess, also leaving the reaction stir too much time was detrimental for enantiomeric excess. It was concluded that perhaps some racemization took place when the product was allowed to stir for more time than is necessary with the catalyst, so the reaction was only stirred the time required to afford full conversion. It was also noticed that 3 bars of H₂ pressure gave rise to greater enantiomeric excess than 2 bars and 1 bar of H₂ pressure was not enough to give full conversion even when left stir overnight. In this way it was found the optimal conditions for this substrate **120** was THF as solvent, with 3 bars of H₂ pressure and stirring for 2 hours to give full conversion and 96 % ee as described by entry 5 of table 5.1.

As can be seen in table 5.2 the screening of reaction conditions for the α -tetralone derived acetamide substrate **121** lead to the achievement of a best enantiomeric excess of 75 % ee with 2 bars of H₂ pressure in MeOH after having stirred for 20 or 3 hours at room temperature. It was possible to achieve a higher enantiomeric excess of up to 83 % while

carrying out the reaction with 2 bars of H₂ in MeOH at 0 °C but at a detriment to conversion when even 26 hours or 66 hours could not yield full conversion.

Table 5.2: The MaxPHOS-Rh catalysed asymmetric hydrogenation of the α -tetralone derived acetamide substrate **121**.

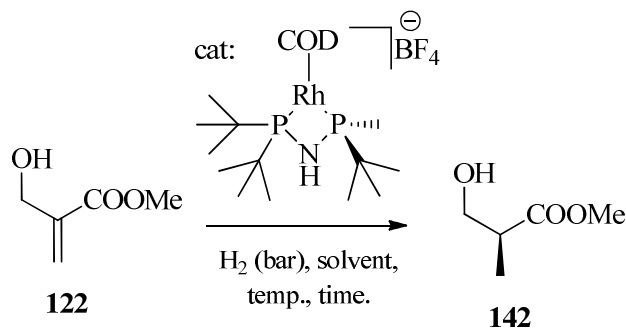


Entry	Solvent	P. (bars)	cat. (mol%)	t (hours)	temp.	conversion (%) ^a	ee (%) ^b
1	MeOH	3	1	20	r.t.	100	64
2	MeOH	2	1	20	r.t.	100	75
3	MeOH	2	1	2	r.t.	88	70
4	MeOH	2	1	3	r.t.	100	75
5	MeOH	1	1	22,5	r.t.	100	59
6	THF	2	1	5	r.t.	0	0
7	TFE	2	1	5	r.t.	0	0
8	MeOH	2	1	26	0 °C	83	83
9	MeOH	2	1	65,6	0 °C	93	70

^a Determined by ¹H NMR. ^b Determined by chiral GC (Beta-DEX 30m column).

It can be seen from table 5.2 that 2 bars of H₂ was optimal as enantiomeric excess dropped drastically as the pressure was lowered to 1 bar. Also other solvents were tested besides MeOH i.e. THF and TFE but no conversion resulted.

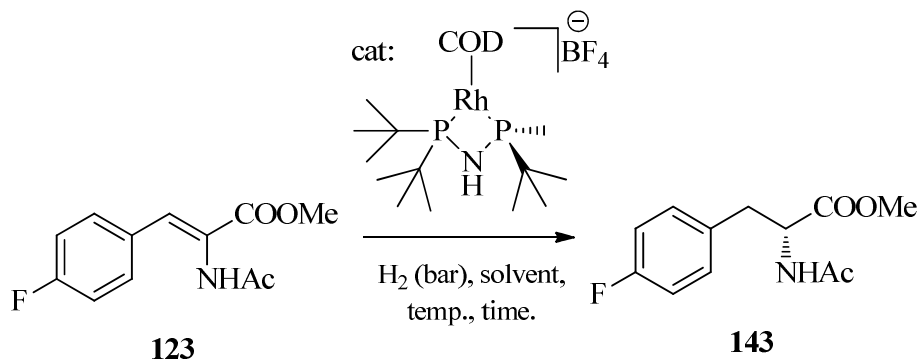
Upon carrying out the asymmetric hydrogenation of the Roche ester precursor **122** it was found reducing the temperature greatly improved the enantiomeric excesses obtained. Poor to mediocre excesses were observed as can be seen from table 5.3 when hydrogenating at 3 bars or 2 bars of H₂ pressure in MeOH or THF. When the reaction was carried out at 0 °C instead of room temperature we saw a best enantiomeric excess of 87 % ee where there had only been 55 % ee when MeOH and 3 bars of H₂ pressure was used. Lowering the temperature even further only served to impede conversion.

Table 5.3: The MaxPHOS-Rh catalysed hydrogenation of the Roche ester **122**.

Entry	Solvent	P. (bars)	cat. (mol%)	t (hours)	conversion (%) ^a	ee (%) ^b	T (°C)
1	MeOH	3	1	20	100	55	r.t.
2	MeOH	2	1	20	100	48	r.t.
3	THF	3	1	2	100	53	r.t.
4	MeOH	3	1	26	100	87	0 °C
5	MeOH	3	1	45	76	86	- 20 °C

^a Determined by ¹H NMR. ^b Determined by chiral GC (Beta-DEX 30m column).

The *para*-fluoro-*Z*-MAC **123** was asymmetrically hydrogenated by the MaxPHOS-Rh complex to desirable enantiomeric excess without much need for optimisation of reaction conditions.

Table 5.4: The asymmetric hydrogenation of the *para*-fluoro-*Z*-MAC **123**.

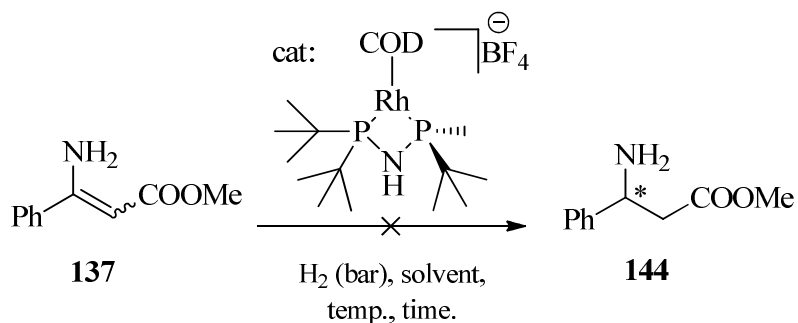
Entry	Solvent	P. (bars)	cat. (mol%)	t (hours)	conversion (%) ^a	ee (%) ^b
1	THF	5	1	17,3	100	97
2	THF	2	1	2,5	49	- ^c
3	THF	2	1	17,3	74,6	- ^c
4	THF	3	1	2,5	100	99

^a Determined by ¹H NMR. ^b Determined by chiral HPLC (Chiralcel OJ). ^c The chiral HPLC was not run.

It had been shown previously within the group that hydrogenating in distilled THF produced best results when asymmetrically hydrogenating the *Z*-MAC substrate and the solvent of choice for this substrate passed from being MeOH to the use of THF from the beginning. A pressure of 5 bars of H₂ stirring overnight was applied to test reactivity and the reaction proceeded with full conversion and 97 % ee. When pressure was reduced to 2 bars full conversion was not observed but with 3 bars of H₂ pressure full conversion was observed along with almost complete enantioselectivity at 99 % ee.

The β³-dehydroamino acid **137** containing a non-acylated enamine was tested at first using what could be considered “standard” reaction conditions of 3 bars of H₂ with 1 mol % of catalyst loading in MeOH but no conversion was observed by ¹H NMR. The catalyst loading was increased to 3 mol % while pressure, solvent and time were remained constant yet still not conversion was observed. The pressure was increased greatly to try and force the reaction by first testing at 10 bars and later at 30 bars of H₂ pressure (entries 3 and 4, table 5.5) while simultaneously testing other solvents but still no conversion was observed. Although reaction conditions were not exhaustively, rigorously and mechanically checked the complete lack of reactivity observed lead to the conclusion that the MaxPHOS-rhodium catalyst was not compatible with this substrate.

Table 5.5: Screening of the Rh-MaxPHOS complex in the attempted hydrogenation of the β³-dehydroamino acid **137**.



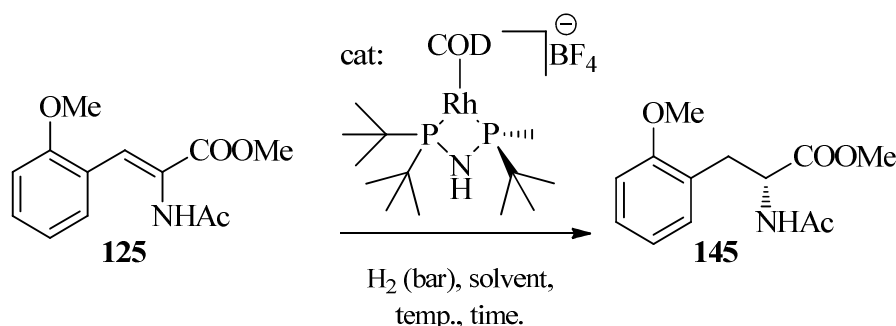
Entry	solvent	P. (bars)	cat. (mol %)	t (hours)	conversion (%) ^a
1	MeOH	3	1	20	0
2	MeOH	3	3	20	0
3	TFE	10	3	20	0
4	THF	30	3	20,5	0

^a Determined by ¹H NMR.

5. MaxPHOS and Asymmetric Hydrogenation

The substrate *o*-MeO-Z-MAC **125** was readily selectively hydrogenated by the MaxPHOS-Rh complex and the optimisation of reaction conditions consisted in reducing the pressure from 3 bars to 2 bars and then to 1 bar of H₂ pressure with the enantiomeric excess observed to increase in each case. In this case the use of THF seemed to hinder the conversion of the reaction (Table 5.6, entry 4) and so the use of MeOH was favoured. When reacted overnight at 1 bar of H₂ full conversion and an optimum enantiomeric excess was observed of 98 % ee (Table 5.6, entry 3). When the reaction time was reduced to 4 hours only 51 % conversion was observed and so it could be concluded that at 1 bar of H₂ pressure optimum enantiomeric excess could be observed but it made for a slow reaction.

Table 5.6: The asymmetric hydrogenation of the *o*-MeO-Z-MAC **125** substrate by the MaxPHOS-Rh-COD complex.



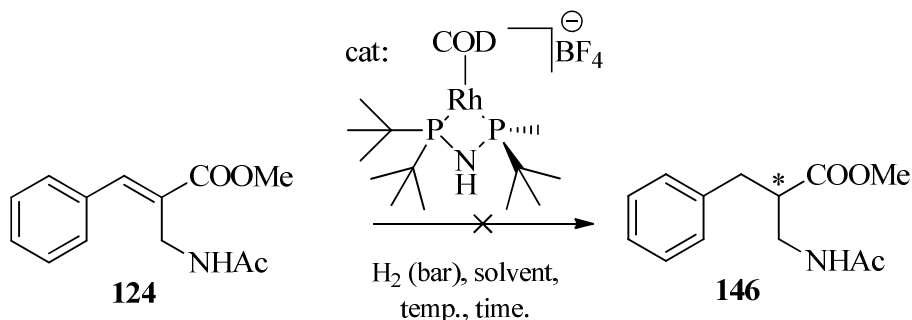
Entry	solvent	P. (bars)	cat. (mol%)	t (hours)	conversion (%) ^a	ee (%) ^b
1	MeOH	3	1	22,5	100	93
2	MeOH	2	1	22,5	100	97
3	MeOH	1	1	22,5	100	98
4	THF	1	1	20	80	96
5	MeOH	1	1	4	51	- ^c

^a Determined by ¹H NMR. ^b Determined by chiral HPLC (Chiralpak AD-H column).

^c The HPLC was not ran.

The hydrogenation of β²-amino acid precursor **124** proved to be troublesome. Various reaction conditions were tested. The crude reaction mixture was analysed by ¹H NMR after the hydrogen pressure was released and the solvent was removed and each time two products were observed in the spectrum as well as a substantial quantity of starting material. Neither of the resulting products corresponded to the literature described product and so it was concluded the MaxPHOS-Rh catalyst was not suitable to hydrogenate this substrate.

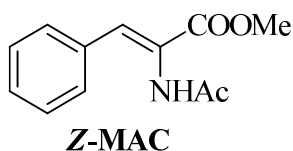
Scheme 5.8: MaxPHOS-Rh catalyst could not cleanly hydrogenate the β -dehydroamino acid **124**.



5.2 The application of the MaxPHOS-Rh catalyst in the asymmetric hydrogenation of the Z-MAC substrate

When probing the efficacy of would-be asymmetric hydrogenation catalysts the Z-MAC is often the first port of call as a substrate to test. As mentioned earlier it is the precursor of an industrially important amino acid in phenylalanine and it is generally regarded that an effective asymmetric hydrogenation catalyst must hydrogenate this substrate in high selectivity or otherwise it must not be considered effective.

Figure 5.5: The Z-MAC substrate.



In this next section it will be described the further investigation of the asymmetric hydrogenation of this substrate by the MaxPHOS-Rh catalyst as regards the optimisation of reaction conditions involving the *in-situ* formation of the catalyst, optimisation of reaction conditions as applied to the reduction of catalyst loading of the reaction and also a very brief investigation into the turn-over frequency (TOF) of this catalyst when catalysing the reduction of this substrate.

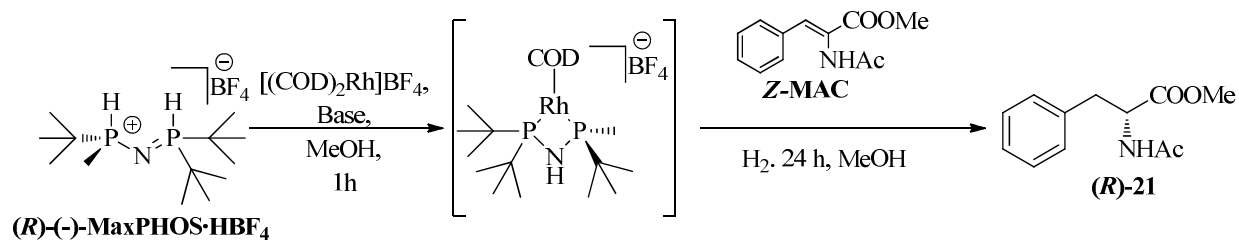
5. MaxPHOS and Asymmetric Hydrogenation

5.2.1 Hydrogenating Z-MAC with *in-situ* formation of the catalyst

The hydrogenation by the MaxPHOS-Rh catalyst of various substrates has been described so far. In all instances so far described these asymmetric hydrogenations were carried out using pre-formed and recrystallized [(MaxPHOS)Rh(COD)]BF₄ complex. Hydrogenation of Z-MAC by means of an *in-situ* formation of the catalyst had been explored briefly²² but a more complete optimisation of its reactions conditions was to constitute part of this work.

The *in-situ* formation of a hydrogenation catalyst is advantageous when the chiral phosphine ligand in question is more bench stable than the resulting chiral ligand-rhodium complex. The MaxPHOS ligand salt can be stored in sample vials under a normal air atmosphere in the laboratory for very long periods of time and with no degradation being appreciated by ¹H NMR. The recrystallized MaxPHOS-rhodium complex is also very stable under air but we have noted by carrying out asymmetric hydrogenations using batches of preformed catalysts having being stored in air for weeks to months, that enantiomeric excesses obtained in hydrogenation of the Z-MAC substrate drop significantly. So it can be concluded that degradation of MaxPHOS-Rh catalyst complex does occur eventually with time and so an *in-situ* formation of catalyst could be advantageous as it negates the need for the catalyst recrystallization and storage under inert atmosphere.

To asymmetrically hydrogenate the Z-MAC substrate employing the method of *in-situ* formation of the catalyst, the MaxPHOS·BF₄ salt was first stirred with the commercial source of rhodium, an organic base in methanol under nitrogen in a flame-dried schlenk tube for an hour. An organic base was employed as it was noted that the ligand to metal complexation takes much more time if one is not employed resulting in a complexation which must be left occur overnight. Once the complexation as described just previously has stirred for an hour, the appropriate aliquot of catalyst complex solution is removed under inert atmosphere using the schlenk tube and transferred *via* syringe to the substrate in the hydrogenation vessel, the vessel is sealed and the hydrogenation is carried out as normal. Using this methodology parameters which could be varied were pressure of hydrogen, catalyst loading with the intention to reduce it to at least 1 mol % but as well the type of organic base used and the equivalents of it employed could be varied also. The solvent was not varied as catalyst formation is preferable in methanol.

Table 5.7: The hydrogenation of *Z*-MAC via an *in-situ* formation of the catalyst.

Entry	Base	Eq. ^a	cat. (mol %)	P. (Bar)	ee (%) ^b
1	Et ₃ N	2	1.5	1	97,8
2	Et ₃ N	14	1.5	1	97,3
3	Et ₃ N	2	3	5	91
4	Et ₃ N	14	3	5	98,1
5	Et ₃ N	2	1.5	5	91,7
6	Et ₃ N	14	1.5	5	98,2
7	DBU	2	3	3	83,9
8	DBU	20	3	3	s.m. ^c
9	DIP	2	3	3	99,2
10	DIP	20	3	3	98,8
11	DIP	2	1	3	98,6
12	DIPEA	2	1	3	98,9
13	TBA	2	1	3	99,1

^a The equivalents of base w.r.t. ligand. ^b Determined by chiral HPLC (Chiralpak AD-H). ^c Only starting material was recovered. The conversion was 100 % in each case, confirmed to a certainty by ¹H NMR.

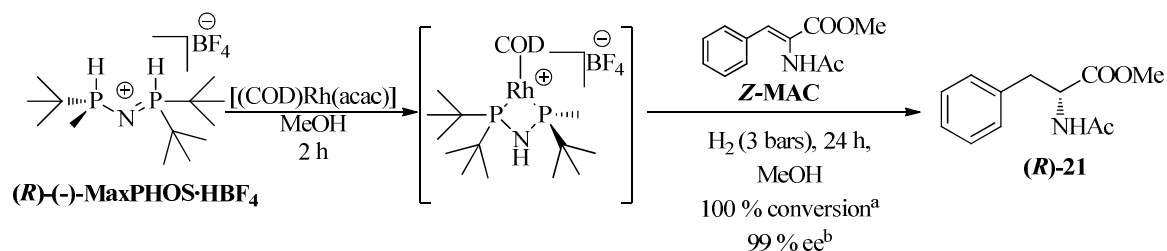
It was noted serendipitously (table 5.7, entry 3-6) that when a large excess of Et₃N with 14 equivalents with respect to ligand was used to form the catalyst it provided greater enantiomeric excess than when only 2 equivalents were used when 5 bars of H₂ were employed with 3 mol % and 1.5 mol % of catalyst loading. This proved not to be the case for the bases DBU (1,8-Diazabicycloundec-7-ene) and DIP (diisopropylamine) where large excess of base hindered or halted the reaction when employed with 3 bars of H₂ pressure and 3 mol % catalyst loading (table 5.7, entry 7-10). It was found that at low catalyst loading of 1

5. MaxPHOS and Asymmetric Hydrogenation

mol % and 3 bars of H₂ pressure, the ideal organic base was TBA (*tert*-butyl amine) as it provided the best enantiomeric excess in the optimisation process of 99.1 % ee.

Coming with the advent of a cleaner, more efficient and quicker method to afford the MaxPHOS rhodium catalyst complex *via* the [(COD)Rh(acac)] rhodium source as described in section 4.1 (scheme 4.9, page 87), came the possibility to use this as the source of rhodium for an *in-situ* asymmetric hydrogenation of the Z-MAC substrate without the presence of an organic base such as those used in the screening outlined in table 5.7.

Scheme 5.9: An *in-situ* asymmetric hydrogenation of Z-MAC by employing the MaxPHOS·HBF₄ salt and [(COD)Rh(acac)].



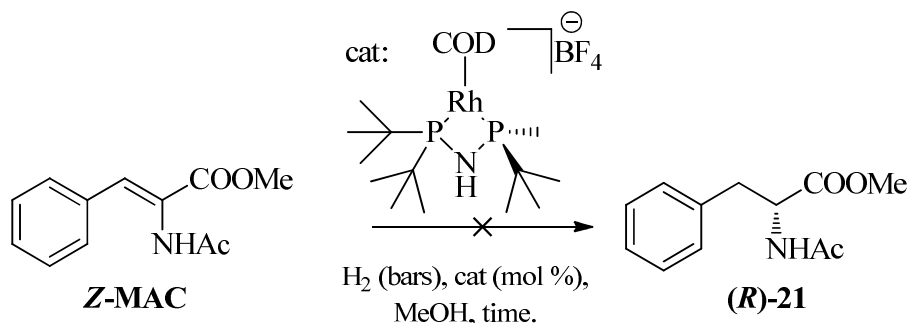
^a 100 % conversion was confirmed by ¹H NMR. ^b Determined by chiral HPLC (Chiralpak AD-H). 1 mol % loading of catalyst was employed.

A slight excess of MaxPHOS·HBF₄ salt to rhodium was used to form the catalyst to ensure there might be no non phosphine-coordinated rhodium present in the reaction which might catalyse hydrogenation in a racemic manner and therefore lower the ultimate enantioselectivity. Formation of the catalyst was allowed two hours to stir to ensure full complexation and was carried out in the hydrogenation vessel so as when the catalyst was assumed to have formed after two hours the vessel could be opened, the substrate simply added and the hydrogenation carried out as normal. In this way it was shown the MaxPHOS·HBF₄ salt could be utilized to catalyse the asymmetric hydrogenation of the Z-MAC substrate with total conversion to hydrogenated product with near perfect enantioselectivity taking advantage of an *in-situ* formation of the chiral organometallic rhodium catalyst.

5.2.2 Reduction of catalyst loading

It has already been discussed in a previous chapter how an industrially utilized, asymmetric hydrogenation catalyst must be powerful enough to catalyse enantioselectively on a grand scale with minute concentrations of catalyst loading. If 1 mol % of catalyst is required to catalyse the transformation, at multi-kilo quantities of substrate, the cost of the source of catalysing metal to form the chiral catalyst might be too great to be considered economically sound and most probably would not be employed on an industrial or pharmaceutical level. Besides the excessive cost of the catalysing metal for an organometallic catalyst which might require high catalyst concentrations also it would not be considered environmentally friendly and therefore safe, to use excessive amounts of a transition metal in an industrial process. Most commonly the most powerful asymmetric hydrogenation catalysts are efficient to 10,000:1 or even 100,000:1 substrate: catalyst ratio. It was with this in mind that an investigation into the power of the MaxPHOS-Rh preformed catalyst complex to catalyse the asymmetric hydrogenation of the Z-MAC substrate at lower concentrations was undertaken.

Table 5.8: Reduction in catalyst loading of the MaxPHOS-rhodium catalysed asymmetric hydrogenation of Z-MAC.



Entry	P. (bars)	cat. (mol%)	conc. (g/mL)	t. (hours)	conversion (%) ^a	ee (%) ^b
1	3	0,1	0,109	22	100	97
2	5	0,1	0,292	4,8	100	97
3	5	0,01	0,292	72	99	98
4	5	0,01	0,292	43	100	99

^a Conversion was confirmed by ¹H NMR. ^b Determined by chiral HPLC (Chiralpak AD-H).

It was noted upon during the investigation into the reduction of the catalyst loading that the reaction became a little unpredictable as can be appreciated from table 5.8, especially entries 1 and 2. When reducing catalyst loading to 0.1 mol % (1000:1 S/C) full conversion was

5. MaxPHOS and Asymmetric Hydrogenation

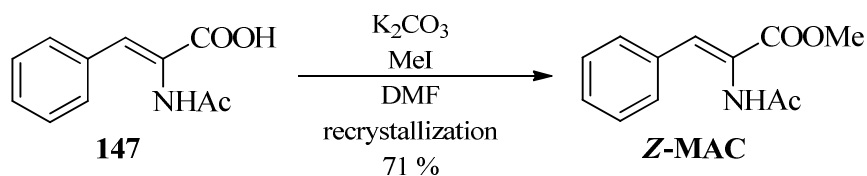
achieved but unfortunately the almost complete enantiomeric excess of 99 % ee was not achieved as 97 % ee was observed, at both 3 bars of H₂ pressure and 5 bars of H₂ pressure. When it was attempted to reduce catalyst loading even further to 0.01 mol % (10,000:1 S/C) loading, we observed the desired 99 % enantiomeric excess.

The conclusion to be drawn from these results is that the MaxPHOS-Rh hydrogenation catalyst can catalyse hydrogenation of this substrate at low catalyst concentrations to full conversion with the very high enantioselectivity required of industrially employed catalysts. However the reaction becomes much more sensitive and enantioselectivities can vary to a very small degree depending perhaps on the substrate batch or the state of the solvent employed; even though in all cases the substrate batches used were completely pure as best can be judged by ¹H NMR and HPLC.

5.2.3 The low enantiomeric excess dilemma

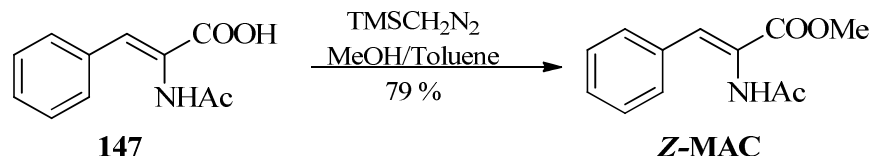
An anomaly began to be noticed where depending on the preparation of the Z-MAC substrate an enantiomeric excess of 96 % ee was consistently observed when asymmetrically hydrogenating using 1 mol % of the MaxPHOS-Rh preformed catalyst complex at 3 bars of H₂ pressure for 2 hours in MeOH (table 5.9, entry 1, page 133). This enantiomeric excess was obtained from substrate batches which were obtained from esterification of α -acetamidocinnamic acid *via* a combination of K₂CO₃ and MeI in DMF with the pure compound obtained after recrystallization from hot hexane/ethyl acetate.

Scheme 5.10: Z-MAC substrate batches prepared in this manner were observed to provide 96 % ee when hydrogenated by the MaxPHOS-Rh.



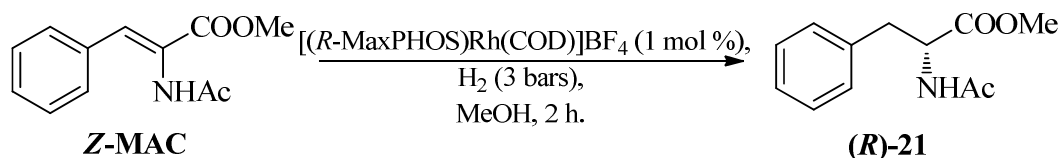
Upon hydrogenating batches of Z-MAC where the esterification process of the α -acetamidocinnamic acid was carried out using trimethylsilyldiazomethane reagent in MeOH/toluene, the MaxPHOS catalysed hydrogenation at 1 mol % catalyst loading, 3 bars of H₂ in MeOH once again provided the desired 99 % ee.

Scheme 5.11: Esterifying the α -acetamidocinnamic acid in this manner gave rise to batches of Z-MAC substrate which would consistently provide 99 % ee in MaxPHOS hydrogenation tests.



This caused some puzzlement until it was realised that the same batch of Z-MAC substrate derived from trimethylsilyldiazomethane (table 5.9, entry 2) would indeed provide 99 % ee when the substrate was used crude after its preparation. However upon recrystallization of the substrate from hexane/ethyl acetate at 80 °C with later cooling, even though the substrate would then have an obviously cleaner aspect to the naked eye with a pure white colour when it had a faint brown one before and also showed a cleaner ^1H NMR spectrum showing no traces of impurity, the recrystallized product provided once again 96 % ee in hydrogenation test using the MaxPHOS ligand (table 5.9 entry 3).

Table 5.9: Recrystallization of substrate proved detrimental to ultimate enantioselectivity obtained.



Entry	Z-MAC preparation	conversion (%) ^a	ee (%) ^b
1	K ₂ CO ₃ /MeI (recrys.) ^c	100	96
2	Trimethylsilyldiazomethane (crude) ^d	100	99
3	Trimethylsilyldiazomethane (recrys.) ^e	100	96
4	Trimethylsilyldiazomethane (column) ^f	100	99

^a Conversion was confirmed by ^1H NMR. ^b Determined by chiral HPLC (Chiralpak AD-H). ^c As scheme 5.10. ^d As scheme 5.11 purifying only by work-up. ^e As scheme 5.11 and later purified by recrystallization. ^f As scheme 5.11 and later purified by flash column chromatography.

In this way it was concluded that recrystallization of Z-MAC was detrimental to enantiomeric excesses obtained from the asymmetric hydrogenation of the MaxPHOS rhodium catalyst and should be avoided with purification by flash column chromatography of the substrate being

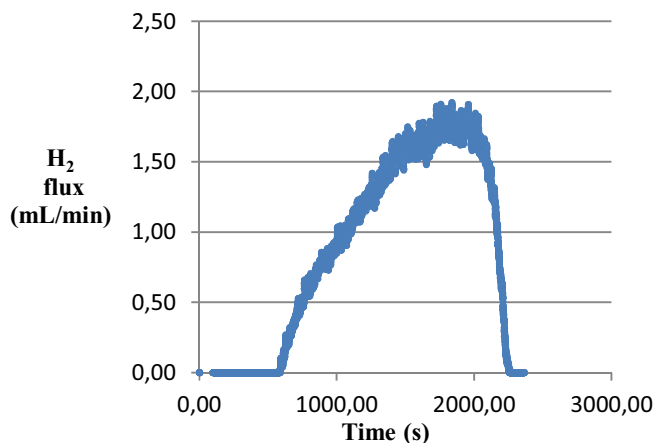
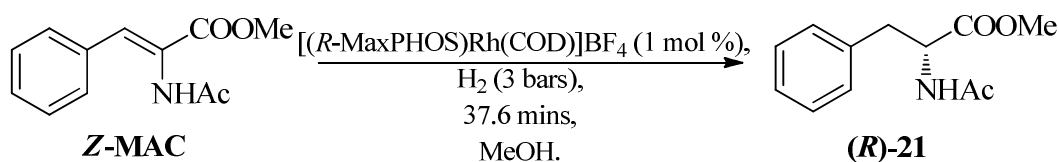
5. MaxPHOS and Asymmetric Hydrogenation

preferable prior to hydrogenation however even crude substrate batches provided better enantiomeric excess than recrystallized ones.

5.2.4 An insight into the speed of reaction and therefore the TOF of the MaxPHOS catalyst.

An experiment was carried out to examine the uptake of hydrogenation during the course of a MaxPHOS-rhodium complex catalysed asymmetric hydrogenation of the Z-MAC substrate. The hydrogenation was carried out using “standard” reaction conditions.

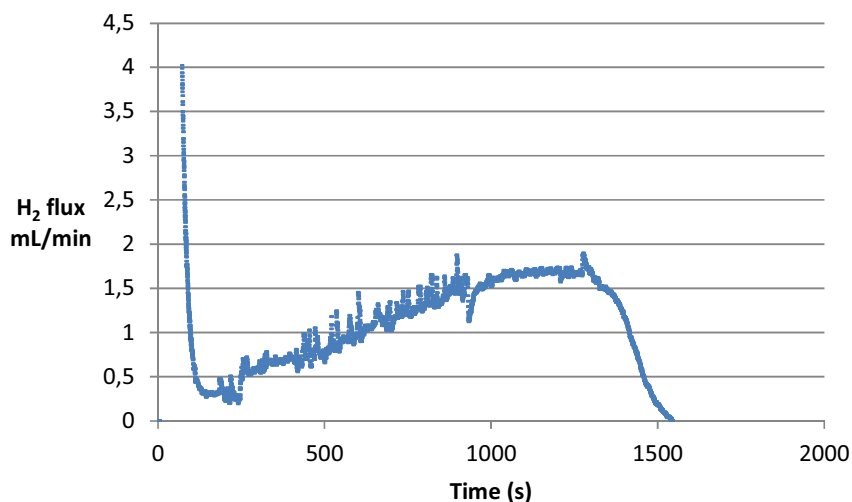
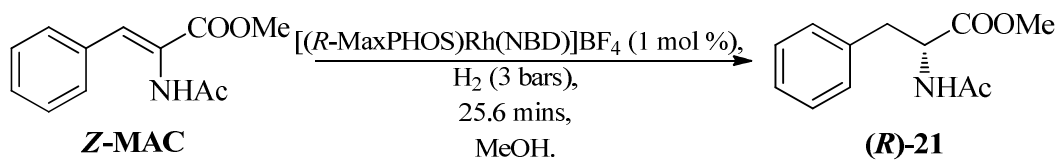
Graph 5.1: The hydrogen flux vs. time of the MaxPHOS rhodium catalysed asymmetric hydrogenation of Z-MAC.



The hydrogenation vessel was charged with catalyst, substrate and solvent under N₂ and subsequently purged of nitrogen by vacuuming and flushing with H₂ three times before being finally charged with 3 bars of hydrogen. At that point instead of the vessel being sealed it was left connected to the hydrogenation system through a gas flux monitoring device which outputs the hydrogen flux to a laptop computer. From the appropriate program interface the flux of gas into the vessel was observed.

As can be somewhat appreciated from graph 5.1 it took 8.1 minutes before the uptake of H₂ began. For the hydrogenation catalyst to become activated the 1,5-cyclooctadiene must be first hydrogenated and released from the complex. This initial period of 8.1 minutes before H₂ uptake is observed might suggest this initial hydrogenation of the 1,5-cyclooctadiene ligand is slow in the case of the MaxPHOS rhodium catalyst but once it occurs and the complex is activated it hydrogenates the substrate rapidly. As the hydrogenation of the substrate continues more catalyst is being activated as more COD is hydrogenated and released from the catalyst and so H₂ uptake increases. Once all the substrate is completely hydrogenated the hydrogen uptake is halted suddenly which occurred after 37.6 minutes after the H₂ pressure having been maintained at 3 bars. It was noted that once activated and hydrogenating; the catalyst took 28 minutes to consume all the substrate.

Graph 5.2: A hydrogen flux experiment employing the [(R)-MaxPHOS)Rh(NBD)]BF₄ preformed catalyst complex.



When norbornadiene replaced 1,5-cyclooctadiene in the MaxPHOS rhodium preformed catalyst a faster reaction was observed for the simple fact that, as is apparent from the graph 5.2, the norbornadiene ligand is instantly hydrogenated and released from the complex to provide activated catalyst to begin hydrogenation. From the graph it is observed the H₂ flux reducing from the high flux rates which are observed during the purging and charging with

5. MaxPHOS and Asymmetric Hydrogenation

H₂ process to instantly begin to rise once again. It rises steadily until all substrate is consumed and falls suddenly with a total recorded time of 25.6 minutes. Slightly shorter than the process described in graph 5.1 which was 28 minutes, possibly due to hydrogenation taking place during the purging process.

From the time observed for this hydrogenation to go to completion, the TOF for the MaxPHOS-rhodium active catalyst in the hydrogenation of the Z-MAC substrate could be estimated.

Figure 5.6: An estimation of the MaxPHOS rhodium catalyst turn-over frequency.

$$TOF = \frac{S(Z)}{(C.Z)(T)} = \frac{(1 \times 10^{-3} \text{ mol})(6.022 \times 10^{23})}{((0.01 \times 10^{-3} \text{ mol})(6.022 \times 10^{23}))(1536\text{s})} = 0.065 \text{ s}^{-1}$$

S = Substrate (mol).

C = Catalyst loading (mol)

T = time of reaction (s)

Z = Avogadro's constant.

This value suggests that one molecule of MaxPHOS rhodium catalyst catalyses 0.065 molecules of substrate to hydrogenated product every second or 3.9 per minute. This value complies with the time which was needed to give full hydrogenation during the reduction in catalyst loading experiments described in table 5.8 (page 131) where at 0.01 mol % 43 hours (154,800 s) of hydrogenation time delivered 100 % conversion. Curiously it could be noted that the reduction of catalyst loading to 0.01 mol % experiment was carried out at 5 bars of hydrogen as it was expected the reaction would take too long and the hydrogen flux experiments described in graphs 5.1 and 5.2 were carried out at 3 bars of hydrogen pressure. This implies that there is no increase in the speed of hydrogenation by increasing the pressure from 3 bars to 5 bars.

Figure 5.7: TOF extrapolated from reduction of catalyst loading.

$$TOF = \frac{10,000 \text{ sub}}{154,800 \text{ s}} = 0.065 \text{ sub. s}^{-1}$$

sub = molecules of substrate

However this TOF value is only applicable for the hydrogenation of this substrate with the MaxPHOS-rhodium catalyst while following the same procedures and using the same hydrogenation apparatus that have been employed in this work within reasonably similar ranges of temperature and pressure. For example, in one instance a hydrogenation of Z-MAC by [(MaxPHOS)Rh(COD)]BF₄ preformed catalyst monitored by hydrogen flux, where the solvent had not been sufficiently saturated with H₂ through a vacuuming and flushing process lead to the reaction time to almost double to 65 minutes. Also it is very feasible to consider that with a different hydrogenation reaction vessel and system with better circulation of hydrogen gas through the solvent a quicker reaction and a higher TOF for this catalyst could then be observed.

5.3 Conclusions

In this chapter it has been described the expansion in the substrate scope of the MaxPHOS-rhodium catalysed asymmetric hydrogenation to include 5 more hydrogenation substrates providing good to very good enantiomeric excesses. The feasibility of asymmetric hydrogenation taking advantage of the *in-situ* formation of the MaxPHOS-rhodium catalyst using the MaxPHOS·HBF₄ phosphonium salt has been proved. An insight into the speed of the asymmetric hydrogenation by the MaxPHOS-Rh catalyst while catalysing the asymmetric hydrogenation of the Z-MAC substrate has been given and also a curious anomaly has been described whereby in the asymmetric hydrogenation of the Z-MAC substrate, recrystallization of the substrate prior to hydrogenation was proven to be detrimental to the eventual enantiomeric excess obtained.

¹ Gridnev, I. D.; Imamoto, T.; Hoge, G.; Kouchi, M.; Takahashi, H. *J. Am. Chem. Soc.* **2008**, *130*, 2560.

² Zhang, Z. G.; Zhu, G. X.; Jiang, Q. Z.; Xiao, D. M.; Zhang, X. M. *J. Org. Chem.* **1999**, *64*, 1774.

³ Ohashi, A.; Kikuchi, S.; Yasutake, M.; Imamoto, T. *Eur. J. Org. Chem.* **2002**, 2535.

5. MaxPHOS and Asymmetric Hydrogenation

-
- ⁴ Bernsmann, H.; van den Berg, M.; Hoen, R.; Minnaard, A. J.; Mehler, G.; Reetz, M. T.; De Vries, J. G.; Feringa, B. L. *J. Org. Chem.* **2005**, *70*, 943.
- ⁵ a) *Phosphorous Ligands in Asymmetric Catalysis*; Börner, A., Ed.; Wiley-WCH: Weinheim, 2008; Vol. I-III. b) Nugent, T. C.; El-Shazly, M. *Adv. Synt. Catal.* **2010**, *352*, 753-819. c) Xie, J.; Zhu, S.; Zhou, Q. *Chem. Rev.* **2011**, *111*, 1713-1760. d) Gómez, A. R.; Adrio, J.; Carretero, J. C. *Angew. Chem. Int. Ed.* **2006**, *45*, 7674-7715.
- ⁶ Tang, W. J.; Chi, Y. X.; Zhang, X. M. *Org. Lett.* **2002**, *4*, 1695.
- ⁷ Mickel, S. J.; Sedelmeier, G. H.; Niederer, D.; Schuerch, F.; Koch, G.; Kuesters, E.; Daeffler, R.; Osmani, A.; Seeger-Weibel, M.; Schmid, E.; Hirni, A.; Schaer, K.; Gamboni, R. *Org. Process Res. Dev.* **2004**, *8*, 107.
- ⁸ Paterson, I.; Delgado, O.; Florence, G. J.; Lyothier, I.; O'Brien, M.; Scott, J. P.; Sereinig, N. *J. Org. Chem.* **2005**, *70*, 150.
- ⁹ Shimizu, H.; Saito, T.; Kumobayashi, H. *Adv. Synth. Catal.* **2003**, *345*, 185.
- ¹⁰ a) Fernandez-Perez, H.; Donald, S. M. A.; Munslow, I. J.; Benet-Buchholz, J.; Maseras, F.; Vidal-Ferran, A. *Chem. Eur. J.* **2010**, *16*, 6495. b) Robert, T.; Abiri, Z.; Sandee, A. J.; Schmalz, H.-G.; Reek, J. N. H. *Tetrahedron-Asymmetry* **2010**, *21*, 2671.
- ¹¹ Burk, M. J.; Feaster, J. E.; Nugent, W. A.; Harlow, R. L. *J. Am. Chem. Soc.* **1993**, *115*, 10125.
- ¹² a) Seebach, D.; Kimmerlin, T.; Sebesta, R.; Campo, M. A.; Beck, A. K. *Tetrahedron* **2004**, *60*, 7455. b) Liu, D. H.; DeGrado, W. F. *J. Am. Chem. Soc.* **2001**, *123*, 7553. c) Cheng, R. P.; DeGrado, W. F. *J. Am. Chem. Soc.* **2001**, *123*, 5162.
- ¹³ a) Huang, H. M.; Liu, X. C.; Chen, S.; Chen, H. L.; Zheng, Z. *Tetrahedron-Asymmetry* **2004**, *15*, 2011. b) Huang, J.-D.; Hu, X.-P.; Duan, Z.-C.; Zeng, Q.-H.; Yu, S.-B.; Deng, J.; Wang, D.-Y.; Zheng, Z. *Org. Lett.* **2006**, *8*, 4367.
- ¹⁴ Jaekel, C.; Krahnert, W.-R.; Paciello, R.; Siegel, W.; Basf Aktiengesellschaft, Germany . 2008, p 31 pp.
- ¹⁵ Burk, M. J.; Casy, G.; Johnson, N. B. *J. Org. Chem.* **1998**, *63*, 6084.
- ¹⁶ a) Bailly, F.; Queffelec, C.; Mbemba, G.; Mouscadet, J.-F.; Pommery, N.; Pommery, J.; Henichart, J.-P.; Cotellet, P. *Eur. J. Med. Chem.* **2008**, *43*, 1222. b) Jursic, B. S.; Sagiraju, S.; Ancalade, D. K.; Clark, T.; Stevens, E. D. *Synth. Commun.* **2007**, *37*, 1709.
- ¹⁷ Yu, C. Z.; Liu, B.; Hu, L. Q. *J. Org. Chem.* **2001**, *66*, 5413.
- ¹⁸ Hoen, R.; Tiemersma-Wegman, T.; Procuranti, B.; Lefort, L.; de Vries, J. G.; Minnaard, A. J.; Feringa, B. L. *Org. Biomol. Chem.* **2007**, *5*, 267.
- ¹⁹ Simons, C.; Hanefeld, U.; Arends, I.; Sheldon, R. A.; Maschmeyer, T. *Chem. Eur. J.* **2004**, *10*, 5829.
- ²⁰ Zhou, Y. G.; Tang, W. J.; Wang, W. B.; Li, W. G.; Zhang, X. M. *J. Am. Chem. Soc.* **2002**, *124*, 4952.
- ²¹ Hsiao, Y.; Rivera, N. R.; Rosner, T.; Krska, S. W.; Njolito, E.; Wang, F.; Sun, Y. K.; Armstrong, J. D.; Grabowski, E. J. J.; Tillyer, R. D.; Spindler, F.; Malan, C. *J. Am. Chem. Soc.* **2004**, *126*, 9918.
- ²² Reves, M.; Ferrer, C.; Leon, T.; Doran, S.; Etayo, P.; Vidal-Ferran, A.; Riera, A.; Verdaguer, X. *Angew. Chem., Int. Ed.* **2010**, *49*, 9452.

Conclusions

6

6. Conclusions

Work began focusing on S-stereogenic *N*-phosphino sulfinamide ligands applied toward asymmetric metal catalysis and especially the asymmetric hydrogenation reaction. The ligand **71-BH₃** was prepared and it formed a neutral complex **73** when coordinated to rhodium which could later be protonated to form its cationic counterpart **74**. The complex **73** hydrogenated hydrogenation substrate *Z*-MAC to a best enantiomeric excess of 42 %. After some time was spent working towards analogues of **71-BH₃** in the attempt to form an *N*-phosphino sulfinamide ligand-rhodium complex which could provide better enantiomeric excess in the rhodium catalysed asymmetric hydrogenation with little progress, attention was shifted towards the MaxPHOS ligand.

The MaxPHOS ligand was coordinated to palladium forming the complex **90**. It was coordinated to a cobaltcarbonyl-alkyne cluster and applied in the catalytic asymmetric Pauson-Khand reaction, forming the Pauson-Khand adduct yielding a noteworthy best enantiomeric excess of 28 % ee with norbornadiene and the butyl-substituted terminal alkyne. The optimized route to the MaxPHOS-rhodium catalyst was discovered taking advantage of [(COD)Rh(acac)] as the source of rhodium. The [(NBD)Rh(MaxPHOS)]BF₄ complex **96** was prepared. The [(CO)₂Rh(MaxPHOS)]BF₄ complex **97** was prepared and was used to examine the carbonyl stretching by FT-IR in analysis of the electronic nature of the ligand especially in comparison with the TCFP ligand.

Several MaxPHOS ligand derivatives were prepared. The diselenide MaxPHOS derivative **99** was used to shed more light on the electronic nature of the phosphine moieties of the ligand. The dioxide and disulphide derivatives **101** and **102** were also prepared. Several mono-chalcogenated MaxPHOS derivatives were prepared. They were coordinated to rhodium and applied in the asymmetric hydrogenation reaction providing a best enantiomeric excess of 21% ee hydrogenating the *Z*-MAC substrate. The mono-sulphide MaxPHOS derivative **106** was coordinated to palladium to form a neutral mono nucleic complex **110** bearing two ligands.

A set of hydrogenation substrates was prepared with which the MaxPHOS-rhodium catalyst had not yet been tested and it was shown to hydrogenate five of them with good to excellent enantioselectivities. The optimized *in-situ* generation of the MaxPHOS-rhodium catalyst and application in asymmetric hydrogenation of *Z*-MAC was discovered. A TOF value was closely estimated for the MaxPHOS-rhodium catalysed asymmetric hydrogenation of the *Z*-

6. Conclusions

MAC substrate by carrying H₂ flux experiments during the course of a two hydrogenation reactions.

The scientific and experimental knowledge of the MaxPHOS ligand as applied in asymmetric catalysis has been expanded during the course of this work, the knowledge of its coordination capacity to different metals, its application in different asymmetric transformations such as the Pauson-Khand and its scope of applicability in the asymmetric hydrogenation has been broadened. The understanding of the electronic nature of the ligand has been enhanced. Key intermediates from its preparation were taken advantage of to develop and prepare new molecular entities, new ligands and new metal-ligand complexes. The knowledge of *N*-phosphino sulfinamide ligands as applied to asymmetric catalysis has also been expanded during this work and new molecular entities of this class and type have been introduced into the knowledge community.

Experimental

7

7.1 General Methods:

7.1.1 Instrumentation:

Polarimetry:

The values of optical rotation ($[\alpha]_D$) have been determined using a Perkin-Elmer polarimeter 241 at 25 °C. A cell with a length of 1 dm and a volume of 1 mL has been used. The concentration is expressed in the form g/100 mL. A sodium lamp with a wavelength of 589 nm has been employed.

Melting points (mp):

All melting points have been obtained using a Büchi B-540 melting point apparatus.

Infrared spectroscopy (IR):

All IR spectrums have been obtained using a Thermo Nicolet Nexus FT-IR fourier transform spectrometer. The samples were prepared by either dissolution in solvent and subsequent formation of a film on a NaCl disc by evaporation of the prepared solution or by the preparation of a KBr disc.

Nuclear Magnetic Resonance Spectroscopy (NMR):

NMR spectra were recorded at room temperature, unless otherwise stated, on a Varian Mercury 400 or Varian inova 300. ^1H NMR and ^{13}C NMR spectra were referenced to residual solvent peaks. ^{31}P NMR spectra were referenced with phosphoric acid. ^{19}F NMR spectra were referenced by the spectrometer without external reference. Signal multiplicities in the ^{13}C spectra have been assigned by DEPT (Direct Enhancement by Polarisation Transfer) and HSQC (Hetero-nuclear Single Quantum Correlation) experiments and are described as C (quaternary), CH (tertiary), CH_2 (secondary) and CH_3 (primary). The following abbreviations were used to define the multiplicities:

7. Experimental

δ : Chemical shift in ppm with trimethylsilane as reference.

J: Coupling constant in Hz.

s, singlet; d, doublet; dd, double doublet; t, triplet; q, quartet; m, multiplet; br, broad.

Mass spectrometry:

Exact masses were obtained from The Mass Spectrometry Core Facility located in the Institute for Research in Biomedicine of the Parc Científic, Barcelona using NanoESI techniques.

Elemental analysis (EA):

Have all been determined by the *Unitat de Tècnics Separatives i Síntesi de Pèptids* (The Separation Techniques and Peptide Synthesis Unit) located at the Parc Científic, Barcelona.

Chromatography:

- **Column chromatography:** The technique of flash column chromatography has been utilized under pressure of air with silica gel (SiO₂) of 35 – 70 μ M as stationary phase or using the TELEDYNE ISCO brand CombiFlash R system.
- **Thin layer chromatography:** Aluminium sheets of Silica gel 60 F₂₅₄ provided by Merck have been employed. The following TLC stains have been used.
 - Anisaldehyde: 9.2 mL of 4-methoxybenzaldehyde, 3.8 mL of glacial acetic acid, 338 mL of EtOH and 12.5 mL of concentrated sulfuric acid (98%).
 - Phosphomolybdic acid: 23 g of phosphomolybdic acid in 400 mL of EtOH (95 %).
 - Potassium permanganate: 3g of potassium permanganate, 300 mL of water, and 5 mL of aqueous NaOH (5 %).

7.1.2 Materials and Techniques:

Solvents:

The solvents used have been dried using the Innovative Technology Inc. Puresolv purification system when anhydrous conditions were needed.

Non-anhydrous solvents which have been used (Hexane, Heptane, EtOAc, absolute EtOH, MeOH, acetonitrile, CHCl_3 , 2-propanol, *tert*-butanol, benzene, DMSO, etc.) have all been of synthesis quality or better.

Cold baths:

0 °C: ice and water.

-20 °C: ice and NaCl.

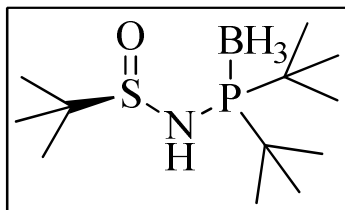
-78 °C: acetone and dry ice.

Reaction conditions:

In general anhydrous reaction conditions have been observed, round-bottom flasks have been flamed using hot air from a heat pistol or have been kept overnight at 60 °C in an oven with a flux of N_2 used subsequently to remove moisture, septums adaptable to the mouth of flasks have been employed, balloons of nitrogen haven been used to ensure an inert atmosphere inside the reaction flask. In certain cases schlenk reaction vessels have been employed to ensure inert conditions, remaining connected to a line supplying nitrogen for the duration of the reaction.

Plastic syringes or glass Hamilton microsyringes of 10, 50, 100 and 250 μL have been utilized to carry out additions to reactions in combination with stainless steel needles. In all cases stirring has been applied using magnetic stirrer bars and magnetic stirrer plates.

For reactions carried out under atmosphere of CO , balloons were used for a pressure of one atmosphere and glass pressure tubes were used for greater pressures. The seal for the glass pressure tubes are equipped with a manual 2-way valve (connector for entry of gas and septum for removal of samples).

7.2 Chapter 3 Experimental**(-)-(R)-N-(di-*tert*-butylphosphino)-2-methylpropane-2-sulfinamide borane, 71-BH₃.**

n-BuLi (1.5 mL, 3.85 mmol) was added dropwise to a solution of (+)-(*R*)-*tert*-butylsulfinamide (0.423g, 3.5 mmol) stirring in THF (30 mL) at $-78\text{ }^{\circ}\text{C}$ under N₂ and the mixture was allowed to stir. After 30 min di-*tert*-butylchlorophosphine (0.731 mL, 3.85 mmol) was slowly

added over approximately 10 min with the temperature maintained at $-78\text{ }^{\circ}\text{C}$. The temperature was allowed to rise to $0\text{ }^{\circ}\text{C}$, the reaction was then stirred for 5 h at $0\text{ }^{\circ}\text{C}$. Upon consumption of the sulfinamide starting material, as monitored by TLC, BH₃·SMe₂ (0.405 mL, 3.85 mmol) was added to the reaction, which was allowed to heat up to room temperature and stirred for 17 h (overnight). To quench the reaction, 30 mL of water was added, the residue was then extracted with ether (3 x 30 mL). Organic extracts were combined and dried over MgSO₄, and solvents were extracted in *vacuo* and pure product (0.581 g, 96 %) was obtained as a white solid after purification by flash column chromatography (SiO₂, Hexanes/EtOAc, 80:20 to 1:1).

Rf : 0.3 (1:1 Hexane:EtOAc, SiO₂).

Mp: 155 – 157 $^{\circ}\text{C}$.

[α]_D = -40.8° (c 1.0, CH₂Cl₂).

IR (KBr): ν_{max} : 2382, 1366 cm⁻¹.

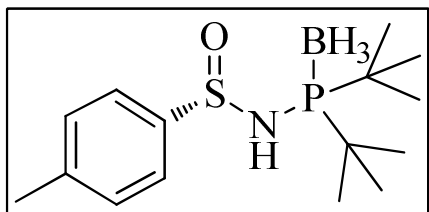
¹H NMR (400 MHz, CDCl₃): δ : 3.73 (s, N-H), 1.36 (d, $J = 13.7\text{ Hz}$, 9H), 1.32 (d, $J = 13.6\text{ Hz}$, 9H), 1.28 (s, 9H) ppm.

¹³C NMR (400 MHz, CDCl₃): δ : 58.19 (d, $J = 4.7\text{ Hz}$, C^q), 35.28 (d, $J = 4.4\text{ Hz}$, C^q), 35.02 (d, $J = 1.8\text{ Hz}$, C^q), 27.40 (dd, $J = 3.9, 2.6\text{ Hz}$, CH₃ X 6), 22.49 (s, CH₃ X 3) ppm.

³¹P NMR (300 MHz, CDCl₃): δ 76.41 – 75.88 (m) ppm.

HRMS (ESI⁺): Calculated for [M + M + Na]⁺ (C₂₄H₆₂B₂N₂NaO₂P₂S₂)⁺, m/z: 581.3806. Observed: 581.38075.

E.A.: Calculated for C₂₅H₆₆B₂N₂O₃P₂S₂ (2M + MeOH): C, 50.85; H, 11.27; N, 4.74; S, 10.86. Observed: C, 51.05; H, 11.10; N, 4.85; S, 11.04.

(+)-(S)-N-(di-tert-butylphosphino)-4-methylphenylsulfonamide borane, 72-BH₃.

n-BuLi (0.43 mL, 1.06 mmol) was added dropwise to the (+)-(S)-*p*-toluenesulfonamide stirring in THF (10 mL) under N₂ at -78 °C. After 50 min of stirring, P^tBu₂Cl (0.2 mL, 1.06 mmol) was slowly added. The solution was allowed to warm up to 0 °C and the

temperature was maintained at 0 °C for 4.5 h. BH₃·SMe₂ (0.1 mL, 1.06 mmol) was added and the reaction was allowed to stir overnight for 17 h at room temperature. The reaction was quenched with NH₄Cl (aq.). The organic layer was washed with water, and the aqueous fractions were combined and washed with EtOAc 3 times. The organic fractions were then combined and dried over MgSO₄, and the solvents were removed in *vacuo*. Pure product was obtained as a white solid (0.20 g, 67 %) after flash column chromatography (SiO₂, Hexanes/EtOAc, 80:20 to 6:4).

Rf : 0.5 (6:4 EtOAc:Hexane, SiO₂).

Mp: 161 °C.

[α]_D = + 79.9 ° (c 1.0, CH₂Cl₂).

IR (KBr): ν_{max}: 2975, 2385, 1469, 1341, 1059, 861 cm⁻¹.

¹H NMR (400 MHz, CDCl₃): δ 7.63 (d, 2H), 7.32(d, 2H), 2.43(s, 3H), 1.36 (d, 9H), 1.28 (d, 9H) ppm.

¹³C NMR (400 MHz, CDCl₃): δ 144.72 (d, *J* = 6.7 Hz, C^q), 142.32 (s, C^q), 130.11 (s, CH X 2), 124.73 (s, CH X 2), 35.21 (d, *J* = 14.6 Hz, C^q), 34.94 (d, *J* = 10.5 Hz, C^q) 27.54 (t, *J* = 2.6 Hz, CH₃ X 6), 21.64 (s, CH₃) ppm.

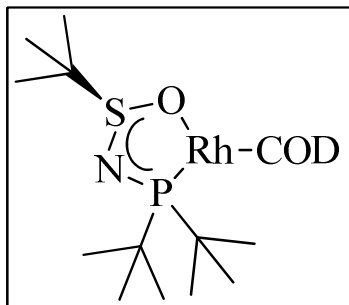
³¹P NMR (300 MHz, CDCl₃): δ 94.2 (m) ppm.

HRMS (ESI+): Calculated for [M + M + Na]⁺ (C₃₀H₅₈B₂N₂NaO₂P₂S₂)⁺, *m/z*: 649.34987. Observed: 649.34936.

E.A.: Calculated for C₁₅H₂₉BNOPS: C, 57.51; H, 9.33; N, 4.47. Observed: C, 57.33; H, 9.33; N, 4.34.

7. Experimental

[((+)-(R)-(tert-butylsulfinyl)(di-tert-butylphosphino)amide)Rh((1Z,5Z)-cycloocta-1,5-diene)], 73.



AgOTf (0.138g, 0.537 mmol) and Rh₂Cl₂COD₂ (0.133g, 0.269 mmol) were added to a round bottom flask under nitrogen, THF (2 mL) was added on top and this was allowed to stir, covered in aluminium foil. To a flame-dried schlenk tube was added the ligand **71-BH₃** (0.15g, 0.537 mmol), followed by DABCO (0.181g, 1.61 mmol) and toluene (5 mL), under nitrogen. It was stirred at 70 °C, monitoring by TLC, stirring and heating was stopped after an hour and it was allowed to cool. After the rhodium had stirred for 2 hours it was filtered through a pad of celite under N₂, washing with dry THF and it was concentrated in *vacuo*. The solution of rhodium was quickly added to the deprotected ligand **2** stirring in the schlenk tube, this was allowed to stir for an hour at room temperature before the residue was concentrated in *vacuo*. It was purified by flash column chromatography (SiO₂, Hexanes/EtOAc, 80:20) to give an orange solid (0.226g, 89 %).

Rf : 0.9 (8:2 Hexane:EtOAc, SiO₂).

[α]_D = + 48 ° (c 0.7, CH₂Cl₂).

IR (KBr): ν_{max} 2936 (broad), 1472, 1358, 1046, 1014, 852 cm⁻¹.

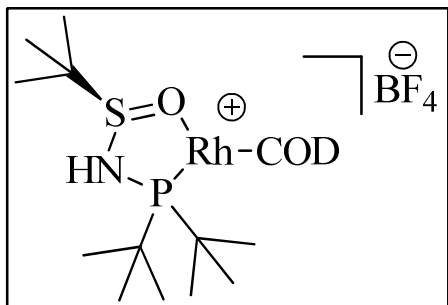
¹H NMR (400 MHz, CDCl₃): δ 5.22(dd, 2H) 4.05(dd, 2H) 2.48 (m, 1H) 2.22(m, 4H) 1.89 (m, 3H) 1.24 (dd, 1 8H) 1.10 (s, 9H) ppm.

¹³C NMR (400 MHz, CDCl₃): δ: 99.21 (dd, *J* = 10.3, 7.9 Hz, CH), 95.98 (dd, *J* = 11.4, 7.2 Hz, CH), 65.24 (d, *J* = 15.2 Hz, CH), 61.52 (d, *J* = 13.9 Hz, CH), 42.62 (d, *J* 13.0 Hz, C), 38.14 (d, *J* = 22.0 Hz, C), 34.72 (s, CH₂) 32.78 (s, CH₂) 30.17 (d, *J* = 50.1 Hz, C), 29.70 (d, *J* = 6.3 Hz, CH₃ X 3), 29.29 (d, *J* = 4.8 Hz, CH₃ X 3), 28.18 (s, CH₂), 27.28 (s, CH₂), 22.47 (s, CH₃ X 3) ppm.

³¹P NMR (300 MHz, CDCl₃): δ: 138.36 (d, *J* = 145.0 Hz) ppm.

HRMS (ESI+): Calculated for [M + H⁺]⁺ (C₂₀H₃₉NOPRhS)⁺, m/z: 476.1623. Observed: 476.1619.

[((+)-(R)-N-(di-*tert*-butylphosphino)-2-methylpropane-2-sulfinamide)Rh((1Z,5Z)-cycloocta-1,5-diene)] BF₄, 74.



The rhodium complex **73** (0.05g, 0.105 mmol) was stirred in anhydrous Et₂O (3 mL) under N₂ in a round bottom flask and to it was added HBF₄·OEt₂ (0.014 mL, 0.105 mmol) dropwise. A precipitate instantly fell out of solution. The supernatant was removed by syringe. The precipitate was washed with dry diethyl ether (3 x 2 mL). Solvent was removed in *vacuo* and later by high vacuum to afford product as a bright yellow powder (0.041g, 69 %).

$[\alpha]_{\text{D}} = + 27.9^{\circ}$ (c 0.32, CH₂Cl₂).

IR (KBr): ν_{max} : 2919, 1471, 1076 cm⁻¹.

¹H NMR (400 MHz, CDCl₃): δ 5.97 (s, 1H), 5.44 – 5.33 (m, 1H), 5.15 (s, 1H), 4.27 (s, 1H), 2.61 – 2.47 (m, 1H), 2.47 – 2.33 (m, 3H), 2.28 – 2.18 (m, 1H), 2.14 – 1.97 (m, 3H), 1.81 (s, 1H, NH), 1.50 (d, $J = 14.6$ Hz, 9H), 1.40 (s, 9H), 1.35 (d, $J = 14.9$ Hz, 9H) ppm.

¹³C NMR: (400 MHz, CDCl₃): δ 105.54 (s, CH), 102.09 (d, $J = 18.7$ Hz, CH), 67.12 (d, $J = 211.0$ Hz, CH), 60.09 (d, $J = 91.0$ Hz, CH), 42.74 (d, $J = 6.2$ Hz, C), 39.62 (dd, $J = 14.7, 3.0$ Hz, C), 33.40 (s, CH₂), 33.12 (s, CH₂), 29.65 (s, CH₃ X 3), 28.98 (s, CH₃ X 3), 27.61 (s, CH₂ X 2), 21.92 (s, CH₃ X 3) ppm.

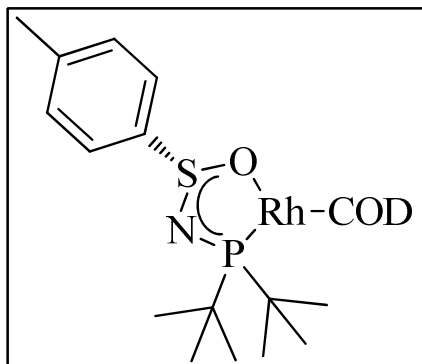
³¹P NMR: (300 MHz, CDCl₃): δ :140.449 (br) ppm.

¹⁹F NMR: (400 MHz, CDCl₃): δ -150.53 (s), -150.59 (s) ppm.

HRMS (ESI+): Calculated for [M]⁺ (C₂₀H₄₀BF₄NOPRhS)⁺, m/z: 476.1617. Observed: 476.1618.

7. Experimental

[((S)-(di-tert-butylphosphino)(p-tolylsulfinyl)amide)Rh((1Z,5Z)-cycloocta-1,5-diene)], 75.



The PNSO ligand **72-BH₃** (0.06g, 0.192 mmol), DABCO (0.065g, 0.575 mmol) and toluene (3 mL) were added to a flame-dried Schlenk tube under N₂ and this solution was heated to 65 °C while stirring. It was stirred for 1.25 h and then allowed to cool to room temperature. After 45 min, [Rh(COD)₂][BF₄] (0.078g, 0.192 mmol) in anhydrous MeOH (2 mL)

was added to the Schlenk flask. After 2 h of stirring, the solvents were removed in *vacuo* and pure product (80 mg, 77 %) was obtained after flash column chromatography (SiO₂, Hexanes/EtOAc, 9 : 1).

Rf: 0.25 (9:1 Hexane:EtOAc, SiO₂).

[α]_D = + 68.4 ° (c 0.55, CH₂Cl₂).

IR (KBr): ν_{max} : 2944 (large), 1588, 1471, 1037 cm⁻¹.

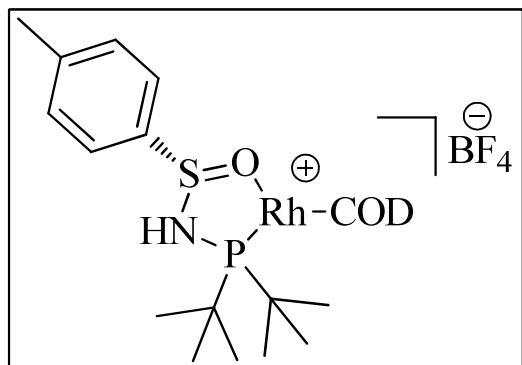
¹H NMR (400 MHz, CDCl₃): δ 7.84 (d, *J* = 8.1 Hz, 2H), 7.22 (d, *J* = 7.9 Hz, 2H), 5.40 – 5.25 (m, 2H), 4.20 – 4.02 (m, 2H), 2.51 – 2.40 (m, 1H), 2.37 (s, 3H), 2.40 – 2.26 (m, 4H), 2.19 – 1.88 (m, 3H), 1.34 (d, *J* = 13.2 Hz, 9H), 0.92 (d, *J* = 13.3 Hz, 9H) ppm.

¹³C NMR (400 MHz, CDCl₃): δ 151.70 (s, C), 139.58 (s, C), 128.71 (s, CH), 124.62 (s, CH), 99.82 (d, *J* = 8.1 Hz, CH), 96.01 (s, CH), 67.67 (d, *J* = 14.7 Hz, CH), 61.51 (d, *J* = 15.6 Hz, CH), 40.75 (d, *J* = 22.3 Hz, C), 37.22 (dd, *J* = 17.4, 3.8 Hz, C), 33.64 (s, CH₂), 33.27 (s, CH₂), 29.48 (d, *J* = 5.4 Hz, CH₃ X 3), 28.51 (d, *J* = 5.6 Hz, CH₃ X 3), 27.82 (s, CH₂), 27.49 (s, CH₂), 21.31 (s, CH₃) ppm.

³¹P NMR (300 MHz, CDCl₃): δ 148.74 (d, *J* = 149.4 Hz) ppm.

HRMS (ESI+): Calculated for [(PNSO)Rh(PNSO)]⁺ (C₃₀H₅₂N₂O₂P₂RhS₂)⁺, *m/z*: 701.19950. Observed: 701.19927.

[((*S*)-*N*-(di-*tert*-butylphosphino)-4-methylbenzenesulfinamide)Rh((1*Z*,5*Z*)-cycloocta-1,5-diene)]BF₄, 76.



The complex **75** (0.042 g, 0.078 mmol) was stirred in anhydrous Et₂O (3 mL) under N₂ and HBF₄·OEt₂ (0.11 mL of a 1:10, HBF₄·OEt₂ : Et₂O solution, 0.078 mmol) was then added. A yellow precipitate quickly formed and fell out of solution. This precipitate was washed several times with

anhydrous Et₂O to yield pure product in quantitative yield (0.051 g, 99 %).

[α]_D = + 55.6 ° (c 0.85, CH₂Cl₂).

IR (KBr): ν_{max} 3506, 3199, 2940 (broad), 1482, 1051 cm⁻¹.

¹H NMR (400 MHz, CDCl₃): δ 8.19 (d, *J* = 8.2 Hz, 2H), 7.43 (d, *J* = 8.0 Hz, 2H), 5.57 – 5.47 (m, 1H), 5.34 – 5.23 (m, 1H), 4.25 (d, *J* = 49.5 Hz, 2H), 2.64 – 2.47 (m, 4H), 2.46 (s, 3H), 2.28 – 2.03 (m, 4H), 1.56 (d, *J* = 14.6 Hz, 9H), 0.90 (d, *J* = 15.0 Hz, 9H) ppm.

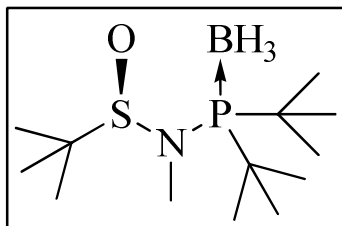
¹³C NMR (400 MHz, CDCl₃): δ 143.96 (s, C), 130.00 (s, CH), 125.10 (s, CH), 109.98 (s, C), 105.87 (s, CH), 100.54 (dd, *J* = 12.0, 7.3 Hz, CH), 73.82 (s, CH), 64.58 (s, CH), 38.10 (s, C), 34.26 (s, CH₂), 32.12 (s, CH₂), 29.50 (d, *J* = 5.9 Hz, CH₃ X 3), 28.35 (s, CH₂), 27.77 (d, *J* = 6.1 Hz, CH₃ X 3), 26.71 (s, CH₂), 21.60 (s, CH₃) ppm.

³¹P NMR (300 MHz, CDCl₃): δ 140.11 (d, *J* = 150.2 Hz) ppm.

HRMS (ESI+): Calculated for [(PNSO)Rh(PNSO)]⁺ (C₃₀H₅₂N₂O₂P₂RhS₂)⁺, *m/z*: 701.19950. Observed: 701.19927.

7. Experimental

(di-*tert*-butyl(*N*,2-dimethylpropan-2-ylsulfinamido)phosphonio)trihydroborate, **78-BH₃**.



The PNSO ligand **71-BH₃** (0.5 g, 1.79 mmol) was stirred in THF (30 mL) at $-78\text{ }^{\circ}\text{C}$ under N_2 and to it was added *n*-BuLi (0.9 mL, 1.97 mmol) drop by drop and it was allowed to stir for 55 minutes. MeI (1.1 mL, 17.9 mmol) was then added directly and quickly. It was allowed to warm up and

left to stir for 24 hours. The reaction was quenched with water and extracted with Et_2O , dried over MgSO_4 and purified by flash column chromatography (SiO_2 , Hexanes/ EtOAc , 9:1 to 1:1) to yield a white solid (0.32 g, 61 %).

$[\alpha]_{\text{D}}^{25}$: $+85.602^{\circ}$ (c 0.013, CH_2Cl_2).

Mp: $122\text{ }^{\circ}\text{C}$.

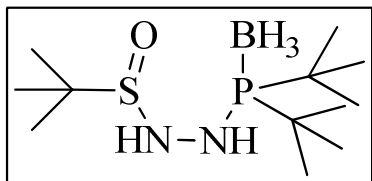
$^1\text{H NMR}$ (400 MHz, CDCl_3): δ .14(s, 3H), 1.46 (s, 9H), 1.26(dd, 18H) ppm

$^{13}\text{C NMR}$ (400 MHz, CDCl_3): δ 63.43 (s, C) 37.37 (s, N- CH_3), 36.87 (d, $J = 31.1\text{ Hz}$, C), 36.51 (d, $J = 26.0\text{ Hz}$, C), 28.72 (s, $\text{CH}_3 \times 6$), 25.14 (s, $\text{CH}_3 \times 3$) ppm.

$^{31}\text{P NMR}$ (300 MHz, CDCl_3): δ 85.54 (m) ppm.

IR (KBr): ν_{max} 3436, 2372, 1649, 1245, 1123 cm^{-1} .

MS ESI: Calculated for $[\text{M} - \text{H}]^+$ ($\text{C}_{13}\text{H}_{33}\text{BNOPS}$), m/z : 292.2030. Observed: 292.2029.

(di-*tert*-butyl(2-(*tert*-butylsulfinyl)hydrazinyl)phosphonio)trihydroborate, 79-BH₃.

Sulfinyl chloride (0.27 mL, 2.2 mmol) was added slowly to the di-*tert*-butyl chloro phosphine salt **83** (0.452 g, 1.99 mmol) and NaHCO₃ (0.836 g, 9.95 mmol) stirring in DMF (40 mL) under N₂. It quickly turned orange in colour. After 1.3 hours stirring, solvents were removed in *vacuo*. The residue obtained was dissolved in DCM (20 mL), it was washed with water (20 mL), the aqueous phase was extracted with DCM (4 X 20 mL), the organic extracts were combined, dried over MgSO₄, solvents were removed in *vacuo* to yield pure product as a white solid (0.676 g, 96 %).

Rf: 0.38 (1:1 Hexane:EtOAc, SiO₂).

Mp: 83 – 89 °C.

¹H NMR (400 MHz, CDCl₃): δ 6.69 (s, N-H), 6.13 (dd, N-H), 1.21 (dd, 18H), 1.15 (s, 9H) ppm.

¹³C NMR (400 MHz, CDCl₃): δ 56.24 (s, C), 35.24 (t, *J* = 28.5 Hz, C X 2), 27.98 (d, *J* = 14.2 Hz, CH₃ X 6), 23.20 (s, CH₃ X 3) ppm.

³¹P NMR (300 MHz, CDCl₃): δ 96 (s) ppm.

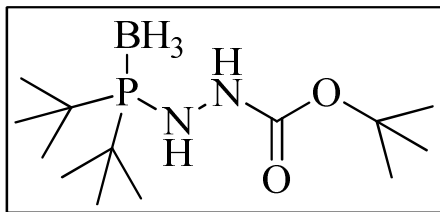
IR (KBr): ν_{max} 3411, 3231, 2956, 1482, 1360, 1008 cm⁻¹.

HRMS (ESI⁺): Calculated for [M + Na]⁺ (C₁₂H₃₂BN₂NaOPS), m/z: 317.1964. Observed: 317.1965.

E.A: Calculated for C₁₂H₃₂BN₂OPS: C, 48.98; H, 10.96; N, 9.52; S, 10.90. Observed: C, 46.55; H, 11.16; N, 7.71; S, 9.43.

7. Experimental

tert-butyl 2-(di-*tert*-butyl(borano)phosphino)hydrazinecarboxylate, **81**.



The *tert*-butylcarbazate (0.456 g, 3.45 mmol) was stirred in THF (10 mL) at $-78\text{ }^{\circ}\text{C}$ under N_2 and *n*-BuLi (1.52 mL, 3.8 mmol) was slowly added to it. It turned from colourless to yellow. After stirring for an hour the di-*tert*-butylchlorophosphine was added dropwise. It was stirred for two hours at $-78\text{ }^{\circ}\text{C}$ before it was allowed to warm up. It was stirred for 6 hours before $\text{BH}_3\cdot\text{SMe}_2$ (0.36 mL, 3.8 mmol) was added. It was stirred overnight, after 65 h stirring, 20 mL of water was added to quench the reaction. It was extracted with diethylether (3 X 20 mL), the organic extracts were combined, dried over MgSO_4 and solvents were removed in *vacuo*. Pure product was obtained as a white solid (0.670 g, 67 %) after flash column chromatography (9:1, Hexane:Ethyl acetate, SiO_2).

Rf : 0.25 (8:2 Hexane:EtOAc, SiO_2).

Mp: 134 - 136 $^{\circ}\text{C}$.

^1H NMR (400 MHz, CDCl_3): δ 6.03(s, 1H), 4.2(d, 1H), 1.46(s, 9H), 1.32 (d, 18H) ppm.

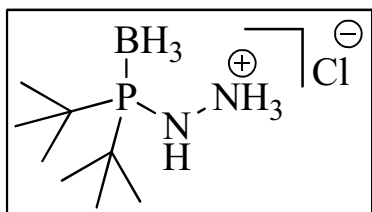
^{13}C NMR (400 MHz, CDCl_3): δ 29.91 (s, C^q) 35.08 (d, $J = 28.1\text{ Hz}$, $\text{C}^q \times 2$), 28.47 (s, $\text{CH}_3 \times 6$), 27.57 (d, $J = 2.1\text{ Hz}$, $\text{CH}_3 \times 6$) ppm.

^{31}P NMR (300 MHz, CDCl_3): δ 95 (d) ppm.

IR (KBr): ν_{max} 3315 (br), 2975, 2379, 1694, 1354, 1162, 1066 cm^{-1} .

HRMS (ESI+): Calculated for $[2\text{M} + \text{Na}]^+(\text{C}_{26}\text{H}_{64}\text{B}_2\text{N}_4\text{NaO}_4\text{P}_2)$, m/z : 603.4487. Observed: 603.4482.

E.A: Calculated for $\text{C}_{13}\text{H}_{32}\text{BN}_2\text{O}_2\text{P}$: C, 53.81; H, 11.11; N, 9.65; Observed: C, 53.40; H, 11.94; N, 9.52.

P-borane complex of 2-(di-*tert*-butylphosphino)hydrazin-1-ium chloride, 83.

The Boc protected hydrazine phosphine **81** (0.366 g, 1.26 mmol) was stirred in HCl·MeOH (1.25 M, 6.1 mL, 7.57 mmol) under N₂. It was stirred for 24 hours before solvents were removed in *vacuo* to yield pure compound as a white solid in quantitative yield (0.284 g).

¹H NMR (400 MHz, CDCl₃): δ 1.16 (d, 18H) ppm.

¹³C NMR (400 MHz, CDCl₃): δ 35.44 (d, *J* = 30.9 Hz, C X 2), 27.34 (d, *J* = 2.2 Hz, CH₃ X 6) ppm.

³¹P NMR (300 MHz, CDCl₃): δ 94 (s) ppm.

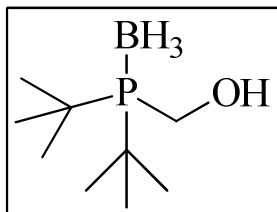
IR (KBr): ν_{max} 2654 – 3161 (br), 2383, 1912, 1593 cm⁻¹.

HRMS (ESI⁺): Calculated for [M – BH₃ + H⁺]⁺ (C₈H₂₂N₂P), *m/z*: 177.1521. Found: 177.1523

E.A: Calculated for C₈H₂₅BClN₂P: C, 42.42; H, 11.12; N, 12.37. Observed: C, 42.85; H, 11.62; N, 12.00.

7. Experimental

(di-*tert*-butyl(hydroxymethyl)phosphonio)trihydroborate, **88**.



The phosphine (di-*tert*-butylphosphonio)trihydroborate **87** (0.253 g, 1.58 mmol) was stirred in 20 mL THF at -78 °C and to it was added *s*-BuLi (3.8 mL, 3.48 mmol) dropwise. The reaction mixture turned a yellow colour. Paraformaldehyde (0.104 g, 3.48 mmol) was added dissolved in 8 mL of THF at -78 °C *via* syringe, washing with a further THF. The reaction was allowed to stir while warming up overnight. After 17 h stirring 50 mL water was added to the reaction, it was extracted with diethyl ether (5 X 50 mL), dried over MgSO₄ and solvent was removed in *vacuo*. The reaction gave pure product in quantitative yield as a white solid (0.317 g).

Rf: 0.38 (8:2 Hexane:EtOAc, SiO₂).

Mp: 139 °C.

¹H NMR (400 MHz, CDCl₃): δ 4.08 (d, CH₂), 1.96 (br s, O-H), 1.31 (d, 18H) ppm.

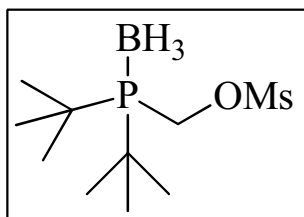
¹³C NMR (400 MHz, CDCl₃): δ 54.44 (d, *J* = 32.9 Hz, CH₂), 31.52 (s, C X 2), 27.92 (d, *J* = 0.8 Hz, CH₃ X 6) ppm.

³¹P NMR (300 MHz, CDCl₃): δ 46 (dd) ppm.

IR (KBr): ν_{max} 3465 (br), 2913, 2362 cm⁻¹.

HRMS (ESI+): Calculated for [M - BH₃ + H⁺]⁺ (C₉H₂₂OP), *m/z*: 177.14028. Observed: 177.1403.

EA: Calculated for C₉H₂₄BOP: C, 56.87; H, 12.73; Observed: C, 56.19; H, 13.68.

(di-tert-butyl(borano)phosphino)methyl methanesulfonate, 89.

The (di-tert-butyl(hydroxymethyl)phosphonio) trihydroborate phosphine **88** (0.123 g, 0.646 mmol) was stirred in DCM (4 mL) at 0 °C and to it was added Et₃N (0.14 mL, 0.969 mmol). MsCl (0.07 mL, 0.904 mmol) was slowly added. It was allowed to stir for 24 hours before 0.1M HCL (5mL), was added. The organic phase was washed with brine (5 mL), and the aqueous was extracted with DCM (3 X 10 mL), the organic fractions were combined and dried over MgSO₄ and solvents were removed in *vacuo*. Pure product was obtained as a white solid (0.113 g, 74 %) after flash column chromatography (8:2, Hexane:DCM increasing to 1:9, Hexane:DCM, SiO₂).

Rf : 0.25 (8:2 Hexane:EtOAc, SiO₂).

Mp: 90 – 93 °C.

¹H NMR (400 MHz, CDCl₃): δ 4.64 (d, 2H), 3.11(s, 3H), 1.40 (d, 18H) ppm.

¹³C NMR (400 MHz, CDCl₃): δ 61.46 (d, *J* = 26.6 Hz, CH₂), 37.51 (s, CH₃), 32.75 (d, *J* = 24.6 Hz, C^q X 2), 28.35 (s, CH₃ X 6) ppm.

³¹P NMR (300 MHz, CDCl₃): δ 46 (dd) ppm.

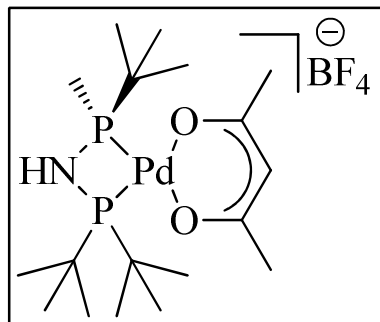
IR (KBr): ν_{max}: 3397, 2917, 2411, 1463, 1361, 1181, 983, 784 cm⁻¹.

HRMS (ESI+): Calculated for [M – H]⁺ (C₁₀H₂₅BO₃PS), m/z: 267.13496. Observed: 267.13481.

E.A.: Calculated for C₁₀H₂₆BO₃PS: C, 44.79; H, 9.77; S, 11.96. Observed: C, 42.63; H, 10.02; S, 11.92.

7. Experimental

7.3 Chapter 4 Experimental



[(MaxPHOS)Pd(acac)]BF₄, 90.

MaxPHOS·HBF₄ phosphonium salt (0.1 g, 0.284 mmol) and Pd(acac)₂ (0.087 g, 0.284 mmol) were stirred at 50 °C in MeOH (2 mL) for 24 hours before heating and stirring were stopped, the solvent was removed in *vacuo* and the complex was obtained (0.064 g, 40%) after recrystallizing from dissolution in minimum dichloromethane and layering on top with diethyl ether.

$[\alpha]_D$: -2.151 ° (c 0.013, CH₂Cl₂).

¹H NMR (400 MHz, CDCl₃): δ 5.96 (s, N-H), 5.37 (s, 1H), 5.35 (s, 1H-free acac), 2.01 (s, 6H, free acac), 1.92 (d, 6H-complexed acac), 1.87 (d, 3H, P-CH₃), 1.45 (t, 18H), 1.31 (d, 9H) ppm.

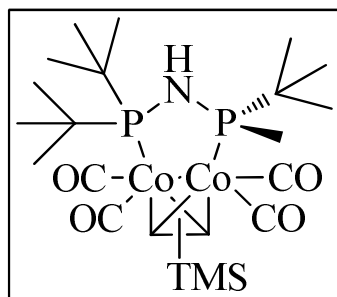
¹³C NMR (400 MHz, CDCl₃): δ 187.41 (C-H, free acac), 101.80 (s, 2 X CH₃, free acac), 100.04 (s, 2 X CH₃, complexed acac), 40.40 (d, C^q), 39.43 (d, C^q), 36.99 (d, C^q), 28.76 (dd, 6 X CH₃), 26.12 (m, 3 X CH₃), 12.47 (d, P-CH₃) ppm.

³¹P NMR (300 MHz, CDCl₃): δ 59.57 (d), 33.51 (d) ppm.

IR (KBr): ν_{max} 3244, 2950, 1568, 1378 cm⁻¹

HRMS (ESI⁺): Calculated for [M]⁺ (C₁₈H₄₁NO₂P₂Pd), m/z: 468.14071. Observed: 468.14064.

E. A: Calculated for C₁₈H₄₁BF₄NO₂P₂Pd: C, 38.7; H, 7.4; N, 2.51. Observed: C, 38.32; H, 7.17; N, 2.84.

[(MaxPHOS)Co₂(CO)₄(C₅H₁₀Si)], **92.**

MaxPHOS·HBF₄ (0.29 g, 0.827 mmol) was stirred with 1,4-diazabicyclo[2.2.2]octane (0.093 g, 0.827 mmol) and dicobalt tetracarbonyl ethynyltrimethylsilane complex (0.3 g, 0.752 mmol) in toluene (4 mL) under N₂ at 80 °C for 1 hour. It was allowed to cool before the solvent was removed in *vacuo* to yield product as a mixture of diastereomers (dr

1:0.8, 0.166 g, 37 %).

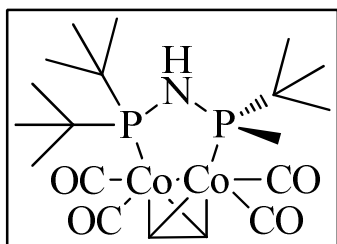
Rf: 0.48 (9:1, Hexane:Ethyl Acetate, SiO₂).

¹H NMR (400 MHz, CDCl₃): δ 5.51 (dd, *J* = 9.5, 7.1 Hz, 1H), 5.37 (dd, *J* = 9.8, 6.0 Hz, 1H), 2.32 (t, *J* = 5.0 Hz, 1H), 2.13 (t, *J* = 5.2 Hz, 1H), 1.88 (s, 1H), 1.25 (d, *J* = 4.5 Hz, 2H), 1.22 (d, *J* = 4.4 Hz, 3H), 1.02 (s, 8H), 0.99 – 0.96 (m, 18H), 0.93 (d, *J* = 4.3 Hz, 15H), 0.88 (d, *J* = 3.4 Hz, 8H) ppm.

³¹P NMR (300 MHz, CDCl₃): δ 133.64 (br s), 110.18 (br s), 105.35 (br s) ppm.

7. Experimental

[(*R*-MaxPHOS)Co₂(CO)₄(C₂H₂)], **93**.



The diastereomeric mixture of complexes of [(MaxPHOS)Co₂(CO)₄(C₂H-TMS)] **92** (0.148 g, 0.250 mmol) was stirred in THF (3 mL) under N₂ and a solution of TBAF (0.4 mL, 0.275 mmol) was added on top. It was monitored by TLC. After 1 hour 40 minutes, the solvent

was removed in *vacuo* and pure complex was obtained as a bright red solid (0.080 g, 61 %) after column chromatography (hexane/Ethyl acetate, SiO₂).

Rf: 0.3 (9:1 Hexane:DCM, SiO₂).

[α]_D: -13.975 ° (c 0.004, CH₂Cl₂).

Mp: 161 °C.

¹H NMR (400 MHz, CDCl₃): δ 5.65 – 5.50 (m, 1H), 2.42 (s, 1H), 1.53 (d, *J* = 6 Hz, 3H), 1.26 (d, *J* = 13.0 Hz, 18H), 1.20 (d, *J* = 14.2 Hz, 9H) ppm.

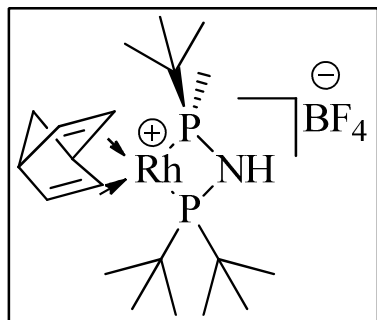
¹³C NMR (400 MHz, CDCl₃): δ 206.74 (s, CO X 4), 74.94 (d, *J* = 16.5 Hz, C-Co X 2), 38.77 (dd, *J* = 12.7, 5.5 Hz, C), 37.96 (dd, *J* = 10.6, 1.9 Hz, C), 35.13 (d, *J* = 23.9 Hz, C), 29.39 – 28.78 (m, CH₃ X 6), 26.25 (d, *J* = 6.7 Hz, CH₃ X 3), 20.04 (d, *J* = 13.2 Hz, P-CH₃) ppm.

³¹P NMR (300 MHz, CDCl₃): δ 135.09 (s), 108.66 (s) ppm.

IR (KBr): ν_{max} 3340, 2952, 2017, 1974, 1949, 1919, 1463 cm⁻¹.

HRMS (ESI⁺): Calculated for [M + H]⁺ (C₁₉H₃₄Co₂NO₄P₂), *m/z*: 520.06216. Observed: 520.06365.

E. A: Calculated for C₁₉H₃₃Co₂NO₄P₂: C, 43.95; H, 6.41; N, 2.70; Observed: C, 44.08; H, 6.73; N, 2.73.

[(*R*-MaxPHOS)Rh(NBD)]BF₄, 96.

(Acetylacetonato)(1,5-cyclooctadiene)rhodium (0.227 g, 0.941 mmol) and MaxPHOS-HBF₄ (0.350 g, 0.996 mmol) were stirred in a flame-dried schlenk tube under N₂ in MeOH (6 mL). It was stirred for 2 hours. The solvent was removed in *vacuo*. The obtained residue was dissolved in minimum DCM (1.6 mL) in a schlenk tube before being frozen in liquid N₂, excess Et₂O was added

on top and the tube was placed in the fridge overnight for the solid to slowly melt, and allow slow diffusion of the two solvent layers to form crystals. The next day the product was isolated as orange crystals (0.330 g, 77 %). The mother liquor was saved; solvents were removed in *vacuo* and recrystallized by layering of Et₂O over DCM once again to form crystals for X-ray analysis.

[α]_D: 97.8933 ° (c 0.005, CH₂Cl₂).

¹H NMR (400 MHz, CDCl₃): δ 5.80 (s, 1H), 5.59 (s, 1H), 5.46 (s, 1H), 5.39 (s, 2H), 4.22 (d, *J* = 10.6 Hz, 2H), 1.72 (s, 2H), 1.67 (d, *J* = 7.6 Hz, 3H), 1.40 – 1.30 (m, 18H), 1.14 (d, *J* = 16.3 Hz, 9H) ppm.

¹³C NMR (400 MHz, CDCl₃): δ 90.02 – 89.38 (m, CH), 86.45 (dd, *J* = 11.0, 6.1 Hz, CH), 82.82 – 82.36 (m, CH), 82.36 – 81.97 (m, CH), 71.03 (d, *J* = 2.0 Hz, CH₂), 56.19 (s, CH), 55.73 (s, CH), 39.06 – 37.96 (m, C X 2), 36.10 – 35.12 (m, C), 28.82 (dd, *J* = 9.5, 6.7 Hz, CH₃ X 6), 26.20 (d, *J* = 6.3 Hz, CH₃ X 3), 12.86 (dd, *J* = 19.0, 2.1 Hz, P-CH₃) ppm.

³¹P NMR (300 MHz, CDCl₃): δ 76.28 (dd, *J* = 136.0, 54.6 Hz), 52.52 (dd, *J* = 138.2, 54.6 Hz) ppm.

¹⁹F NMR (300 MHz, CDCl₃): δ -150.26 (s) ppm.

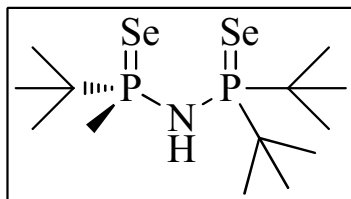
IR (KBr): ν_{max} 3273, 2950, 2868, 2348, 1048 cm⁻¹.

MS ESI: Calculated for [M]⁺ (C₂₂H₄₅NP₂Rh), *m/z*: 458.16073. Observed: 458.16040.

E. A: Calculated for C₂₀H₃₉BF₄NP₂Rh: C, 44.06; H, 7.21; N, 2.57. Observed: C, 38.15; H, 6.67; N, 2.36.

7. Experimental

(S)-P-(tert-butyl)-N-(di-tert-butylphosphoroselenoyl)-P-methylphosphinoselenoic amide, 99.



MaxPHOS·HBF₄ (0.1g, 0.285 mmol), Na₂CO₃ (0.151g, 1.42 mmol) and selenium powder (0.112g, 1.42 mmol) were stirred in MeOH (4 mL) at 50 °C for 17.5 hours. The following day stirring and heating was stopped, the solvent was removed in *vacuo*, the residue was suspended in EtOAc and then filtered over a short pad of silica, it was washed with HCl (0.1 M, 20 mL), the aqueous phase was extracted with EtOAc (3 X 20 mL), the organic fractions were combined, dried over MgSO₄, solvents were removed in *vacuo*. Pure product was obtained as a yellow/orange solid (0.093g, 78 %) after column chromatography (Hexane/EtOAc, SiO₂).

Rf: 0.65 (9:1 Hexane:EtOAc, SiO₂).

[α]_D: 29.160 ° (c 0.005, EtOAc).

Mp: 103 – 110 °C.

¹H NMR (400 MHz, CDCl₃): δ 3.01 (s, N-H), 2.53 (d, 3H), 1.40 (m, 27H) ppm.

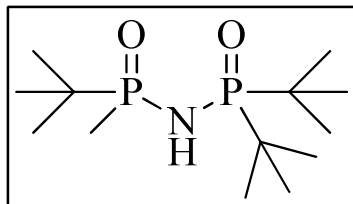
¹³C NMR (400 MHz, CDCl₃): δ 42.60 (d, *J* = 40.9 Hz, C^q), 41.62 (d, *J* = 43.9 Hz, C^q), 38.01 (d, *J* = 54.5 Hz, C^q), 28.08 (dd, *J* = 33.8, 2.4 Hz, CH₃ X 6), 25.35 (d, *J* = 2.6 Hz, CH₃ X 3), 18.22 (d, *J* = 51.8 Hz, P-CH₃) ppm.

³¹P NMR (300 MHz, CDCl₃): δ 102.60 (d, *J* = 43.0 Hz), 99.40 (d, *J* = 43.7 Hz), 96.94 – 95.50 (m), 87.39 (d, *J* = 43.7 Hz), 84.35 (d, *J* = 43.6 Hz), 81.30 (d, *J* = 43.7 Hz) ppm.

IR (KBr): ν_{max} 3308, 2905 (large), 2353, 1470, 1265, 1181, 906 cm⁻¹.

HRMS (ESI+): Calculated for [M – H]⁺ (C₁₃H₃₀NP₂Se₂), *m/z*: 422.01784. Observed: 422.01849.

E.A: Calculated for C₁₃H₃₁NP₂Se₂: C, 37.06; H, 7.42; N, 3.32; C, 39.35; H, 8.13; N, 3.40.

P-(tert-butyl)-N-(di-tert-butylphosphoryl)-P-methylphosphinic amide, 101.

MaxPHOS·HBF₄ (0.04g, 0.114 mmol) and Na₂CO₃ (0.036, 0.342 mmol) were stirred in MeOH (2 mL) at 0 °C for 30 minutes. H₂O₂·H₂O (0.03 mL, 0.342 mmol) was added to the reaction and it was allowed to stir for an hour. The reaction was quenched with the addition of HCl (0.1 M, 5 mL), it was extracted with EtOAc, the organic fractions were combined, dried over MgSO₄ and solvents were removed in *vacuo* to yield product as a white solid (0.014g, 41 %).

Rf: 0.5 (9:1 DCM:MeOH, SiO₂).

Mp: 90 °C.

¹H NMR (400 MHz, CDCl₃): δ 1.81 (d, 3H), 1.30 (dd broad, 27H) ppm.

¹³C NMR (400 MHz, CDCl₃): δ 37.39 (d, *J* = 73.8 Hz, C^q), 33.71 (d, *J* = 90.6 Hz, C^q), 30.28 (d, *J* = 77.4 Hz, C^q), 26.91 (s, CH₃ X 6), 24.75 (s, CH₃ X 3), 11.33 (d, *J* = 78.6 Hz, P-CH₃) ppm.

³¹P NMR (300 MHz, CDCl₃): δ 60.2 (br s), 52.9 (br s) ppm.

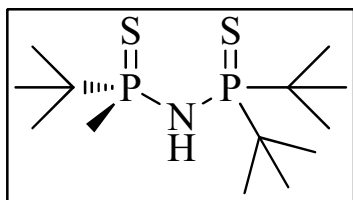
IR (KBr): ν_{max} 2938 (br), 2709, 1469 cm⁻¹.

HRMS (ESI+): Calculated for [M + H⁺] (C₁₃H₃₂NO₂P₂), *m/z*: 296.1908. Observed: 296.1900.

E.A: Calculated for C₁₃H₃₁NO₂P₂: C, 52.87; H, 10.58; N, 4.74; Observed: C, 52.15; H, 11.64. N, 3.84.

7. Experimental

P-(*tert*-butyl)-*N*-(di-*tert*-butylphosphorothioyl)-P-methylphosphinothioic amide, 102.



MaxPHOS·HBF₄ (0.1g, 0.285 mmol), Na₂CO₃ (0.151g, 1.42 mmol) and sulfur powder (0.046g, 1.42 mmol) were stirred in MeOH (4 mL) at 50 °C for 17.5 hours. The following day stirring and heating was stopped, the solvent was removed in *vacuo*, the residue was suspended in EtOAc and then filtered over a short pad of silica, it was washed with HCl (0.1 M, 20 mL), the aqueous phase was washed with EtOAc (3 X 20 mL), the organic fractions were combined, dried over MgSO₄, solvents were removed in *vacuo* to yield Pure product as an off-white solid (0.082g, 88 %).

Rf: 0.35 (95:5 Hexane:EtOAc, SiO₂).

[α]_D: 15.9 ° (c 0.006, EtOAc).

Mp: 129 – 131 °C.

¹H NMR (400 MHz, CDCl₃): δ 2.88 (s, N-H), 2.29 (d, 3H), 1.40 (m, 27H) ppm.

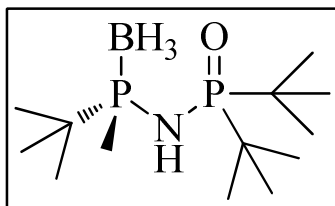
¹³C NMR (400 MHz, CDCl₃): δ 41.53 (d, C), 41.06 (dd, C), 37.31(dd, C), 27.59 (d, CH₃ X 6), 24.83(s, CH₃ X 3), 17.46(d, P-CH₃) ppm.

³¹P NMR (300 MHz, CDCl₃): δ 96.78 (d), 87.79 (d) ppm.

IR (KBr): ν_{max} 3355, 2949, 2342, 1475 cm⁻¹.

HRMS (ESI+): Calculated for [M + H]⁺ (C₁₃H₃₂NP₂S₂), m/z: 328.14459. Observed: 328.14455.

E.A: Calculated for C₁₃H₃₁NP₂S₂: C, 47.68; H, 9.54; N, 4.28; S, 19.58. Observed: C, 47.06; H, 9.43; N, 4.27; S, 19.79.

(tert-butyl((di-tert-butylphosphoryl)amino)(methyl)phosphonio)trihydroborate, 103.

The MaxPHOS-BH₃ **39** (0.15 g, 0.541 mmol), Na₂CO₃ (0.17 g, 1.6 mmol) and H₂O₂·H₂O (0.015 mL, 1.6 mmol) were stirred in MeOH (2 mL) for an hour. The solvent was removed in *vacuo*, and the residue was suspended in EtOAc and then filtered over a short pad of silica. Solvents were again removed in *vacuo* to yield pure product as a white solid (0.099 g, 62 %).

Rf: 0.5 (1:1 Hexane:EtOAc, SiO₂).

[α]_D: -14.370 ° (c 0.006, CH₂Cl₂).

Mp: 100 °C.

¹H NMR (400 MHz, CDCl₃): δ 2.29 (d, N-H), 1.80 (d, 3H), 1.29 (m, 27H) ppm.

¹³C NMR (400 MHz, CDCl₃): δ 37.96 (d, 2 X C^q), 32.10 (d, C^q), 27.29 (d, 6 X CH₃), 25.08 (d, 3 X CH₃), 7.85 (d, P-CH₃) ppm.

³¹P NMR (300 MHz, CDCl₃): δ 81.13 (br m), 61.61 (d) ppm.

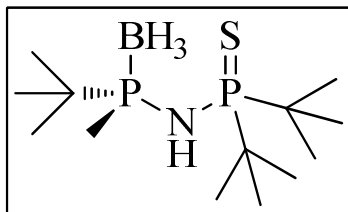
IR (KBr): ν_{max} 3580, 3346, 2952m 2866, 2380, 2331, 1629 cm⁻¹.

HRMS (ESI+): Calculated for [M + H]⁺ (C₁₃H₃₅BNOP₂), m/z: 294.22815. Observed: 294.22819.

E.A: Calculated for C₁₃H₃₄BNOP₂: C, 53.26; H, 11.69; N, 4.78. Observed: C, 52.32; H, 11.78; N, 4.76.

7. Experimental

(R)-(tert-butyl((di-tert-butylphosphorothioyl)amino)(methyl)phosphonio) trihydroborate, 104.



The MaxPHOS-BH₃ **39** (0.134g, 0.483 mmol), Na₂CO₃ (0.153g, 1.45 mmol) and sulphur powder (0.046, 1.45 mmol) were stirred in MeOH (5 mL) at 50 °C for an hour. Stirring and heating was stopped, the solvent was removed in *vacuo*, and the residue was suspended in EtOAc and then filtered over a short pad of silica. Solvents were again removed in *vacuo* to yield pure product as a white solid (0.127 g, 85%).

Rf: 0.8 (8:2 Hexane: EtOAc, SiO₂).

[α]_D: -4.940 ° (c 0.005, CHCl₃).

Mp: 108 – 113 °C.

¹H NMR (400 MHz, CDCl₃): δ 2.52 (s (br), N-H), 1.94 (d, 3H), 1.38 (dd, 18H), 1.27 (d, 9H) ppm.

¹³C NMR (400 MHz, CDCl₃): δ 41.49 (C X 2), 32.34 (d, C), 27.81 (d, 6 X CH₃), 25.54 (d, 3 X CH₃), 8.56 (d, P-CH₃) ppm.

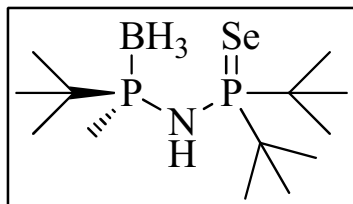
³¹P NMR (300 MHz, CDCl₃): δ 98.05 (d), 84.82 (br m) ppm.

IR (KBr): ν_{\max} 3363, 2951, 2396, 1473 cm⁻¹.

HRMS (ESI+): Calculated for [M – H]⁺ (C₁₃H₃₃BNP₂S), m/z: 308.18965. Observed: 308.18961.

E.A: Calculated for C₁₃H₃₄BNP₂S: C, 50.49; H, 11.08; N, 4.53; S, 10.37. Observed: C, 51.03; H, 11.38; N, 4.68; S, 10.05.

(tert-butyl((di-tert-butylphosphoroselenoyl)amino)(methyl)phosphonio) trihydroborate, 105.



The MaxPHOS-BH₃ **39** (0.107g, 0.386 mmol), Na₂CO₃ (0.122g, 1.16 mmol) and selenium powder (0.092, 1.16 mmol) were stirred in MeOH (5 mL) at 50 °C for an hour. Stirring and heating was stopped, the solvent was removed in *vacuo*, and the residue was suspended in EtOAc and then filtered over a short pad of silica. Solvents were again removed in *vacuo* to yield pure product as a yellow solid (0.117 g, 85%).

Rf : 0.65 (8:2 Hexane:EtOAc, SiO₂).

[α]_D: 5.908 ° (c 0.004, CH₂Cl₂).

Mp: 145 – 155 °C.

¹H NMR (400 MHz, CDCl₃): δ 2.68 (br s, N-H), 2.01 (d, 3H), 1.36 (m, 27H) ppm.

¹³C NMR (400 MHz, CDCl₃): δ 42.01 (C^q), 41.05(C^q), 32.21 (C^q) 27.78(dd, 6 X CH₃), 25.45 (s, 3 X CH₃), 8.47 (d, P-CH₃) ppm.

³¹P NMR (300 MHz, CDCl₃): δ 101.73 (d, sat), 98.55 (d, P=Se), 95.37 (d, sat), 86.43 (m, P-BH₃) ppm.

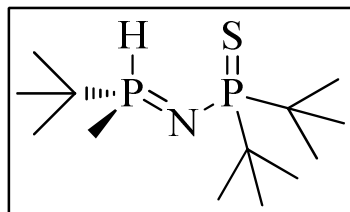
IR (KBr): ν_{max} 3311, 2961 (br), 2380 (br) cm⁻¹.

HRMS (ESI⁺): Calculated for [M – H]⁺ (C₁₃H₃₃BNP₂Se), m/z: 356.13410. Observed: 356.13470.

E.A: Calculated for C₁₃H₃₄BNP₂Se: C, 43.84; H, 9.62; N, 3.93. Observed: C, 44.00; H, 10.21; N, 3.87.

7. Experimental

(*R*)-P,P-di-*tert*-butyl-*N*-(*tert*-butyl(methyl)phosphoranylidene)phosphinothioic amide, **106**.



The mono-sulphur boron-protected MaxPHOS **104** (0.303g, 0.979 mmol) and 1,4-diazabicyclo[2.2.2]octane (0.385g, 3.43 mmol) were stirred in toluene (4 mL) at 70 °C under nitrogen for one hour. Solvent was removed in *vacuo* and pure product was obtained as a white solid (0.260g, 90 %) after column chromatography (Hexane:Ethyl acetate, 8:2, SiO₂).

Rf: 0.47 (8:2 Hexane: EtOAc, SiO₂).

[α]_D: -39.259 ° (c 0.005, CH₂Cl₂).

Mp: 90 °C.

¹H NMR (400 MHz, CDCl₃): δ 6.64 (d, 441 Hz, 1H), 1.67 (d, 3H), 1.3 (dd, 18H), 1.21 (d, 9H) ppm.

¹³C NMR (400 MHz, CDCl₃): δ 40.85 (d, C^q), 39.18 (d, C^q), 29.91 (s, C^q), 27.77 (d, 6 X CH₃), 24.57 (d, 3 X CH₃), 9.61 (d, P-CH₃) ppm.

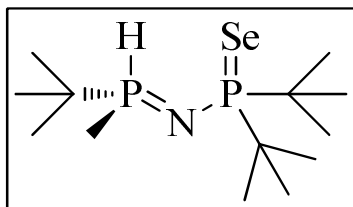
³¹P NMR (300 MHz, CDCl₃): δ 86.60 (s), 27.44 (s) ppm.

IR (KBr): ν_{\max} 2956 (br), 2303, 1476, 1171 cm⁻¹.

HRMS (ESI⁺): Calculated for [M + H]⁺ (C₁₃H₃₂NP₂S), m/z: 296.17252. Observed: 296.17232.

E.A: Calculated for C₁₃H₃₁NP₂S: C, 52.86; H, 10.58; N, 4.74; S, 10.85. Observed: C, 53.26; H, 11.18; N, 4.86; S, 10.4.

P,P-di-*tert*-butyl-*N*-(*tert*-butyl(methyl)phosphoranylidene)phosphinoselenoic amide, 107.



The mono-seleniated boron-protected MaxPHOS **105** (0.044g, 0.124 mmol) and 1,4-diazabicyclo[2.2.2]octane (0.042g, 0.371 mmol) were stirred in toluene (3 mL) at 70 °C under nitrogen for one hour. Solvent was removed in *vacuo* and pure product was obtained as a white solid (0.035g, 83 %) after column chromatography (Hexane/Ethyl acetate, SiO₂).

Rf: 0.5 (8:2 Hexane: EtOAc, SiO₂).

[α]_D: -67.446 ° (c 0.006, CH₂Cl₂).

Mp: 103 – 104 °C.

¹H NMR (400 MHz, CDCl₃): δ 7.15 (m, 0.5H), 6.03 (m, 0.5H), 1.65 (dd, 3H), 1.31 (dd, 18H), 1.21 (d, 9H) ppm.

¹³C NMR (400 MHz, CDCl₃): δ 40.87 (d, C), 39.06(d, C), 29.61(dd, C), 27.7 (d, 6 X CH₃), 24.41(s, 3 X CH₃), 9.52 (d, P-CH₃) ppm.

³¹P NMR (300 MHz, CDCl₃): δ 85.39(d), 30.67 (d) ppm.

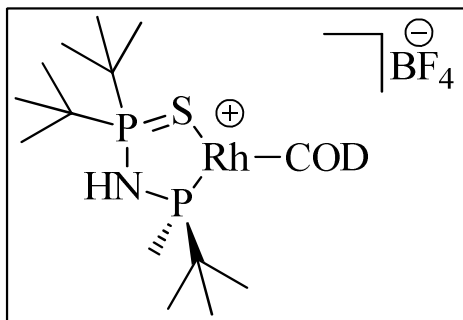
IR (KBr): ν_{max} 2932 (br), 2306, 1467 cm⁻¹.

HRMS (ESI+): Calculated for [M + H]⁺ (C₁₃H₃₂NP₂Se), m/z: 344.11697. Observed: 344.11702.

E.A: Calculated for C₁₃H₃₁NP₂Se: C, 45.61; H, 9.13; N, 4.09. Observed: C, 45.05; H, 8.87; N, 4.05.

7. Experimental

[(*R*-Mono-S-MaxPHOS)Rh(COD)]BF₄, **108**.



The mono-S-MaxPHOS **106** (0.016 g, 0.054 mmol) and [Rh(COD)₂]BF₄ (0.022 g, 0.054 mmol) were stirred in MeOH (2 mL) for 5 hours. The solvent was removed in *vacuo* to yield the complex as an orange/yellow solid (0.030 g, 94 %).

[α]_D: 110.219 ° (c 0.008, CH₂Cl₂).

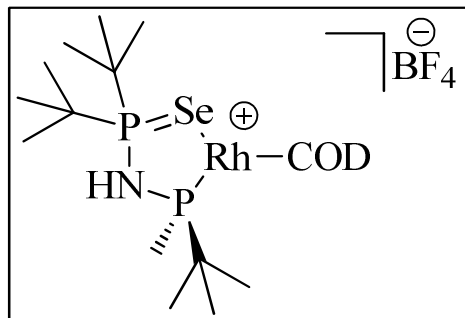
¹H NMR (400 MHz, CDCl₃): δ 5.57 (br s, CH), 5.37 (br s, CH), 4.16 (br s, CH), 4.07 (br s, CH), 2.48 – 2.01 (m, 8H, CH₂ X 4), 1.63 (d, J = 7.1 Hz, 3H), 1.48 (dd, J = 16.8, 4.3 Hz, 18H), 1.26 (d, J = 15.5 Hz, 9H) ppm.

¹³C NMR (400 MHz, CDCl₃): δ 102.67 (m, CH), 101.86 (m, CH), 80.72 (d, J = 12.8 Hz, CH), 71.38 (d, J = 11.9 Hz, CH), 40.00 (d, J = 42.8 Hz, C), 39.14 (dd, J = 43.8, 3.7 Hz, C), 37.78 (dd, J = 24.8, 1.5 Hz, C), 34.45 (d, J = 3.5 Hz, CH₂), 31.05 (s, CH₂), 30.27 (s, CH₂), 28.14 (d, J = 1.5 Hz, CH₃ X 3), 27.62 (d, J = 1.2 Hz, CH₃ X 3), 27.40 (d, J = 5.8 Hz, CH₃ X 3), 10.64 – 10.05 (m, P-CH₃) ppm.

³¹P NMR (300 MHz, CDCl₃): δ 115.80 (dd, J = 21.0, 3.2 Hz), 113.67 (d, J = 21.0 Hz), 112.41 (d, J = 20.9 Hz) ppm.

IR (KBr): ν_{max} 3211, 2968, 2877, 1465 cm⁻¹.

HRMS (ESI⁺): Calculated for [M]⁺ (C₂₁H₄₃NP₂RhS), m/z : 506.16410. Observed: 506.16375.

[(R-Mono-Se-MaxPHOS)Rh(COD)]BF₄, 109.

The mono-Se-MaxPHOS **107** (0.026 g, 0.08 mmol) and [Rh(COD)₂]BF₄ (0.032 g, 0.08 mmol) were stirred in MeOH (2 mL) for 5 hours. The solvent was removed in *vacuo* to yield the complex as a yellow/orange solid (0.047 g, 92 %).

[α]_D: 106.429 ° (c 0.009, CH₂Cl₂).

¹H NMR (400 MHz, CDCl₃): δ 5.50 (dd, J = 100.2, 35.4 Hz, 2H), 4.06 (d, J = 102.0 Hz, 2H), 2.62-1.96 (m, 4 X CH₂), 1.60 (d, J = 7.0 Hz, 3H), 1.49 (dd, J = 22.3, 17.2 Hz, 18H), 1.26 (d, J = 15.5 Hz, 9H) ppm.

¹³C NMR (400 MHz, CDCl₃): δ 107.48 (d, J = 7.6 Hz, CH), 102.10 – 99.95 (m, CH), 81.25 (d, J = 12.8 Hz, CH), 71.40 (d, J = 11.5 Hz, CH), 40.52 (d, J = 34.2 Hz, C), 39.25 (dd, J = 35.8, 3.7 Hz, C), 38.04 (dd, J = 26.3, 1.5 Hz, C), 34.88 (d, J = 3.4 Hz, CH₂), 31.11 (s, CH₂), 30.27 (s, CH₂), 29.68 (s, CH₂), 28.54 (s, CH₃ X 3), 27.81 (s, CH₃ X 3), 27.66 (d, J = 5.7 Hz, CH₃ X 3), 10.09 – 9.42 (m, P-CH₃) ppm.

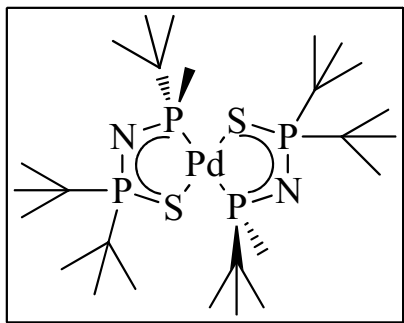
³¹P NMR (300 MHz, CDCl₃): δ 115.68 (dd, J = 154.1, 25.0 Hz, P-Rh), 113.03 (dd, J = 24.9, 3.1 Hz, sat), 110.69 (dd, J = 24.9, 3.4 Hz, P=Se), 108.35 (dd, J = 25.0, 3.5 Hz, sat) ppm.

IR (KBr): ν_{\max} 3217, 2950, 2825, 1721 cm⁻¹.

HRMS (ESI⁺): Calculated for [M]⁺ (C₂₁H₄₃NP₂RhSe), m/z : 554.10855. Observed: 554.10826.

7. Experimental

[(Mono-S-MaxPHOS)₂Pd], 110.



Mono-S-MaxPHOS **106** (0.06 g, 0.185 mmol) and Pd(acac)₂ (0.028 g, 0.093 mmol) were stirred in MeOH (2 mL) at 50 °C and to the reaction was added Et₃N (0.03 mL, 0.231 mmol). Pure complex was obtained as colourless oil (0.041 g, 63 %) after column chromatography (Hexane/Ethyl acetate, SiO₂).

[α]_D: 72.394 ° (c 0.006, CH₂Cl₂).

Rf: 0.38 (8:2 Hexane:EtOAc, SiO₂).

Mp: 243 °C.

¹H NMR (400 MHz, CDCl₃): δ 1.62 (d, *J* = 12 Hz, 3H), 1.42 (d, *J* = 14.7 Hz, 9H), 1.26 (d, *J* = 14.7 Hz, 9H), 1.14 (t, *J* = 7.5 Hz, 9H) ppm.

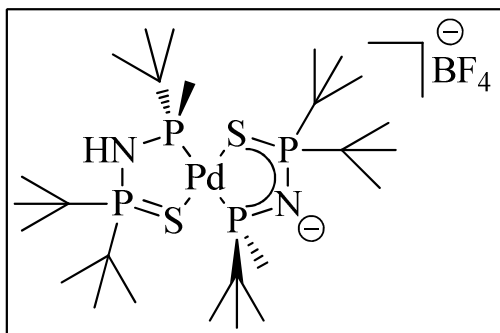
¹³C NMR (400 MHz, CDCl₃): δ 39.92 (d, *J* = 53.0 Hz, C), 39.02 – 38.13 (m, C), 29.58 (d, *J* = 45.5 Hz, C), 29.46 (s, CH₃ X 3), 28.55 (s, CH₃ X 3), 26.87 (t, *J* = 3.3 Hz, CH₃ X 3), 18.01 (s, P-CH₃) ppm.

³¹P NMR (300 MHz, CDCl₃): δ 113.91 (t, *J* = 46.9 Hz), 105.00 (t, *J* = 47.4 Hz) ppm.

IR (KBr): ν_{max} 2947, 2898, 2860 cm⁻¹.

HRMS (ESI+): Calculated for [M + H⁺]⁺ (C₂₆H₆₁N₂P₄PdS₂), *m/z*: 695.22560. Observed: 695.22545.

E.A.: Calculated for C₂₆H₆₀N₂P₄PdS₂: C, 44.92; H, 8.70; N, 4.03; S, 9.22. Observed: C, 45.63; H, 9.27; N, 4.05; S, 8.73.

[(Pd(mono-S-MaxPHOS))₂BF₄], 111.

The [(Mono-S-MaxPHOS)₂Pd] **110** (0.032 g, 0.046 mmol) was stirred in hexane (2 mL) under N₂ and to it was added HBF₄·OEt₂ (0.006 mL, 0.046 mmol), a precipitate quickly fell out of solution, the supernatant solution was removed by pipette. The precipitate was washed several times with hexane. The precipitate was

recrystallized by dissolving in the minimum amount of dichloromethane and on top, slowly layering diethylether to yield slightly greyish crystals suitable for X-ray crystallography (0.029 g, 81 %).

[α]_D: 184.83 ° (c 0.005, CH₂Cl₂).

¹H NMR (400 MHz, CDCl₃): δ 6.35 (d, *J* = 11.1 Hz, 1H), 2.11 (s, 3H), 1.60 (d, *J* = 17.5 Hz, 9H), 1.44 (d, *J* = 17.8 Hz, 9H), 1.33 (t, *J* = 9.0 Hz, 9H) ppm.

¹³C NMR (400 MHz, CDCl₃): δ 41.44 (d, *J* = 38.4 Hz, C), 41.20 (d, *J* = 37.4 Hz, C), 28.25 (d, *J* = 81.87 Hz), 28.41 (s, CH₃ x 3), 27.48 (s, CH₃ x 3), 26.60 (t, *J* = 3.2 Hz, CH₃ x 3), 13.24 – 12.79 (m, P-CH₃) ppm.

³¹P NMR (300 MHz, CDCl₃): δ 124.63 (t, *J* = 26.6 Hz), 117.95 (t, *J* = 26.8 Hz) ppm.

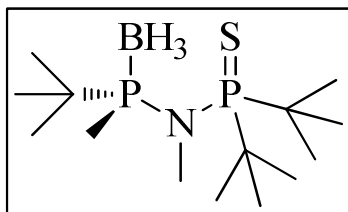
IR (KBr): 3161, 2970, 2628 (small), 1476, 1406, 1308, 1088, 897, 625 cm⁻¹.

HRMS (ESI⁺): Calculated for [M]⁺ (C₂₆H₆₁N₂P₄PdS₂), *m/z*: 695.22560. Observed: 695.22476.

E.A.: Calculated for C₂₆H₆₁BF₄N₂P₄PdS₂: C, 39.88; H, 7.85; N, 3.58; S, 8.19. Observed: C, 36.23; H, 7.33; N, 3.4; S, 7.10.

7. Experimental

(R)-(tert-butyl((di-tert-butylphosphorothioyl)(methyl)amino)(methyl)phosphonio) trihydroborate, 112.



The mono-S-MaxPHOS-BH₃ **104** (0.449 g, 1.45 mmol) was stirred in THF (3 mL) and to it was added *n*-BuLi (0.7 mL, 1.74 mmol), dropwise. The reaction was stirred for 50 minutes before MeI (0.9 mL, 14.5 mmol) was added. It was allowed to slowly heat up to room temperature and then stirred for a total of 50 minutes at room temperature before water (15 mL) was added to quench the reaction. It was extracted with EtOAc (3 X 15 mL), the organic fractions were combined, dried over MgSO₄, solvents were removed in *vacuo* and pure product was obtained as a white solid (0.396 g, 84 %) after column chromatography (Hexane/Ethyl acetate, SiO₂).

Rf: 0.75 (8:2 Hexane : EtOAc, SiO₂).

[α]_D: -29.582 ° (c 0.06, CHCl₃).

Mp: 52 °C.

¹H NMR (400 MHz, CDCl₃): δ 2.35 (d, *J* = 9.9 Hz, 3H), 1.35 (dd, *J* = 16.5, 9.2 Hz, 21H), 1.17 (d, *J* = 13.8 Hz, 9H) ppm.

¹³C NMR (400 MHz, CDCl₃): δ 42.45 (d, C^q), 42.04 (d, C^q), 32.62 (d, C^q), 27.51 (m, CH₃ X 6), 25.26 (d, 3 X CH₃), 14.50 (d, P-CH₃), 12.81 (d, N-Me) ppm.

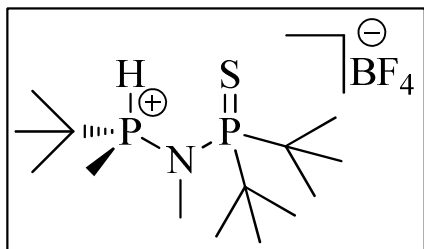
³¹P NMR (300 MHz, CDCl₃): δ 59.24 (d, *J* = 24.0 Hz), 57.43 (ddd, *J* = 104.2, 75.8, 19.2 Hz) ppm.

IR (KBr): ν_{\max} 2974, 2891, 2864, 2362, 2330, 1488 cm⁻¹.

HRMS (ESI+): Calculated for [M + H⁺]⁺ (C₁₄H₃₇BNP₂S), *m/z*: 324.22095. Observed: 324.22099.

E.A: Calculated for C₁₄H₃₆BNP₂S: C, 52.02; H, 11.22; N, 4.33; S, 9.92. Observed: C, 52.32; H, 12.60; N, 4.45; S, 9.59.

[(*R*)-*tert*-butyl((*di-tert*-butylphosphorothioyl)(methyl)amino)(methyl)phosphonium] BF₄, 113.



The Mono-S-N-methyl-MaxPHOS-BH₃ **112** (0.396 g, 1.21 mmol) was stirred in MeOH (5 mL) under N₂ and HBF₄·OEt₂ (0.83 mL, 6.05 mmol) was slowly added. The reaction was heated to 50 °C and it was stirred for 2 hours and 45 minutes before heating and

stirring were stopped and solvents were removed in *vacuo*. The residue obtained was dissolved in EtOAc (15 mL) and washed with aqueous NaHCO₃ (15 mL), the aqueous phase was washed with EtOAc (2 X 15 mL), the organic fractions were combined, dried over MgSO₄, solvents were removed in *vacuo* to provide pure product as a white solid (0.455 g, 95 %).

¹H NMR (400 MHz, CDCl₃): δ 7.89 – 7.77 (m, 0.5H, P-H), 6.68 – 6.54 (m, 0.5H, P-H), 2.43 (d, *J* = 10.9 Hz, 3H, N-CH₃), 1.86 (dd, *J* = 12.9, 4.2 Hz, 3H, P-CH₃), 1.40 (dd, *J* = 17.3, 10.7 Hz, 18H, CH₃ X 6), 1.31 (d, *J* = 18.7 Hz, 9H, CH₃ X 3) ppm.

¹³C NMR (400 MHz, CDCl₃): δ 42.84 (d, *J* = 53.7 Hz, C^q), 42.56 – 41.82 (m, C^q), 31.82 (dd, *J* = 75.9, 4.3 Hz, C^q), 27.39 (d, *J* = 17.5 Hz, CH₃ X 6), 23.89 (s, CH₃ X 3), 13.23 (s, N-CH₃), 9.31 (d, *J* = 59.9 Hz, P-CH₃) ppm.

³¹P NMR (300 MHz, CDCl₃): δ 73.42 (d, *J* = 35.0 Hz), 27.38 (d, *J* = 35.1 Hz) ppm.

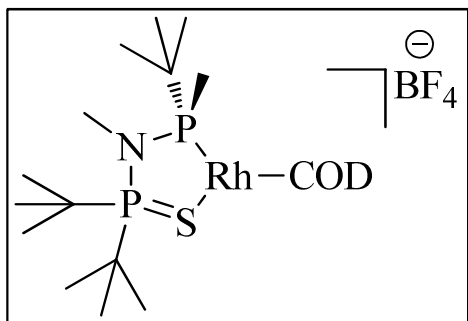
¹⁹F -RMN (400 MHz, CDCl₃): δ 152.58 ppm.

IR (KBr): ν_{max} 3385 (br), 2962, 1474 cm⁻¹.

HRMS (ESI⁺): Calculated for [M]⁺ (C₁₄H₃₄NP₂S), *m/z*: 310.18817. Observed: 310.18817.

7. Experimental

[(*N*-Me-mono-*S*-MaxPHOS)Rh(COD)]BF₄, 115.



The [Mono-*S*-*N*-Me-MaxPHOS]BF₄ **113** (0.08 g, 0.201 mmol), NaHCO₃ (0.017 g, 0.201 mmol) and [Rh(COD)₂]BF₄ (0.082 g, 0.201 mmol) were stirred in MeOH in a schlenk tube under N₂ for 19 hours. The MeOH was removed under *vacuo* and then suspended in Et₂O (10 mL) and stirred. The minimum amount of dichloromethane (3 mL) was

added dropwise to the suspension until dissolution occurred. The solution was transferred to another round-bottom flask and the solvent was removed in *vacuo* to yield pure complex (0.077 g, 63 %). Crystals suitable for X-ray crystallography were formed by dissolving the solid in the minimum amount of dichloromethane and layering an excess of Et₂O on top.

¹H NMR (400 MHz, CDCl₃): δ 5.51 – 4.38 (CH X 4), 2.88 (d, *J* = 6.1 Hz, 3H), 2.47 – 1.9 (m, CH₂ X 4), 1.47 (dd, *J* = 16.9, 4.8 Hz, 18H), 1.33 (d, 15 Hz, P-CH₃), 1.06 (d, *J* = 15.1 Hz, 9H) ppm.

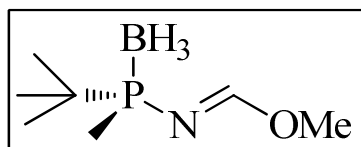
¹³C NMR (400 MHz, CDCl₃): δ 101.27 (dd, *J* = 253.2, 8.5 Hz, CH X 2), 84.76 (d, *J* = 13.4 Hz, CH), 76.22 (s, CH), 42.91 (d, *J* = 37.4 Hz, C), 42.14 – 41.36 (m, C), 34.97 (d, *J* = 3.7 Hz, CH₂), 31.12 (s, CH₂), 30.35 (s, CH₂), 30.13 (d, 45.5 Hz, C), 28.61 (s, 3 X CH₃), 28.14 (s, 3 X CH₃), 27.57 (s, CH₂), 27.17 (d, *J* = 5.1 Hz, 3 X CH₃), 19.30 (d, *J* = 4.1 Hz, P-Me) 14.45 (d, *J* = 31.9 Hz, N-Me) ppm.

³¹P NMR (300 MHz, CDCl₃): δ 101.62 (d, 124 Hz), 101.41 (s) ppm.

IR (KBr): ν_{max} 3487 (br), 2923, 1565 cm⁻¹.

HRMS (ESI⁺): Calculated for [M]⁺ (C₂₂H₄₅NP₂RhS), *m/z*: 520.17975. Observed: 520.17870.

**P-borane complex of (*R,E*)-methyl *N*-(*tert*-butyl(methyl)phosphino) formimidate,
116.**



The aminophosphine **3** (0.1 g, 0.752 mmol) and *para*-toluenesulfonic acid (0.001 g, 0.0008 mmol) were stirred in trimethyl orthoformate (2 mL) while heating at 90 °C. It was stirred for 30 minutes before it was removed from the silicon bath. Solvents were removed in *vacuo* to yield pure product as a colourless oil (0.110 g, 83 %).

Rf: 0.75 (8:2 Hexane:EtOAc, SiO₂).

[α]_D: -62.072 ° (c 0.006, CH₂Cl₂).

¹H NMR (400 MHz, CDCl₃): δ 8.09(d, 1H), 3.79 (s, 3H), 1.36 (d, 3H), 1.13 (d, 9H) ppm.

¹³C NMR (400 MHz, CDCl₃): δ 53 (s, OMe), 29 (d, ⁹C), 24 (s, Bu^t), 10 (d, H₃C-P) ppm.

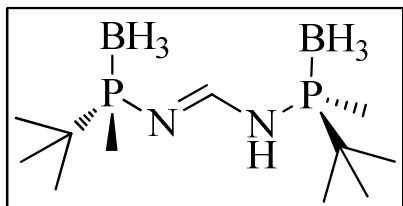
³¹P NMR (300 MHz, CDCl₃): δ 74.42 (dd) ppm.

IR (KBr): ν_{max} 2949, 2375, 1632, 1248, 931 cm⁻¹.

HRMS (ESI+): Calculated for [M - CH₃ - H⁺ + H⁺]⁺ (C₆H₁₆BNOP), m/z: 160.10571.
Found: 160.10578.

7. Experimental

P-borane complex of *N, N'*-bis(*tert*-butyl(methyl)phosphino) formimidamide, **117**.



The (R)-(amino(*tert*-butyl)(methyl)phosphonio) trihydroborate amino phosphine **3** (0.098 g, 0.737 mmol) and NaH (0.053 g, 2.21 mmol) were stirred under N₂ in THF (4 mL) at 50 °C. After 20 minutes stirring after no more bubbles could be seen emerging from the bubbler, the imidate phosphine **116** (0.129 g, 0.737 mmol) was added to the reaction dissolved in THF (1 mL). After 20 minutes one drop of ^tBuOH was added. The reaction was stirred for another 20 minutes by which time it was obvious by TLC that no more imidate phosphine **116** remained. Stirring was stopped and the reaction was allowed to cool. Aqueous NH₄Cl (10 mL) was added to quench the reaction, it was extracted with EtOAc (3 X 20 mL), the organic fractions were combined, dried over MgSO₄ and solvents were removed in *vacuo*. Pure compound was isolated as a white solid (0.024g, 7 %) after column chromatography (Hexane/Ethyl Acetate, SiO₂).

Rf: 0.3 (7:3 Hexane: EtOAc, SiO₂).

[α]_D: -65.450 ° (c 0.008, CH₂Cl₂).

Mp: 124.9 – 128 °C.

¹H NMR (400 MHz, CDCl₃): δ 8.14 (t, *J* = 14.4 Hz, 1H), 1.50 (d, *J* = 8.6 Hz, 6H), 1.19 (d, *J* = 14.7 Hz, 18H) ppm.

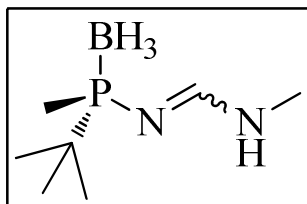
¹³C NMR (400 MHz, CDCl₃): δ 161.12 (d, *J* = 126.6 Hz, C-H), 30.44 (d, *J* = 42.9 Hz, C^q), 24.43 (s, CH₃ X 3), 9.99 – 8.47 (m, P-CH₃) ppm.

³¹P NMR (300 MHz, CDCl₃): δ 76.85 (br s) ppm.

IR (KBr): ν_{max} 3284, 2963, 2370, 1622 cm⁻¹.

HRMS (ESI+): Calculated for [M + H]⁺ (C₁₁H₃₃B₂N₂P₂), *m/z*: 277.22996. Observed: 277.22996.

P-borane complex of (*R*)-*N*-(methylformimidamido)-*N'*-*tert*-butyl(methyl) phosphine, 118.



The imidate phosphine **116** (0.076g, 0.434 mmol) was stirred in MeOH (1 mL) under N₂ and to it was added MeNH₂ (8M in EtOH), (0.27 mL, 2.17 mmol). It was stirred for 30 minutes before solvents were removed in *vacuo*. The residue obtained was dissolved in DCM, it was washed with water, the aqueous layer was washed with DCM, the organic extracts were combined, dried over MgSO₄, solvents were removed in *vacuo* to yield pure product as a white solid (0.093g) in quantitative yield.

Rf: 0.2 (8:2, Hexane:EtOAc, SiO₂).

[α]_D: -132.85° (c 0.004, CH₂Cl₂).

Mp: 105 – 110 °C.

¹H NMR (400 MHz, CDCl₃): δ (*E*): 8.03 (dd, C-H, *J* = 20Hz), 5.18 (br s, N-H), 2.9 (d, CH₃), 1.3(d, P-CH₃), 1.1 (d, 9H). (*Z*) 7.84 (d, C-H, *J* = 20 Hz), 2.98 (s, 3H), 1.28 (d, P-CH₃), 1.09 (d, 9H) ppm.

¹³C NMR (400 MHz, CDCl₃): δ 159.70(C-H), 29.49 (C^q), 26.99 (N-CH₃), 24.33 (3 X CH₃), 10.68 (P-CH₃) ppm.

³¹P NMR (300 MHz, CDCl₃): δ 73.13 (m) ppm.

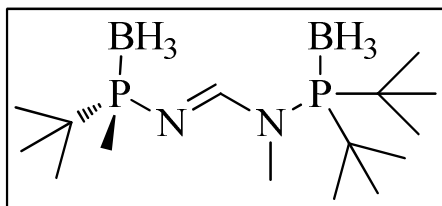
IR (KBr): ν_{max} 3359, 2971, 2362, 1623 cm⁻¹.

HRMS (ESI+): Calculated for [M + H]⁺ (C₇H₂₁BN₂P), m/z: 175.15299. Observed: 175.15300.

E.A: Calculated for C₇H₂₀BN₂P: C, 48.31; H, 11.58; N, 16.10. Observed: C, 49.26; H, 12.13; N, 15.43.

7. Experimental

P-borane complex of (*R,E*)- *N*-(di-*tert*-butylphosphino)-*N*-(methylformimidamide)-*N'*-*tert*-butyl(methyl)phosphine, 119.



The amidine-phosphine **118** (0.164 g, 0.942 mmol) was stirred under nitrogen in THF (5 mL) at $-78\text{ }^{\circ}\text{C}$ and to it was added *n*-BuLi (0.45 mL, 1.13 mmol). It was allowed to stir for 45 minutes at $-78\text{ }^{\circ}\text{C}$ before $\text{P}^t\text{Bu}_2\text{Cl}$ was added directly, it was allow to stir while warming up. After 3.5 hours $\text{BH}_3\cdot\text{SMe}_2$ was added. The reaction was stirred for a further hour before water (5 mL) was added, it was extracted with DCM (3 X 5 mL), the organic fractions were combined and dried over MgSO_4 and solvents were removed in *vacuo*. Pure product was obtained as a white solid (0.179 g, 57 %) after flash column chromatography (9:1, Hexane:Ethyl Acetate, SiO_2).

Rf: 0.75 (Hx:EtOAc, 8:2, SiO_2).

$[\alpha]_D$: -59.508° (c 0.0073, CH_2Cl_2).

Mp: $119 - 127\text{ }^{\circ}\text{C}$.

^1H NMR (400 MHz, CDCl_3): δ 8.55 (d, $J = 20.0$ Hz, 1H), 3.24 (d, $J = 7.4$ Hz, 3H), 1.4 (d, 18H, $J = 15$ Hz), 1.38 (s, 3H), 1.16 (d, $J = 14.1$ Hz, 10H) ppm.

^{13}C NMR (400 MHz, CDCl_3): δ 164.56 (s, C-H), 37.27 (d, $J = 23.4$ Hz, $\text{C}^q \times 2$), 34.71 (s, N- CH_3), 29.76 (d, $J = 43.4$ Hz, C^q), 28.58 (s, $\text{CH}_3 \times 6$), 24.56 (s, $\text{CH}_3 \times 3$), 10.44 (d, $J = 43.2$ Hz, P- CH_3) ppm.

^{31}P NMR (300 MHz, CDCl_3): δ 104.77 (d, $J = 71.2$ Hz), 77.25 (dd, $J = 119.0, 48.6$ Hz) ppm.

IR (KBr): ν_{max} 2962, 2360, 1610 cm^{-1} .

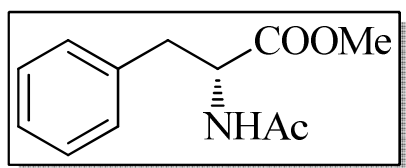
HRMS (ESI+): Calculated for $[\text{M} + \text{H}]^+$ ($\text{C}_{15}\text{H}_{41}\text{B}_2\text{N}_2\text{P}_2$), m/z : 333.2931. Observed: 333.2932.

E.A: Calculated for $\text{C}_{15}\text{H}_{40}\text{B}_2\text{N}_2\text{P}_2$: C, 54.26; H, 12.14; N, 8.44. Observed: C, 54.30; H, 12.45; N, 8.32.

7.4 General Procedure for Hydrogenations using MaxPHOS-Rh catalyst

A pressure tube equipped with a stirrer bar was loaded with substrate and the [(*R*)-MaxPHOS)Rh(COD)]BF₄ catalyst. In the dry box under N₂, anhydrous solvent was added to the vessel and the vessel was sealed.. It was then removed from the dry box and transferred to the hydrogenation facility where it was vacuumed and filled with H₂ three times before being charged with the given pressure of H₂. The reaction vessel was returned to the laboratory where it was left to stir for the given time. After that time had elapsed, stirring was stopped and the pressure was released from the vessel. The reaction mixture was diluted with EtOAc before being vacuum filtered over a short pad of silica. The EtOAc/MeOH filtrate was then filtered through a PTFE 0,45 μm HPLC tab. The solvent was removed in *vacuo*. ¹H NMR and chiral HPLC or chiral GC was performed on the resulting residue.

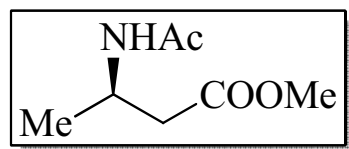
7.5 ¹H NMR and HPLC data of hydrogenated substrates



(-)-(*R*)-methyl 2-acetamido-3-phenylpropanoate, **21**.

HPLC: CHIRALPAK AD-H, 90 % Heptane-10 % IPA, 1 mL/min, λ = 220 nm, *t_R* isomer = 8.8, *t_S* isomer = 12.3 min.

¹H NMR (400 MHz, CDCl₃): δ 7.33 – 7.22 (m, 1H), 7.12 – 7.07 (m, 1H), 5.93 (d, *J* = 6.6 Hz, NH), 4.89 (dt, *J* = 7.8, 5.8 Hz, 1H), 3.73 (s, 3H), 3.12 (m, *J* = 13.9, 5.7 Hz, 2H), 1.98 (s, 3H) ppm



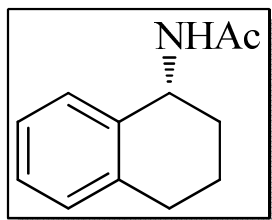
(+)-(*R*)-methyl 3-acetamidobutanoate, **140**.

¹H NMR (400 MHz, CDCl₃): δ 6.04 (s, 1H), 3.70 (s, 3H), 2.63 – 2.45 (m, 2H), 1.96 (s, 3H), 1.23 (d, *J* = 6.8 Hz, 3H)

ppm.

GC: Beta-DEX 30m column 80 °C(3min)---5 °C/min---210 °C(5min), *t_S* isomer = 19.5 min, *t_R* isomer = 19.8 min.

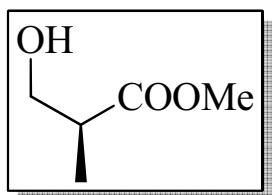
7. Experimental



(+)-(R)-N-(1,2,3,4-tetrahydronaphthalen-1-yl)acetamide, 141.

$^1\text{H NMR}$ (400 MHz, CDCl_3): δ 7.28 (d, $J = 5.6$ Hz, 1H), 7.20 – 7.15 (m, 2H), 7.11 – 7.07 (m, 1H), 5.69 (d, $J = 6.0$ Hz, 1H), 5.18 (dd, $J = 13.6, 5.5$ Hz, 1H), 2.86 – 2.69 (m, 2H), 2.09 – 2.03 (m, 1H), 2.02 (s, 3H), 1.87 – 1.78 (m, 3H) ppm.

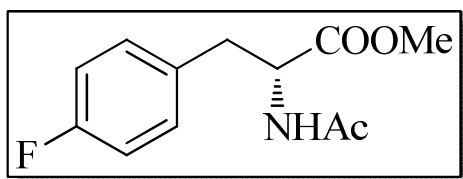
GC: 200°C, det T 300 °C, inj T 220°C; split 50:1 flux 1.0mL/min, carrier: He
2mg/ml Heptane: IPA 1:1, t_S isomer = 13.5 min, t_R isomer = 13.873 min.



(+)-(S)-methyl 3-hydroxy-2-methylpropanoate, 142.

$^1\text{H NMR}$ (400 MHz, CDCl_3) δ 3.75 – 3.70 (m, 5H), 2.69 (pd, $J = 7.2, 4.8$ Hz, 1H), 1.19 (d, $J = 7.3$ Hz, 3H) ppm.

GC: 200°C, det T 300 °C, inj T 220°C; split 50:1 flux 1.0mL/min, carrier: He 2mg/ml Heptane: IPA 1:1, t_S isomer = 10.3 min, t_R isomer = 10.2 min.

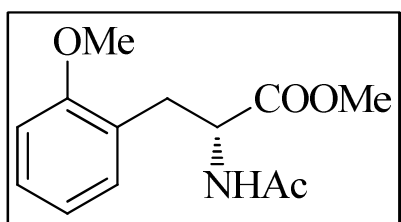


(-)-(R)-methyl-2-acetamido-3-(4-fluorophenyl)propanoate, 143.

$^1\text{H NMR}$ (400 MHz, CDCl_3) δ 7.08 – 6.95 (m, 4H), 5.90 (s, 1H), 4.87 (dt, $J = 7.7, 5.7$ Hz, 1H),

3.73 (s, 3H), 3.10 (m, $J = 14.0, 5.8$ Hz, 2H), 2.00 (s, 3H) ppm.

HPLC: Chiralcel OJ column; Heptane/ IPA (90:10), 2mg/ mL in Heptane/ IPA 1:1, t_S isomer = 20.2 min, t_R isomer = 15.2 min.



(-)-(R)-methyl-2-acetamido-3-(2-methoxyphenyl)propanoate, 145.

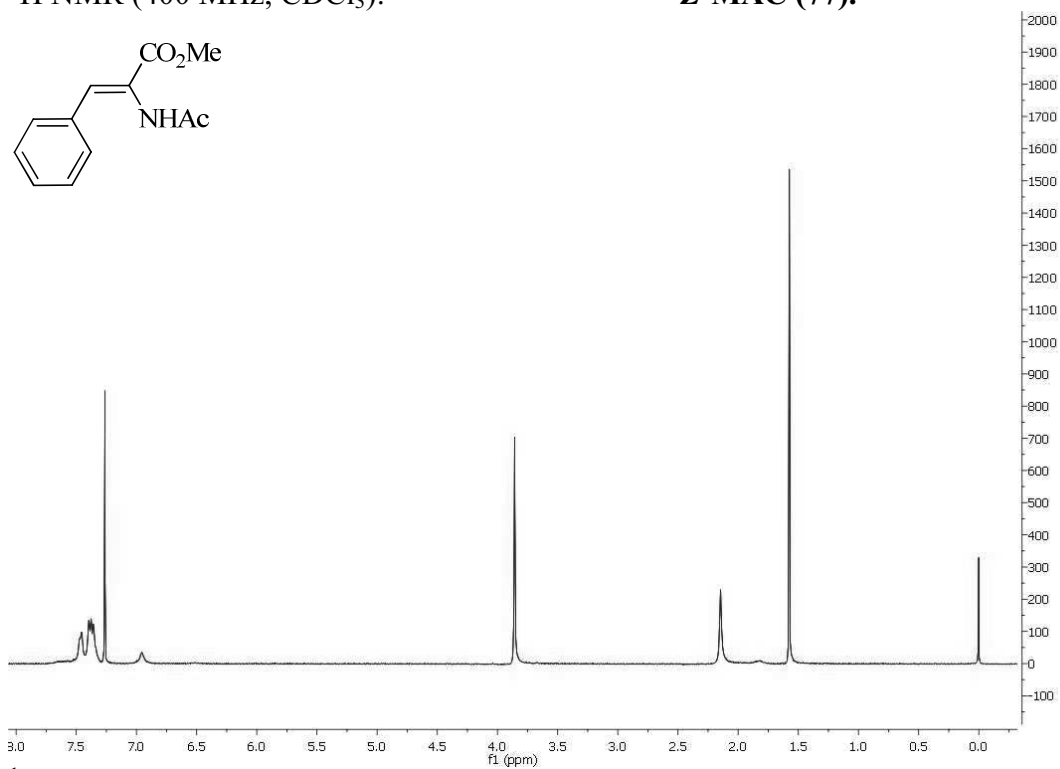
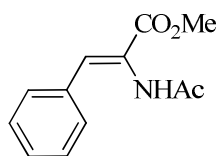
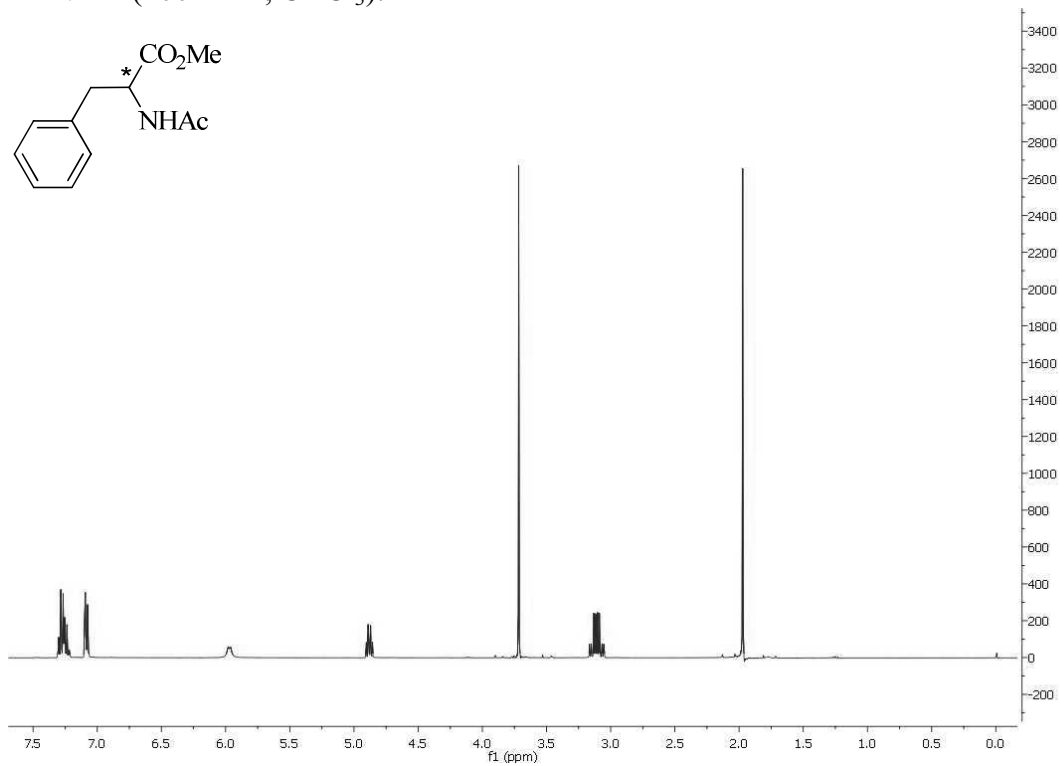
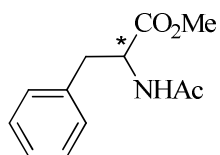
$^1\text{H NMR}$ (400 MHz, CDCl_3) δ 7.30 – 7.19 (m, 1H), 7.07 (dd, $J = 7.4, 1.7$ Hz, 1H), 6.93 – 6.83 (m, 2H), 6.29 (s, 1H), 4.75 (dd, $J = 13.4, 7.1$ Hz, 1H), 3.84 (s,

3H), 3.70 (s, 3H), 3.10 (d, $J = 7.2$ Hz, 2H), 1.93 (s, 3H) ppm.

HPLC: Chiralpak AD-H column; Heptane/IPA 90:10, 2mg/ mL in Heptane/ IPA 1:1, t_S isomer = 17.9 min, t_R isomer = 12.2 min.

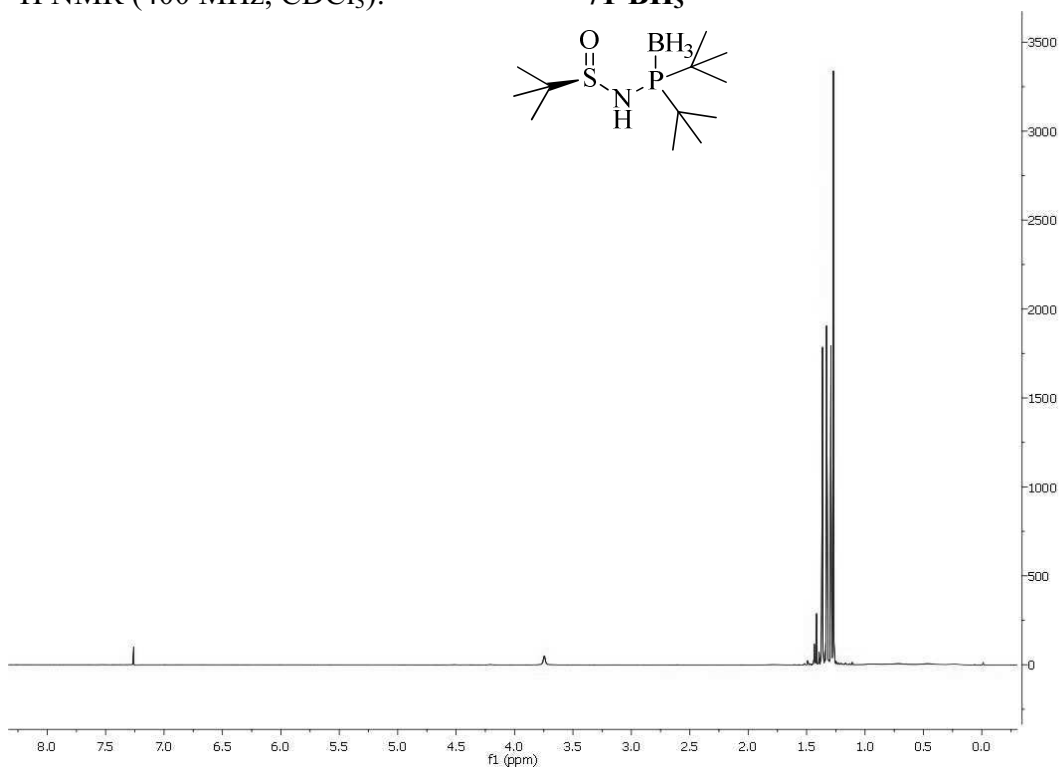
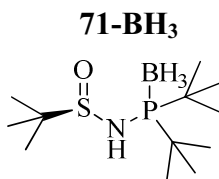
Spectra



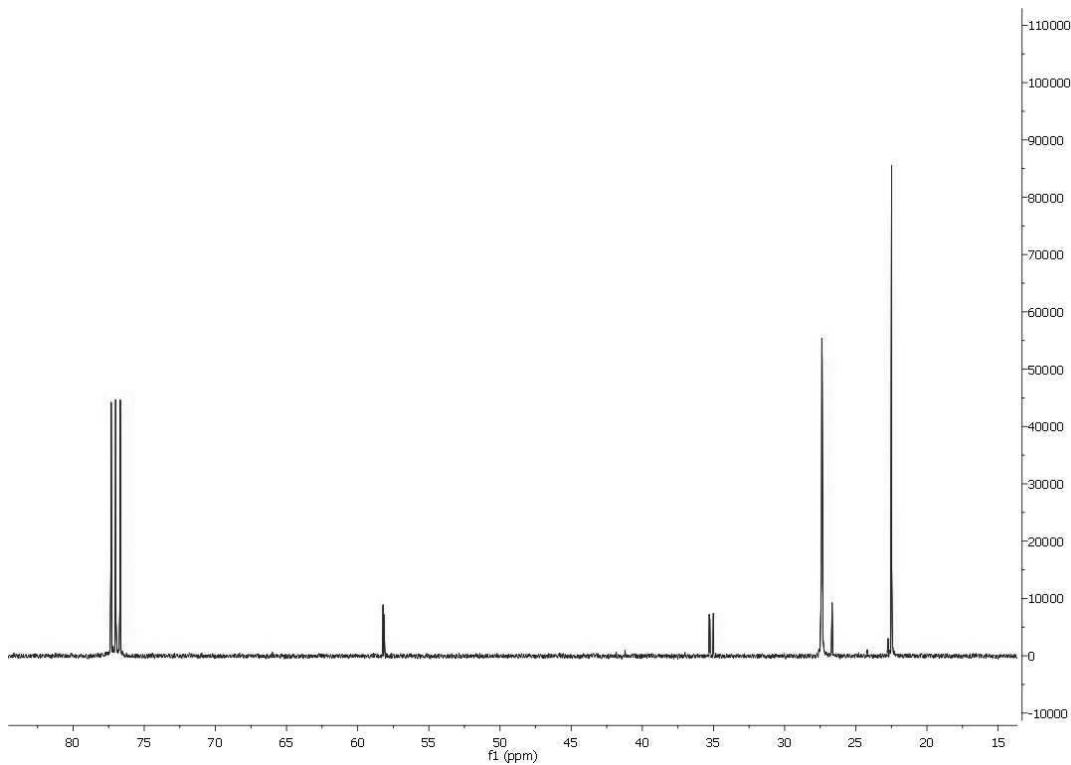
^1H NMR (400 MHz, CDCl_3):**Z-MAC (77).** ^1H NMR (400 MHz, CDCl_3):**21**

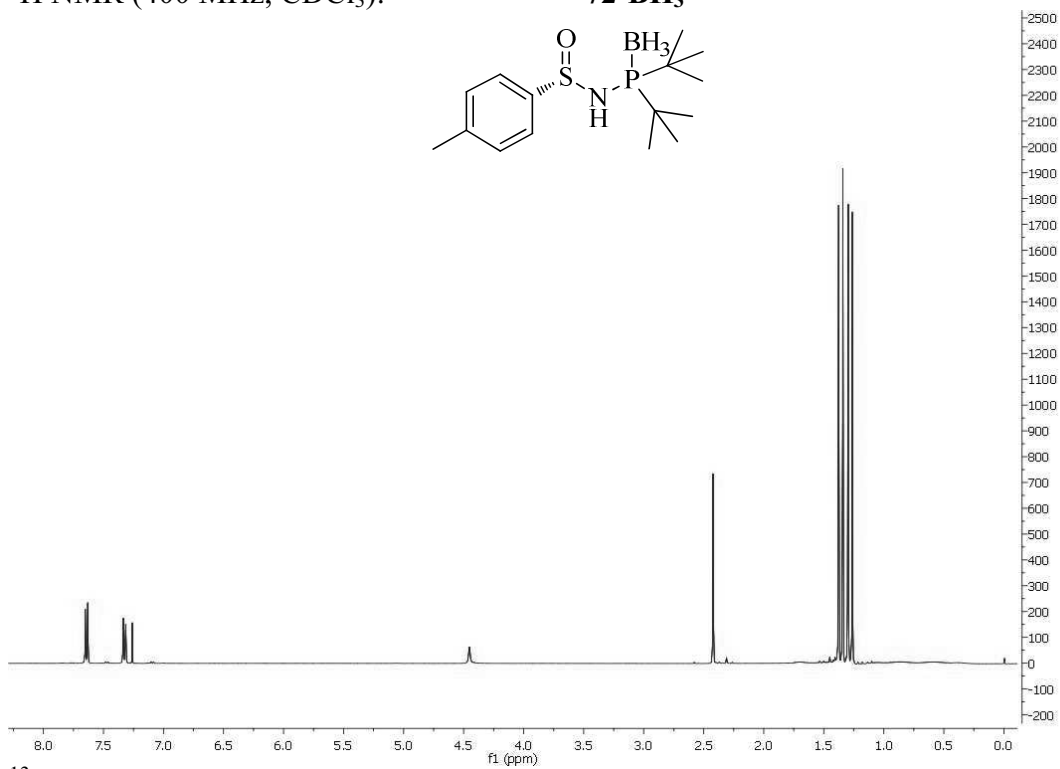
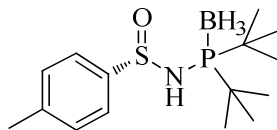
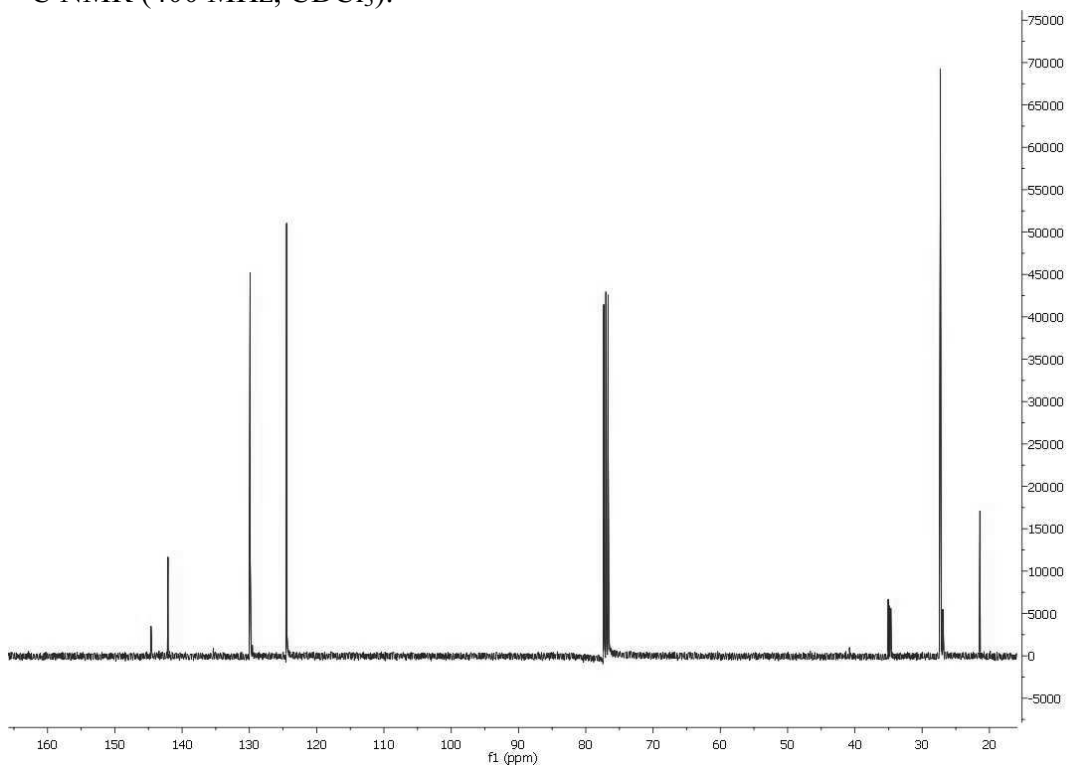
8. Spectra

^1H NMR (400 MHz, CDCl_3):



^{13}C NMR (400 MHz, CDCl_3):

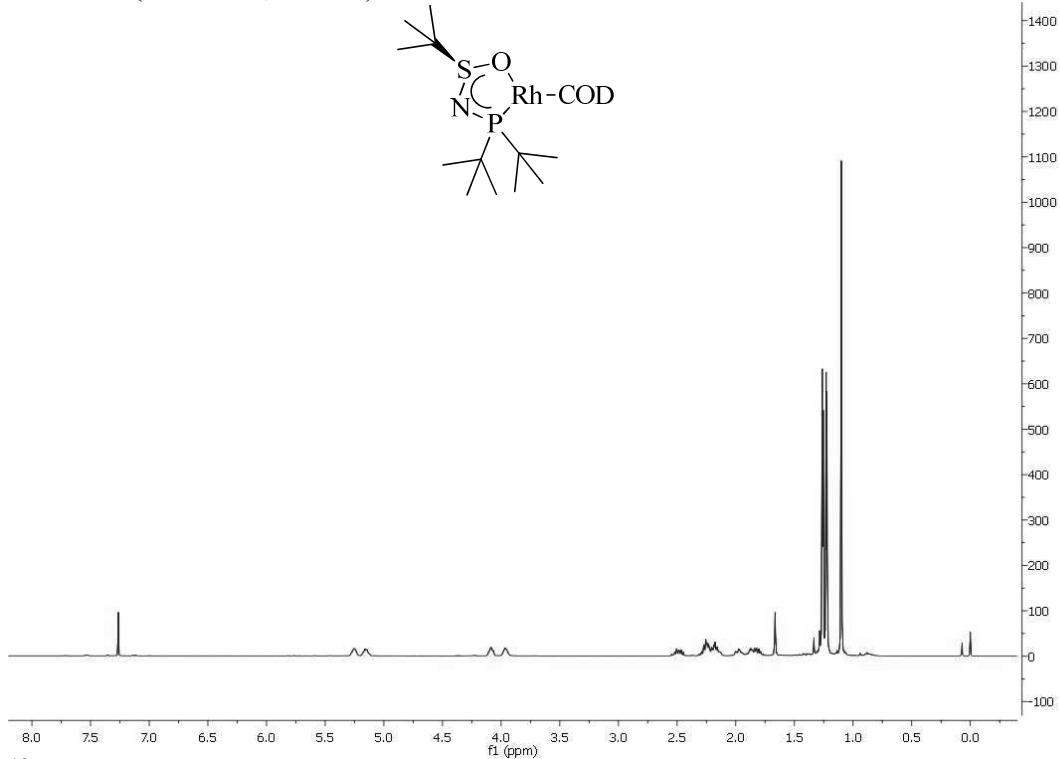
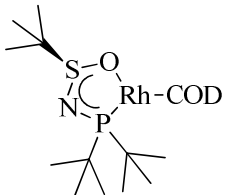


^1H NMR (400 MHz, CDCl_3):**72-BH₃** ^{13}C NMR (400 MHz, CDCl_3):

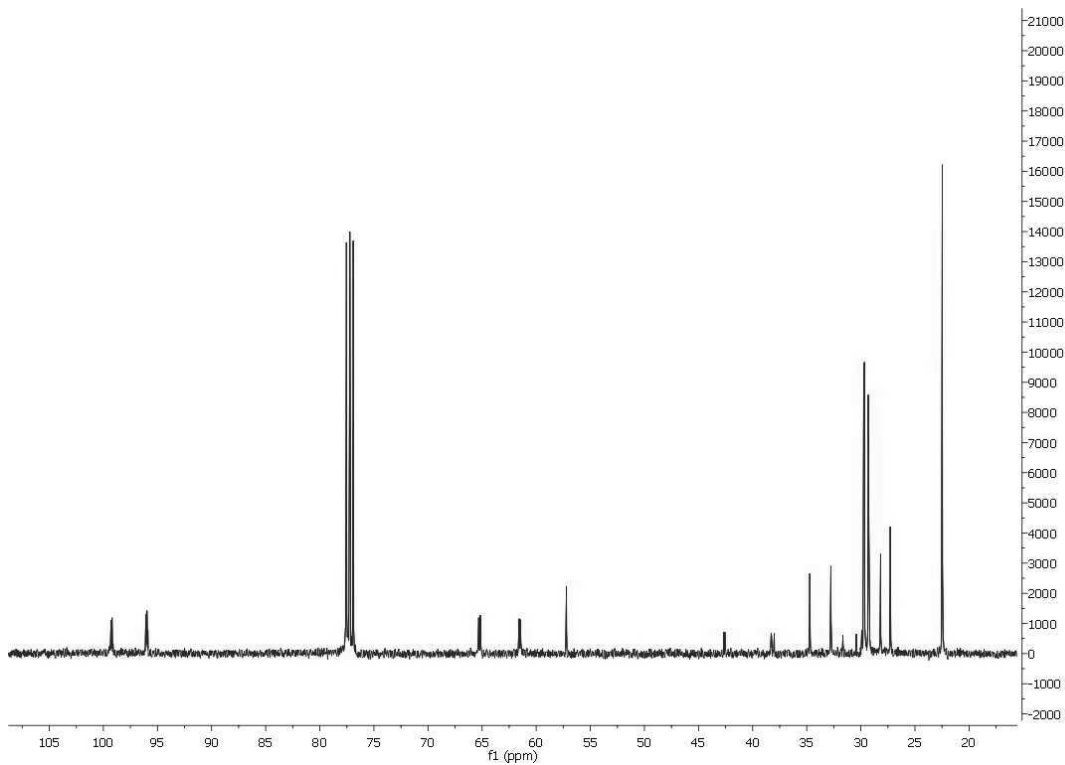
8. Spectra

^1H NMR (400 MHz, CDCl_3):

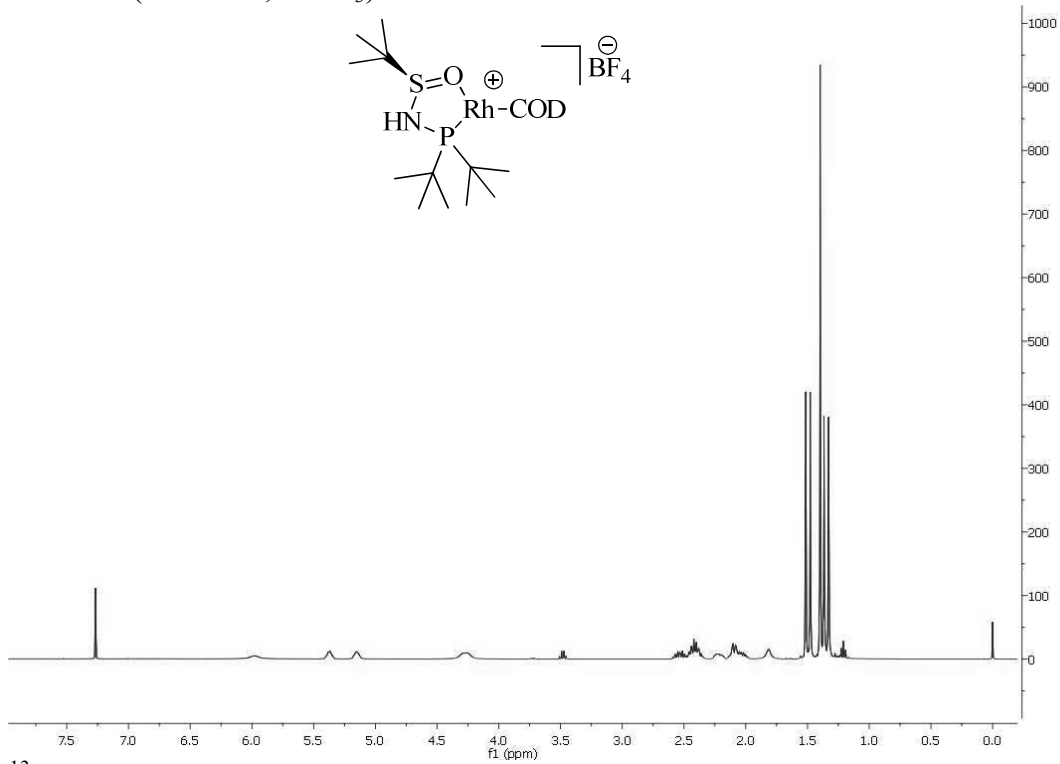
73



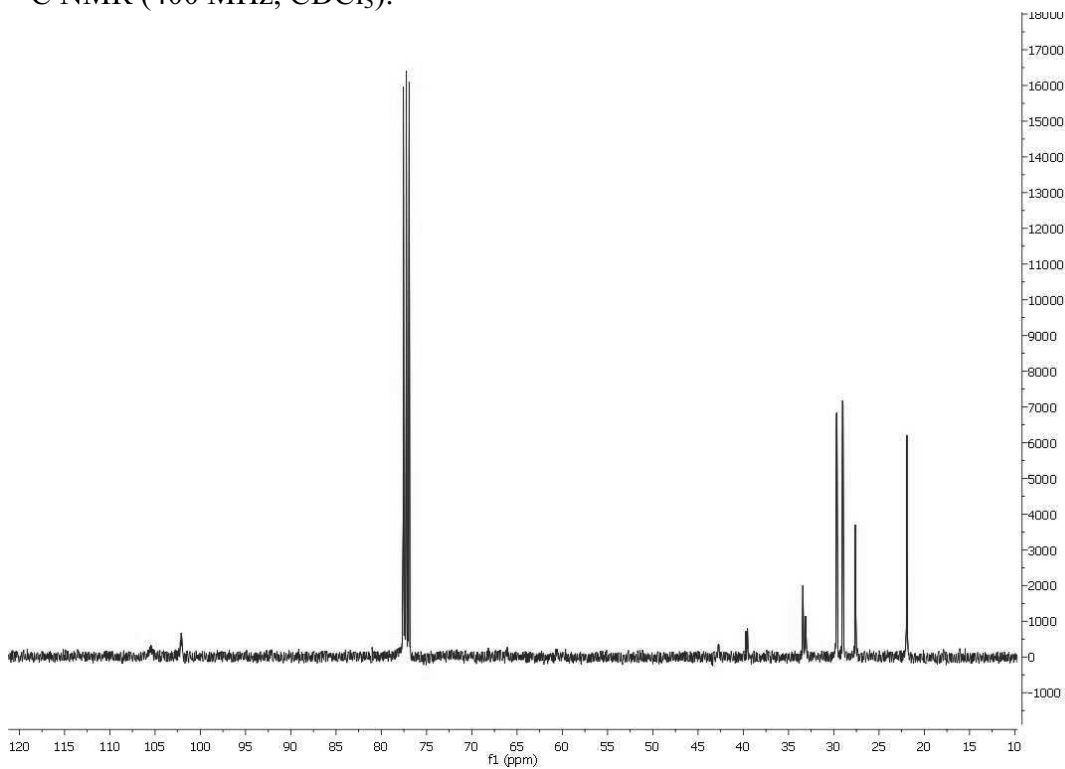
^{13}C NMR (400 MHz, CDCl_3):



^1H NMR (400 MHz, CDCl_3): **74**

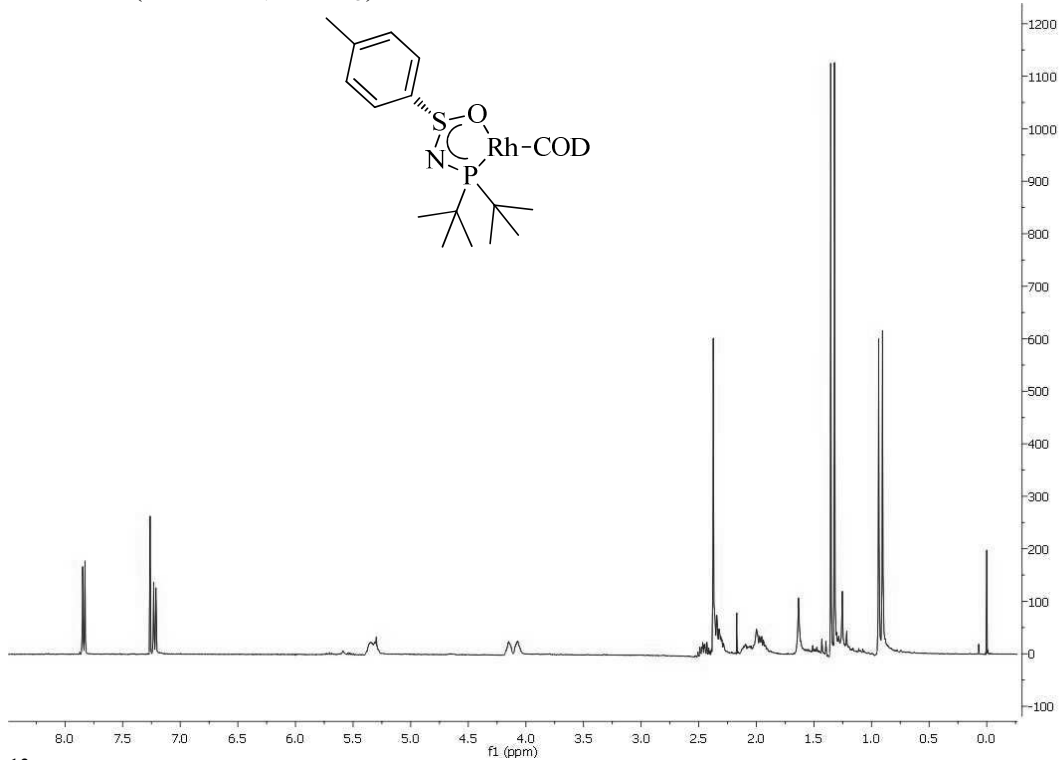


^{13}C NMR (400 MHz, CDCl_3):

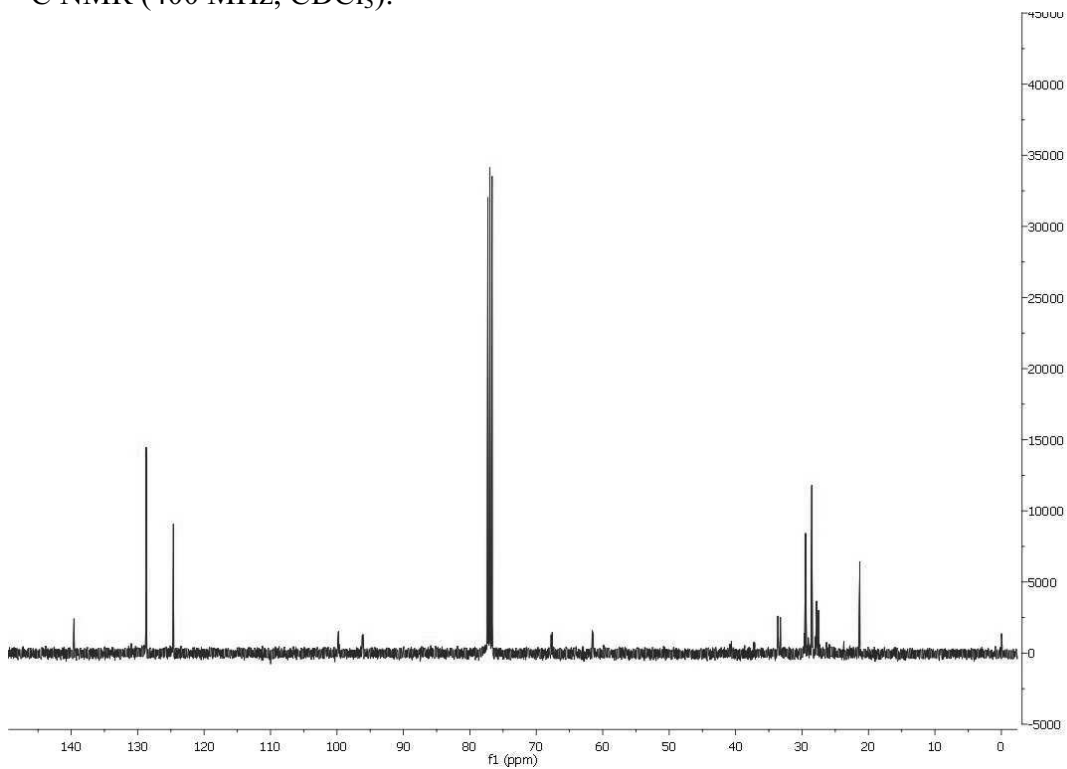


8. Spectra

^1H NMR (400 MHz, CDCl_3): **75**

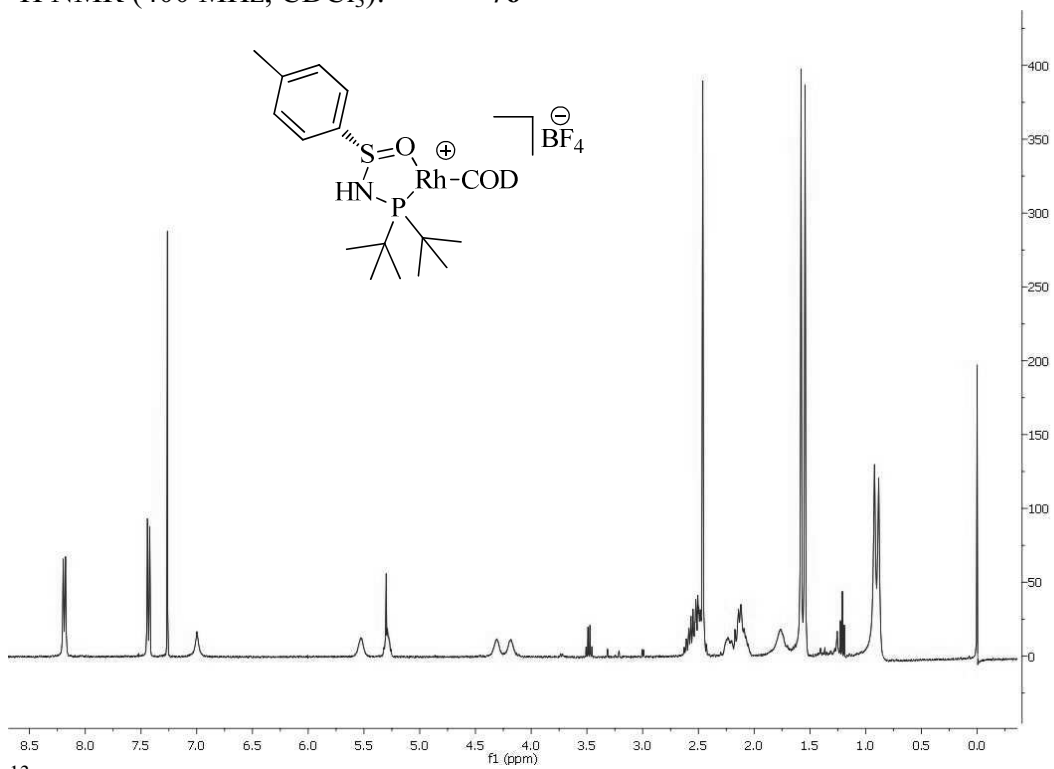
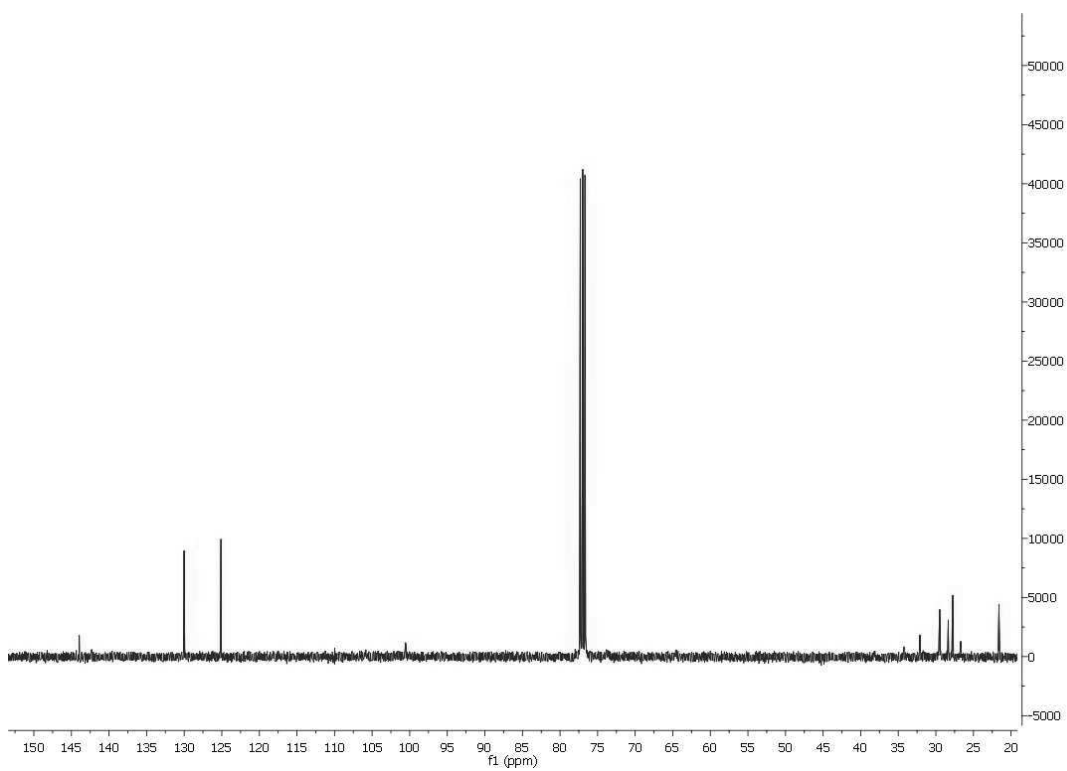


^{13}C NMR (400 MHz, CDCl_3):



^1H NMR (400 MHz, CDCl_3):

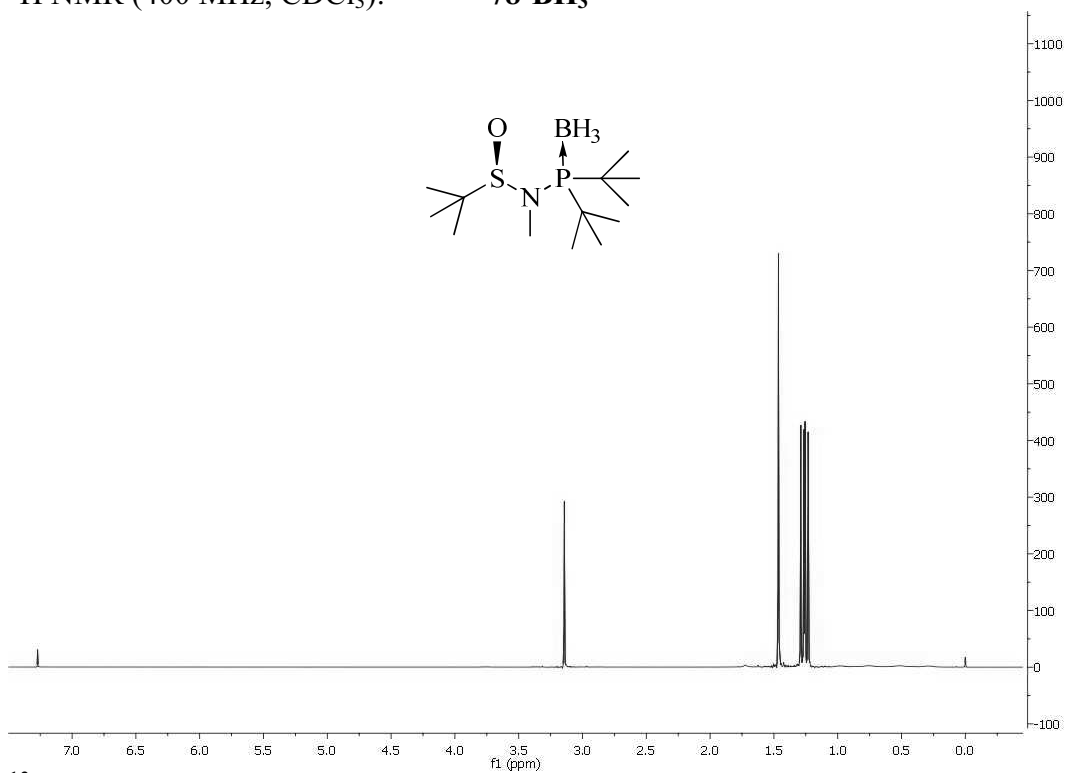
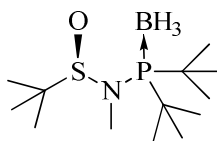
76

 ^{13}C NMR (400 MHz, CDCl_3):

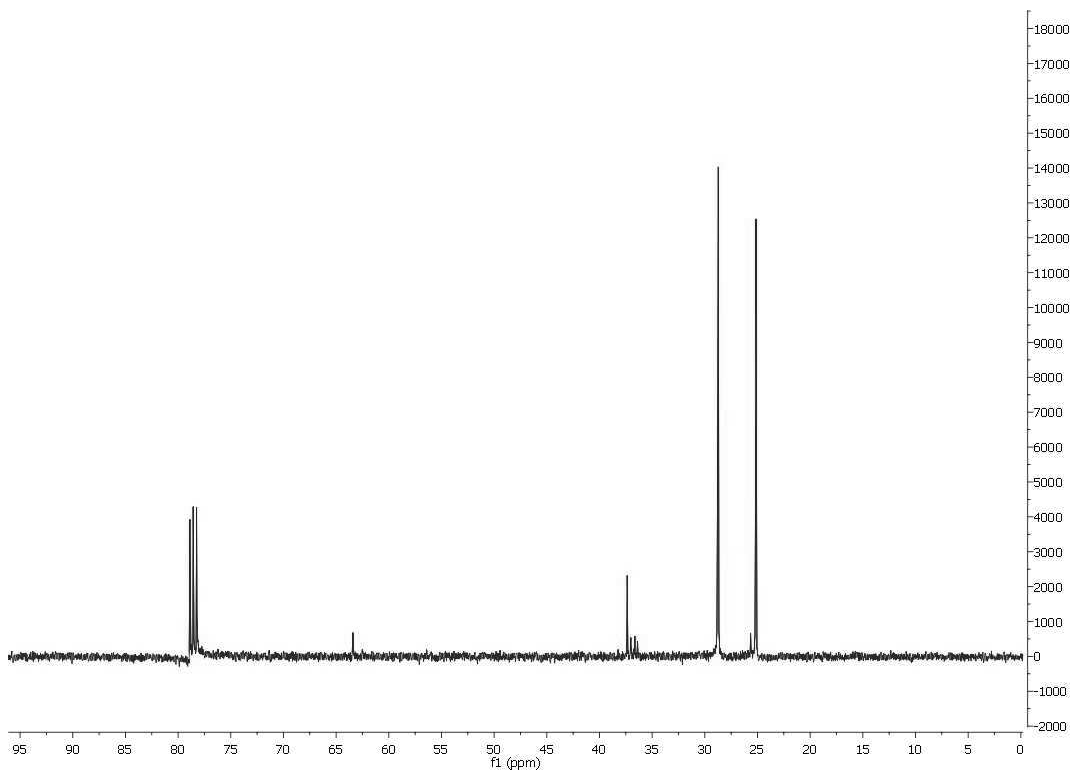
8. Spectra

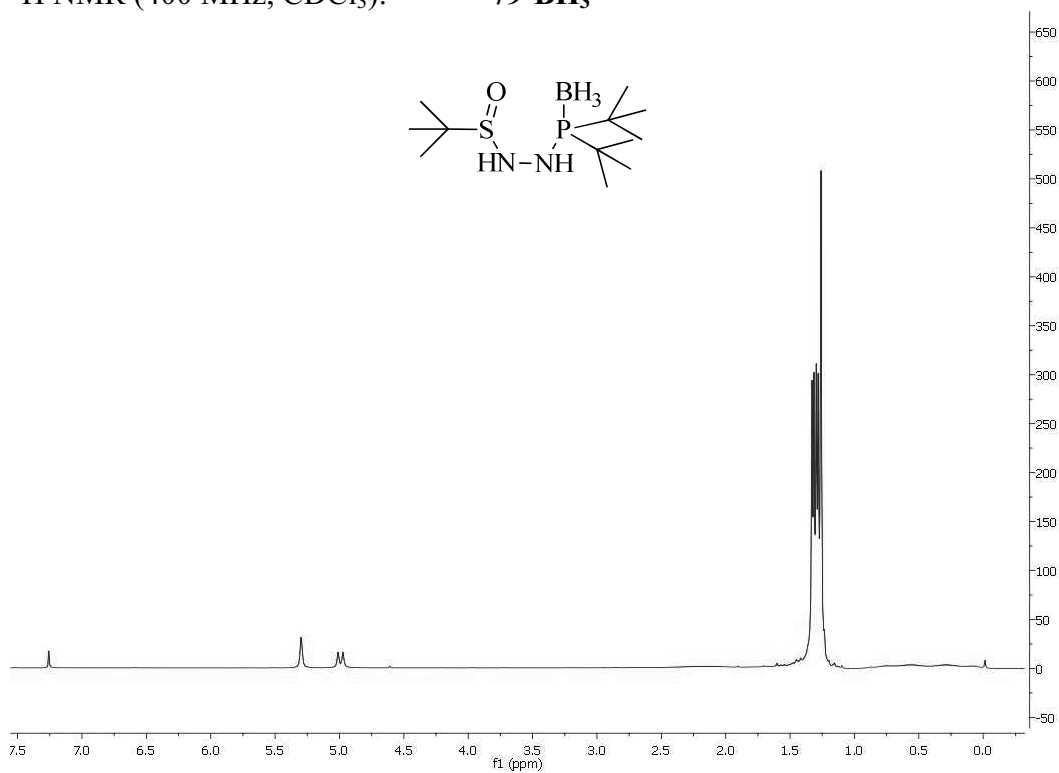
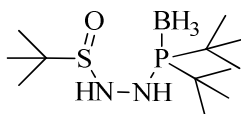
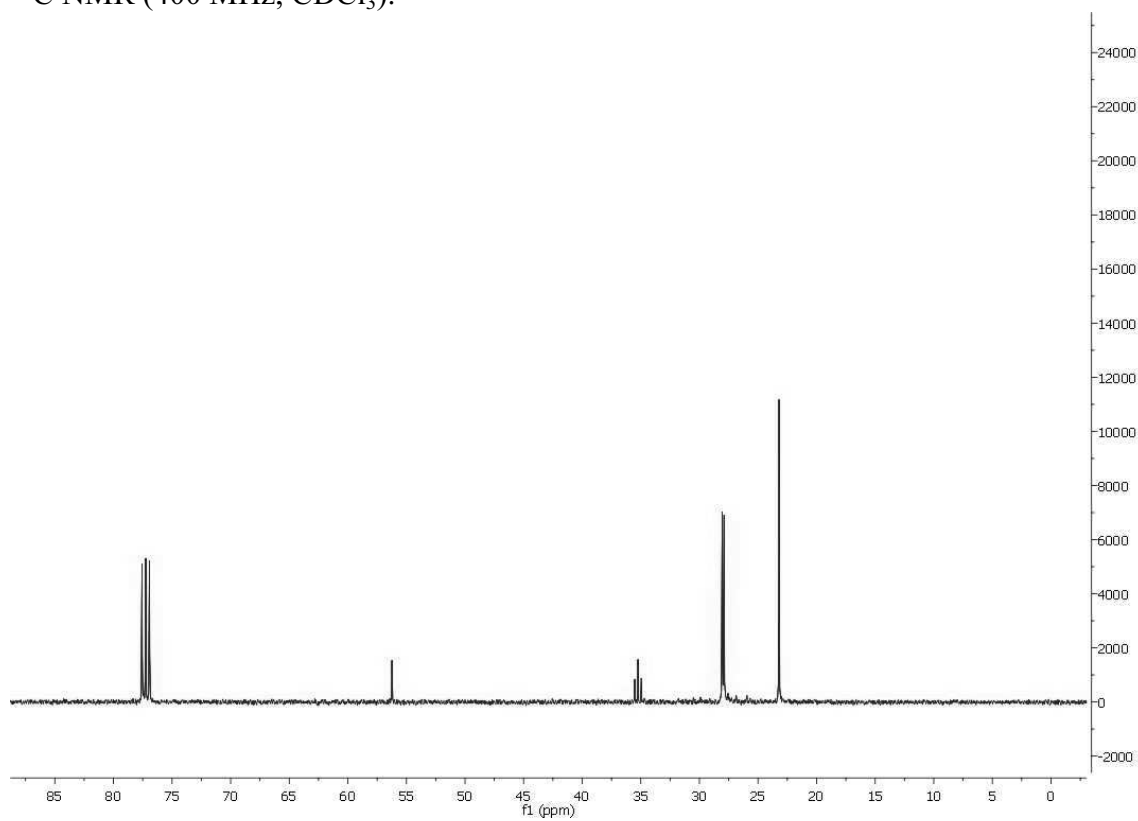
^1H NMR (400 MHz, CDCl_3):

78-BH₃



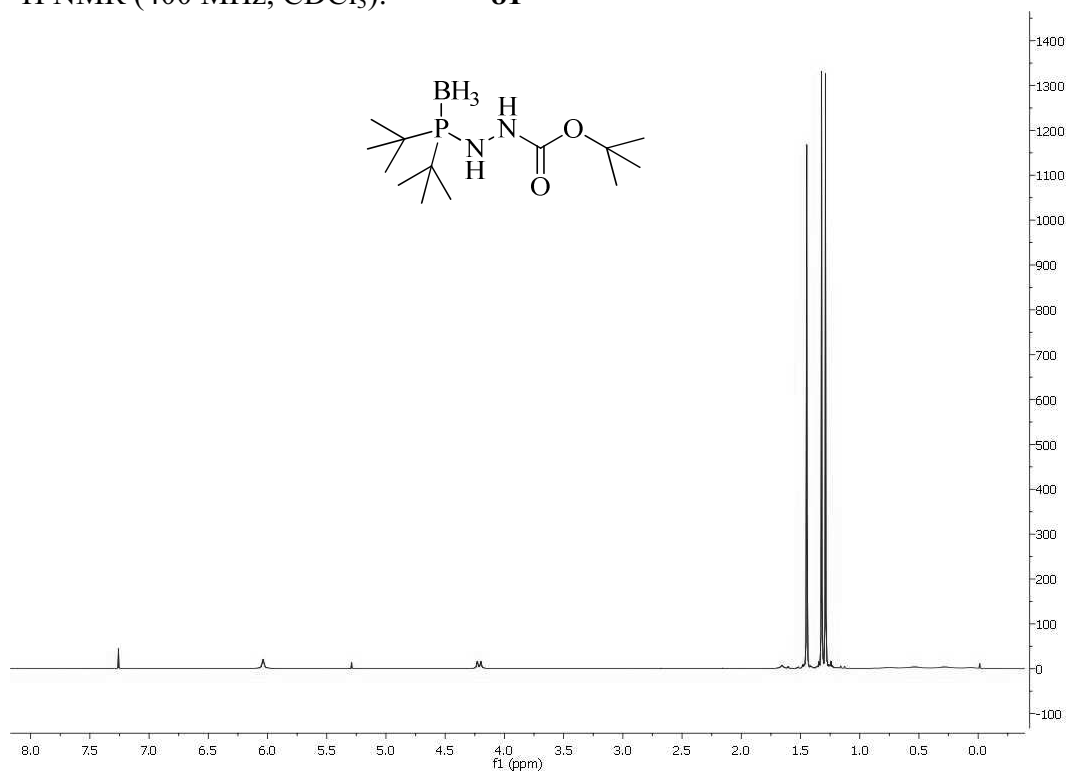
^{13}C NMR (400 MHz, CDCl_3):



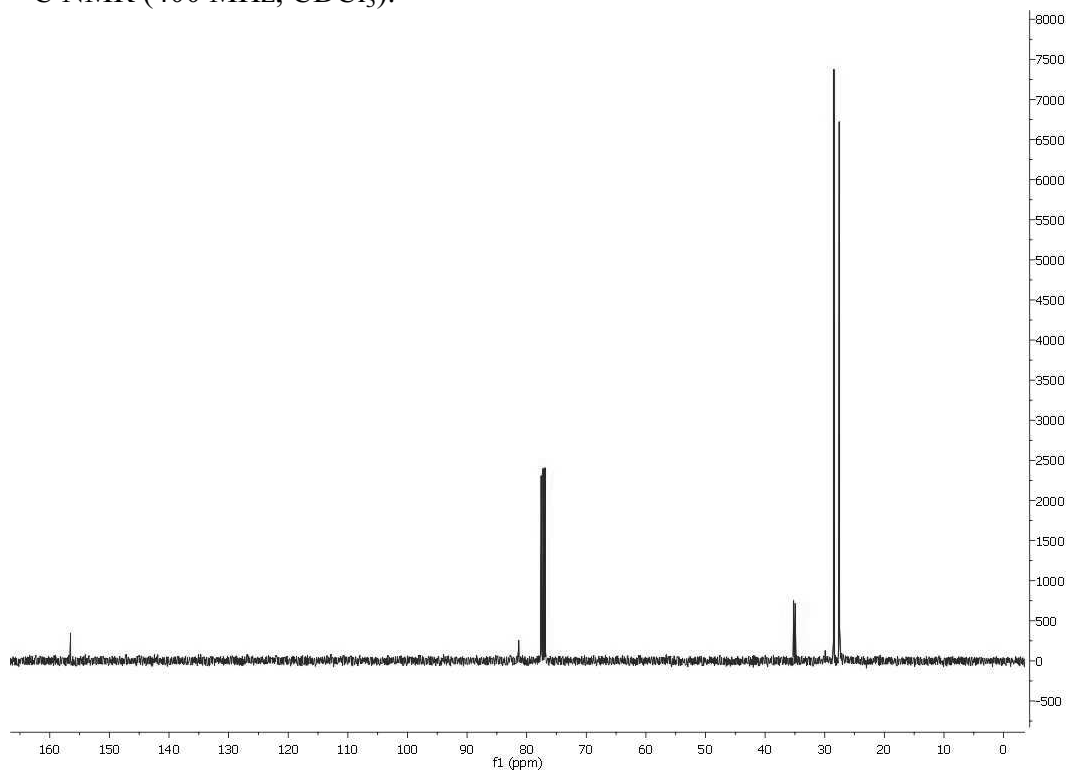
^1H NMR (400 MHz, CDCl_3):**79-BH₃** ^{13}C NMR (400 MHz, CDCl_3):

8. Spectra

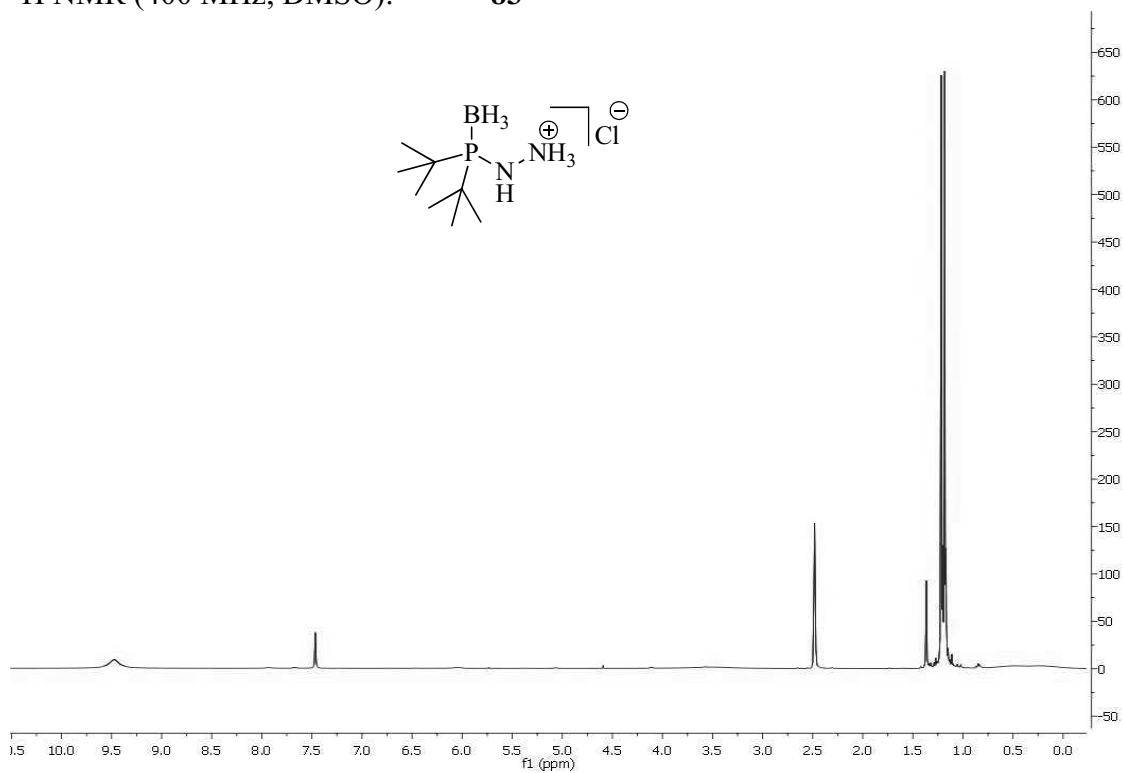
^1H NMR (400 MHz, CDCl_3): **81**



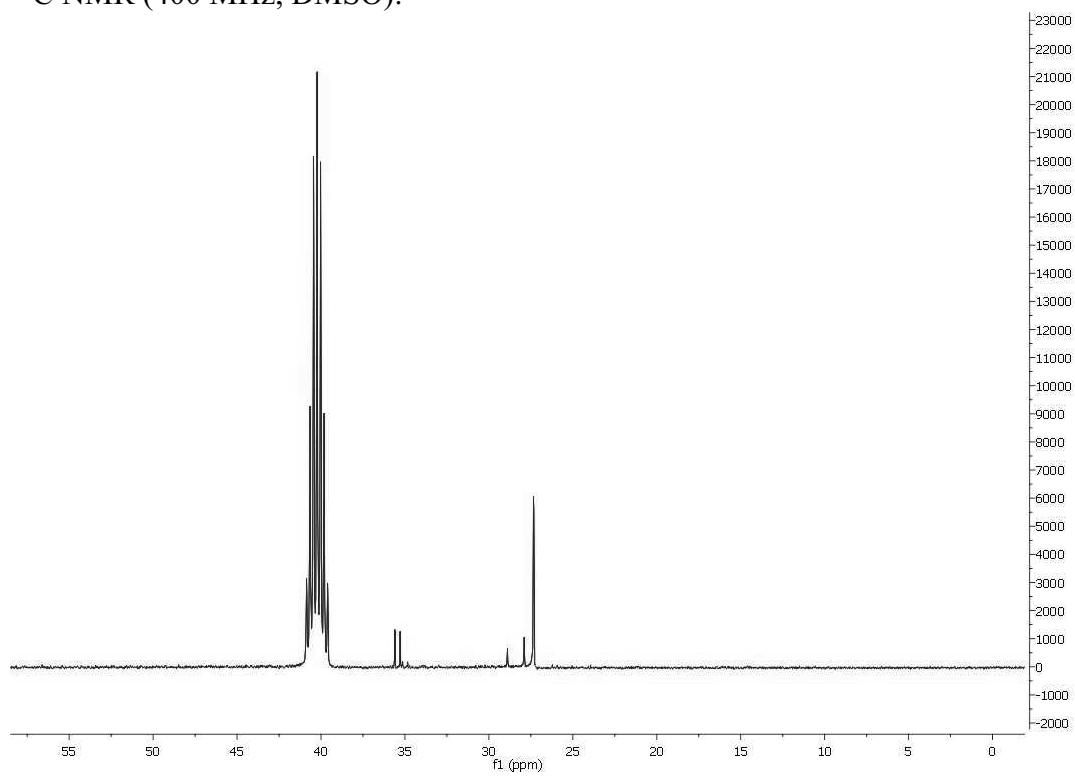
^{13}C NMR (400 MHz, CDCl_3):



^1H NMR (400 MHz, DMSO): **83**



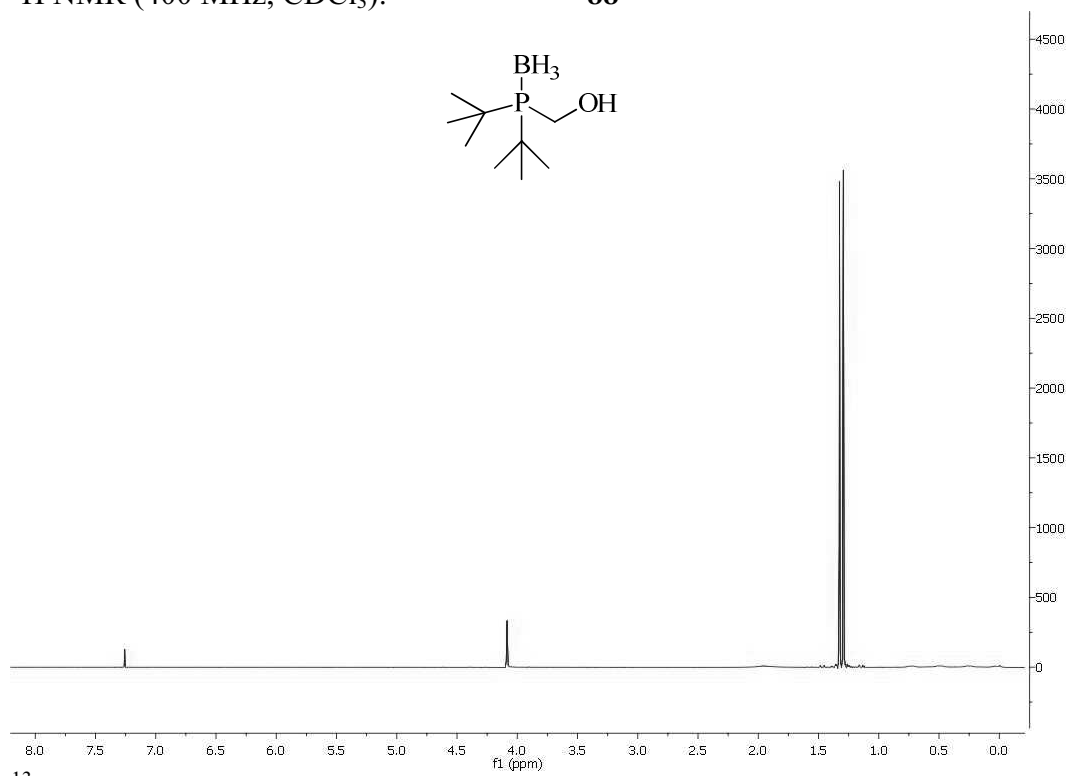
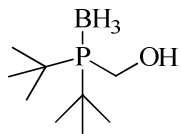
^{13}C NMR (400 MHz, DMSO):



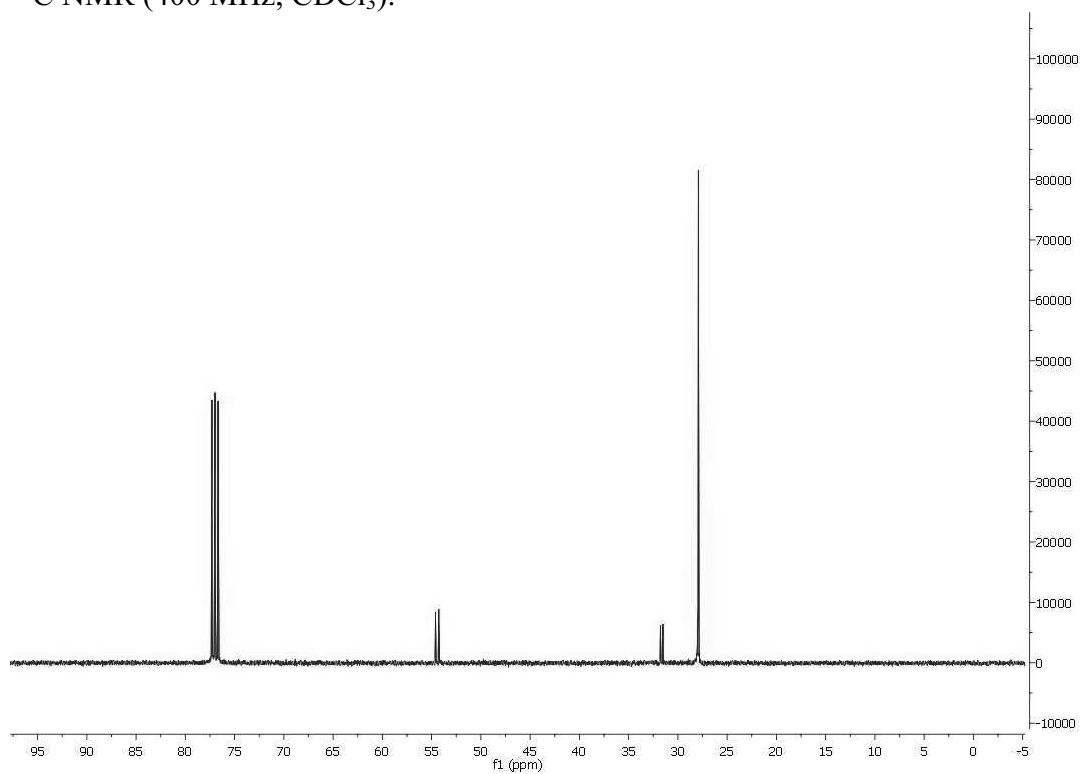
8. Spectra

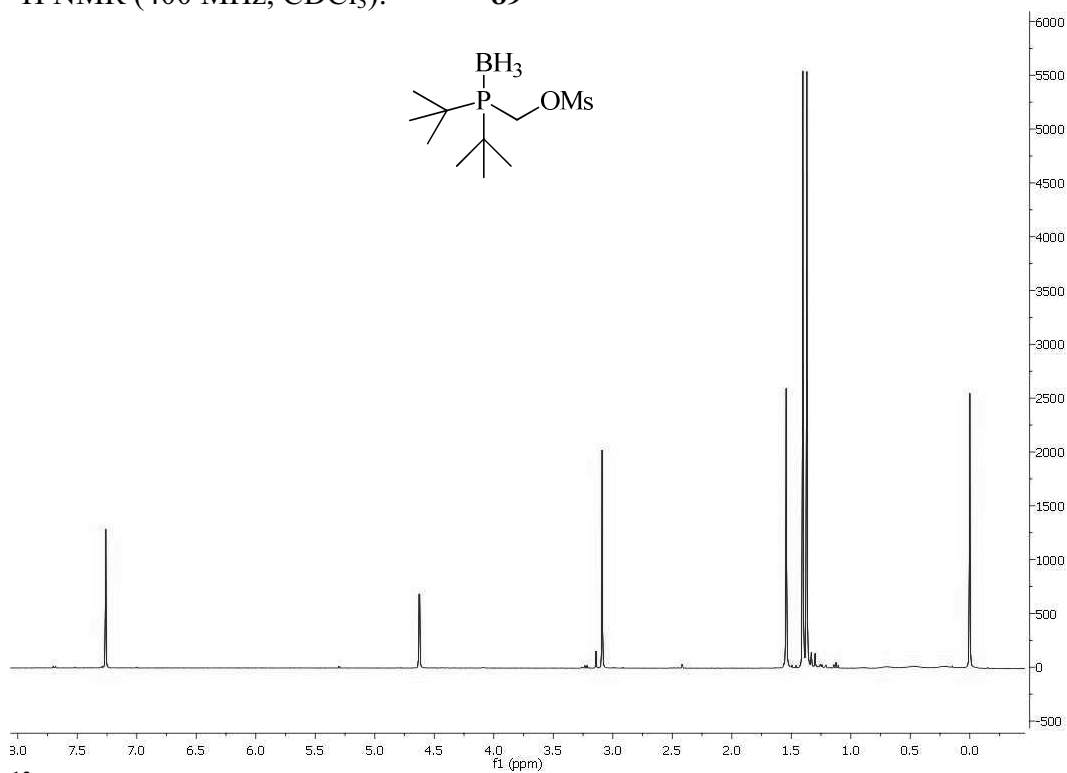
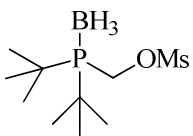
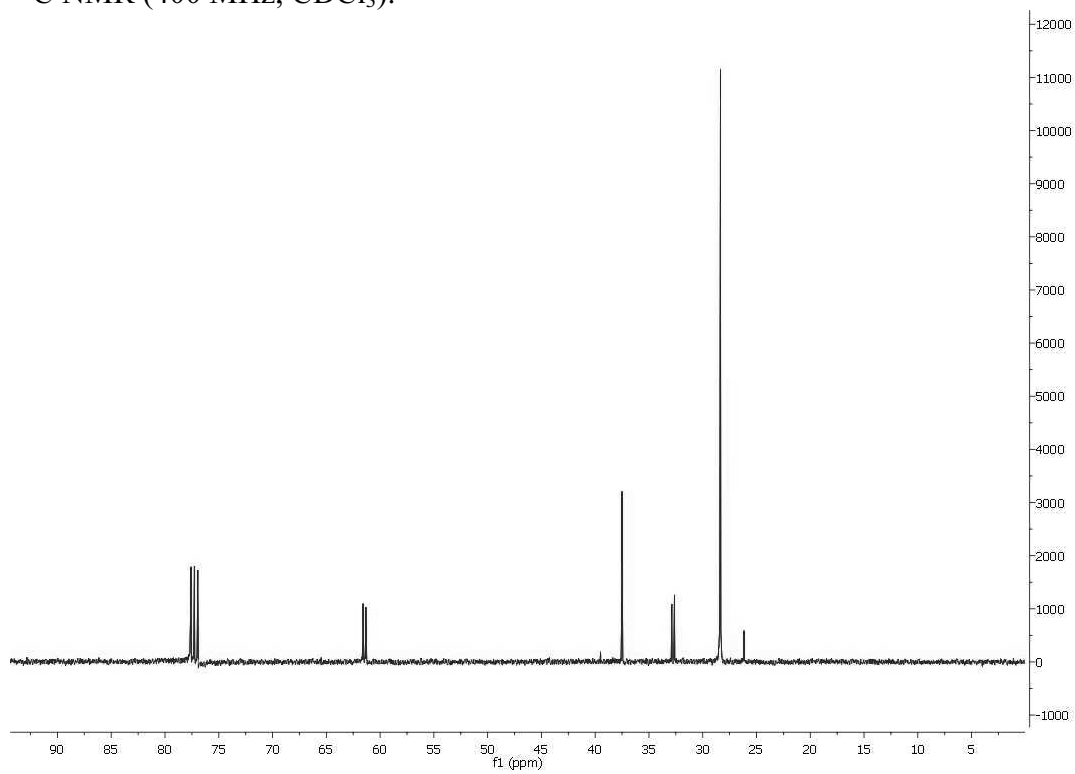
^1H NMR (400 MHz, CDCl_3):

88



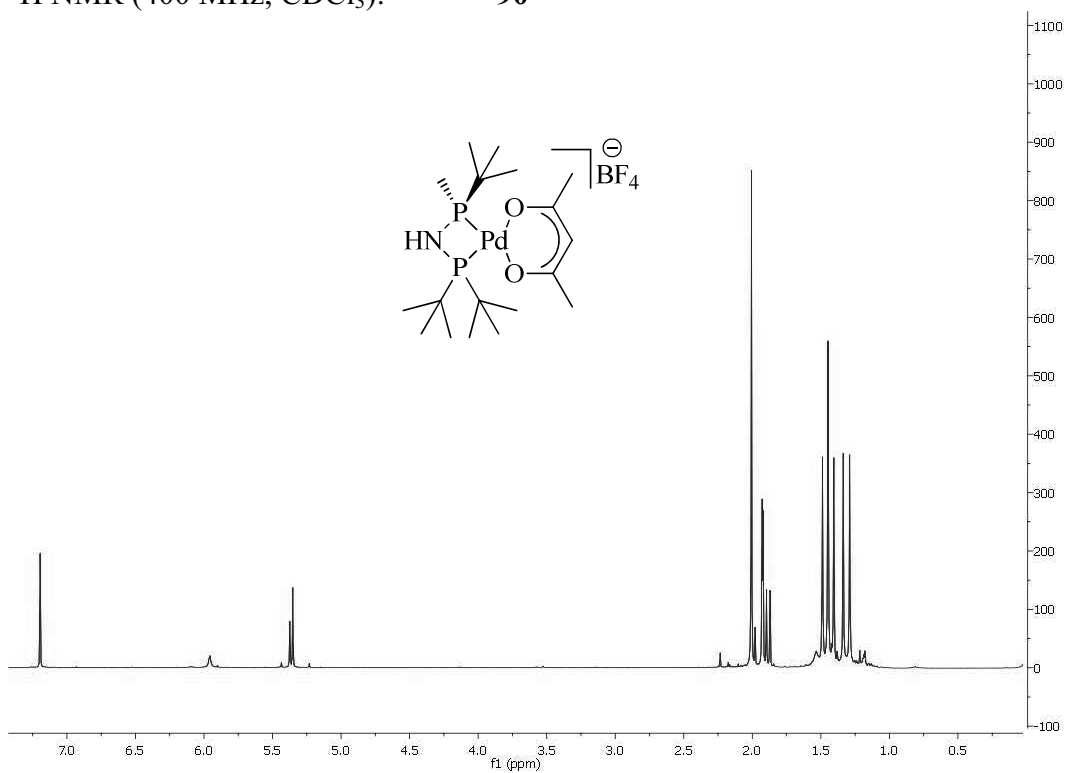
^{13}C NMR (400 MHz, CDCl_3):



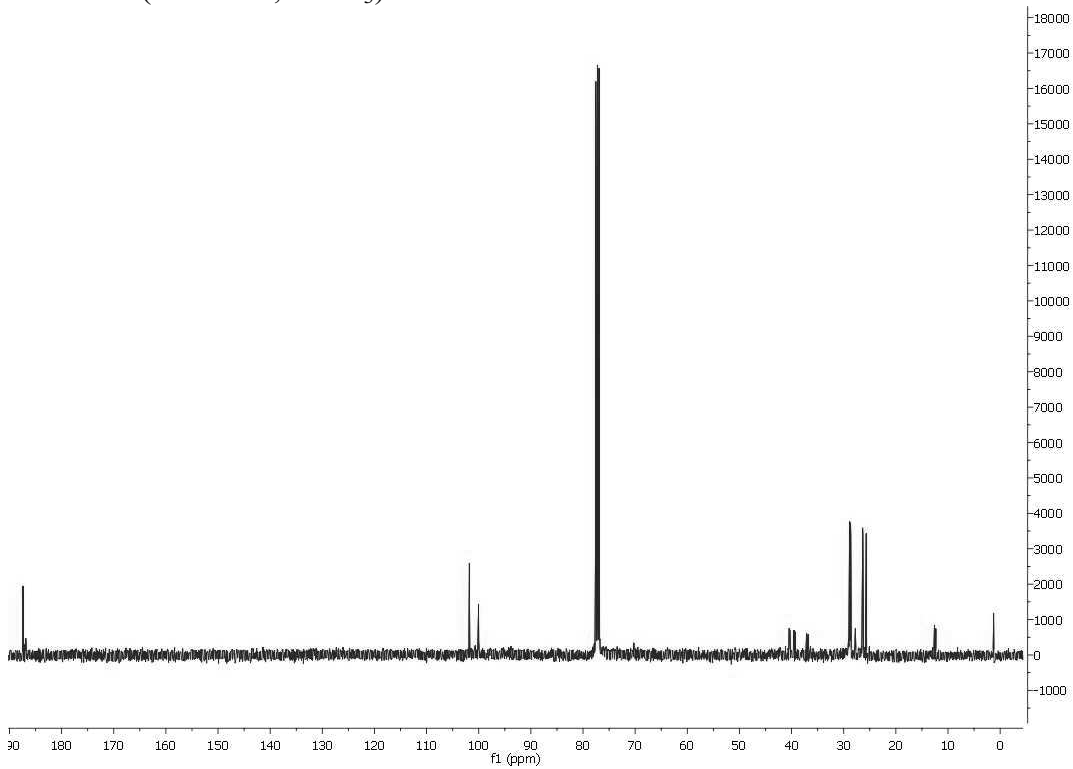
^1H NMR (400 MHz, CDCl_3):**89** ^{13}C NMR (400 MHz, CDCl_3):

8. Spectra

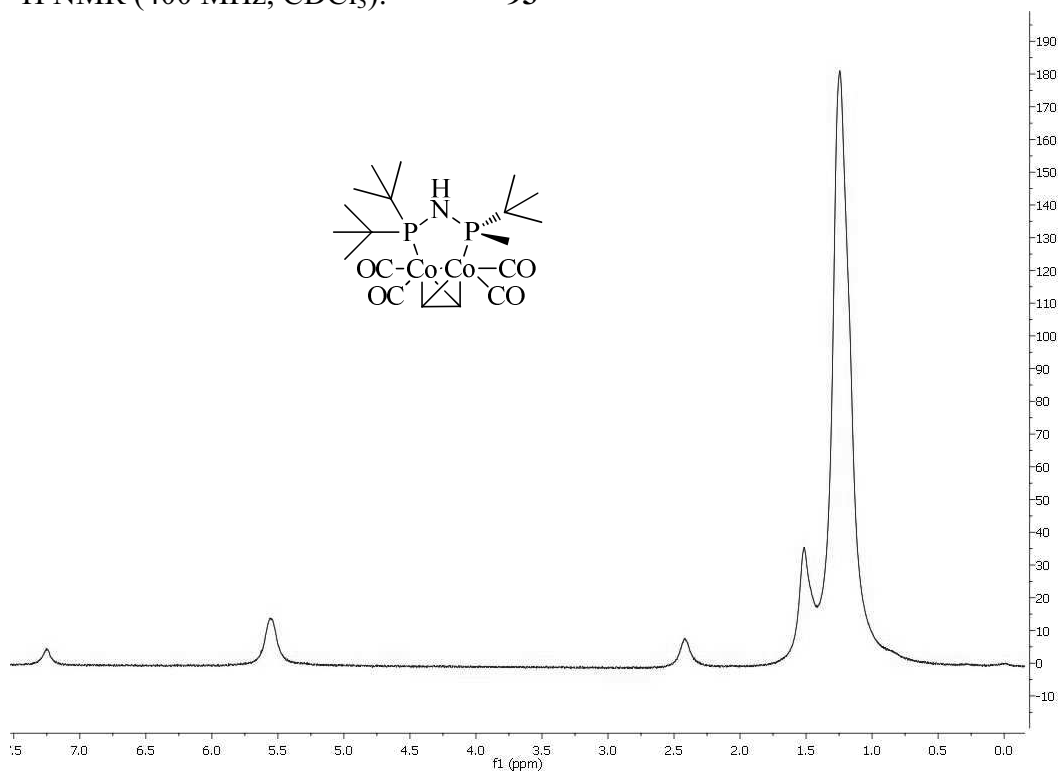
^1H NMR (400 MHz, CDCl_3): **90**



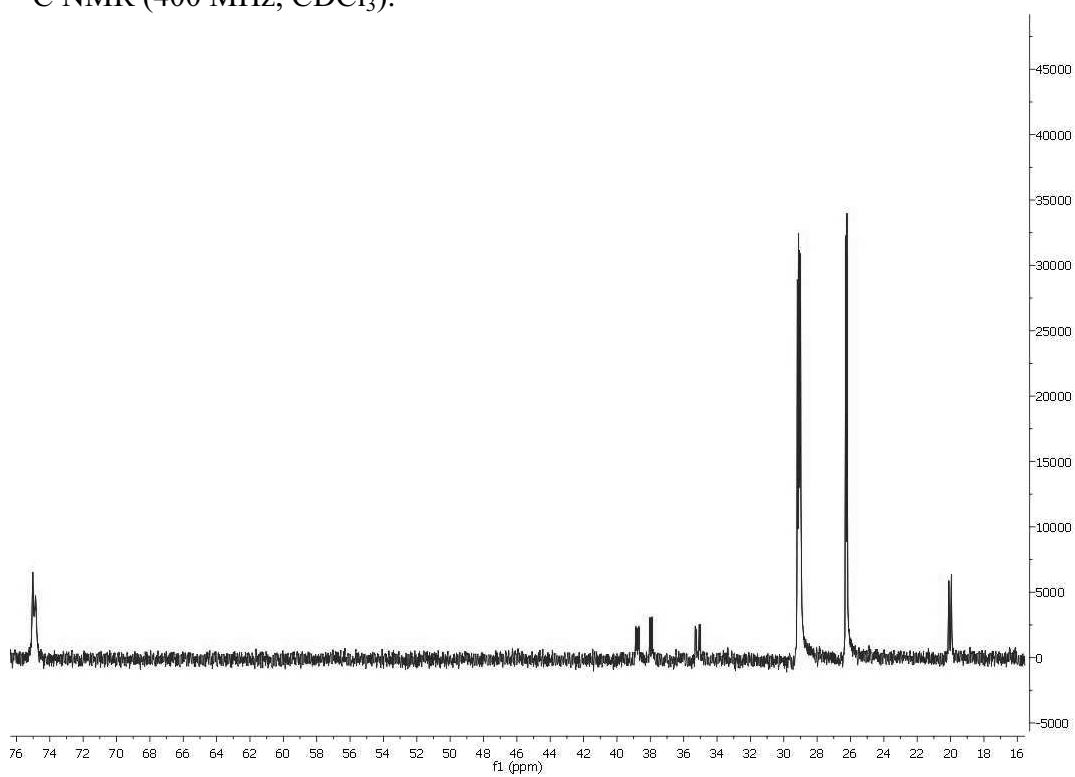
^{13}C NMR (400 MHz, CDCl_3):



^1H NMR (400 MHz, CDCl_3): **93**

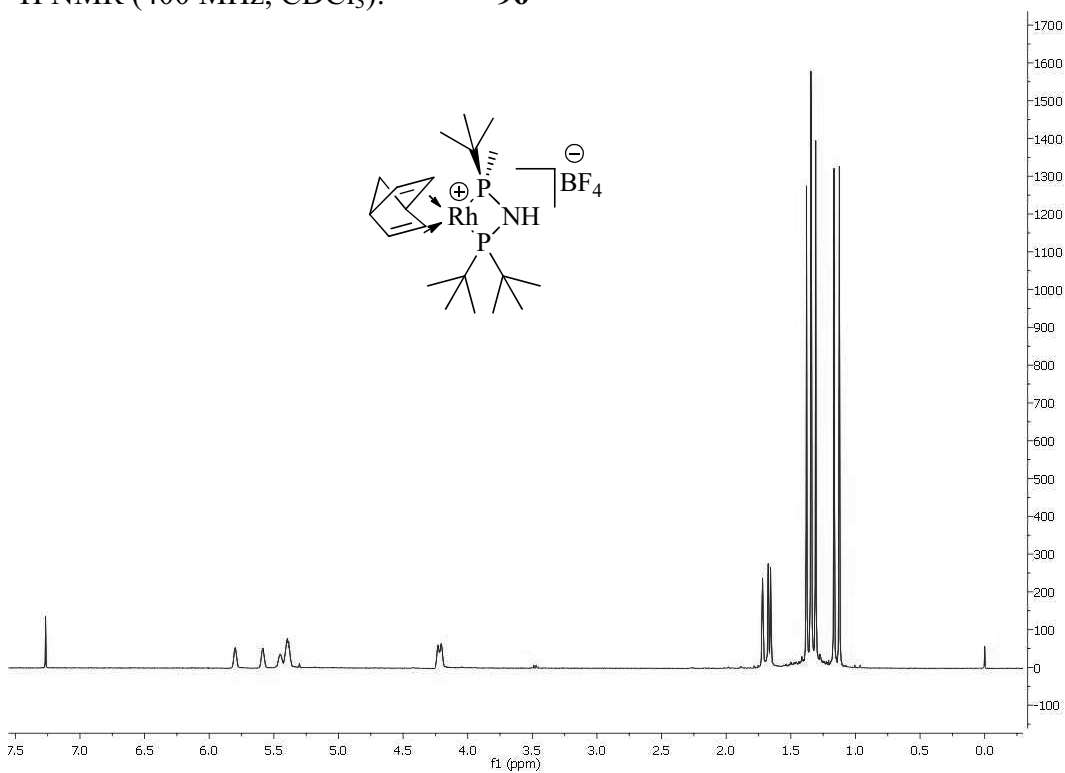


^{13}C NMR (400 MHz, CDCl_3):

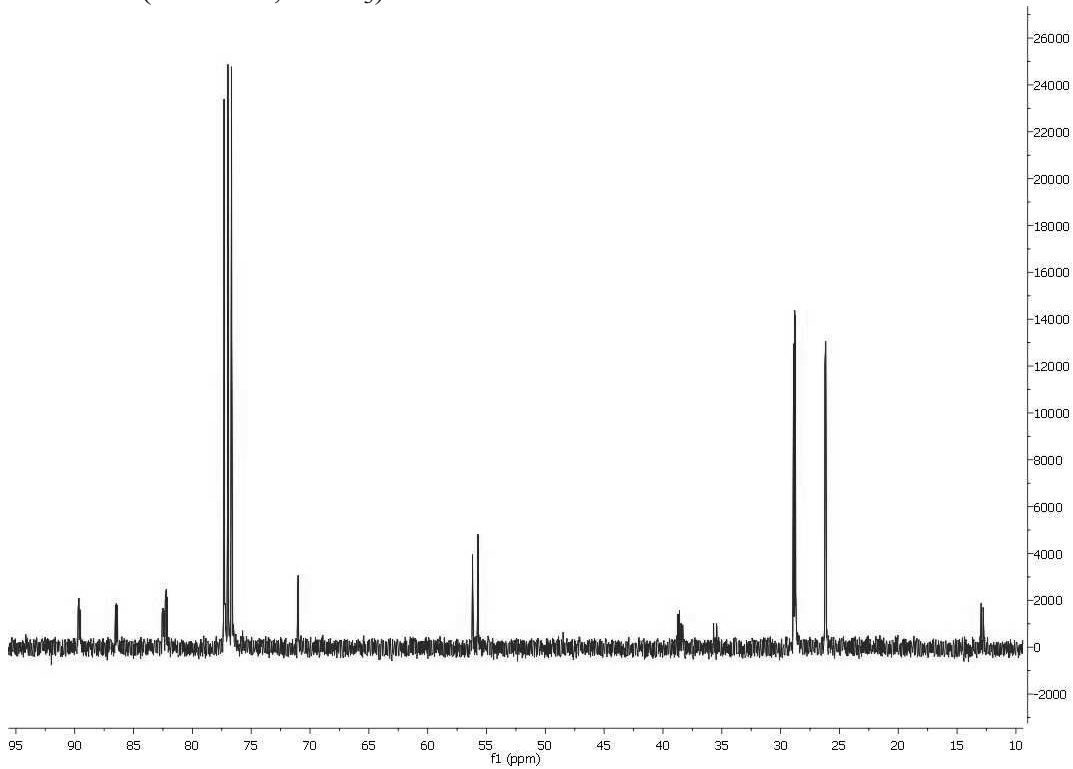


8. Spectra

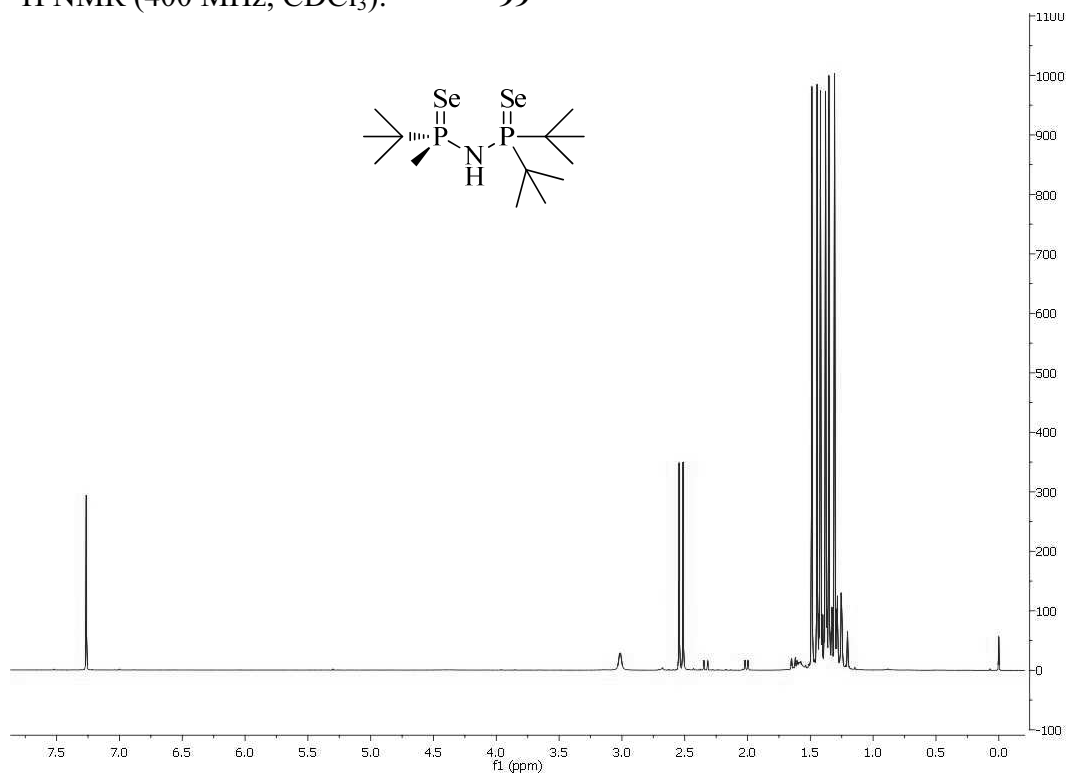
^1H NMR (400 MHz, CDCl_3): **96**



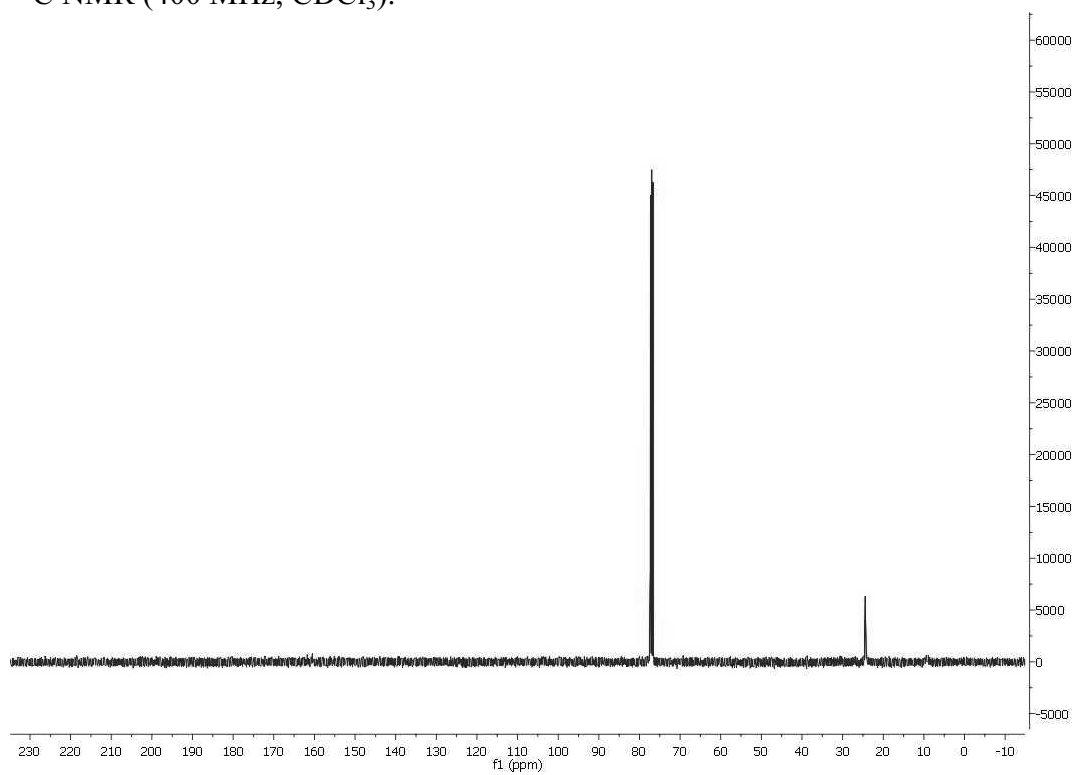
^{13}C NMR (400 MHz, CDCl_3):



^1H NMR (400 MHz, CDCl_3): **99**

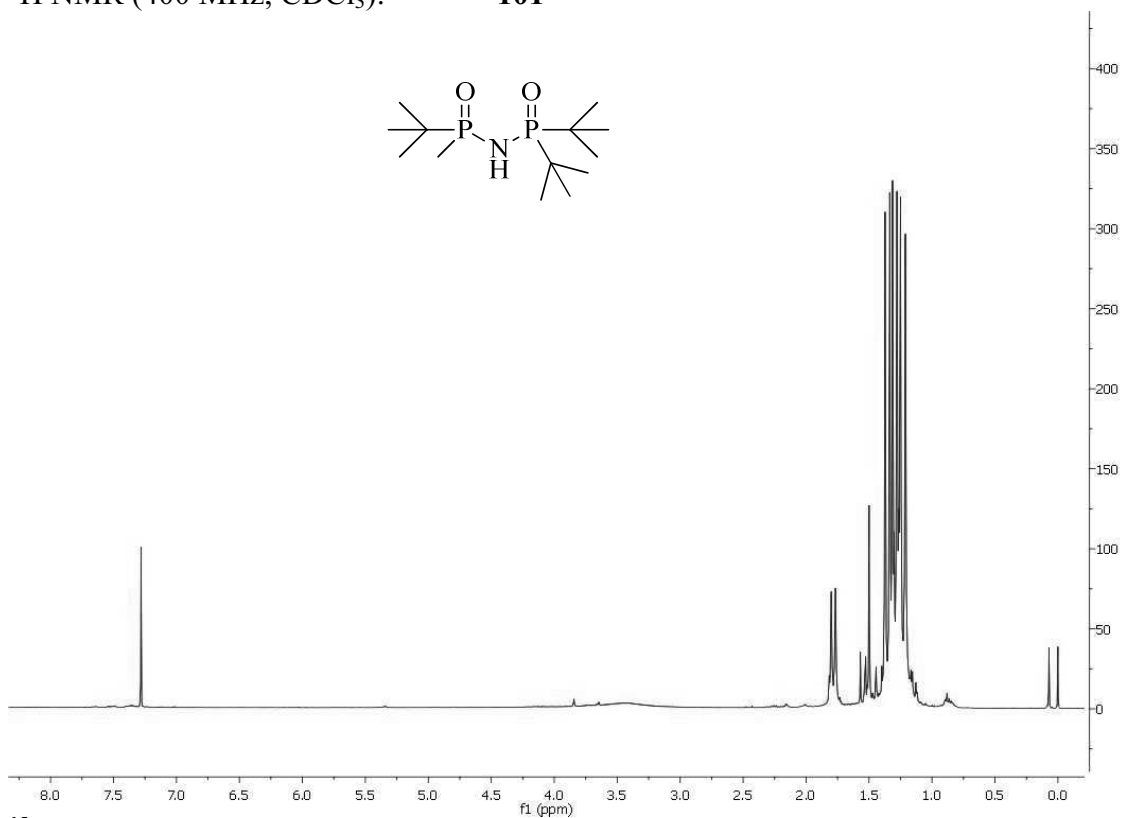


^{13}C NMR (400 MHz, CDCl_3):

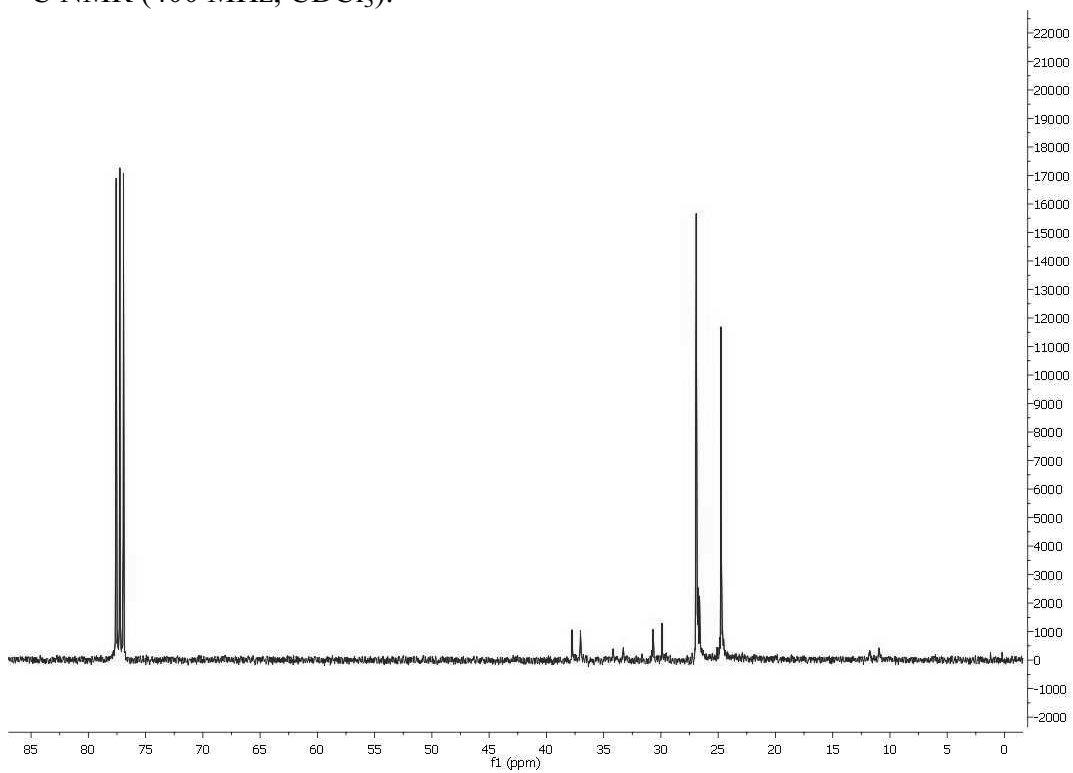


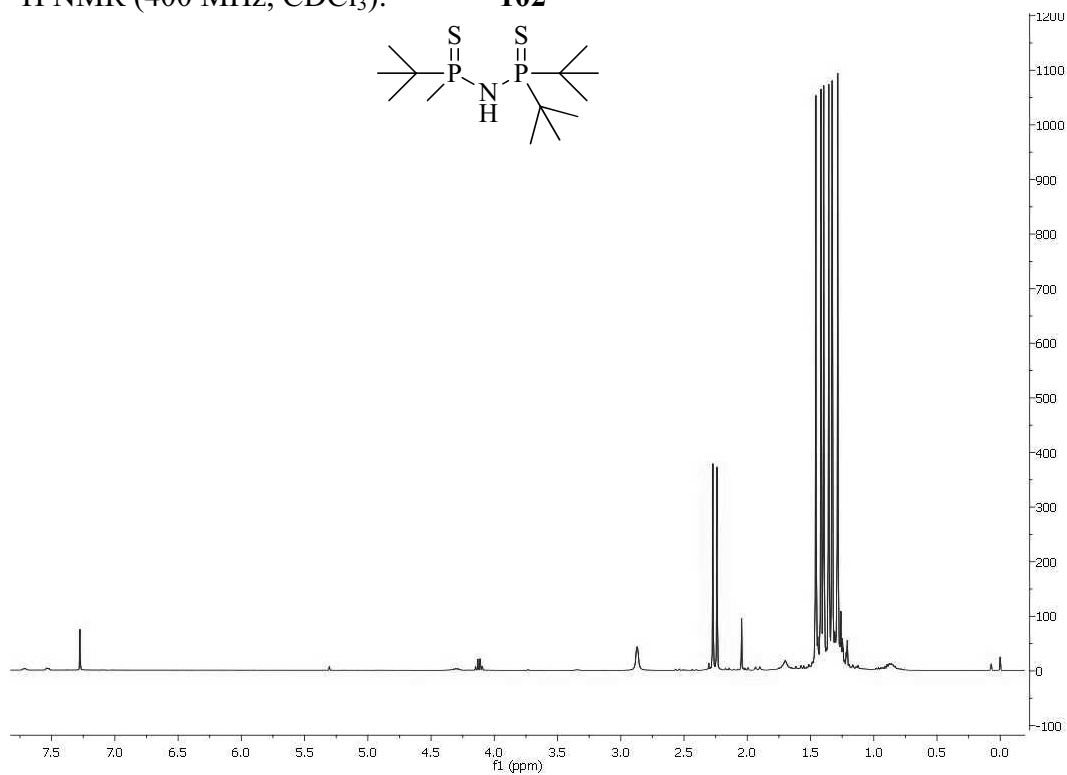
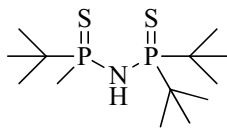
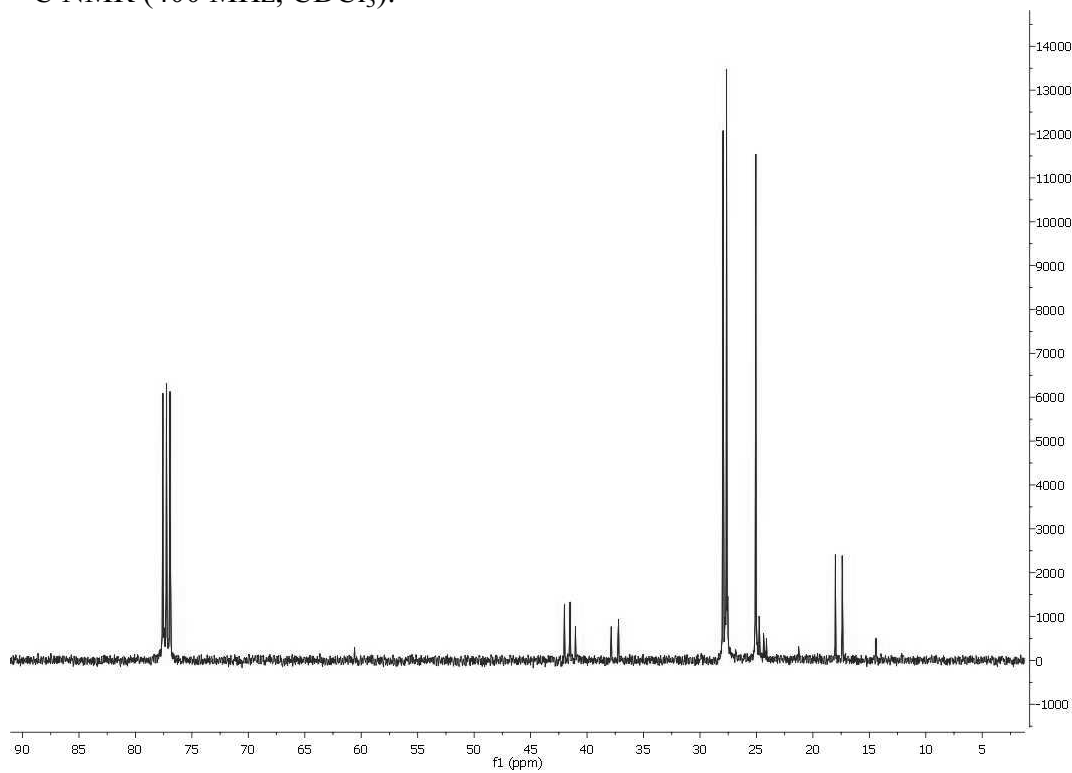
8. Spectra

^1H NMR (400 MHz, CDCl_3): **101**



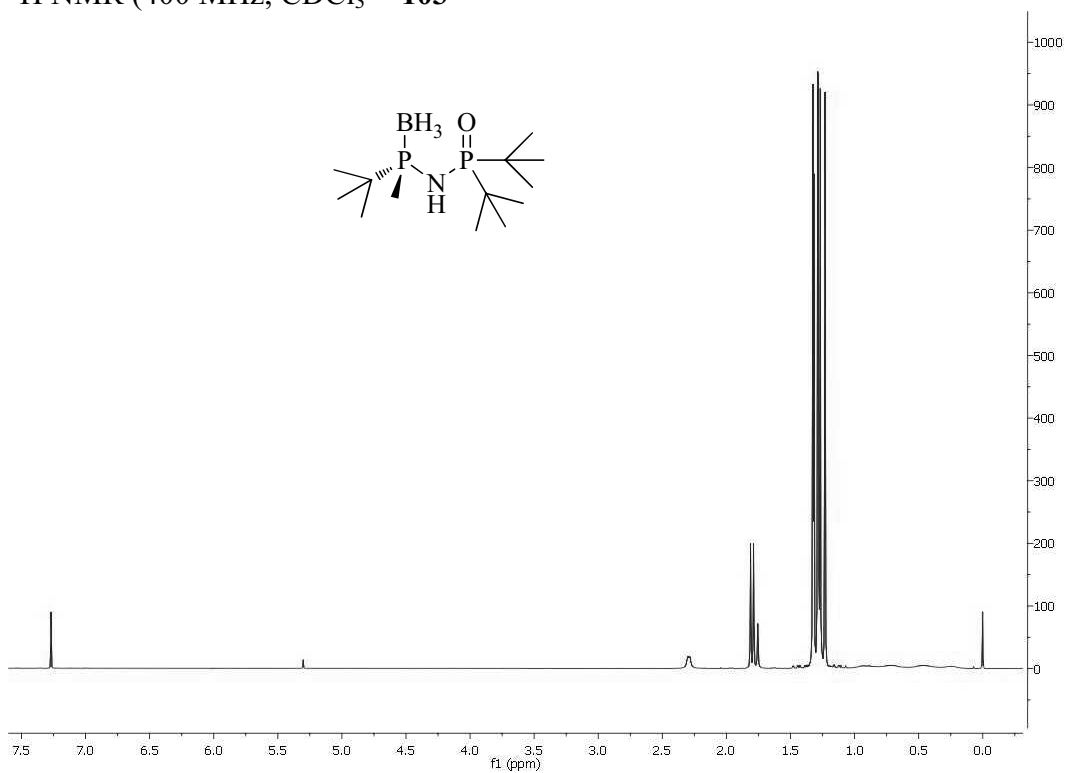
^{13}C NMR (400 MHz, CDCl_3):



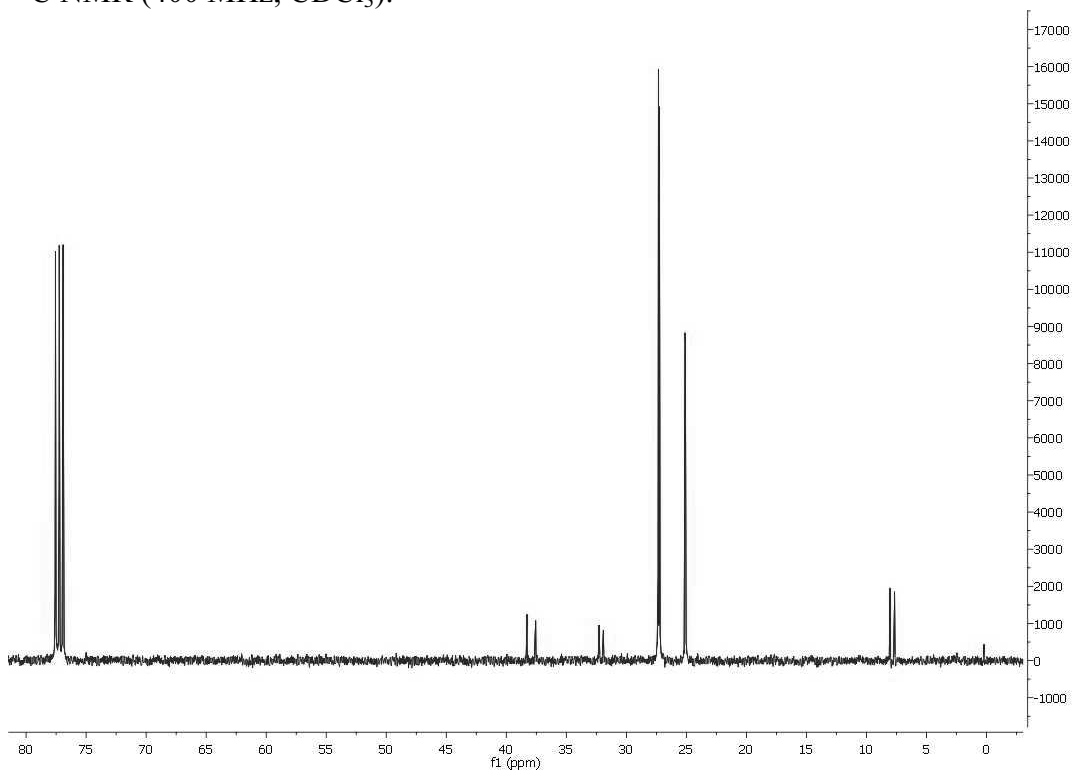
^1H NMR (400 MHz, CDCl_3):**102** ^{13}C NMR (400 MHz, CDCl_3):

8. Spectra

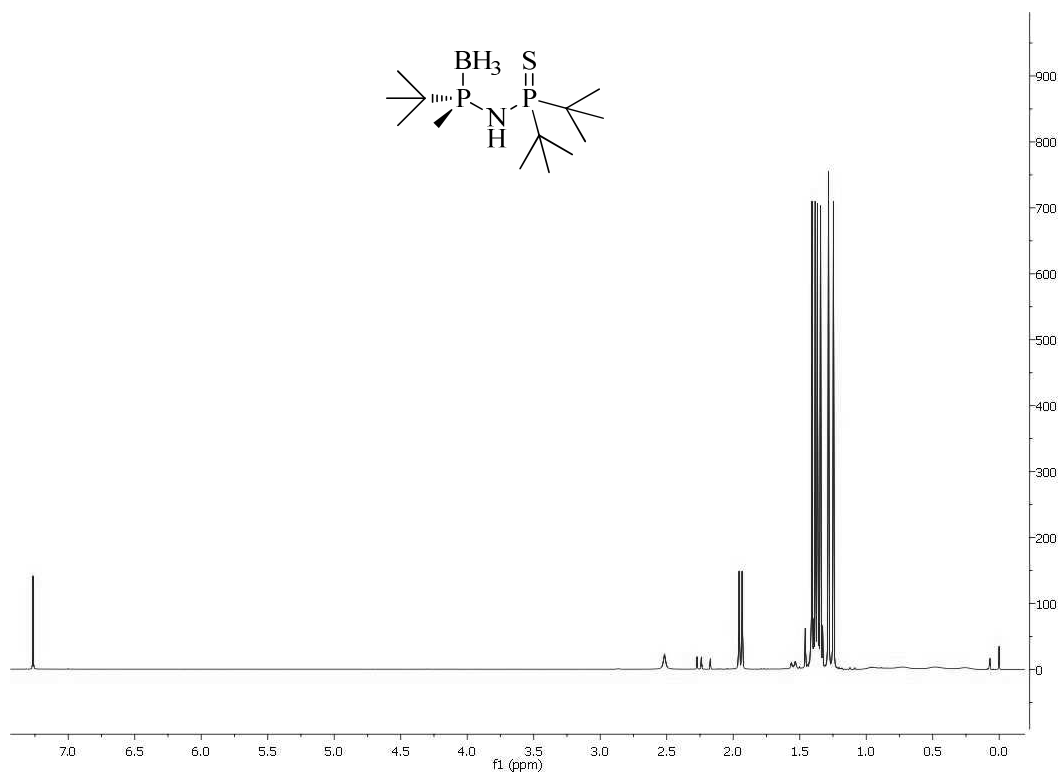
^1H NMR (400 MHz, CDCl_3) **103**



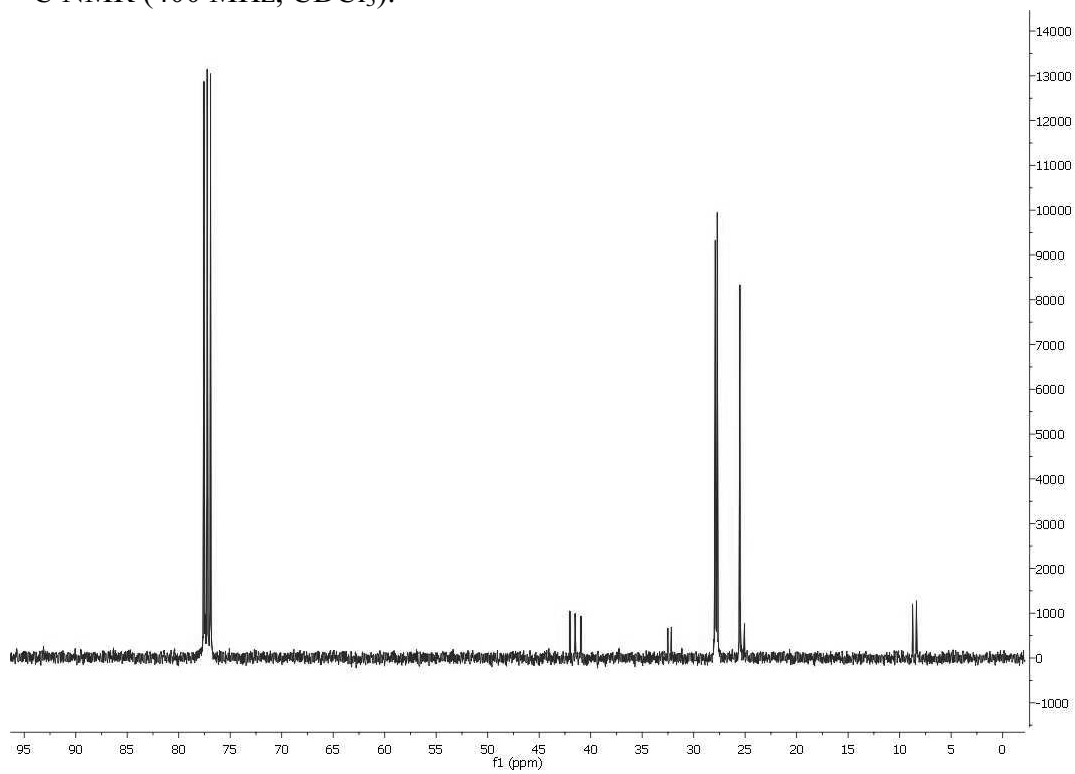
^{13}C NMR (400 MHz, CDCl_3):



^1H NMR (400 MHz, CDCl_3): **104**

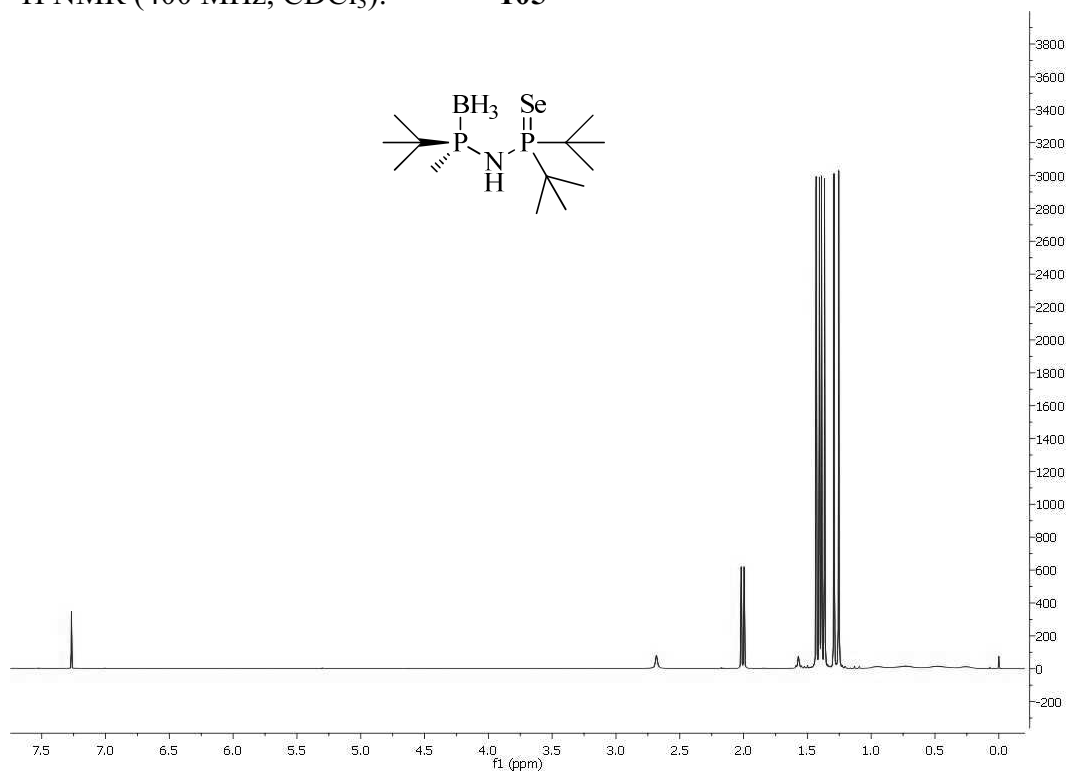


^{13}C NMR (400 MHz, CDCl_3):

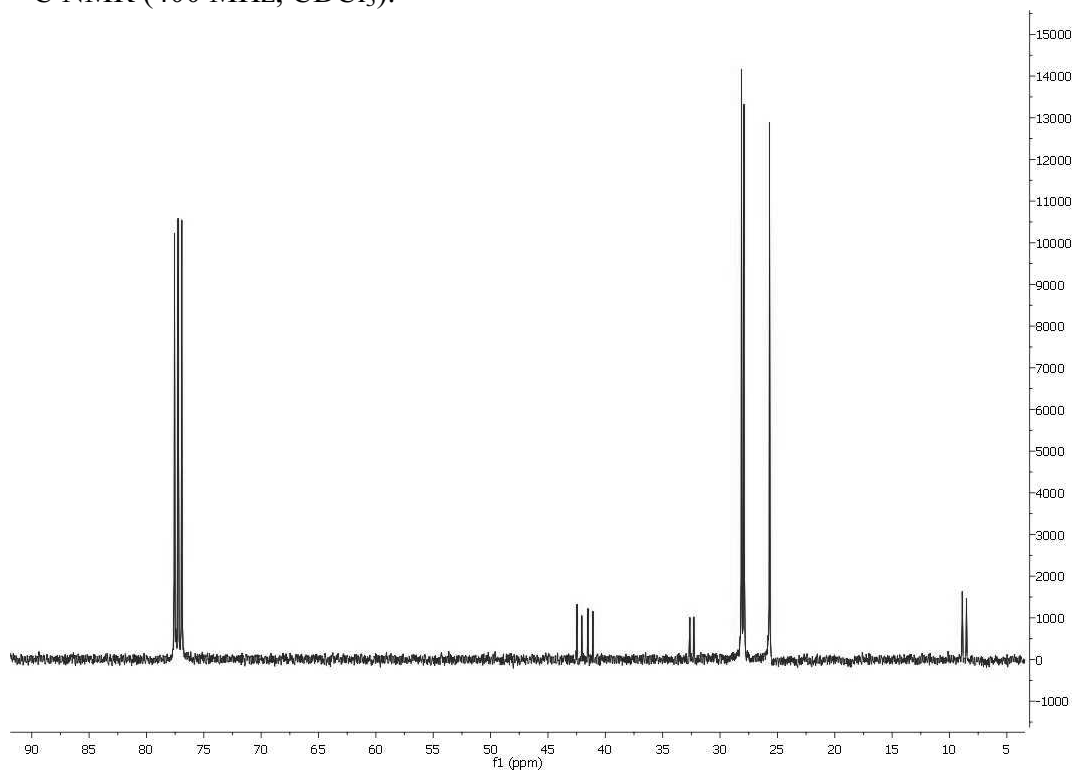


8. Spectra

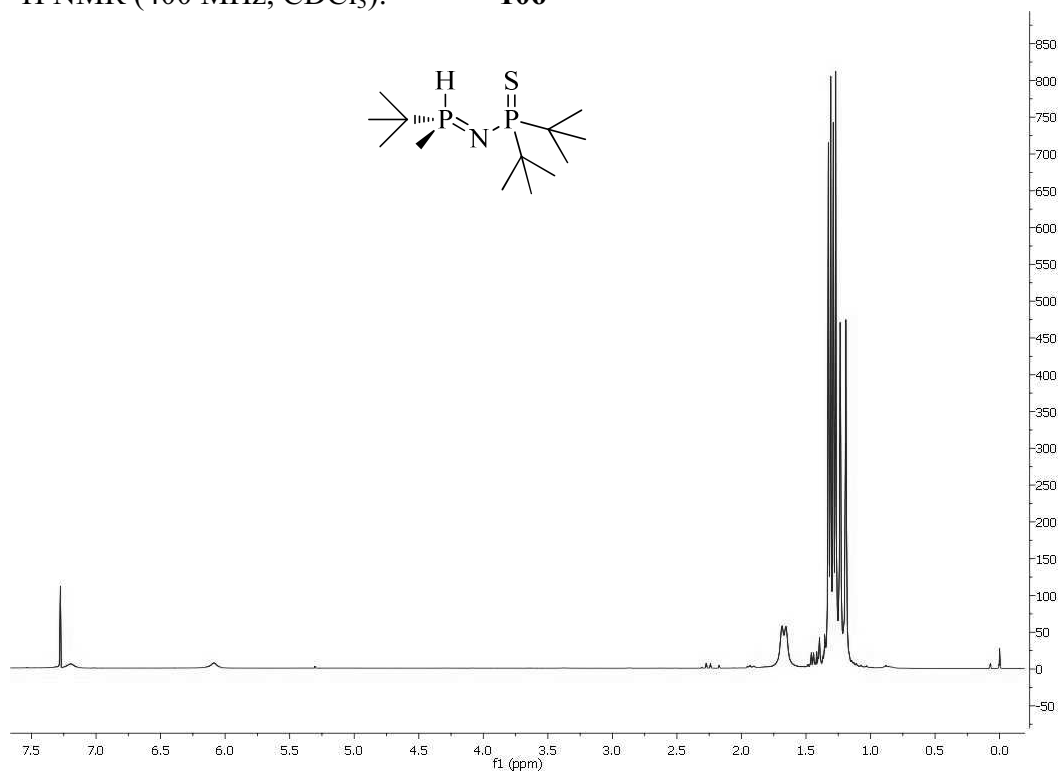
^1H NMR (400 MHz, CDCl_3): **105**



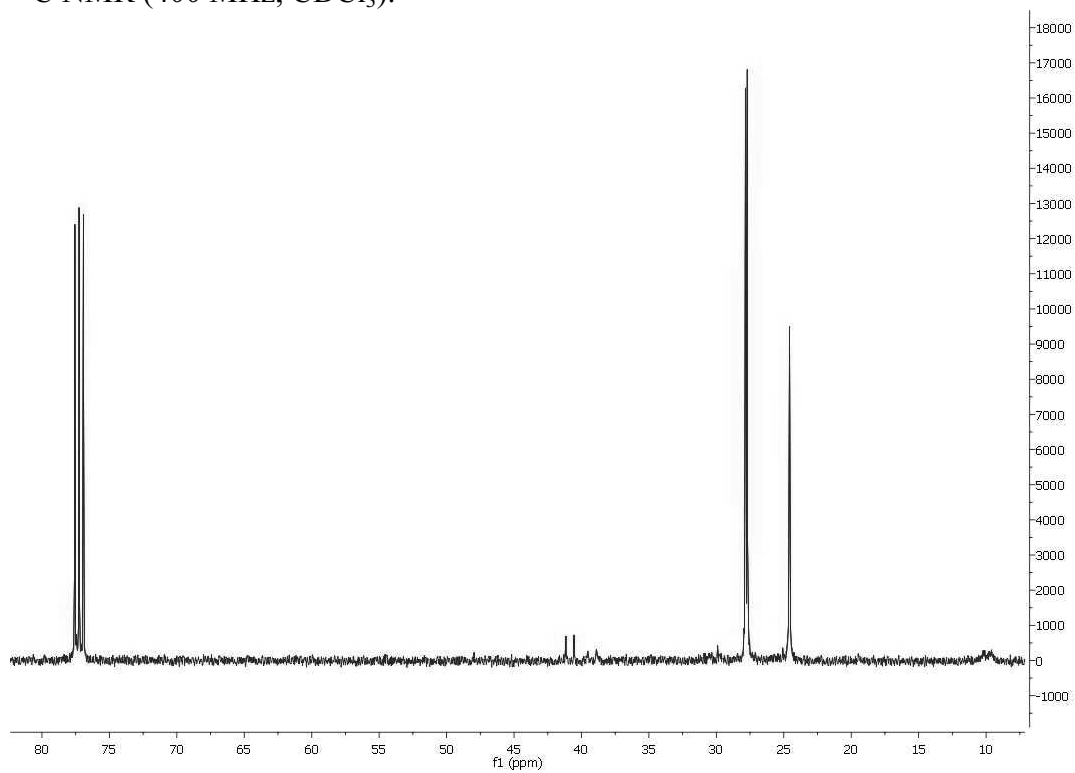
^{13}C NMR (400 MHz, CDCl_3):



^1H NMR (400 MHz, CDCl_3): **106**

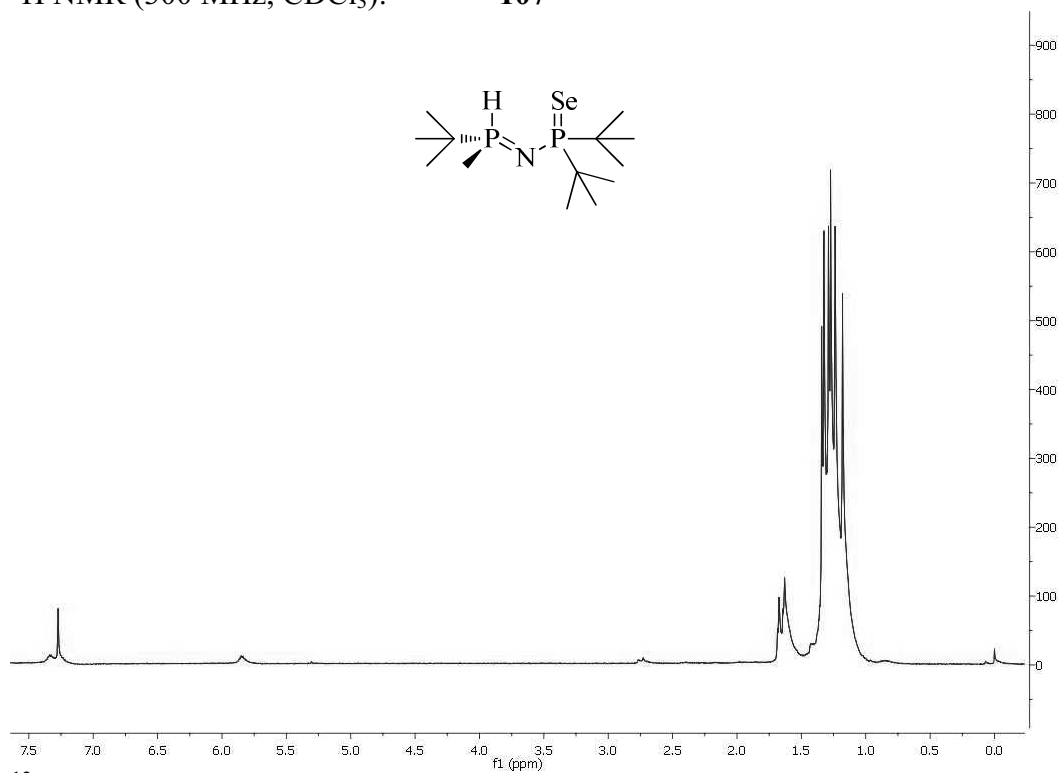


^{13}C NMR (400 MHz, CDCl_3):

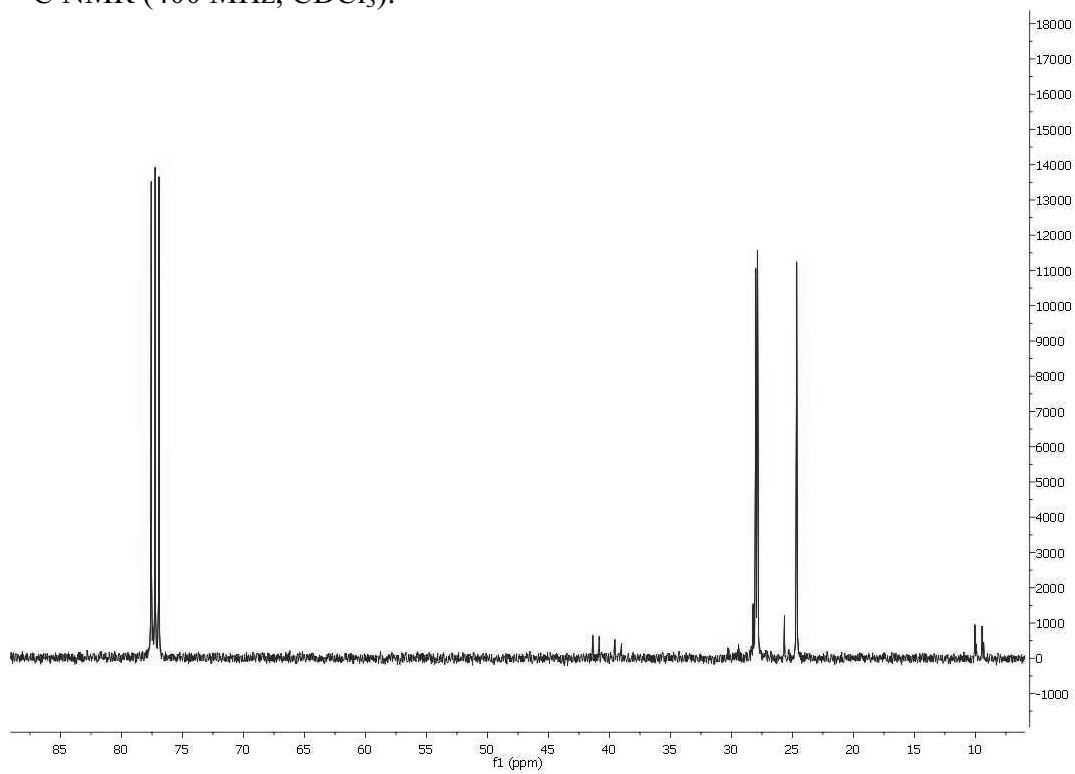


8. Spectra

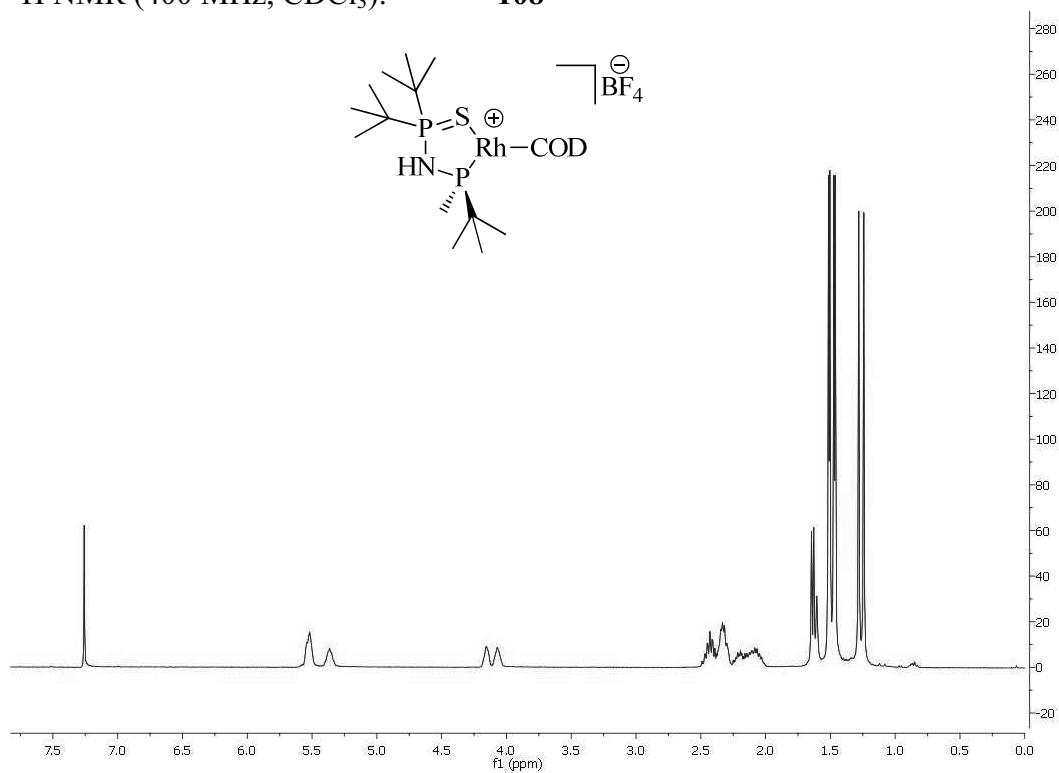
^1H NMR (300 MHz, CDCl_3): **107**



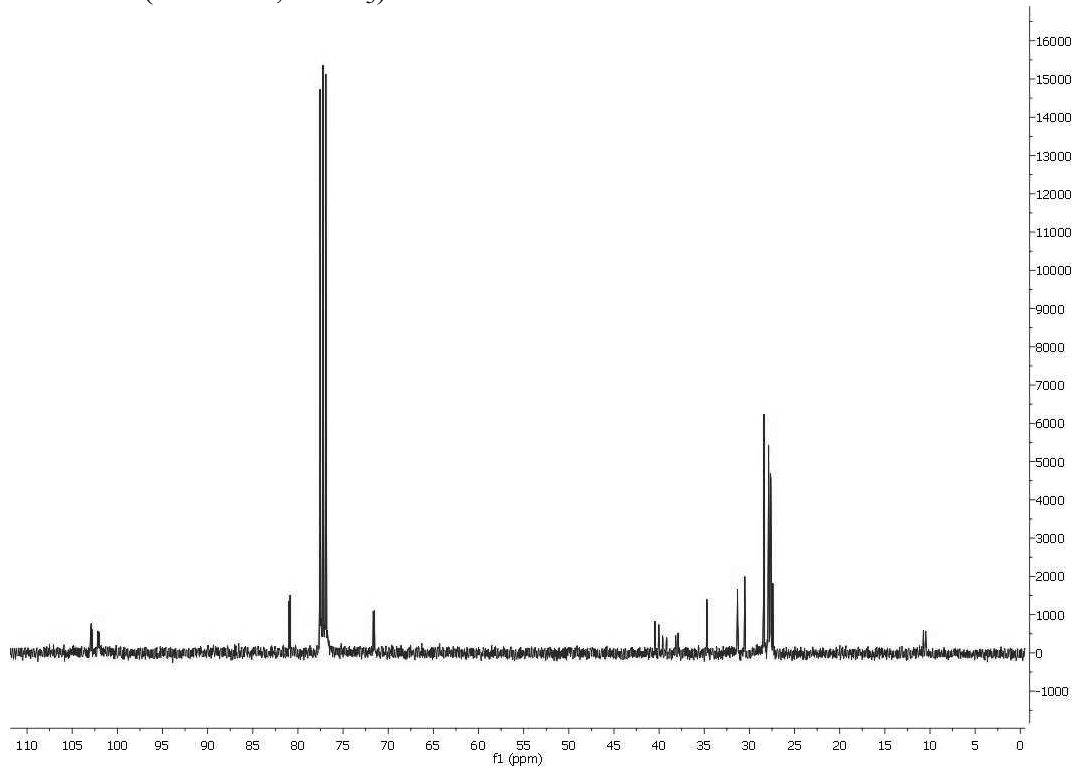
^{13}C NMR (400 MHz, CDCl_3):



^1H NMR (400 MHz, CDCl_3): **108**

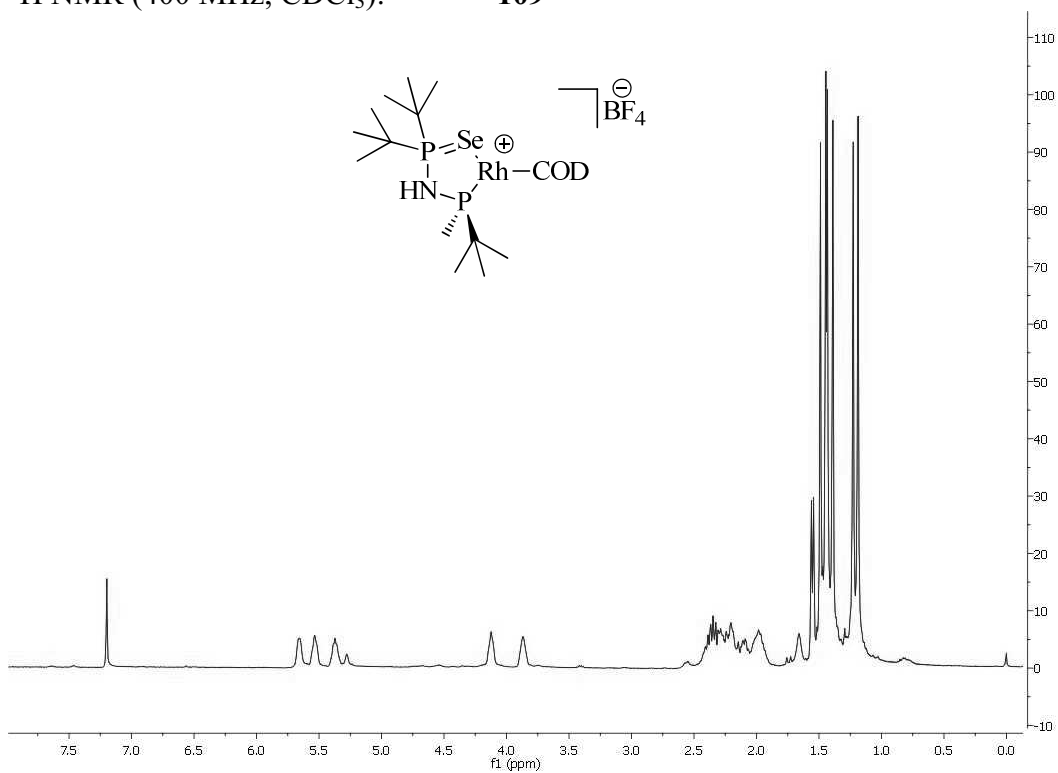


^{13}C NMR (400 MHz, CDCl_3):

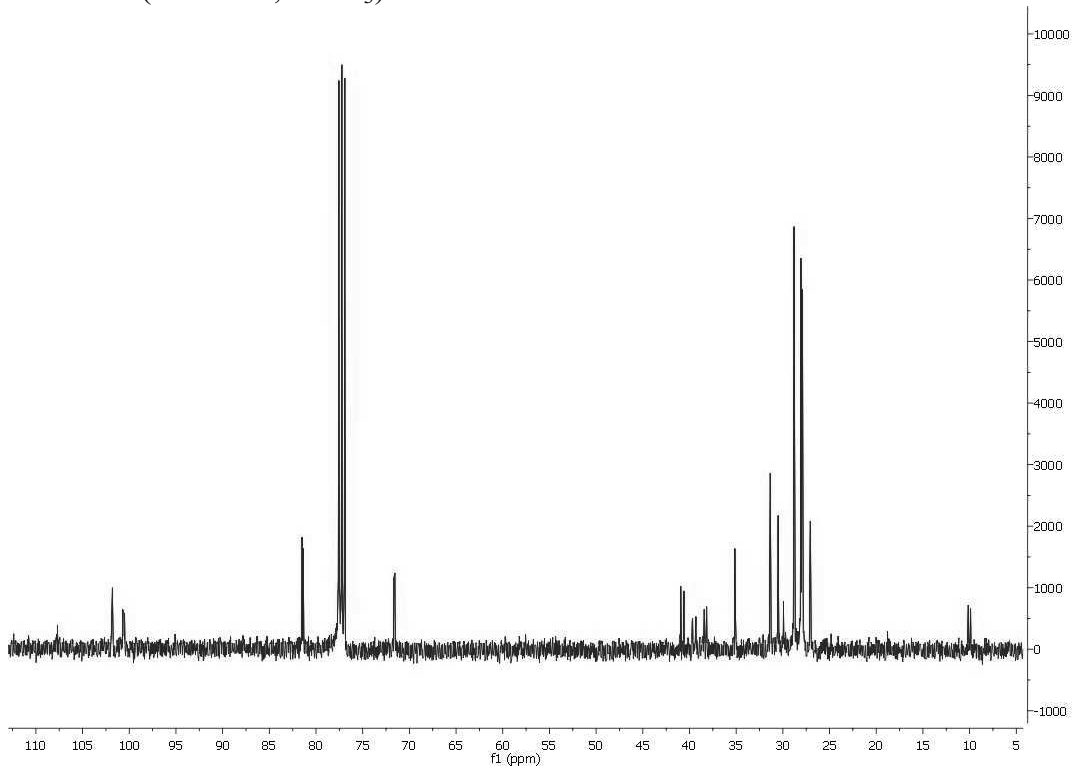


8. Spectra

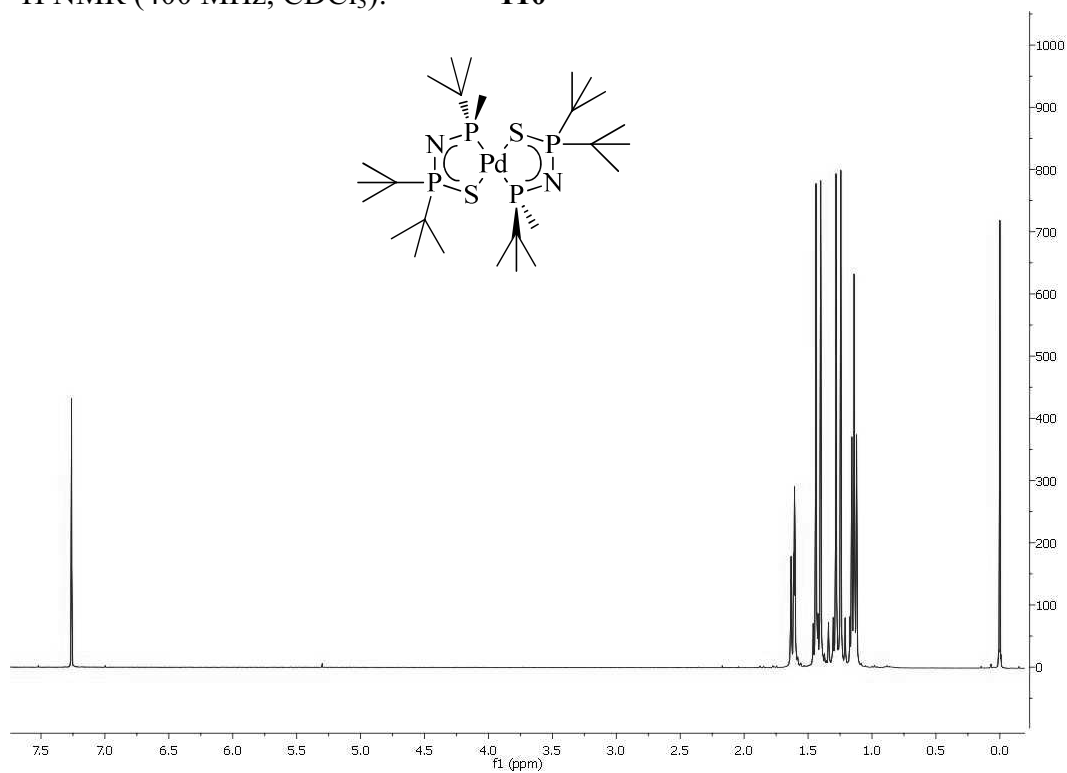
^1H NMR (400 MHz, CDCl_3): **109**



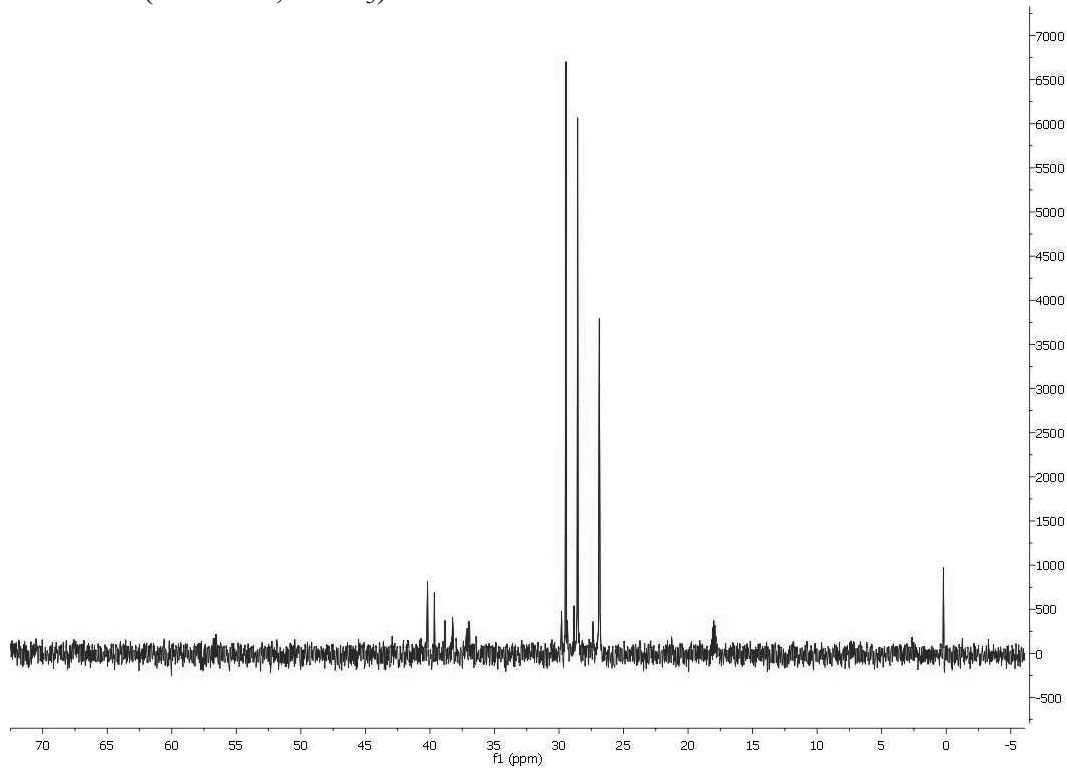
^{13}C NMR (400 MHz, CDCl_3):



^1H NMR (400 MHz, CDCl_3): **110**

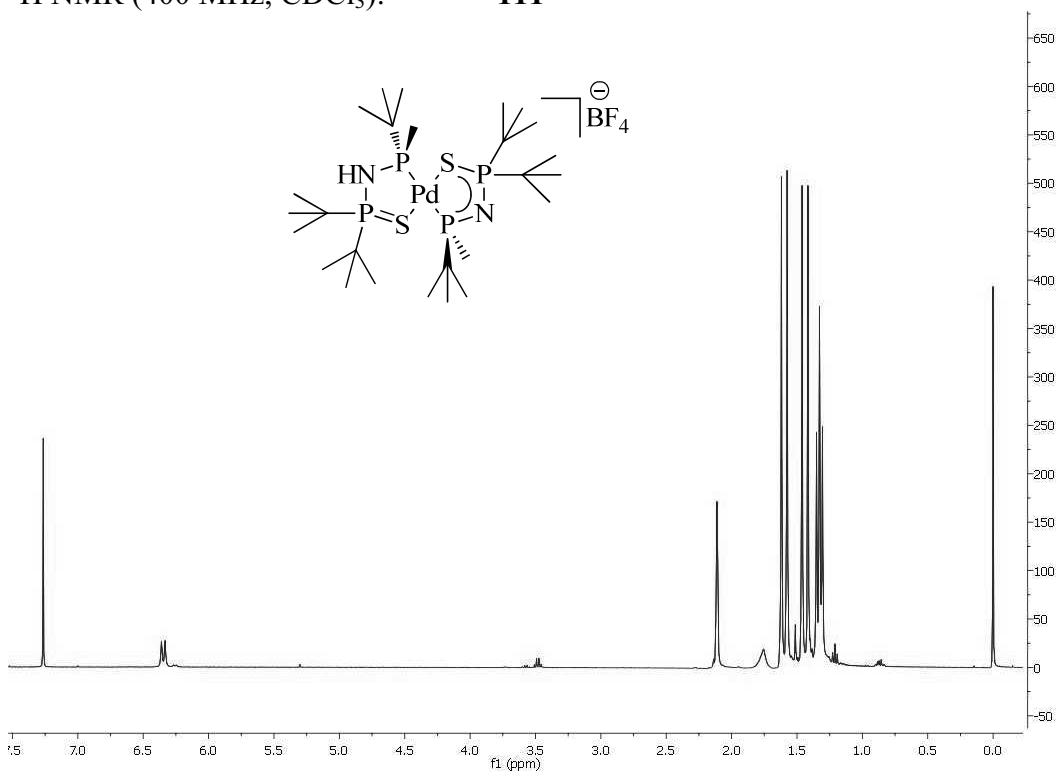


^{13}C NMR (400 MHz, CDCl_3):

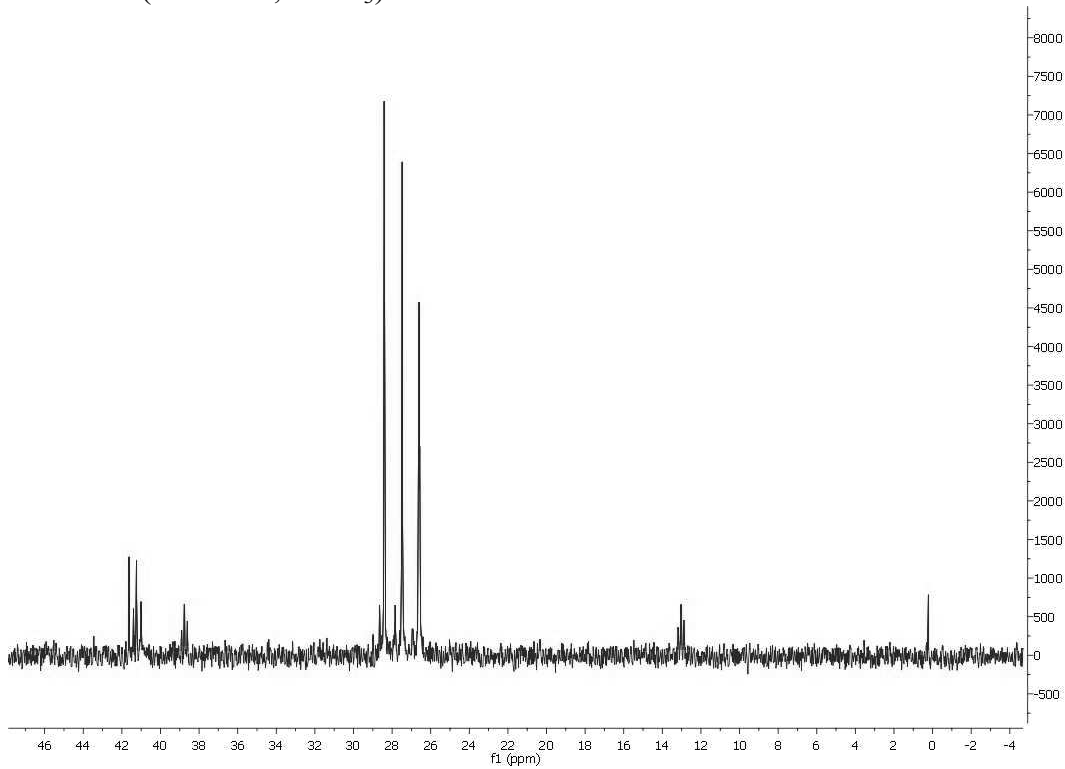


8. Spectra

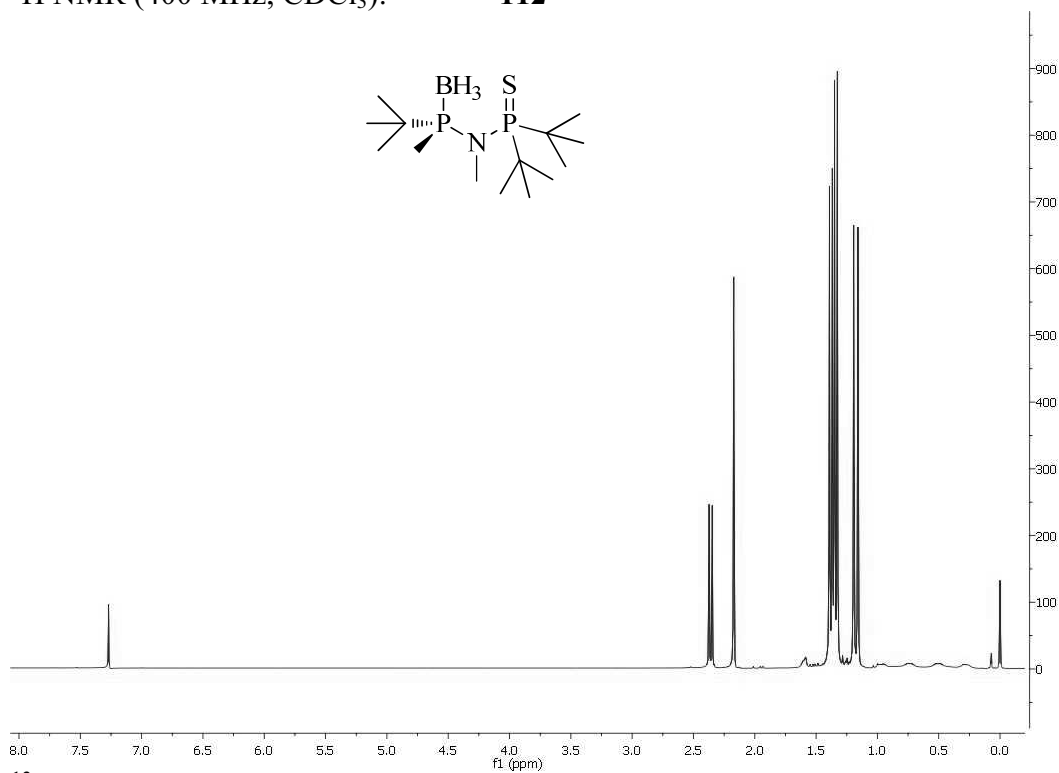
^1H NMR (400 MHz, CDCl_3): **111**



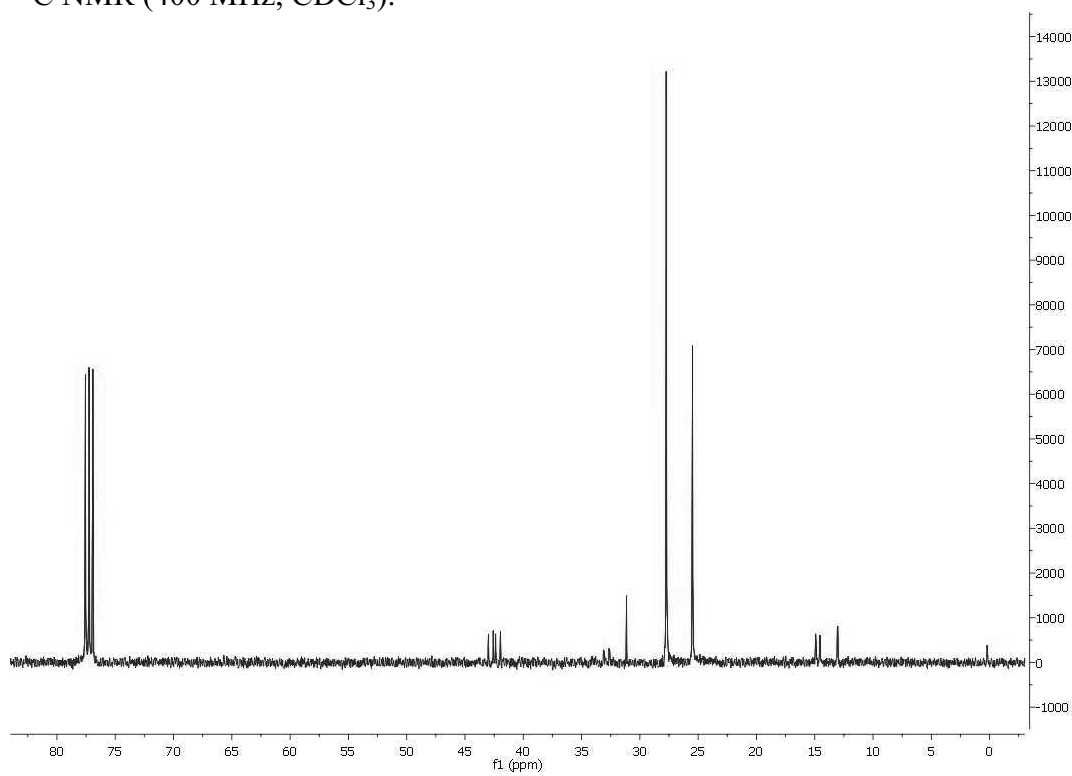
^{13}C NMR (400 MHz, CDCl_3):



^1H NMR (400 MHz, CDCl_3): **112**



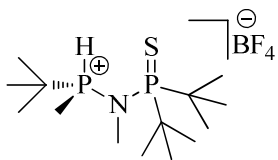
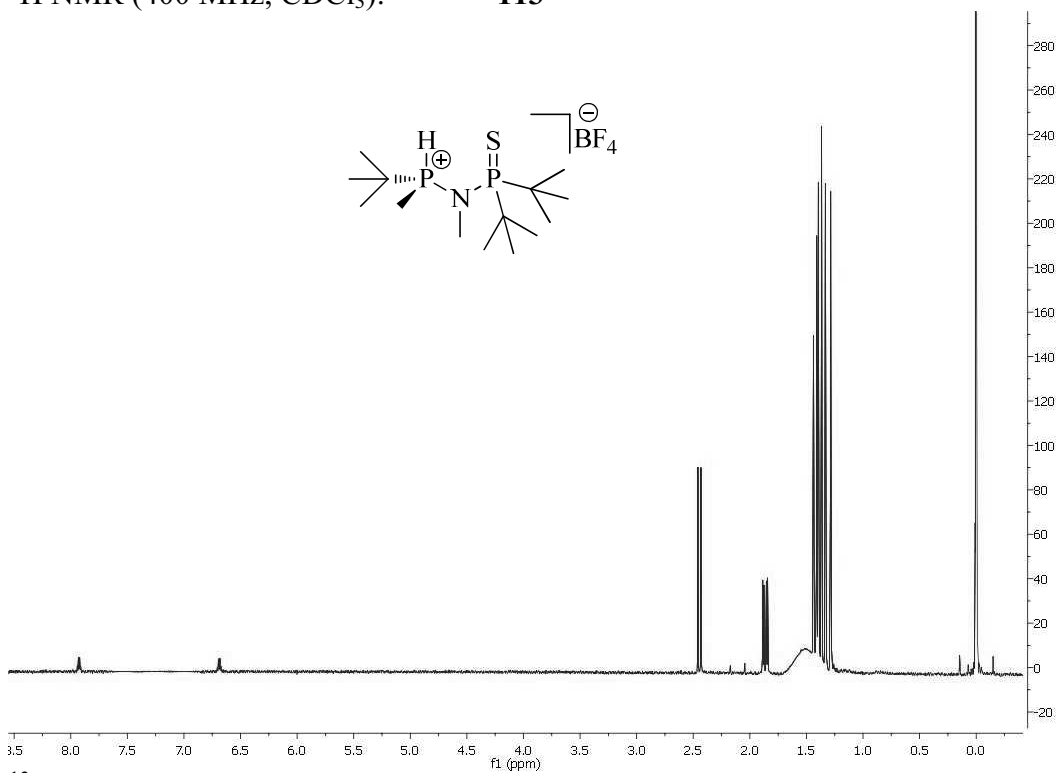
^{13}C NMR (400 MHz, CDCl_3):



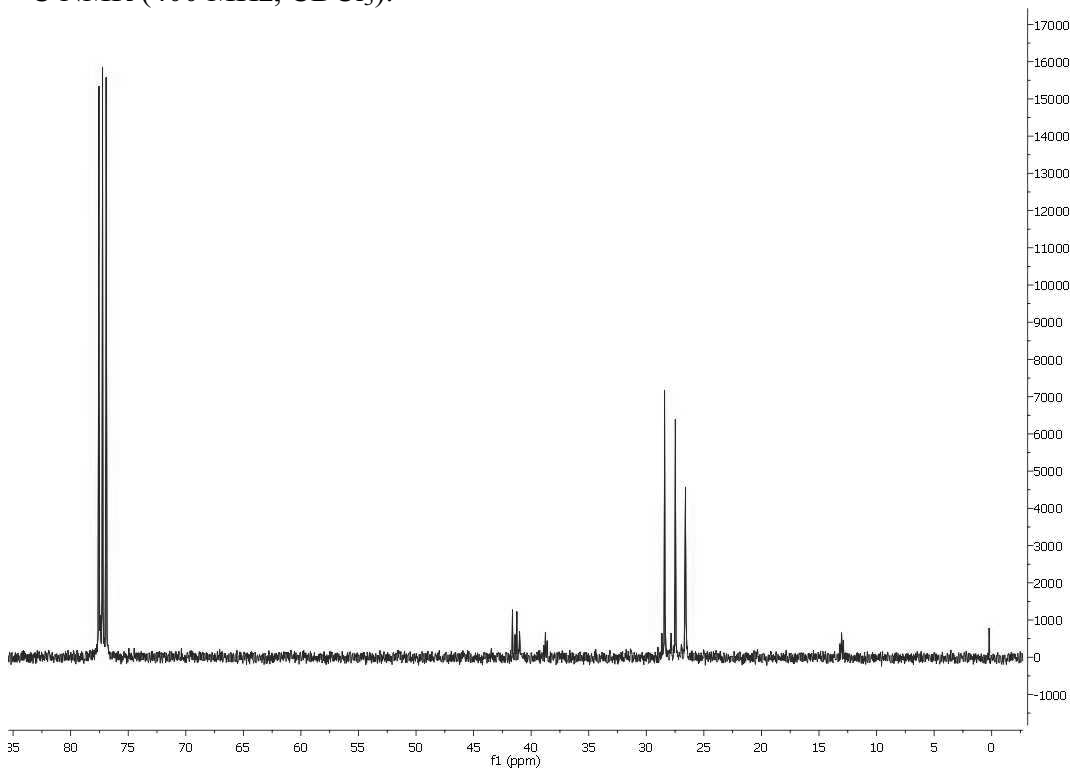
8. Spectra

^1H NMR (400 MHz, CDCl_3):

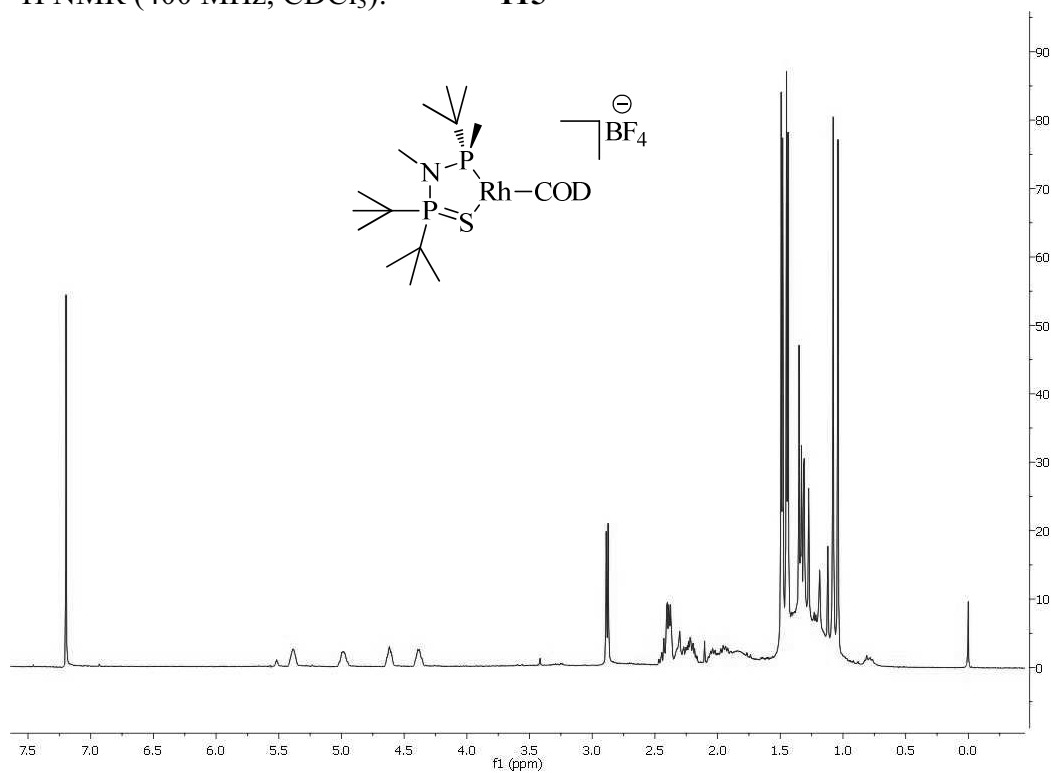
113



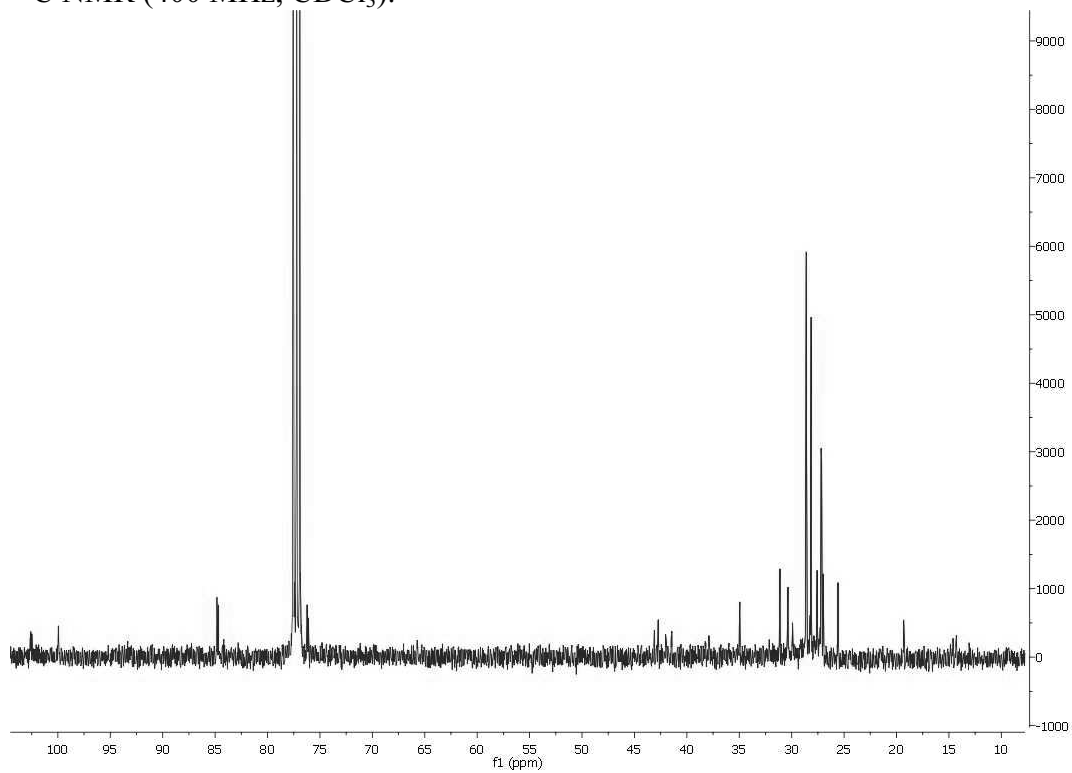
^{13}C NMR (400 MHz, CDCl_3):



^1H NMR (400 MHz, CDCl_3): **115**

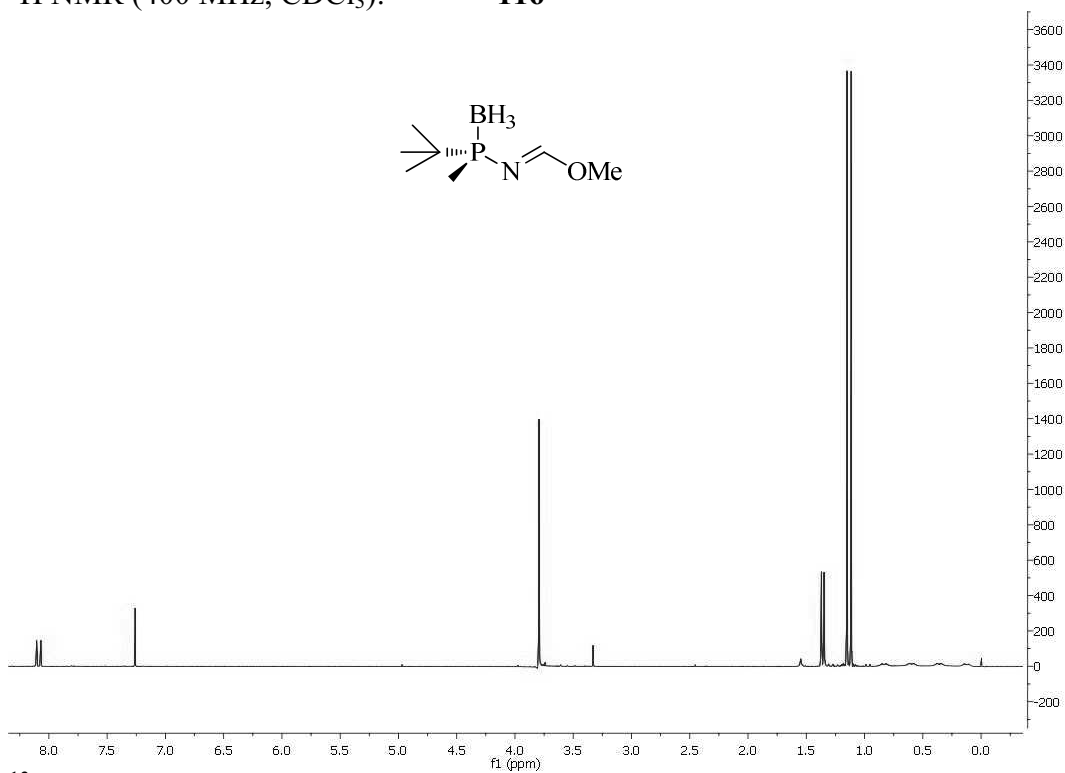


^{13}C NMR (400 MHz, CDCl_3):

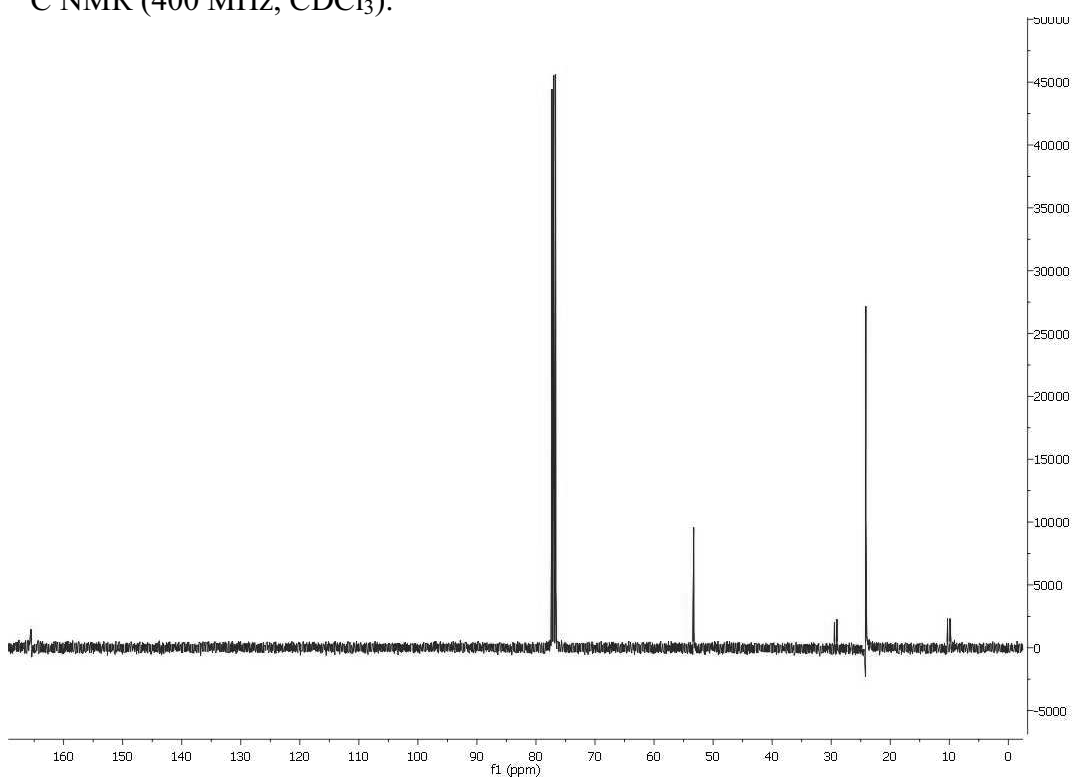


8. Spectra

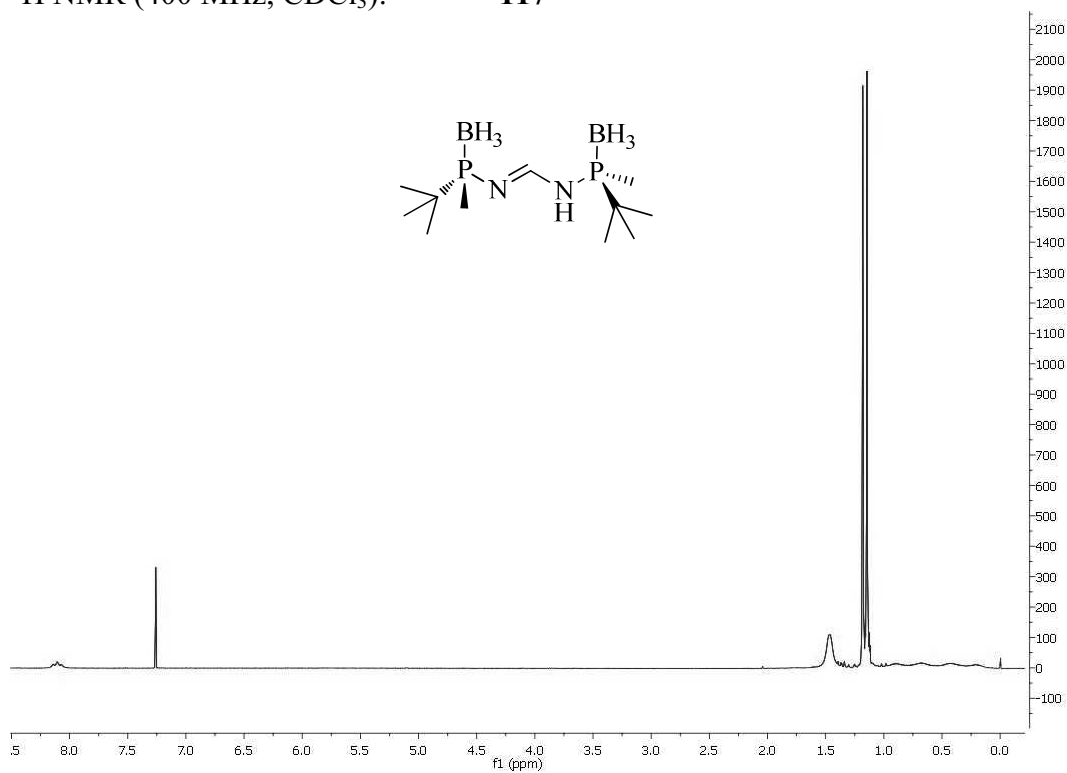
^1H NMR (400 MHz, CDCl_3): **116**



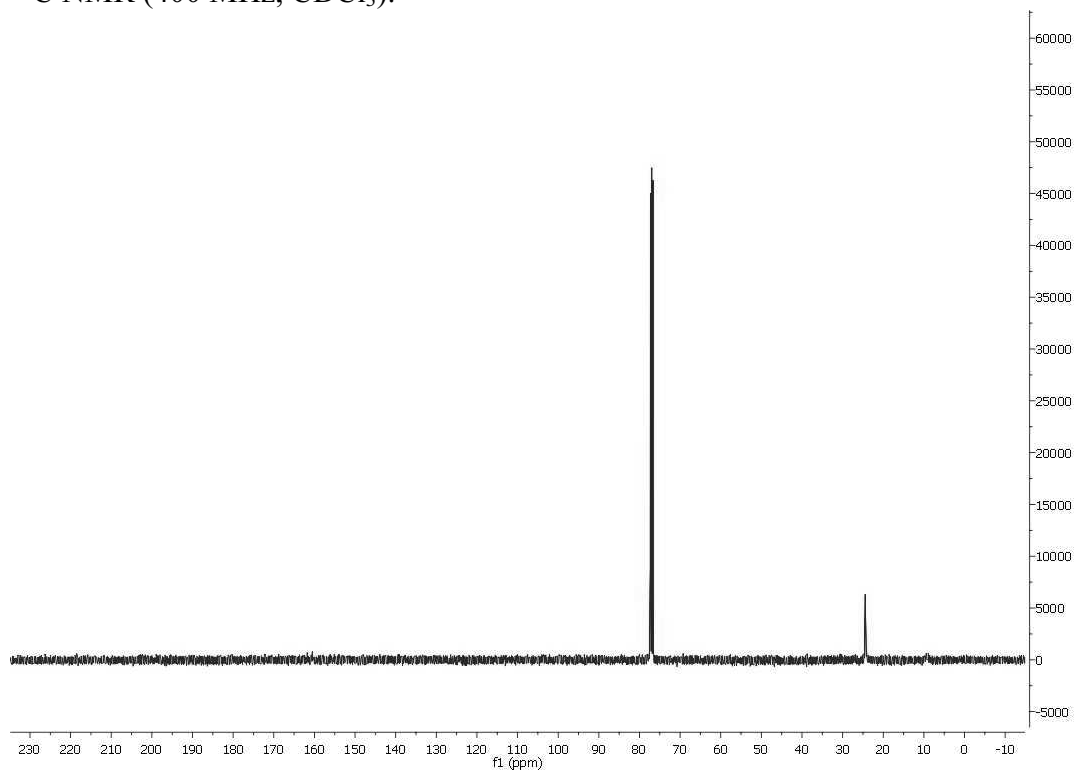
^{13}C NMR (400 MHz, CDCl_3):



^1H NMR (400 MHz, CDCl_3): **117**

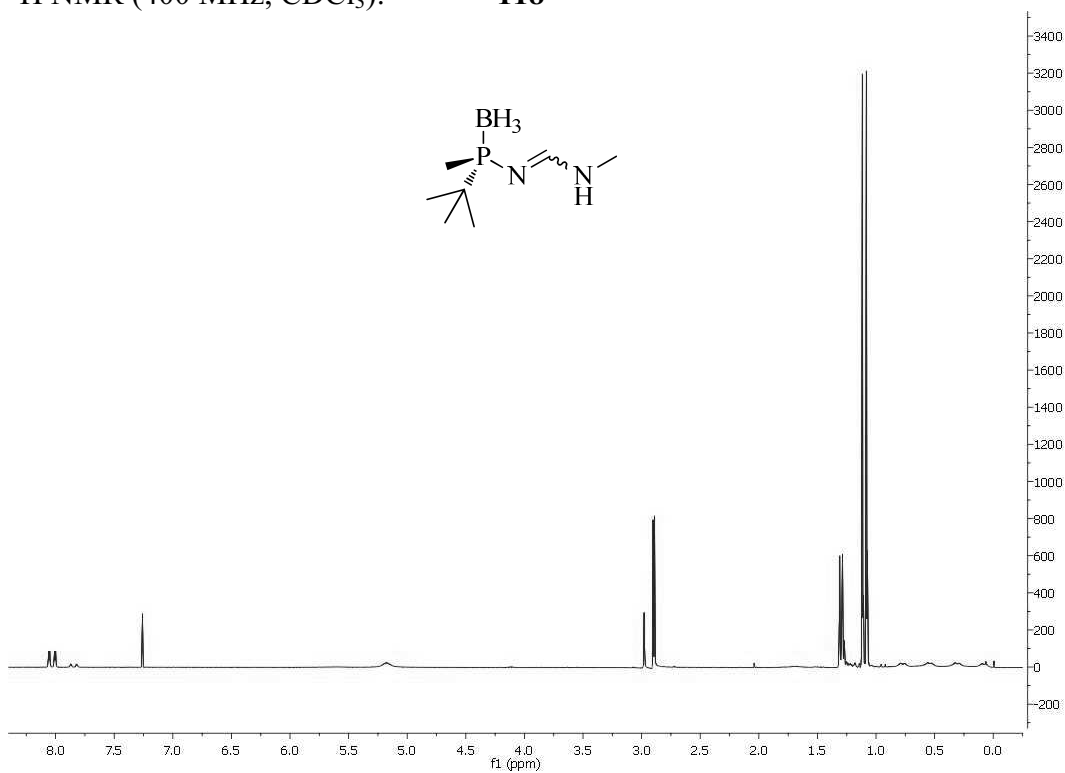


^{13}C NMR (400 MHz, CDCl_3):

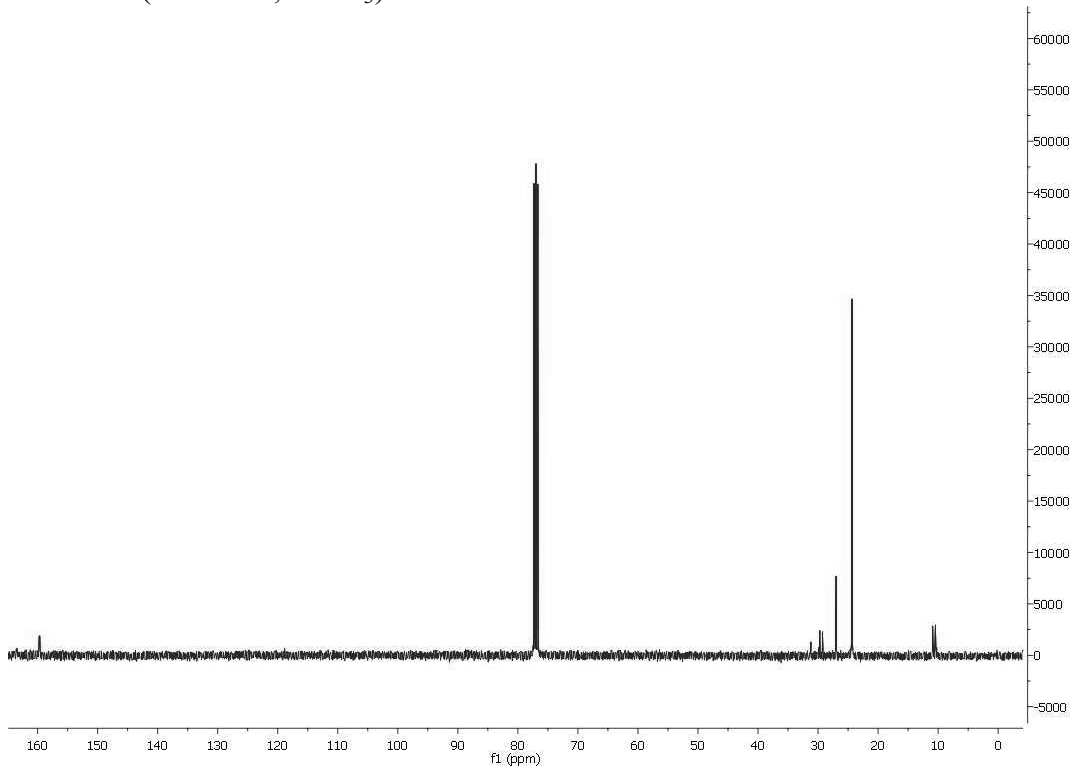


8. Spectra

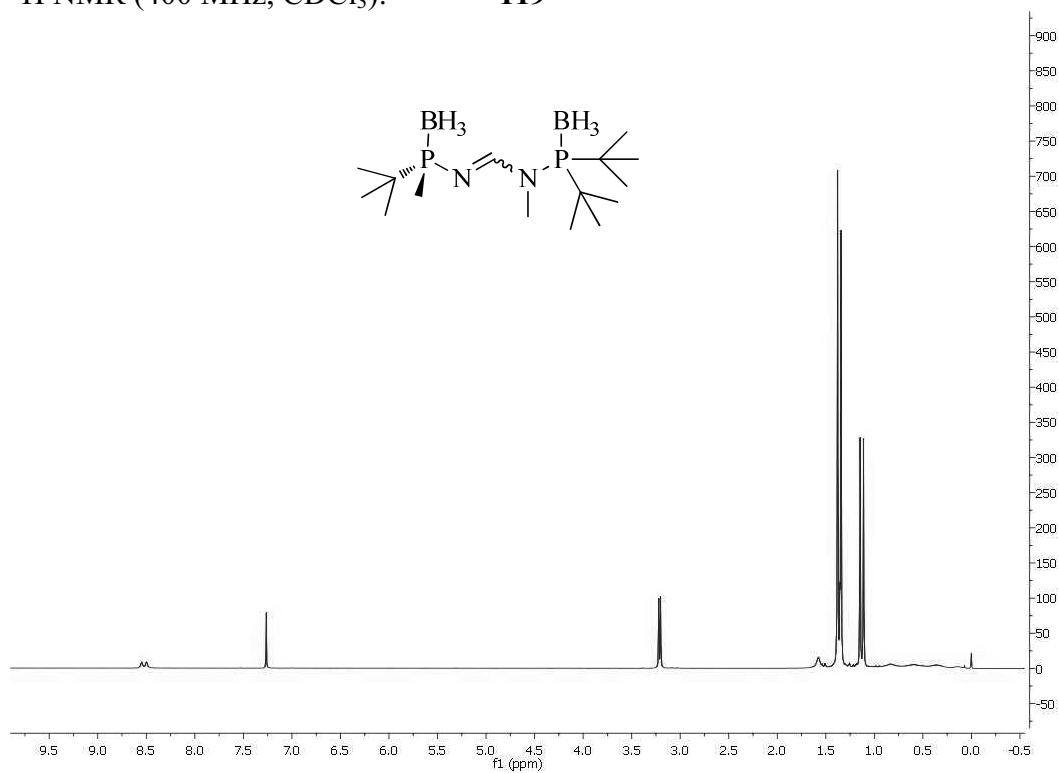
^1H NMR (400 MHz, CDCl_3): **118**



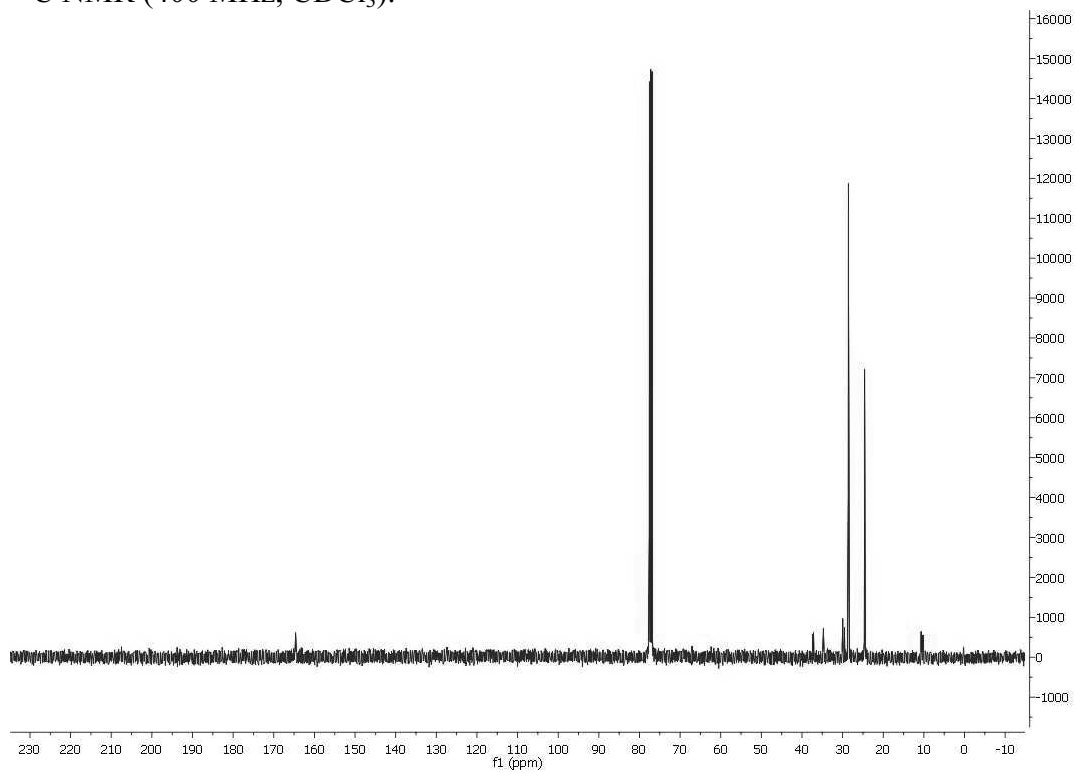
^{13}C NMR (400 MHz, CDCl_3):



^1H NMR (400 MHz, CDCl_3): **119**



^{13}C NMR (400 MHz, CDCl_3):



Appendix I:
X-ray diffraction data

9

Figure 1: Crystal data and structure refinement for **74-S**.

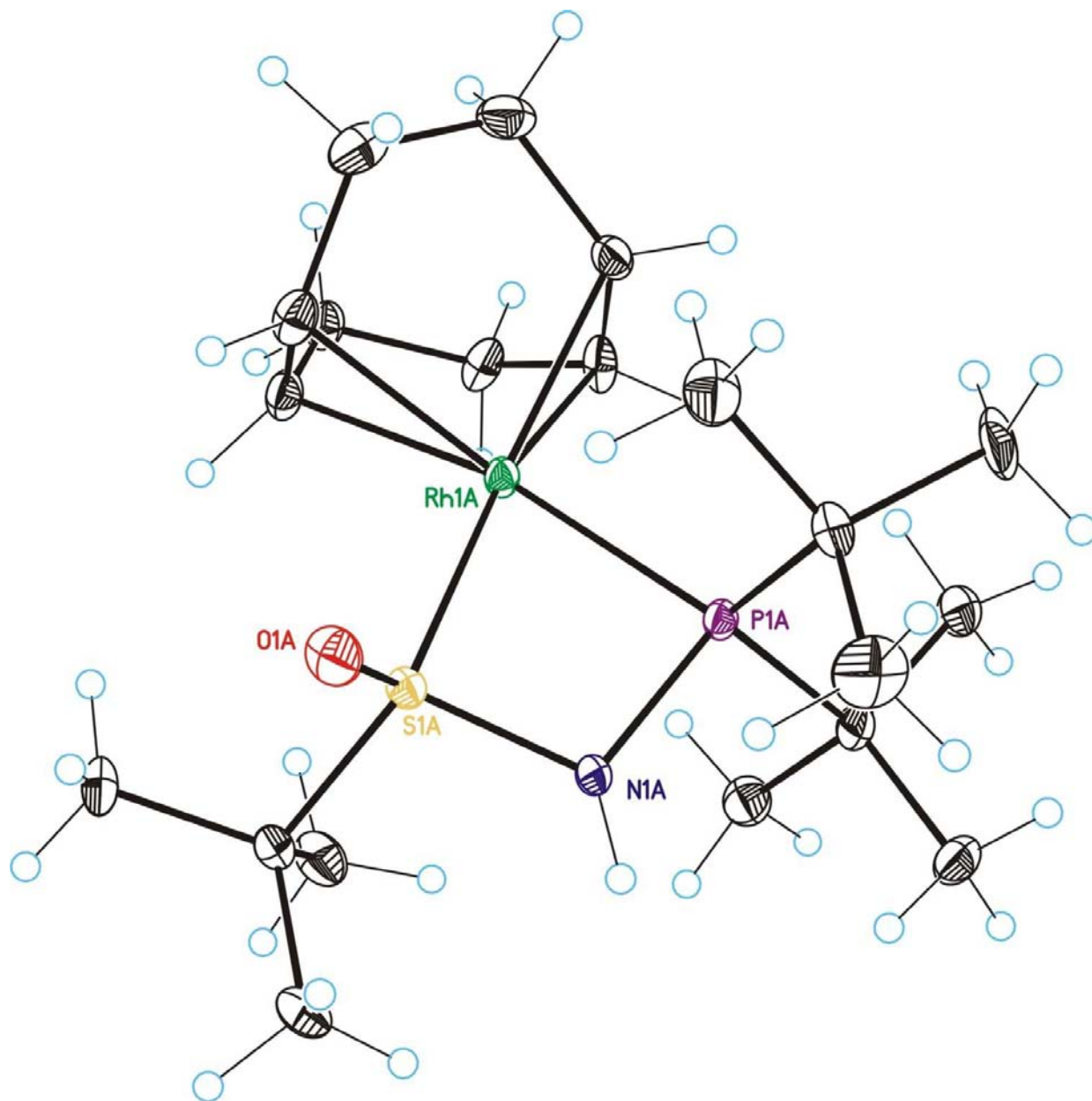


Table 1: Crystal data and structure refinement for **74-S**.

Identification code	74-S	
Empirical formula	C ₂₀ H ₄₀ B ₄ F ₄ N O P Rh S	
Formula weight	563.28	
Temperature	100(2) K	
Wavelength	0.71073 Å	
Crystal system	Triclinic	
Space group	P1	
Unit cell dimensions	a = 9.8358(5) Å	= 85.202(2) °.
	b = 10.2704(5) Å	= 70.937(3) °.
	c = 12.8909(6) Å	= 84.064(2) °.
Volume	1222.47(10) Å ³	
Z	2	
Density (calculated)	1.530 Mg/m ³	
Absorption coefficient	0.892 mm ⁻¹	
F(000)	584	
Crystal size	0.30 x 0.10 x 0.10 mm ³	
Theta range for data collection	1.67 to 33.23 °.	
Index ranges	-15 ≤ h ≤ 15 , -15 ≤ k ≤ 15 , -19 ≤ l ≤ 19	
Reflections collected	12439	
Independent reflections	11265 [R(int) = 0.0399]	
Completeness to theta = 33.23 °	0.912 %	
Absorption correction	Empirical	
Max. and min. transmission	0.9161 and 0.7757	
Refinement method	Full-matrix least-squares on F ²	
Data / restraints / parameters	12439 / 3 / 559	
Goodness-of-fit on F ²	1.050	
Final R indices [I > 2σ(I)]	R1 = 0.0538 , wR2 = 0.1379	
R indices (all data)	R1 = 0.0607 , wR2 = 0.1426	
Absolute Structure Flack parameter	x = 0.00(
Largest diff. peak and hole	4.714 and -0.969 e.Å ⁻³	

Figure 2: Crystal data and structure refinement for **90**.

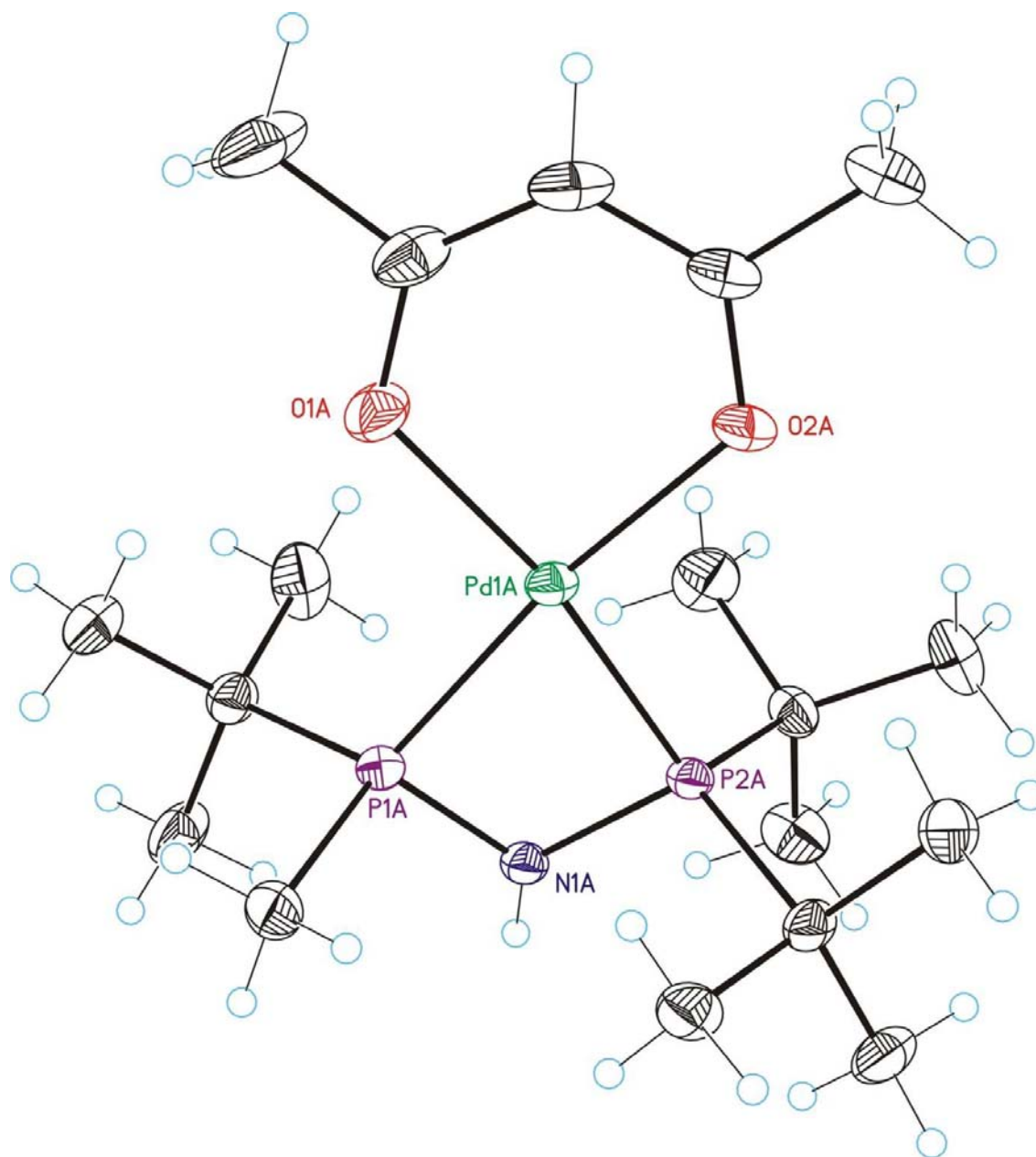


Table 2: Crystal data and structure refinement for **90**.

Identification code	90	
Empirical formula	C ₁₈ H ₃₈ B F ₄ N O ₂ P ₂ Pd	
Formula weight	555.64	
Temperature	100(2)K	
Wavelength	0.71073 Å	
Crystal system	Monoclinic	
Space group	P2(1)	
Unit cell dimensions	a = 8.2540(8) Å	a = 90.00 °.
	b = 23.726(2) Å	b = 107.584(2) °.
	c = 13.4822(12) Å	g = 90.00 °.
Volume	2516.9(4) Å ³	
Z	4	
Density (calculated)	1.466 Mg/m ³	
Absorption coefficient	0.907 mm ⁻¹	
F(000)	1144	
Crystal size	0.20 x 0.20 x 0.20 mm ³	
Theta range for data collection	1.58 to 29.98 °.	
Index ranges	-11 ≤ h ≤ 11, -31 ≤ k ≤ 33, -18 ≤ l ≤ 18	
Reflections collected	26406	
Independent reflections	12370 [R(int) = 0.0230]	
Completeness to theta = 29.98 °	0.902 %	
Absorption correction	Empirical	
Max. and min. transmission	0.8394 and 0.8394	
Refinement method	Full-matrix least-squares on F ²	
Data / restraints / parameters	12370 / 405 / 671	
Goodness-of-fit on F ²	1.054	
Final R indices [I > 2σ(I)]	R ₁ = 0.0225, wR ₂ = 0.0582	
R indices (all data)	R ₁ = 0.0230, wR ₂ = 0.0588	
Flack parameter	x = -0.015(12)	
Largest diff. peak and hole	0.880 and -0.607 e.Å ⁻³	

Figure 3: Crystal data and structure refinement for **96**.

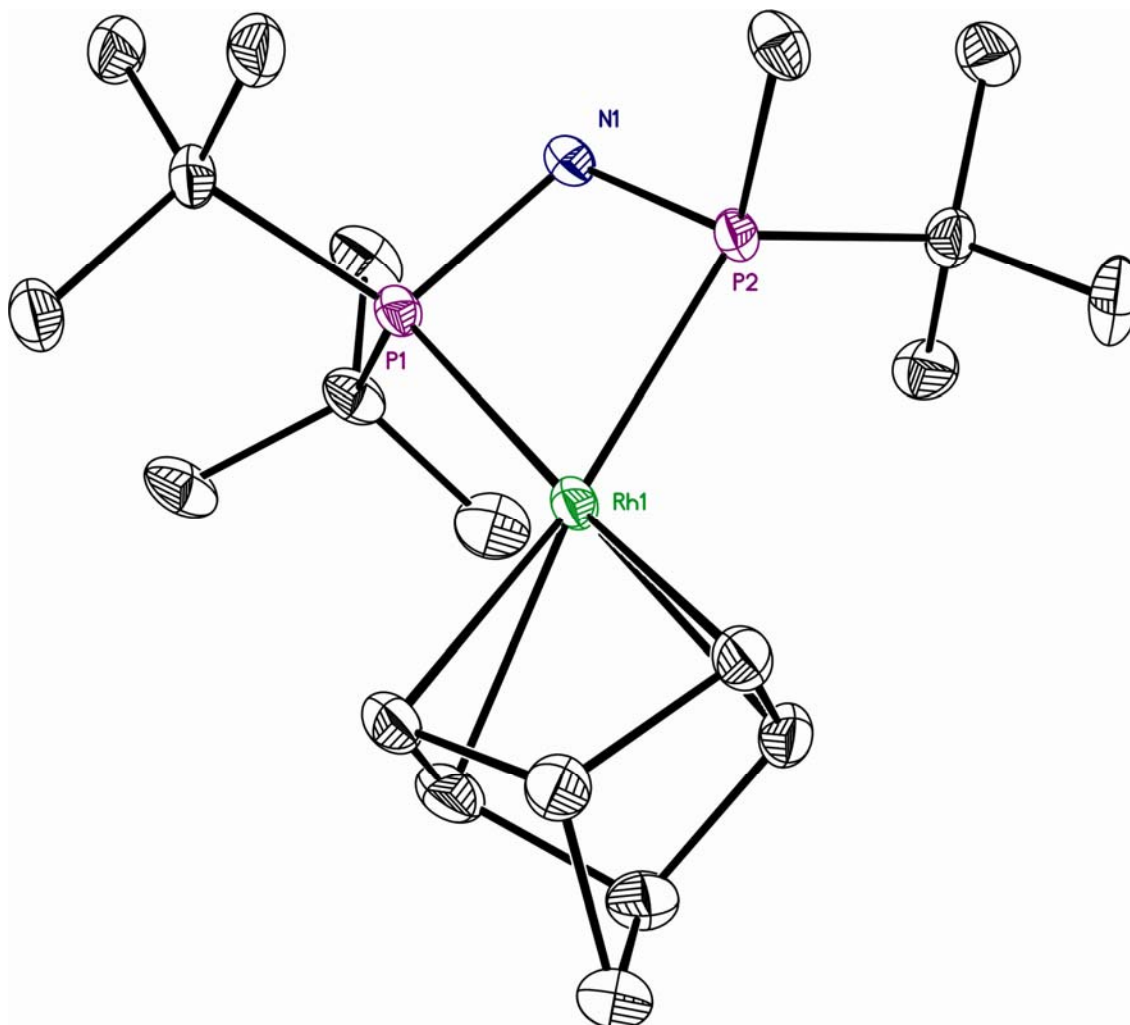


Table 3: Crystal data and structure refinement for **96**.

Identification code	96	
Empirical formula	C ₂₀ H ₃₉ B F ₄ N P ₂ Rh	
Formula weight	545.18	
Temperature	100(2)K	
Wavelength	0.71073 Å	
Crystal system	Orthorhombic	
Space group	P2(1)2(1)2(1)	
Unit cell dimensions	a = 10.4917(4) Å	a = 90.00 °.
	b = 15.2866(5) Å	b = 90.00 °.
	c = 15.4985(6) Å	g = 90.00 °.
Volume	2485.69(16) Å ³	
Z	4	
Density (calculated)	1.457 Mg/m ³	
Absorption coefficient	0.852 mm ⁻¹	
F(000)	1128	
Crystal size	0.40 x 0.40 x 0.30 mm ³	
Theta range for data collection	1.87 to 33.15 °.	
Index ranges	-12 ≤ h ≤ 15, -20 ≤ k ≤ 23, -23 ≤ l ≤ 10	
Reflections collected	19990	
Independent reflections	9211 [R(int) = 0.0714]	
Completeness to theta = 33.15 °	0.969 %	
Absorption correction	Empirical	
Max. and min. transmission	0.7841 and 0.7268	
Refinement method	Full-matrix least-squares on F ²	
Data / restraints / parameters	9211 / 0 / 272	
Goodness-of-fit on F ²	1.009	
Final R indices [I > 2σ(I)]	R1 = 0.0432, wR2 = 0.1006	
R indices (all data)	R1 = 0.0485, wR2 = 0.1031	
Flack parameter	x = -0.02(2)	
Largest diff. peak and hole	0.883 and -1.671 e.Å ⁻³	

Figure 4: Crystal data and structure refinement for **108**.

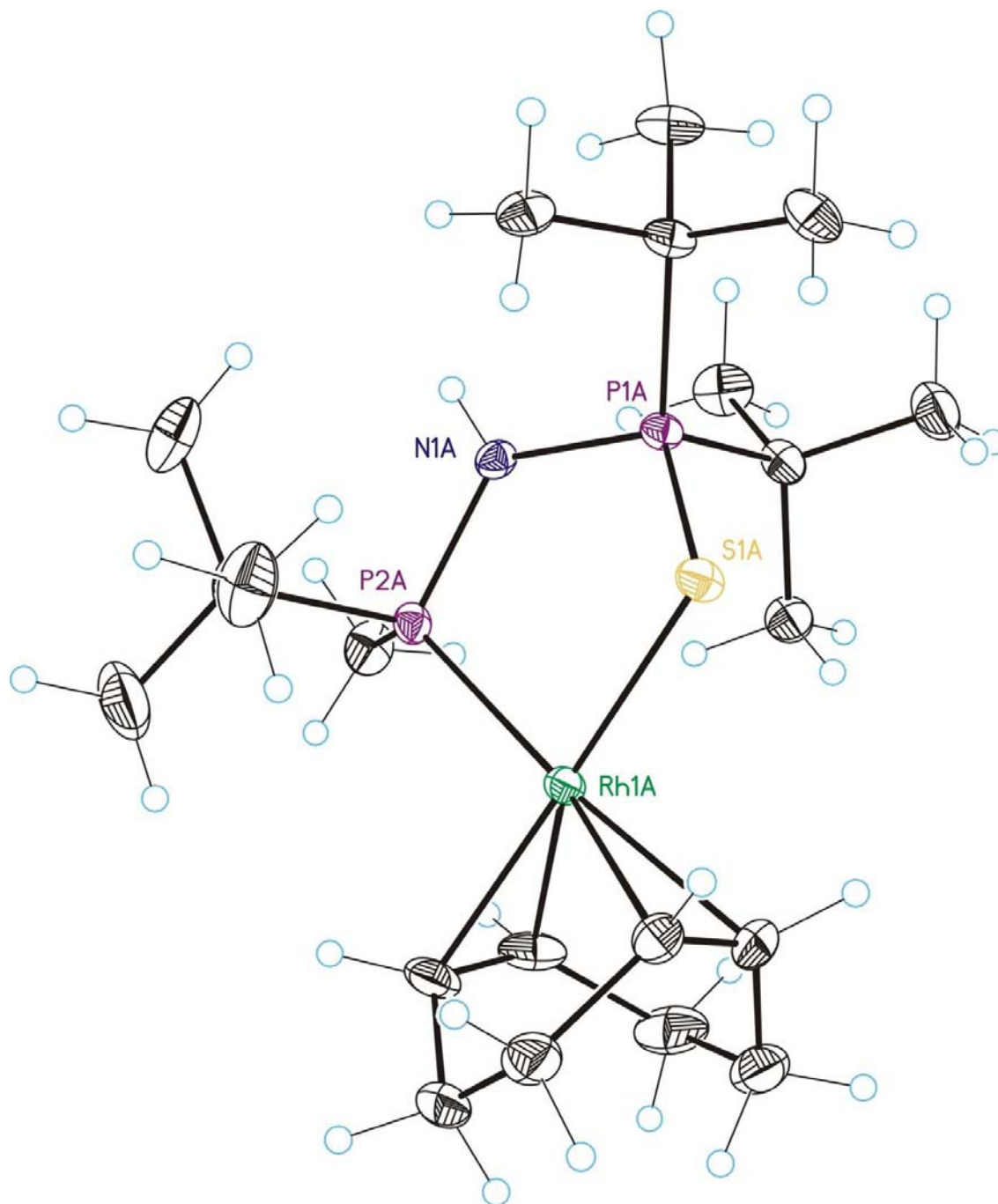


Table 4: Crystal data and structure refinement for **108**.

Identification code	108
Empirical formula	C ₂₁ H ₄₃ B F ₄ N P ₂ Rh S
Formula weight	593.28
Temperature	100(2) K
Wavelength	0.71073 Å
Crystal system	Orthorhombic
Space group	P2(1)2(1)2(1)
Unit cell dimensions	a = 10.0539(7) Å a = 90.00 °. b = 20.9220(14) Å b = 90.00 °. c = 24.9649(17) Å g = 90.00 °.
Volume	5251.3(6) Å ³
Z	8
Density (calculated)	1.501 Mg/m ³
Absorption coefficient	0.890 mm ⁻¹
F(000)	2464
Crystal size	0.30 x 0.20 x 0.20 mm ³
Theta range for data collection	1.27 to 28.89 °.
Index ranges	-13 ≤ h ≤ 13, -27 ≤ k ≤ 28, -32 ≤ l ≤ 33
Reflections collected	12827
Independent reflections	11867 [R(int) = 0.0364]
Completeness to theta = 28.89 °	0.947 %
Absorption correction	Empirical
Max. and min. transmission	0.8942 and 0.7846
Refinement method	Full-matrix least-squares on F ²
Data / restraints / parameters	12827 / 0 / 579
Goodness-of-fit on F ²	1.098
Final R indices [I > 2σ(I)]	R1 = 0.0268, wR2 = 0.0552
R indices (all data)	R1 = 0.0311, wR2 = 0.0652
Absolute Structure Flack parameter	x = -0.023(15)
Largest diff. peak and hole	0.773 and -0.349 e.Å ⁻³

Figure 5: Crystal data and structure refinement for **111**.

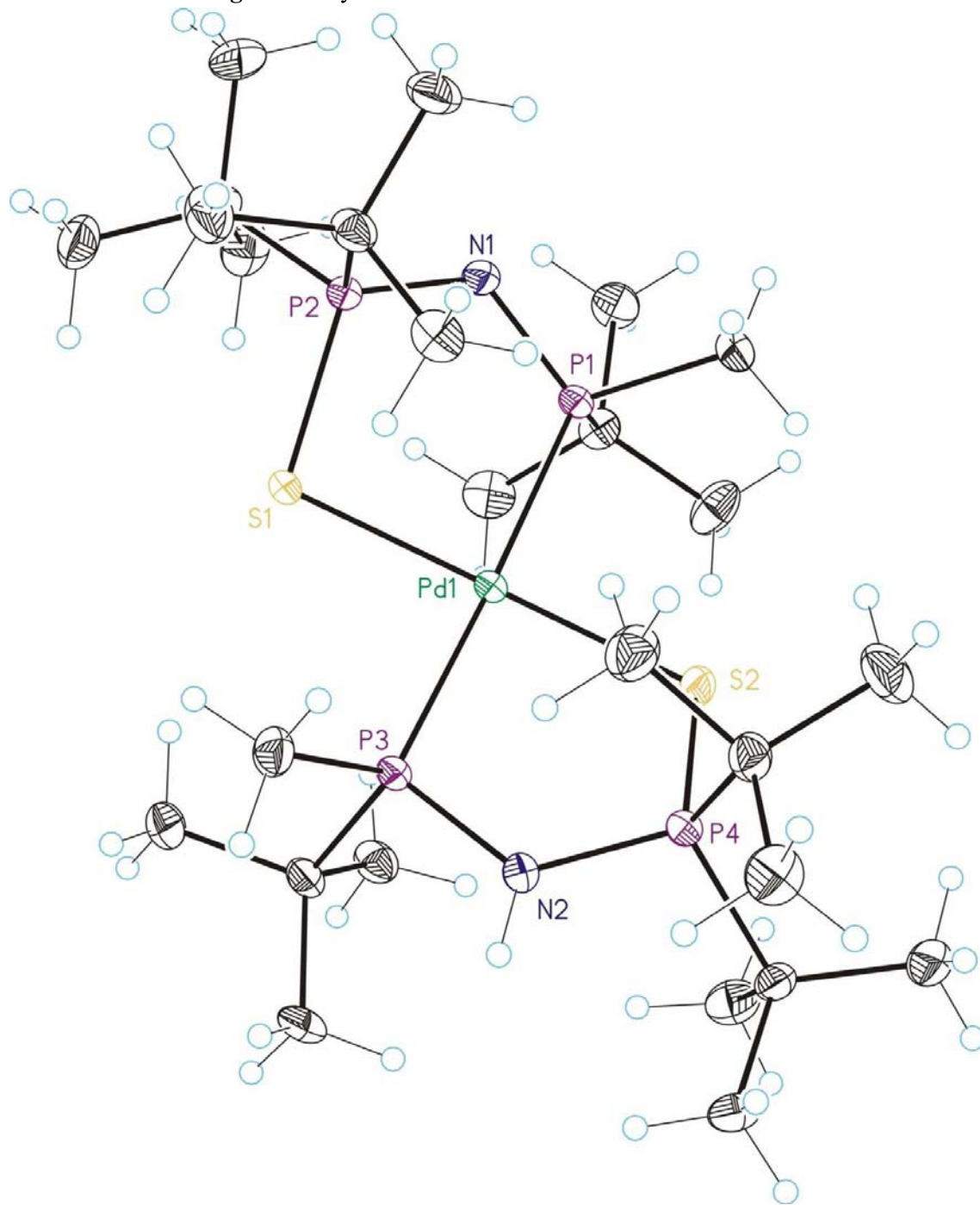
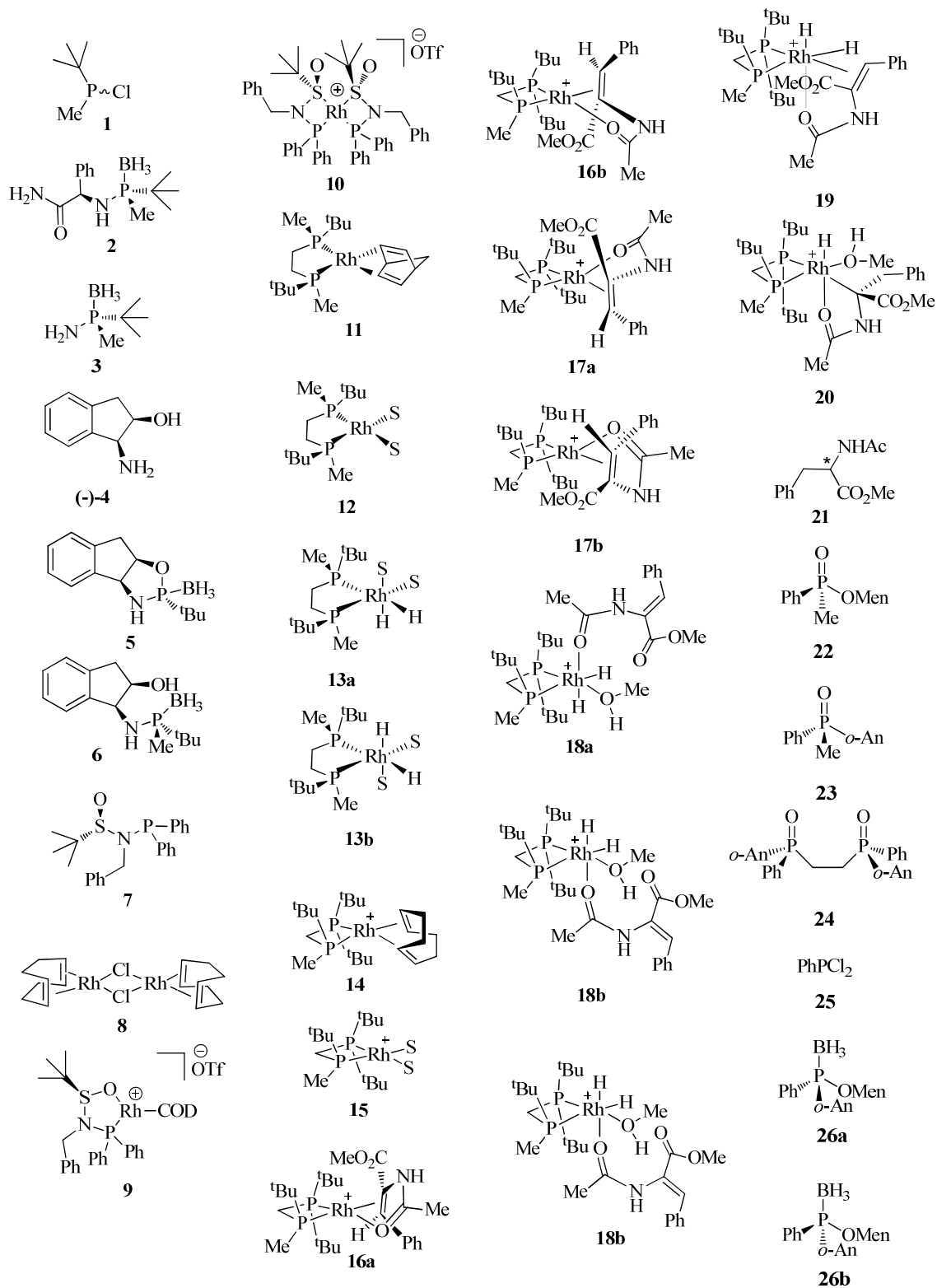


Table 5: Crystal data and structure refinement for **111**.

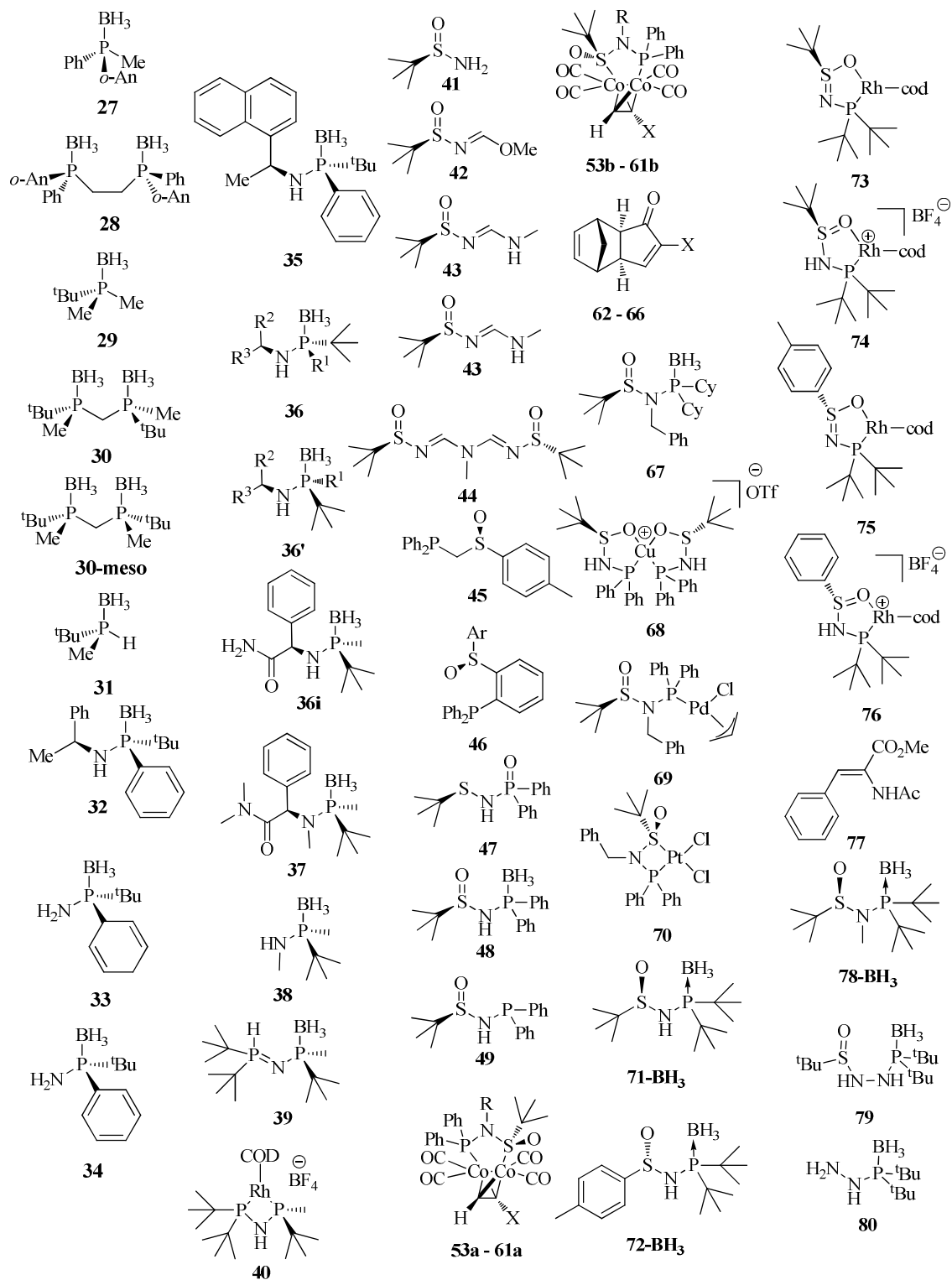
Identification code	111
Empirical formula	C ₂₇ H ₆₃ B Cl ₂ F ₄ N ₂ P ₄ Pd S ₂
Formula weight	867.90
Temperature	100(2) K
Wavelength	0.71073 Å
Crystal system	Orthorhombic
Space group	P2(1)2(1)2(1)
Unit cell dimensions	a = 10.7736(8) Å a = 90.00 °. b = 17.6502(13) Å b = 90.00 °. c = 21.3183(15) Å g = 90.00 °.
Volume	4053.8(5) Å ³
Z	4
Density (calculated)	1.422 Mg/m ³
Absorption coefficient	0.890 mm ⁻¹
F(000)	1808
Crystal size	0.2 x 0.2 x 0.2 mm ³
Theta range for data collection	1.50 to 29.78 °.
Index ranges	0 ≤ h ≤ 14, 0 ≤ k ≤ 24, 0 ≤ l ≤ 29
Reflections collected	101129
Independent reflections	6229 [R(int) = 0.0485]
Completeness to theta = 29.78 °	0.975 %
Absorption correction	Empirical
Max. and min. transmission	0.8533 and 0.7781
Refinement method	Full-matrix least-squares on F ²
Data / restraints / parameters	6229 / 78 / 446
Goodness-of-fit on F ²	1.055
Final R indices [I > 2σ(I)]	R1 = 0.0294, wR2 = 0.0649
R indices (all data)	R1 = 0.0363, wR2 = 0.0667
Absolute Structure Flack parameter	x = 0.41(2)
Largest diff. peak and hole	0.854 and -0.619 e.Å ⁻³

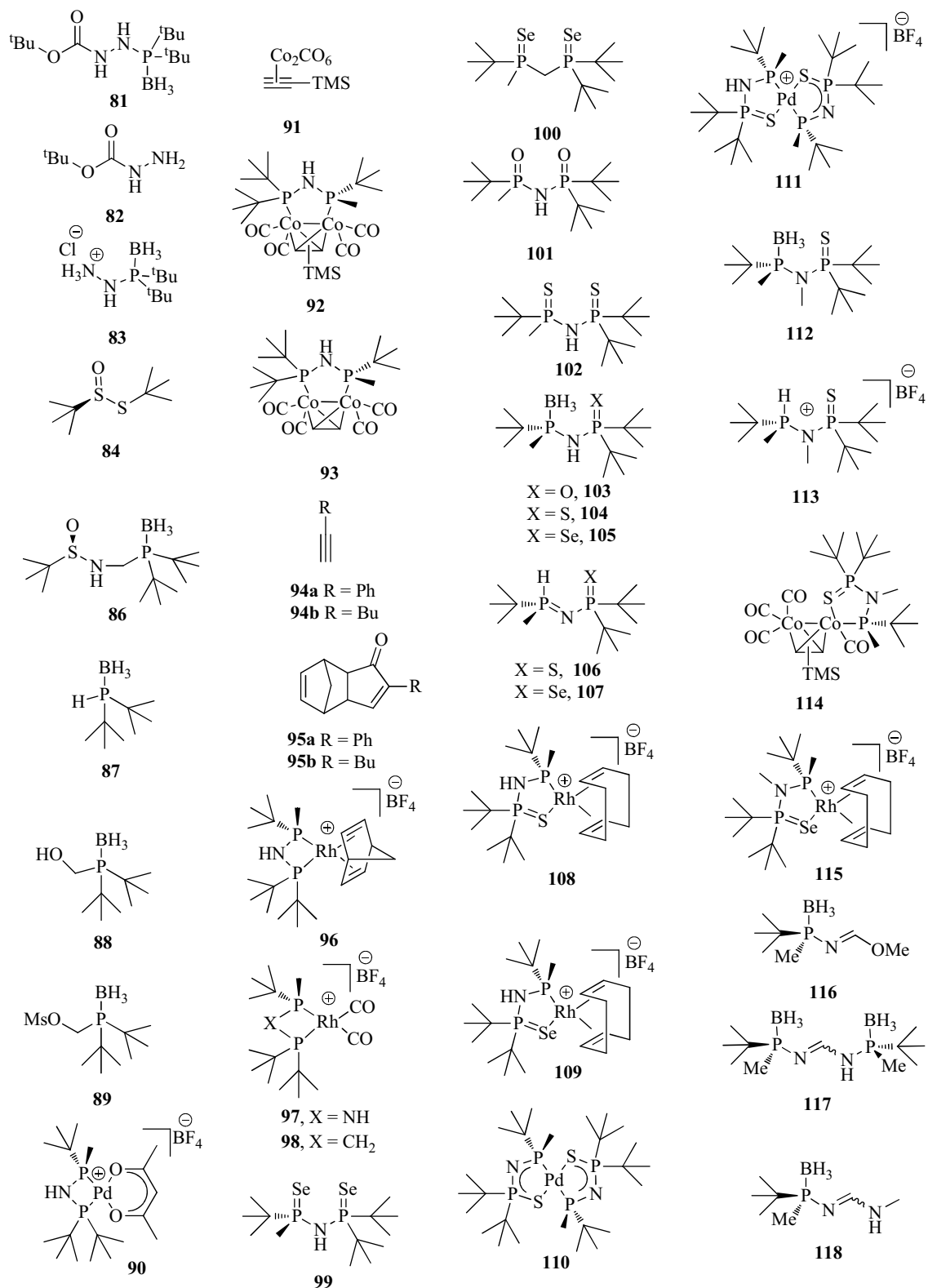
Appendix II:
Index of Structures

10

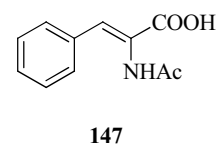
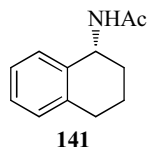
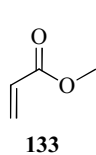
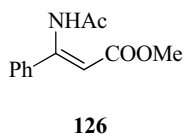
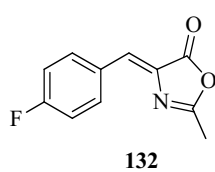
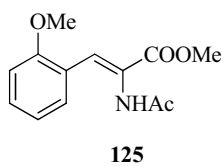
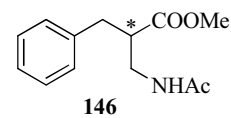
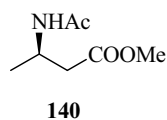
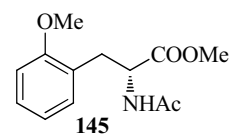
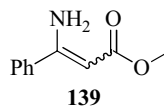
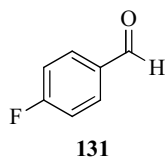
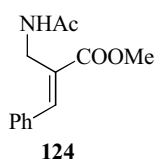
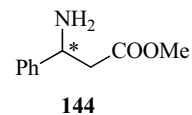
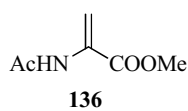
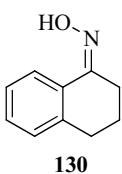
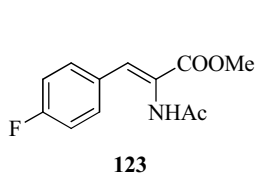
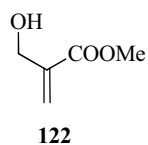
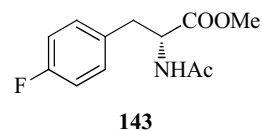
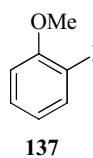
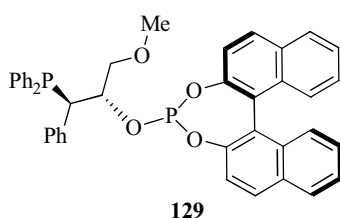
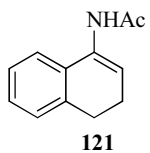
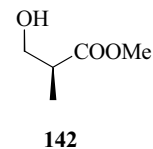
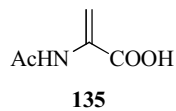
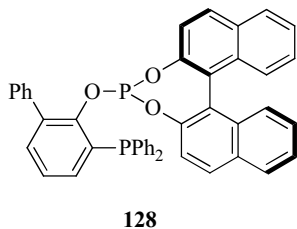
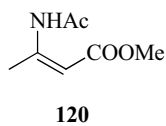
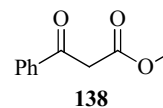
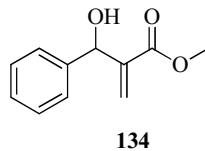
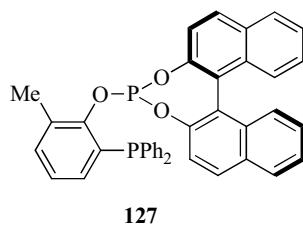
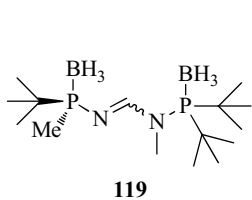


10. Appendix II: Index of Structures





10. Appendix II: Index of Structures



**Appendix III:
Detailed Index**

11

1 Introduction.....	3
2 Background.....	13
2.1 Chiral Phosphorus and Asymmetric Hydrogenation.....	13
2.2 Asymmetric Hydrogenation.....	17
2.3 Strategies employed in the synthesis of chiral phosphorus.....	26
2.4 The development of MaxPHOS.....	36
2.5 The optimized route to MaxPHOS.....	41
2.6 <i>P, S</i> ligands with chirality on sulphur.....	44
3 <i>N</i> -Phosphino sulfinamide ligands.....	57
3.1 The <i>tert</i> -butyl and <i>p</i> -tolyl sulfinamide derived ligands.....	57
3.1.1 The synthesis and examination of the ligands and their complexes.....	58
3.1.2 Hydrogenations of Z-MAC catalysed by the PNSO-Rh complexes.....	63
3.2 Attempts towards the synthesis of PNSO analogues.....	66
3.2.1 The <i>N</i> -methyl PNSO ligand.....	67
3.2.2 The PNNSO ligand.....	69
3.2.3 The attempt to introduce a carbon atom into the PNSO scaffold.....	74
3.3 Conclusions.....	77
4 P-stereogenic phosphine ligands.....	81
4.1 New MaxPHOS complexes.....	81
4.1.1 Coordinating MaxPHOS to palladium, copper and nickel.....	82
4.1.2 Coordinating MaxPHOS to cobalt and rhodium.....	84
4.2 Examining the electronic nature of the MaxPHOS ligand.....	89
4.2.1 Examination of carbonyl stretching frequencies.....	89
4.2.2 Examination of $J(^{31}\text{P}-^{77}\text{Se})$ coupling frequencies.....	91
4.3 Derivatives of MaxPHOS-BH ₃ as ligands.....	94
4.3.1 The preparation of the mono-chalcogenated MaxPHOS derivatives.....	94
4.3.2 The mono-chalcogenated MaxPHOS derivative metal complexes.....	98
4.4 Towards the synthesis of C ₁ /C ₂ P*-stereogenic amidine ligands.....	107
4.5 Conclusions.....	110

5 MaxPHOS and asymmetric hydrogenation.....	115
5.1 Exploring the substrate scope of the MaxPHOS-Rh catalyst.....	115
5.1.1 The choice of substrates.....	115
5.1.2 The methodologies employed to prepare the new substrate set.....	118
5.1.3 Testing the MaxPHOS-Rh catalyst against the new substrate set	122
5.2 The application of the MaxPHOS-Rh catalyst in the asymmetric hydrogenation of the Z-MAC substrate.....	127
5.2.1 Hydrogenating Z-MAC with <i>in-situ</i> formation of the catalyst.....	128
5.2.2 Reduction of catalyst loading.....	131
5.2.3 The low enantiomeric excess dilemma.....	132
5.2.4 An insight into the speed of reaction and therefore the TOF of the MaxPHOS catalyst.....	134
5.3 Conclusions	137
6 Conclusions.....	141
7 Experimental	145
7.1 General methods.....	145
7.1.1 Instrumentation.....	145
7.1.2 Materials and techniques.....	146
7.2 Chapter 3 Experimental.....	148
(-)-(R)- <i>N</i> -(di- <i>tert</i> -butylphosphino)-2-methylpropane-2-sulfinamide borane, 71-BH₃	148
(+)-(<i>S</i>)- <i>N</i> -(di- <i>tert</i> -butylphosphino)-4-methylphenylsulfinamide borane, 72-BH₃	149
[[(+)-(R)-(tert-butylsulfinyl)(di- <i>tert</i> -butylphosphino)amide)Rh((1 <i>Z</i> ,5 <i>Z</i>)-cycloocta-1,5-diene)], 73	150
[[(+)-(R)- <i>N</i> -(di- <i>tert</i> -butylphosphino)-2-methylpropane-2-sulfinamide) Rh ((1 <i>Z</i> ,5 <i>Z</i>)-cycloocta-1,5-diene)] BF ₄ , 74	151
[[(<i>S</i>)-(di- <i>tert</i> -butylphosphino)(<i>p</i> -tolylsulfinyl)amide)Rh((1 <i>Z</i> ,5 <i>Z</i>)-cycloocta-1,5-diene)], 75	152
[[(<i>S</i>)- <i>N</i> -(di- <i>tert</i> -butylphosphino)-4-methylbenzenesulfinamide) Rh ((1 <i>Z</i> ,5 <i>Z</i>)-cycloocta-1,5-diene)]BF ₄ , 76	153
(di- <i>tert</i> -butyl (N,2-dimethylpropan-2-ylsulfinamido)phosphonio) trihydroborate, 78-BH₃	154

(di-tert-butyl(2-(tert-butylsulfinyl)hydrazinyl)phosphonio)trihydroborate, 79-BH₃	155
<i>tert</i> -butyl 2-(di-tert-butyl(borano)phosphino)hydrazinecarboxylate, 81	156
[<i>tert</i> -butyl 2-(di-tert-butylphosphino)hydrazinecarboxylate]BH ₃ , 83	157
(di-tert-butyl(hydroxymethyl) phosphonio)trihydroborate, 88	158
(di-tert-butyl(borano)phosphino)methyl methanesulfonate, 89	159
7.3 Chapter 4 experimental.....	160
[(MaxPHOS)Pd(acac)]BF ₄ , 90	160
[(MaxPHOS)Co ₂ (CO) ₄ (C ₅ H ₁₀ Si)], 92	161
[(MaxPHOS)Co ₂ (CO) ₄ (C ₂ H ₂)], 93	162
[(MaxPHOS)Rh(NBD)]BF ₄ , 96	163
(S)-P-(<i>tert</i> -butyl)-N-(di- <i>tert</i> -butylphosphoroselenoyl)-P-methylphosphinoselenoic amide, 99	164
P-(<i>tert</i> -butyl)-N-(di- <i>tert</i> -butylphosphoryl)-P-methylphosphinic amide, 101	165
P-(<i>tert</i> -butyl)-N-(di- <i>tert</i> -butylphosphorothioyl)-P-methylphosphinothioic amide, 102	166
(<i>tert</i> -butyl)((di- <i>tert</i> -butylphosphoryl)amino)(methyl)phosphonio trihydroborate, 103	167
(<i>R</i>)-(tert-butyl)((di- <i>tert</i> -butylphosphorothioyl)amino)(methyl)phosphonio trihydroborate, 104	168
(<i>tert</i> -butyl)((di- <i>tert</i> -butylphosphoroselenoyl)amino)(methyl)phosphonio trihydroborate, 105	169
(<i>R</i>)-P,P-di- <i>tert</i> -butyl-N-(<i>tert</i> -butyl(methyl)phosphoranylidene) phosphinothioic amide, 106	170
P,P-di- <i>tert</i> -butyl-N-(<i>tert</i> -butyl(methyl)phosphoranylidene) phosphinoselenoic amide, 107	171
[(<i>R</i> -Mono-S-MaxPHOS)Rh(COD)]BF ₄ , 108	172
[(<i>R</i> -Mono-Se-MaxPHOS)Rh(COD)]BF ₄ , 109	173
[(Mono-S-MaxPHOS) ₂ Pd], 110	174
[(Pd(mono-S-MaxPHOS) ₂]BF ₄ , 111	175
(<i>R</i>)-(tert-butyl)((di- <i>tert</i> -butylphosphorothioyl)(methyl)amino)(methyl) phosphonio trihydroborate, 112	176

[(<i>R</i>)-tert-butyl((di-tert-butylphosphorothioyl)(methyl)amino)(methyl)phosphonium] BF ₄ , 113	177
[(<i>N</i> -Me-mono-S-MaxPHOS)Rh(COD)]BF ₄ , 115	178
(<i>R,E</i>)-(tert-butyl((methoxymethylene)amino)(methyl)phosphonio)trihydroborate, 116	179
(2 <i>R,6R,E</i>)-2,6-di-tert-butyl-2,6-dimethyl-3,5-diaza-2,6-diphospha-1,7-diborahept-3-ene-2,6-diium-1,7-diuide, 117	180
2-(tert-butyl)-2-methyl-3,5-diaza-2-phospha-1-borahex-3-en-2-ium-1-uide, 118	181
(<i>R,E</i>)-2,6,6-tri-tert-butyl-2,5-dimethyl-3,5-diaza-2,6-diphospha-1,7-diborahept-3-ene-2,6-diium-1,7-diuide, 119	182
7.4 General Procedure for Hydrogenations using MaxPHOS-Rh catalyst.....	183
7.5 ¹ H NMR and HPLC data of hydrogenated substrates.....	183
(-)-(<i>R</i>)-methyl 2-acetamido-3-phenylpropanoate, 21	183
(+)-(<i>R</i>)-methyl 3-acetamidobutanoate, 140	183
(+)-(<i>R</i>)- <i>N</i> -(1,2,3,4-tetrahydronaphthalen-1-yl)acetamide, 141	184
(+)-(<i>S</i>)-methyl 3-hydroxy-2-methylpropanoate, 142	184
(-)-(<i>R</i>)-methyl-2-acetamido-3-(4-fluorophenyl) propanoate, 143	184
(-)-(<i>R</i>)-methyl-2-acetamido-3-(2-methoxyphenyl) propanoate, 145	184
8 Spectra.....	187
9 Appendix I: X-ray diffraction data.....	225
10 Appendix II: Index of structures.....	237
11 Appendix III: Detailed index.....	243
12 Appendix IV: Publications, Posters, Congresses.....	249
13 Appendix V: Summary in Spanish.....	255

Appendix IV: Publications

Congresses

Posters

12

12.1 Publications

“Primary and Secondary Aminophosphines as Novel P-Stereogenic Building Blocks for Ligand Synthesis”. Reves, M.; Ferrer, C.; Leon, T.; Doran, S.; Etayo, P.; Vidal-Ferran, A.; Riera, A.; Verdaguer, X. *Angew. Chem., Int. Ed.* **2010**, *49*, 9452.

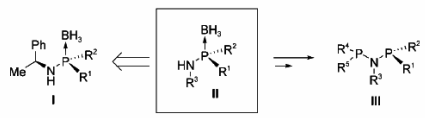
Communications

P Ligands DOI: 10.1002/anie.201004041

Primary and Secondary Aminophosphines as Novel P-Stereogenic Building Blocks for Ligand Synthesis**

Marc Revés, Catalina Ferrer, Thierry León, Sean Doran, Pablo Etayo, Anton Vidal-Ferran, Antoni Riera,* and Xavier Verdaguer*

Chiral phosphine ligands are central to asymmetric metal catalysis.^[1] The effect of the majority of these ligands arises from the chirality of their backbones; however, P-stereogenic (P*) ligands have garnered renewed interest.^[2] After the decisive work of Knowles and co-workers with PAMP and DIPAMP ligands, several efficient syntheses of all-carbon P* compounds have been reported.^[3,4] In contrast, P* compounds that contain heteroatoms directly linked to the phosphorus center are scarce, and have found little application in catalysis. This class of substances includes secondary



Scheme 1. Strategy explored to synthesize P*-aminophosphine building blocks.

“Neutral vs. cationic rhodium (I) complexes of bulky N-phosphino sulfonamide ligands: Coordination modes and its influence in the asymmetric hydrogenation of Z-MAC.”

Doran, S.; Achard, T.; Riera, A.; Verdaguer, X. *J. Organomet. Chem.* **2012**, *717*, 135.

Journal of Organometallic Chemistry 717 (2012) 135–140

Contents lists available at SciVerse ScienceDirect

Journal of Organometallic Chemistry

journal homepage: www.elsevier.com/locate/jorganchem

ELSEVIER

Journal of Organometallic Chemistry

Neutral vs. cationic rhodium (I) complexes of bulky N-phosphino sulfonamide ligands: Coordination modes and its influence in the asymmetric hydrogenation of Z-MAC

Seán Doran, Thierry Achard, Antoni Riera*, Xavier Verdaguer*

Unitat de Recerca en Síntesi Asimètrica (URSA-PCB), Institute for Research in Biomedicine (IRB Barcelona) and Departament de Química Orgànica, Universitat de Barcelona, c/Baldri Reixac 10, E-08028 Barcelona, Spain

ARTICLE INFO

Article history:
Received 8 May 2012
Received in revised form 28 June 2012
Accepted 8 July 2012

Keywords:
P,S and P,O ligands
Rhodium
Asymmetric hydrogenation
Sulfonamides

ABSTRACT

Here we report the synthesis of a new *N*-di-*tert*-butylphosphino-*tert*-butylsulfonamide (PNSO) ligand and its corresponding *p*-tolylsulfonamide analog. The coordination of these compounds to rhodium to form a neutral and apolar complex is described, followed by the subsequent protonation of said complexes to quantitatively form the more orthodox, cationic rhodium species containing a tetrafluoroborate counterion. The crystallographic structure of the *tert*-butylsulfonamide-derived cationic species was obtained and is elucidated. It outlines coordination from the sulfonamide group to the rhodium atom and shows no preference between O- and S-coordination as both complexes can be seen in one unit cell of the crystal. The efficacies of the neutral species and the salt species were tested in the asymmetric hydrogenation of methyl (Z)- α -acetamido cinnamate (Z-MAC). The *p*-tolylsulfonamide-derived complexes gave no hydrogenation while the *tert*-butylsulfonamide-derived ones produced hydrogenation with complete conversion but low enantioselectivities. The stereochemical outcome of the reaction was analyzed by means of the quadrant method.

© 2012 Elsevier B.V. All rights reserved.

12.2 Congress and Poster



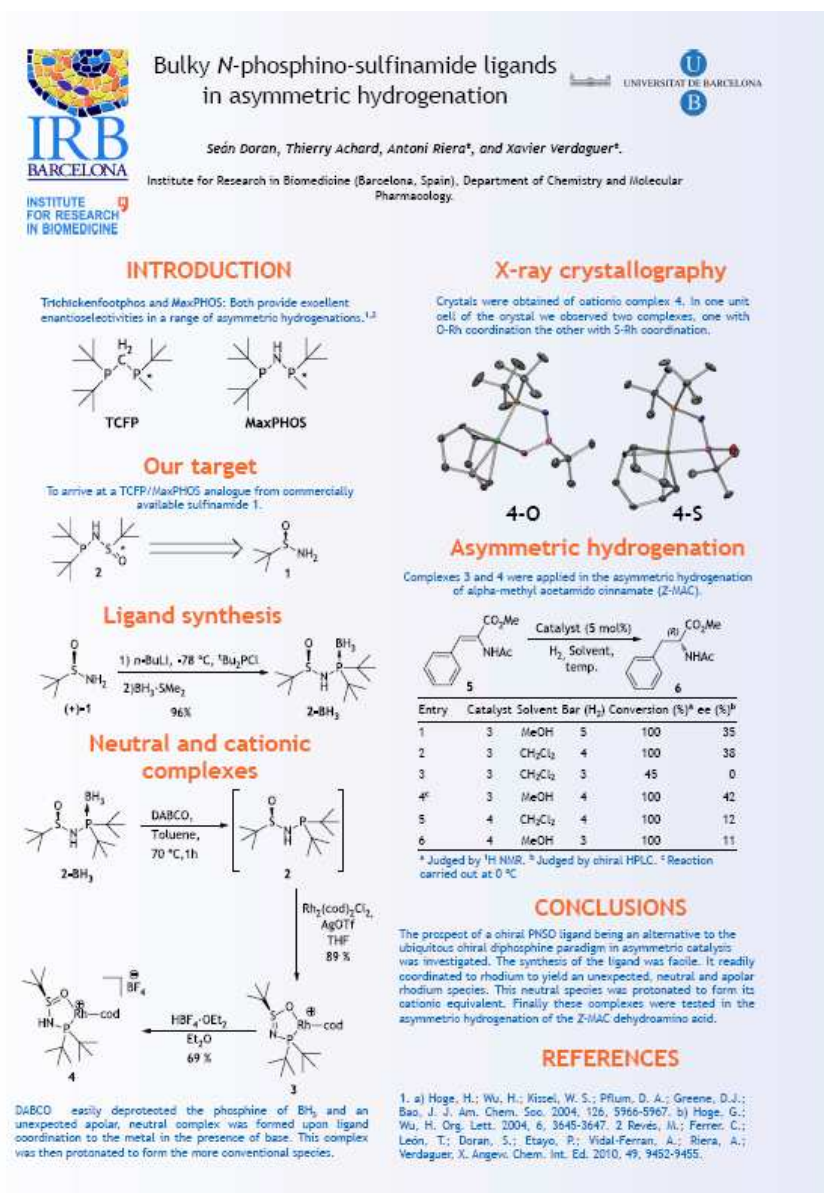
13th Tetrahedron Symposium
CHALLENGES IN BIOORGANIC & ORGANIC MEDICINAL CHEMISTRY

26 - 29 June 2012
AMSTERDAM,
THE NETHERLANDS

“The 13th Tetrahedron Symposium: Challenges in Bioorganic & Organic Medicinal Chemistry”. *Amsterdam, Netherlands. 26 – 29 June, 2012.*

Contribution type: Poster.

“Bulky *N*-Phosphino Sulfinamide Ligands in Asymmetric Hydrogenation.” Seán Doran, Thierry Achard, Xavier Verdaguer, Antoni Riera.



Bulky *N*-phosphino-sulfinamide ligands in asymmetric hydrogenation

Seán Doran, Thierry Achard, Antoni Riera^a, and Xavier Verdaguer^a.

Institute for Research in Biomedicine (Barcelona, Spain), Department of Chemistry and Molecular Pharmacology.

INTRODUCTION

Trichickenfootphos and MaxPHOS: Both provide excellent enantioselectivities in a range of asymmetric hydrogenations.^{1,2}

Our target

To arrive at a TCFP/MaxPHOS analogue from commercially available sulfinamide 1.

Ligand synthesis

1) *n*-BuLi, -78 °C, ^tBu₂PCl
2) BH₃·SMe₂

96%

Neutral and cationic complexes

DABCO, Toluene, 70 °C, 1h

Rh₂(cod)₂Cl₂, AgOTf, THF, 89%

HBF₄·OEt₂, Et₂O, 69%

X-ray crystallography

Crystals were obtained of octahedral complex 4. In one unit cell of the crystal we observed two complexes, one with O-Rh coordination the other with S-Rh coordination.

Asymmetric hydrogenation

Complexes 3 and 4 were applied in the asymmetric hydrogenation of alpha-methyl acetoamido cinnamate (Z-MAC).

Entry	Catalyst	Solvent	Bar (H ₂)	Conversion (%) ^a	ee (%) ^b
1	3	MeOH	5	100	35
2	3	CH ₂ Cl ₂	4	100	38
3	3	CH ₂ Cl ₂	3	45	0
4 ^c	3	MeOH	4	100	42
5	4	CH ₂ Cl ₂	4	100	12
6	4	MeOH	3	100	11

^a Judged by ¹H NMR. ^b Judged by chiral HPLC. ^c Reaction carried out at 0 °C.

CONCLUSIONS

The prospect of a chiral PNSO ligand being an alternative to the ubiquitous chiral diphosphine paradigm in asymmetric catalysis was investigated. The synthesis of the ligand was facile. It readily coordinated to rhodium to yield an unexpected, neutral and apolar rhodium species. This neutral species was protonated to form its cationic equivalent. Finally these complexes were tested in the asymmetric hydrogenation of the Z-MAC dehydroamino acid.

REFERENCES

1. a) Hoge, H.; Wu, H.; Kitzel, W. S.; Pflum, D. A.; Greene, D. J.; Bao, J. *J. Am. Chem. Soc.* 2004, 126, 5966-5967. b) Hoge, G.; Wu, H. *Org. Lett.* 2004, 6, 3645-3647. 2. Revés, M.; Ferrer, C.; León, T.; Doran, S.; Etayo, P.; Vidal-Ferran, A.; Riera, A.; Verdaguer, X. *Angew. Chem. Int. Ed.* 2010, 49, 9452-9455.

DABCO easily deprotected the phosphine of BH₃ and an unexpected apolar, neutral complex was formed upon ligand coordination to the metal in the presence of base. This complex was then protonated to form the more conventional species.

Apéndice V:

Resumen en Español

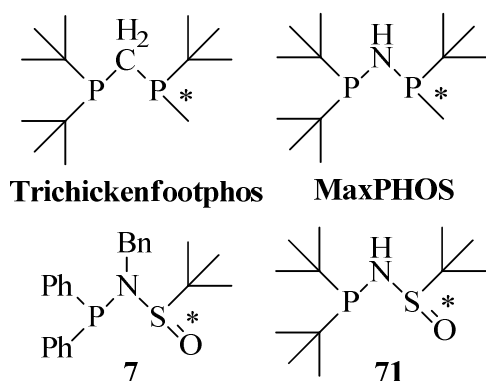
13

13.1 Los ligandos N-phosphino sulfinamida

13.1.1 Los ligandos *tert*-butilo y *p*-tolilo

En los antecedentes (capítulo 2) se destacó la importancia de los ligandos bidentados en catálisis asimétrica y aun más en hidrogenación asimétrica. Algunos de los ligandos como el BINAP y el DuPHOS aportan mucha reactividad al metal con el que se complejan y conducen a excesos enantioméricos muy altos en las transformaciones asimétricas en las cuales son usados. Además de ser muy buenos como ligandos quirales, los ligandos DIOP, BINAP y el DuPHOS, se destacaron en el momento de su descubrimiento porque su quiralidad no residía en el átomo del fósforo sino en la estructura del ligando. Ligandos como *trichickenfootphos* y MaxPHOS también destacan en el campo de hidrogenación asimétrica, porque su quiralidad reside en el átomo de fósforo y tienen simetría C_1 en vez de C_2 . Los ligandos que tienen su quiralidad en fósforo pueden ser muy efectivos en catálisis asimétrica, pero uno de sus inconvenientes es que normalmente son difíciles y laboriosos de preparar.

Figura 13.1: Similitud estructural entre los ligandos TCFP, MaxPHOS, el ligando PNSO **7** y el nuevo ligando PNSO **71**.



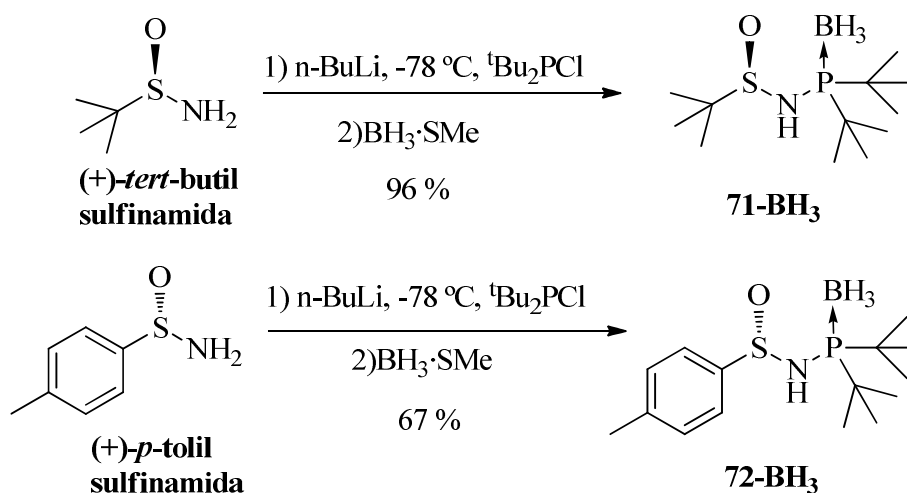
Dada la experiencia de nuestro grupo con los ligandos tipo PNSO especialmente en la reacción Pauson-Khand, pensamos que los ligandos PNSO podrían ser aplicados a la reacción de hidrogenación asimétrica como un análogo de los ligandos *trichickenfootphos* y MaxPHOS. Pensamos que un ligando PNSO que diera buenos excesos enantioméricos en

transformaciones asimétricas sería mas atractivo como ligando porque la preparación de los ligandos PNSO suele ser muy fácil con esquemas de reacción de una o dos etapas.

13.1.1.1 Síntesis y preparación de los ligandos

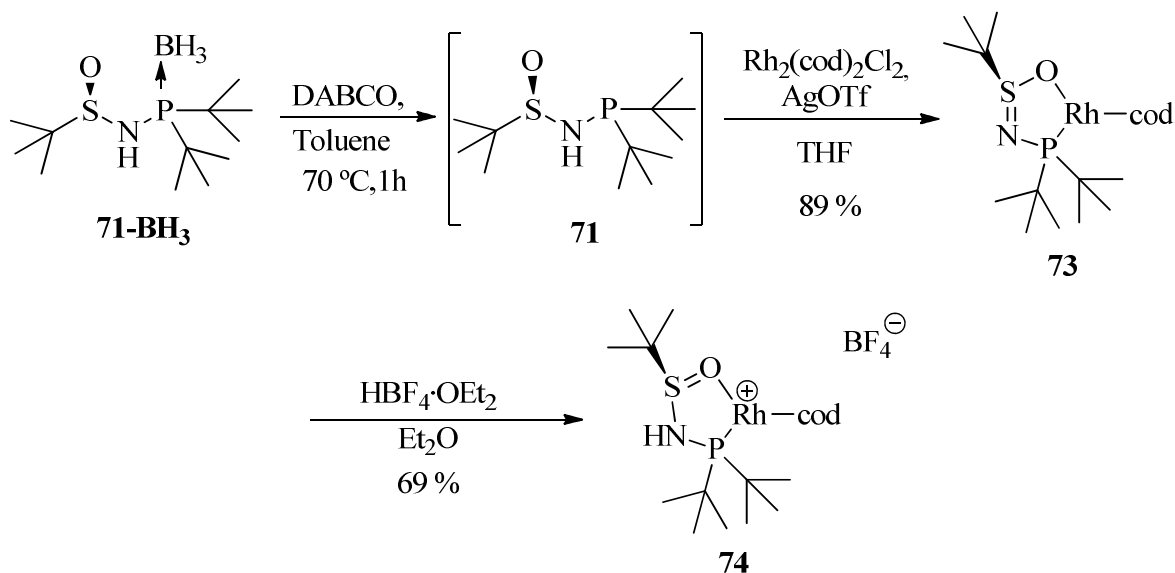
El ligando PNSO **71-BH₃** fue fácilmente preparado a partir de la (+)-*tert*-butil sulfinamida en sólo una etapa tal como está descrito en la esquema 13.1. El producto fue aislado como un sólido blanco, estable al aire después de cromatografía en columna. El ligando PNSO **72-BH₃** fue preparado exactamente de la misma manera.

Esquema 13.1: Preparación de los ligandos.



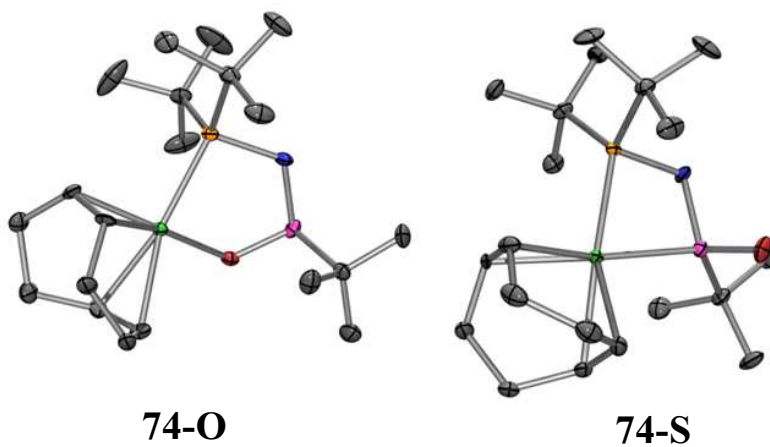
El ligando PNSO **71-BH₃** fue desprotegido del borano con facilidad, agitando el compuesto con un exceso de DABCO en tolueno a 70 °C bajo nitrógeno durante una hora siguiendo la reacción por capa fina. La mezcla de ligando desprotegido, se añadió sobre el rodio el cual había sido activado con AgOTf. Se formó el complejo neutro **73** con baja polaridad que purificamos mediante cromatografía en columna. El complejo era muy soluble en muchos diferentes disolventes desde hexano hasta metanol lo cual hizo muy difícil preparar cristales para análisis de Rayos-X. Fue por esa razón que decidimos protonar el complejo neutro para formar el complejo catiónico **74**.

Esquema 13.2: Desprotección de borano del ligando **71-BH₃**, y coordinación del ligando desprotegido con el rodio para formar un complejo neutro seguido por la protonación de dicho complejo neutro para formar el complejo catiónico.



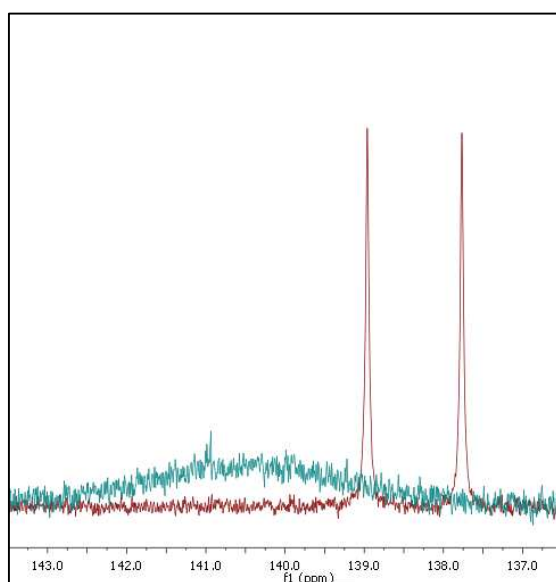
Con el complejo **74** se llevó a cabo una recristalización mediante un proceso de “layering”.

Figure 13.2: Dibujo Ortep para la estructura cristal del complejo **74-O** y **74-S** con 50 % de probabilidad de elipsoides. Las dos diferentes estructuras coexisten en una única celda cristalina.



El análisis de difracción de Rayos-X nos mostró que en una única celda cristalina coexistían dos estructuras diferentes. Una cuyo enlace metal-ligando se daba a través del átomo de oxígeno y otra cuyo enlace metal-ligando era a través del átomo de azufre. Por supuesto, con un enlace P-Rh en ambos casos. Esta información nos indicó que no existía preferencia entre la coordinación O-Rh o S-Rh sino que había un equilibrio entre los dos modos de coordinación que no favorecía ni uno ni otro.

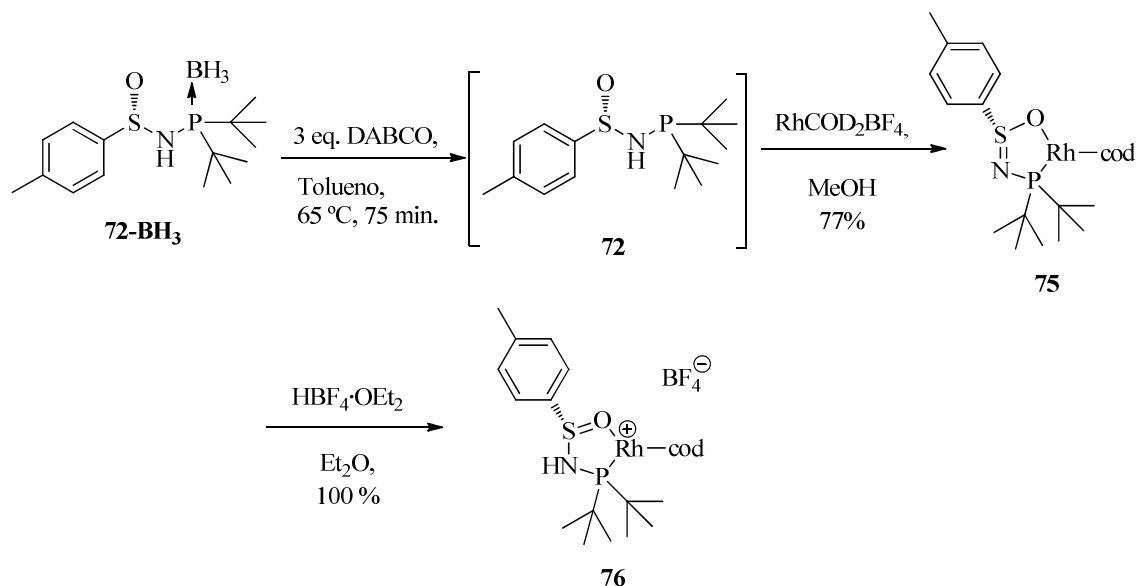
Figure 13.3: Espectros ^{31}P RMN de los complejos **73** (rojo) y **74** (verde) superpuestos.



El análisis del espectro ^{31}P RMN del complejo **74** nos respalda lo que ya nos había indicado el análisis de Rayos-X: que el complejo existía en un equilibrio fluxional de modos de coordinación, lo cual daba lugar a una señal de fósforo ancha. Por otro lado la señal de fósforo del complejo **73** se ve mucho mas definida, sugiriendo que el complejo en solución existía en un estado físico menos fluxional y mas rígido en la escala de tiempo de RMN.

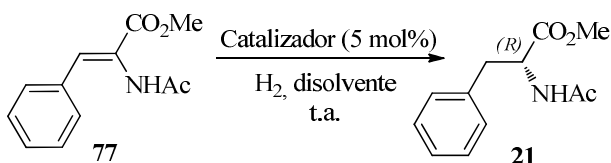
El ligando PNSO **72-BH₃** fue desprotegido y coordinado con rodio exactamente de la misma manera que el ligando **71-BH₃**. Tal como esperábamos, la coordinación dio lugar al complejo neutro **75**. El complejo neutro fue protonado mediante la adición de $\text{HBF}_4 \cdot \text{OEt}_2$ en dietil éter. El precipitado resultante fue filtrado y lavado con abundante dietil éter para proporcionar el complejo **76** como un sólido amarillo brillante.

Esquema 13.3: Desprotección de borano del ligando **72-BH₃**, y coordinación del ligando desprotegido con el rodio para formar un complejo neutro seguido por la protonación de dicho complejo neutro para formar el complejo catiónico.



13.1.1.2 Hidrogenaciones del sustrato Z-MAC catalizado por los complejos PNSO-Rh

Se probaron los complejos **73**, **74**, **75** y **76** como catalizadores en la hidrogenación asimétrica del sustrato Z-MAC y los resultados están representados en la tabla 13.1. Como se aprecia en las entradas 1 y 2 de la tabla 13.1 los complejos **75** y **76** no catalizaron la hidrogenación del sustrato Z-MAC. Como se puede ver en las entradas 3 y 4, el complejo catiónico **74** podía catalizar la hidrogenación del sustrato pero con bajos excesos enantioméricos. El complejo neutro **73** consiguió catalizar la hidrogenación del sustrato Z-MAC con un exceso enantiomérico máximo de 42 % conseguido cuando la reacción se llevaba a cabo a una presión de H_2 de 4 bares, en metanol y una temperatura de 0 °C. Cambiando el disolvente por cloruro de metileno no se consiguió aumentar los excesos enantioméricos, el uso de THF daba lugar a malos rendimientos y exceso enantiomérico nulo. Ningún aditivo añadido, como Et_3N o TBA, consiguió mejorar los resultados.

Tabla 13.1: Hidrogenación del dehidroamino ácido Z-MAC utilizando varios complejos PNSO-Rh.

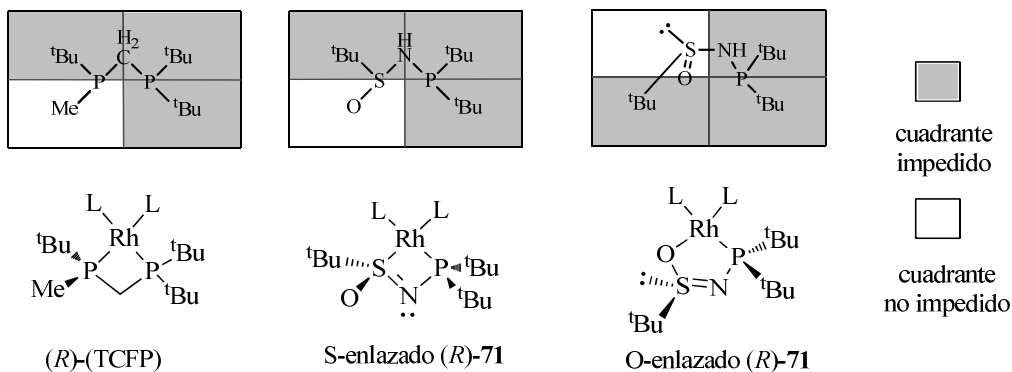
Entrada	Cat.	Disolvente	Bar (H ₂)	Conversión (%) ^a	ee (%) ^b
1	75	MeOH	3	0	0
2	76	MeOH	3	0	0
3	74	MeOH	3	100	11
4	74	CH ₂ Cl ₂	4	100	12
5	73	MeOH	5	100	35
6	73	CH ₂ Cl ₂	4	100	38
7	73	CH ₂ Cl ₂	3	45	0
8 ^c	73	MeOH	4	100	42
9	73	MeOH	30	100	8
10	73	CH ₂ Cl ₂	25	100	6
11	73	THF	5	90	0
12	73	TFE	5	100	13
13 ^d	73	MeOH	5	100	32
14 ^e	73	MeOH	5	100	11

a) Conversiones a producto hidrogenado determinado por ¹H RMN. b) Excesos enantioméricos determinado por HPLC en columna quiral. c) Reacción a 0 ° C. d) 10 mol % de Et₃N usado. e) 10 mol % of *tert*-butilamina usado.

13.1.1.3 Hidrogenaciones del sustrato Z-MAC catalizadas por los complejos PNSO-Rh

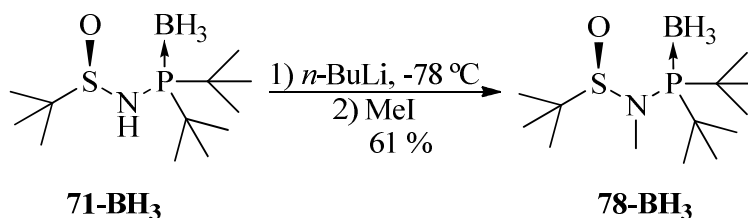
Analizamos el ligando (*R*)-**71** por el método de cuadrantes y llegamos a la conclusión de que si el ligando coordinaba el átomo de metal a través del átomo de azufre tendría el mismo espacio impedido que el ligando (*R*)-TCFP y por lo tanto debería dar la misma configuración del sustrato hidrogenado. El ligando (*R*)-TCFP una vez coordinado con rodio hidrogena el sustrato Z-MAC dando el producto con la configuración (*R*)-**21**. El complejo **73** también dio un exceso de la configuración R de producto **21**. Así que llegamos a la conclusión que se favorecía el modo de coordinación S-Rh durante el proceso de hidrogenación. También había que tener en cuenta que el modo de coordinación S-Rh podría dar lugar a un catalizador más activo y que en realidad los dos modos de coordinación S-Rh y O-Rh podían co-existir en cualquiera proporción en solución.

Figura 13.4: Análisis de cuadrantes para el S- y O-enlazado ligando (*R*)-**71**, y comparación con el ligando (*R*)-TCFP. Configuraciones absolutas referidas al ligando libre.

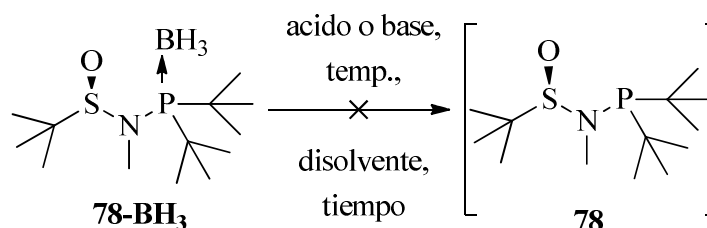


13.1.2.1 Preparación de análogos PNSO: el N-Me ligando PNSO

Quisimos modificar la estructura PNSO para formar ligandos parecidos a los ligandos **71** y **72** y luego probarlos en la reacción de hidrogenación asimétrica. Se nos ocurrió la idea de metilar el ligando **71-BH₃** en la posición NH con la esperanza de que un cambio así pudiera dar lugar a un complejo de rodio con un modo de coordinación mas definido. En ese caso esperábamos ver mejores excesos enantioméricos en la reacción de hidrogenación que catalizaría.

Esquema 13.4: Metilación del ligando **71-BH₃**.

Se metiló el grupo amino secundario del ligando **71-BH₃** mediante una reacción con *n*-BuLi a baja temperatura y posterior adición de un gran exceso de yodometano. Una vez aislado después de cromatografía en columna, se sometió el compuesto **78-BH₃** a diferentes condiciones de desprotección para quitar el grupo protector borano.

Tabla 13.2: Desprotección de BH₃ del ligando PNSO N-metilado.

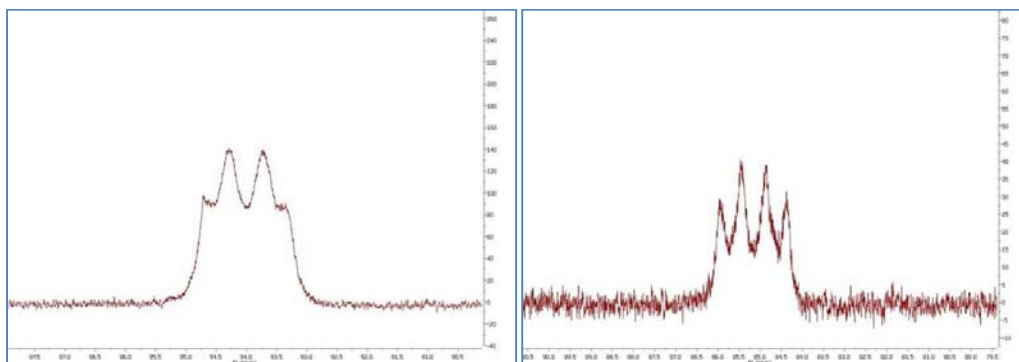
Entrada	Ácido o Base	Disolvente	Temp. (°C)	Tiempo (h)	Rend. ^a
1	DABCO	Tolueno	80	22	p.p.
2	TFA	-- ^b	t.a.	18	descomp.
3	TFA	-- ^b	t.a.	1	descomp.
4	HF ₄ ·OEt ₂	CH ₂ Cl ₂	t.a.	19	descomp.
5	Morfolina	CH ₂ Cl ₂	t.a.	18	p.p.
6	NHEt ₂	-- ^b	45	41	p.p.

^a Deducido mediante una combinación de ³¹P, ¹H RMN y TLC. ^b Reactivo usado como disolvente.

Se descubrió que la adición de un grupo metilo en el N fortalecía el enlace P-BH₃ en tal grado que los métodos más usuales para desproteger un grupo borano de una fosfina como DABCO y NHEt₂ ya no funcionaban. Otros métodos para eliminar los grupos borano especialmente

difíciles de desproteger son los ácidos fuertes como $\text{HBF}_4 \cdot \text{OEt}_2$ y TFA, pero estos ácidos solo consiguieron descomponer el compuesto **78-BH₃**. Por lo tanto, no se encontró una manera para desproteger **78-BH₃**.

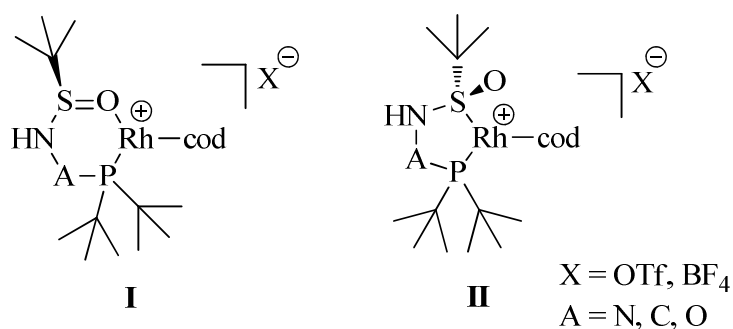
Figura 13.5: Comparación de los espectros ^{31}P RMN del ligando **71-BH₃** (a la izquierda) y el espectro ^{31}P RMN del compuesto **78-BH₃** (a la derecha).



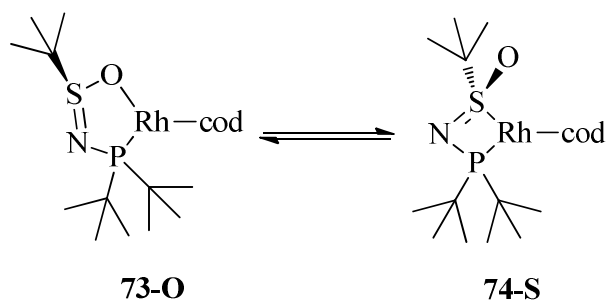
La comparación de espectros de ^{31}P RMN de compuestos con fosfinas protegidas con borano, nos daba una indicación de lo fuerte que era el enlace P-BH₃. A la izquierda en la figura 13.5 se ve una imagen del espectro de ^{31}P RMN del ligando **71-BH₃** y su señal se aprecia como un cuarteto ancho. Por otro lado, a la derecha de la figura 13.5 se ve el espectro del ^{31}P RMN del compuesto **78-BH₃** y se puede apreciar una señal de fosfina bastante más definida, lo cual indica que el enlace P-BH₃ es más fuerte y que será más difícil eliminar el borano.

13.1.2.2 Inserción de un átomo adicional en la estructura PNSO: Nitrógeno

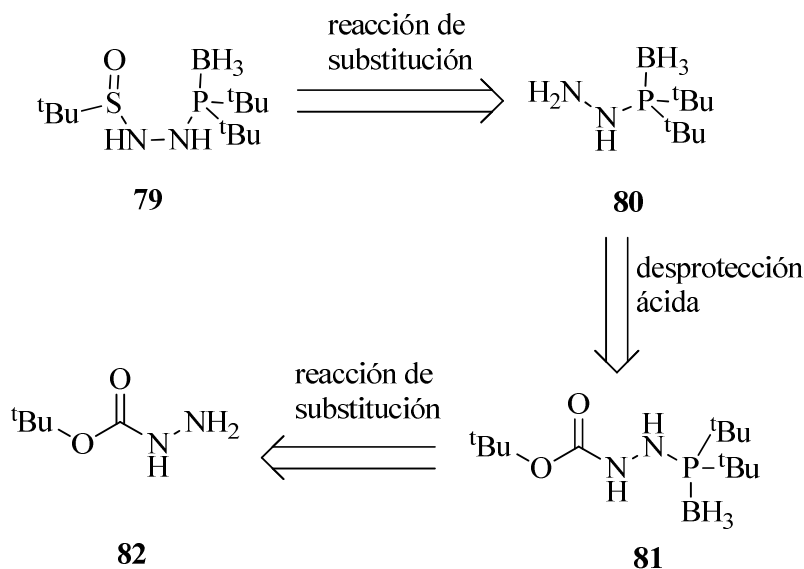
Pensamos que si pudiéramos introducir un átomo adicional entre los átomos de N y P en los ligandos PNSO, ya fuera nitrógeno, carbono u oxígeno, podríamos influir en el modo de coordinación de los ligandos. Esto podría favorecer una coordinación tipo P, S en detrimento de tipo P, O.

Figura 13.6: Un átomo adicional en la plantilla PNSO.

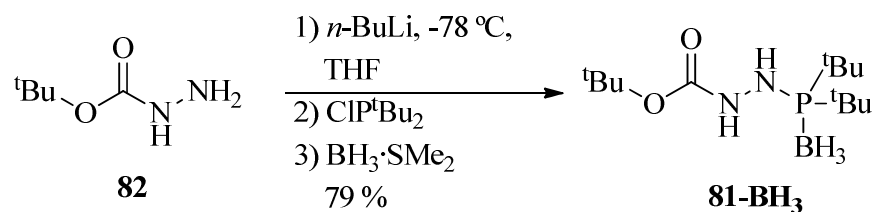
Esperábamos que con la adición de otro átomo en la secuencia PNSO hubiese menos tensión en el anillo formado en la coordinación S-Rh alrededor del metal, de tal manera que ésta coordinación estuviese favorecida y nos diese un complejo mas definido. Esperábamos ver un catalizador que catalizase la hidrogenación asimétrica con mejores excesos enantioméricos.

Figura 13.7: O- contra S- coordinación

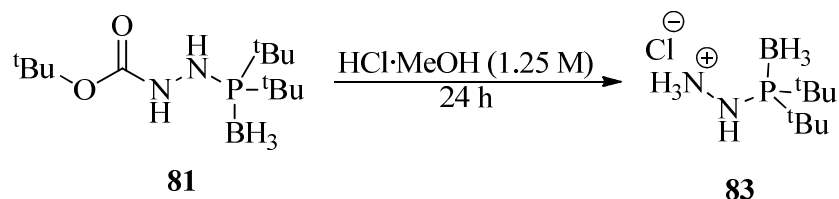
Nuestra primera idea era introducir un átomo de nitrógeno adicional entre la unidad sulfóxido y la fosfina. Planteamos como estrategia el análisis retrosintético dibujado en el esquema 13.5. Quisimos empezar desde la hidrazina **82**, uniéndola con el grupo di-*tert*-butil fosfina para conseguir la molécula **82**. Con el compuesto **81** en mano, desprotegeríamos el grupo protector Boc mediante una desprotección ácida para llegar a tener la hidrazina-fosfina **80**. Luego reaccionaríamos el compuesto **80** con una fuente de sulfóxido para conseguir el nuevo ligando “PNNSO” **79**. Al principio optaríamos por una fuente de sulfóxido racémica como el *tert*-butilo cloruro de sulfinilo para comprobar las características y propiedades físicas de la molécula.

Esquema 13.5: Análisis retro-sintético del ligando PNNSO.

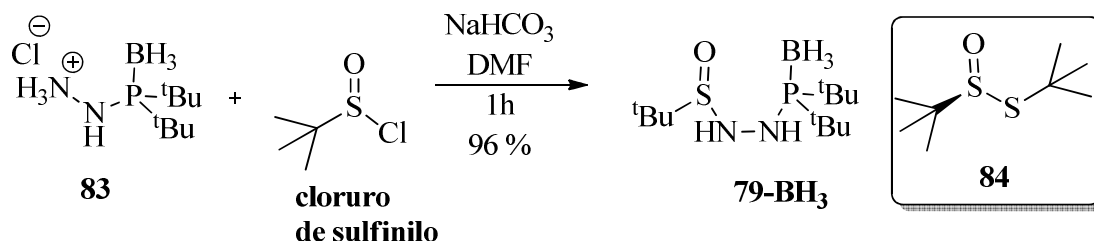
Se formó el anión a 78 °C con *n*-BuLi en la boc-protégida hidracina, luego se añadió la clorofosfina con posterior adición del $\text{BH}_3\cdot\text{SMe}_2$ para proteger el grupo fosfino. El producto **81-BH₃** se obtuvo en estado puro después de tratamiento acuoso y cromatografía en columna.

Esquema 13.6: Preparación de la hidrazina-fosfina **81** protegida con los grupos protectores correspondientes Boc y BH_3 

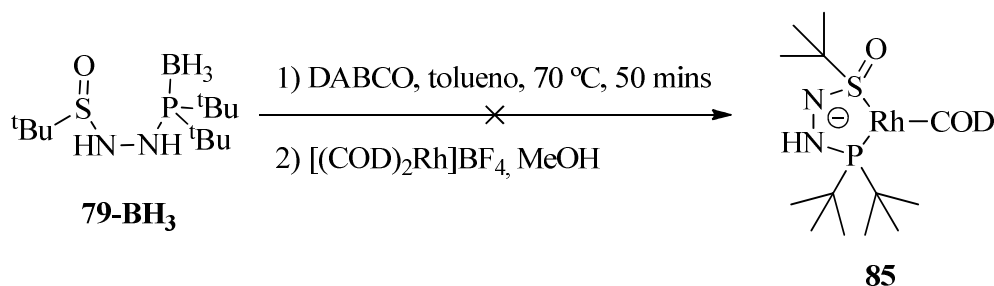
Agitando la fosfina **81-BH₃** bajo una atmósfera de nitrógeno en un exceso de ácido clorhídrico y posteriormente quitando el disolvente en vacío fue suficiente para obtener la fosfina **83** en forma de sal.

Esquema 13.7: Desprotección del grupo protector Boc.

Se reaccionó la fosfina **83** con *tert*-butil-cloruro de sulfinilo en presencia de la base inorgánica NaHCO₃ en DMF para obtener el compuesto **79-BH₃** con buen rendimiento después de un tratamiento acuoso y cromatografía en columna. El nuevo compuesto **79-BH₃** fue preparado de forma racémica con la intención de comprobar que las propiedades del compuesto eran las adecuadas. Una vez comprobado que las eran se pensó en el compuesto **84** para preparar la fosfina de forma enantioméricamente pura ya que este es comercialmente asequible.

Esquema 13.8: Preparación de la fosfino-borano **79-BH₃**.

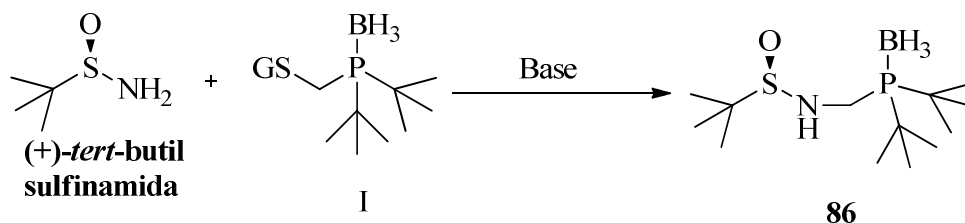
Tras varios intentos de desproteger del borano y coordinar el ligando **79-BH₃** con rodio se concluyó que no era factible preparar el complejo **85**. Parecía que el problema no residía en la etapa de desprotección del borano, ya que se apreciaba por capa fina pero al añadir rodio a la reacción se formaban muchos productos distintos y el producto **85** deseado no podía aislarse.

Esquema 13.9: Pérdida de integridad de la estructura PNNSO.

13.1.2.3 La inserción de un átomo adicional en la estructura PNSO: Carbono

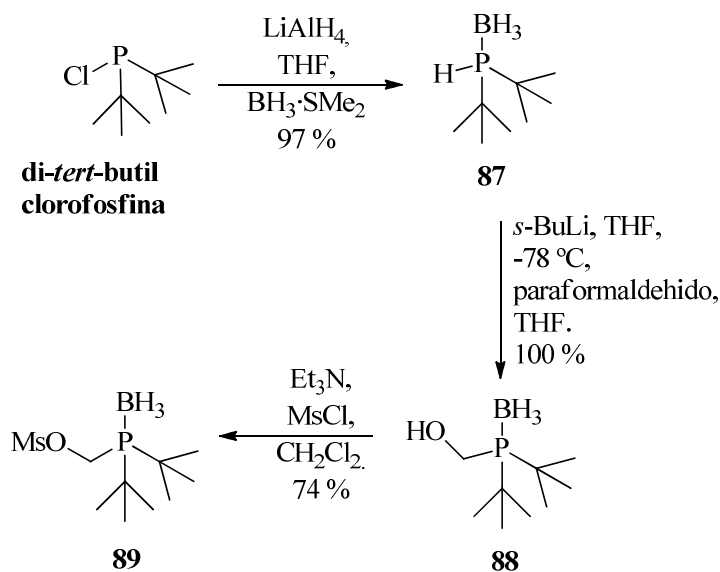
Para introducir un átomo de carbono en el ligando PNSO. Pensó en acoplar la *tert*-butilsulfonamida comercial con un sintón fosfina que contuviese un buen grupo saliente (esquema 13.10).

Esquema 13.10: Una estrategia alternativa para introducir otro átomo en la secuencia PNSO.



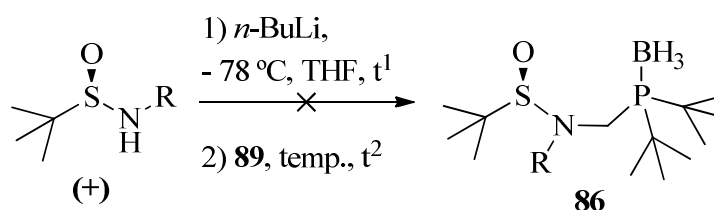
Se decidió utilizar la química de Hoge *et al.* para conseguir preparar una fosfina de tipo I (esquema 13.10). Proseguimos con el esquema de reacción 13.11 para preparar la fosfina **89** que se muestra a continuación.

Esquema 13.11: La preparación de la fosfina **89**.



Se realizaron varios intentos para sintetizar el compuesto **86** pero sólo se observó producto de partida o producto descompuesto como se aprecia en la tabla 13.3. Por otro lado, se empleó la sulfonamida substituida por un grupo benzilo con la esperanza de que actuara mejor como nucleófilo pero tampoco se produjo el resultado esperado.

Tabla 13.3: La reacción de las *tert*-butilsulfonamidas con di-*tert*-butilfosfinamesilato-borano **89**.



Entrada	R	<i>n</i> -BuLi (eq.)	<i>t</i> ¹ (h)	temp. (°C)	<i>t</i> ² (h)	yield ^a
1	H	1,2	0,8	- 78 °C a t.a.	19	p.p.
2	H	1,1	1,3	- 78 °C a 60 °C	25	descomp.
3	Bn	1,2	1	- 78 °C a t.a.	18	p.p.

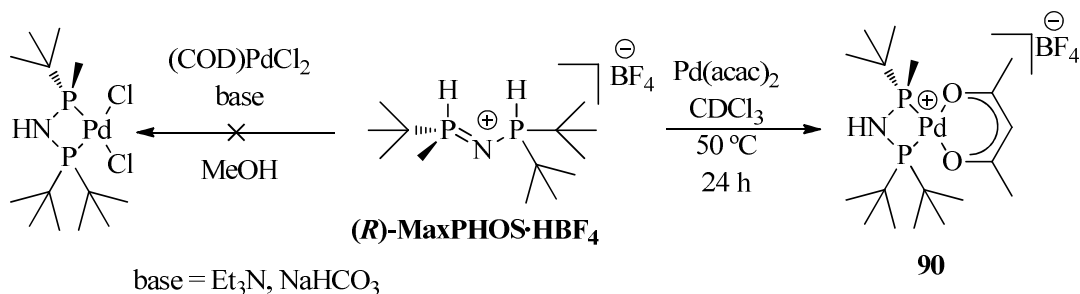
^a Deducido por TLC de la reacción y ¹H RMN del residuo aislado después de un work-up acuoso.

13.2 Los ligandos aminofosfinas P-stereogénicos

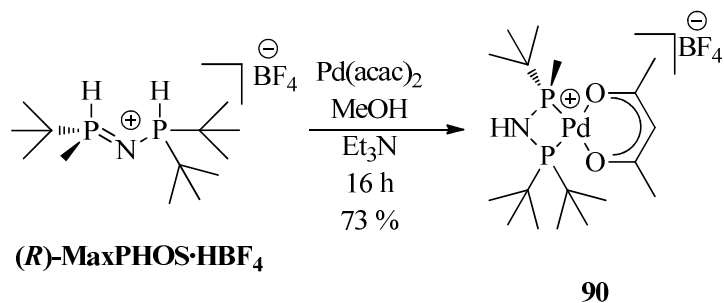
En el capítulo 4 se trató de explorar a fondo el ligando MaxPHOS. Intentamos explorar los diferentes metales a los cuales podíamos complejar el ligando MaxPHOS para generar nuevos complejos. Así como se investigaba la naturaleza electrónica del ligando. Se descubrieron nuevos análogos y derivados del ligando MaxPHOS. Del mismo modo, exploramos los diferentes complejos y aplicaciones que tenían los distintos análogos y sus derivados.

13.2.1 Nuevos complejos de MaxPHOS

En primera instancia se deseaba coordinar el ligando MaxPHOS con paladio. Con (COD)PdCl₂ como fuente de paladio no se pudo obtener complejo. Se cambió la fuente de paladio a [Pd(acac)]₂ y esta vez si se formó el complejo deseado. La reacción se llevó a cabo dentro de un tubo de resonancia comprobando la evolución de la reacción con espectros de ¹H RMN y ³¹P RMN llevados a cabo en distintos intervalos de tiempo. Se pudo apreciar la coordinación total del ligando después de 24 horas.

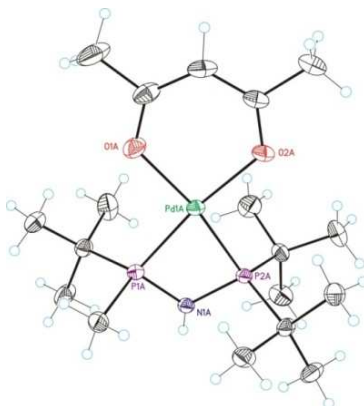
Esquema 13.12: Intentos de complejar MaxPHOS con paladio.

Se observó que con la adición de Et₃N, el ligando MaxPHOS podía ser complejado con paladio mas rápidamente y sin necesidad de calentar. Se obtuvo el complejo puro después de una recristalización.

Esquema 13.13: Formación del complejo [(MaxPHOS)Pd(acac)]BF₄ **90**.

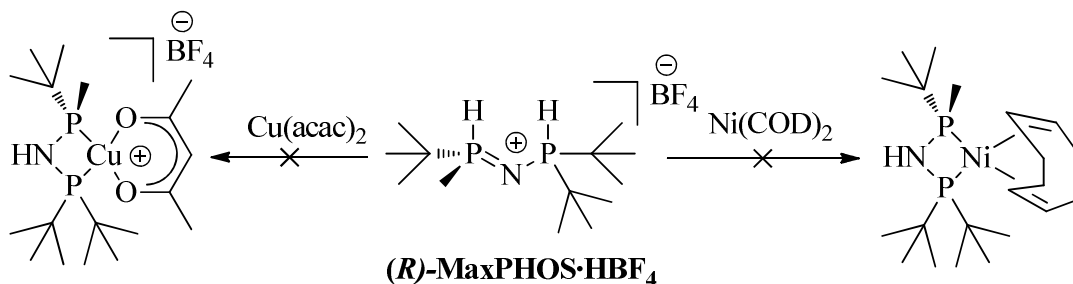
Se obtuvieron cristales adecuados para análisis de difracción Rayos-X después de un proceso de *layering* de éter sobre el complejo disuelto en la mínima cantidad de cloruro de metileno. En la fig. 13.8 se representan los resultados obtenidos del análisis de Rayos-X del complejo **90**.

Figura 13.8: Dibujo ORTEP del complejo [(MaxPHOS)Pd(acac)]BF₄ **90** donde el contra-ion está omitido por claridad.



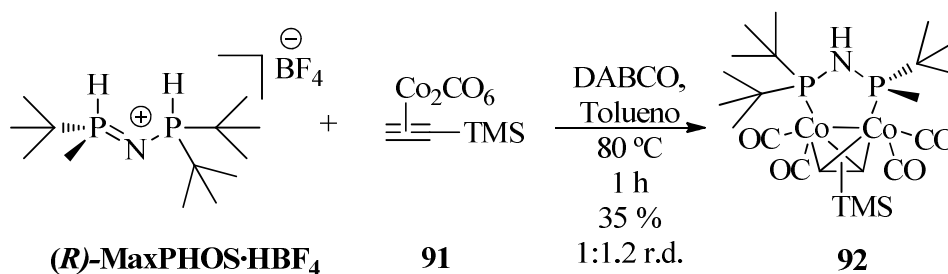
Se hicieron pruebas para la coordinación de MaxPHOS con cobre y con níquel. Estas reacciones se llevaron a cabo dentro de tubos de resonancia en CDCl_3 siguiendo la evolución de las reacciones con experimentos de ^1H y ^{31}P RMN, no dieron lugar a resultados concluyentes.

Esquema 13.14: Intentos fallidos de coordinar el ligando MaxPHOS con cobre y níquel.



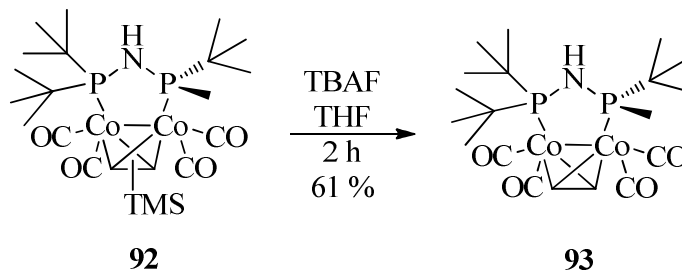
Logramos coordinar el ligando MaxPHOS a un clúster alquino-dicobalto para obtener el producto **92** como mezcla de diastereoisómeros 1:1.2 después de cromatografía en columna.

Esquema 13.15: Preparación del complejo MaxPHOS dicobalto.



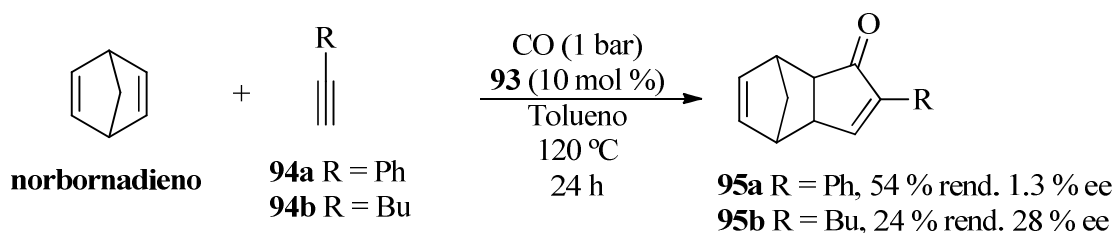
Mediante tratamiento del complejo **92**, compuesto de una mezcla de diastereoisómeros, con TBAF en THF se consiguió eliminar el grupo TMS con facilidad, obteniendo el producto puro **93** después de cromatografía en columna.

Esquema 13.16: Eliminación el grupo TMS para obtener el complejo **93**.



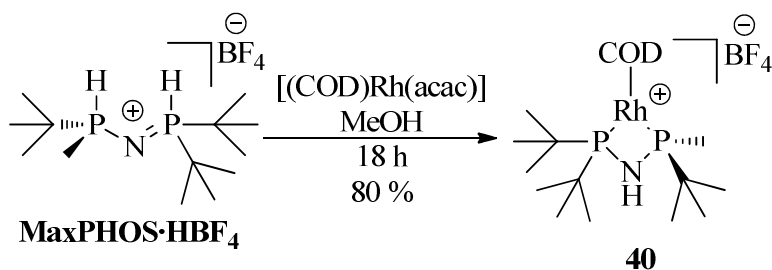
Se probó el complejo **93** como catalizador en la reacción Pauson-Khand asimétrica y catalítica. Se probaron dos diferentes alquinos terminales, uno sustituido por un grupo butilo, el otro con un grupo fenilo y el alqueno utilizado fue norbornadieno en ambos casos. Destacamos el resultado obtenido en la reacción de PK utilizando el alquino **94b** ya que dio un ee comparable a los mejores resultados obtenidos en la reacción de PK catalítica hasta el momento.

Esquema 13.17: Aplicación del clúster **93** en la reacción Pauson-Khand asimétrica y catalítica fue investigada.



Desarrollamos una nueva ruta para obtener el complejo de rodio-MaxPHOS a partir de $[(\text{COD})\text{Rh}(\text{acac})]$. Su ventaja era que evitaba la necesidad de usar NaHCO_3 y también la posterior separación y filtración de las sales inorgánicas como hacía falta cuando se empleaba $[(\text{COD})_2\text{Rh}]\text{BF}_4$.

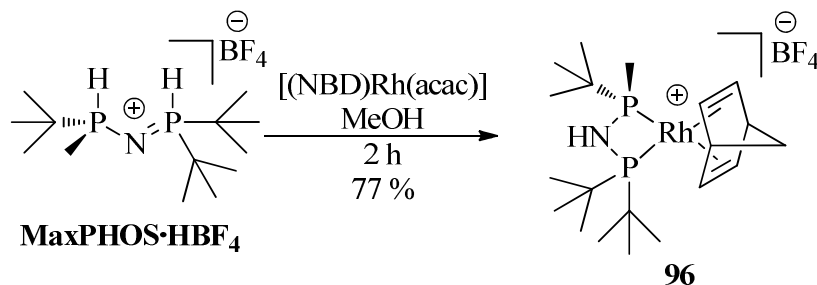
Esquema 13.18: Ruta optimizada para la obtención del complejo MaxPHOS-Rh.



Tal y como se hizo el complejo $[(\text{COD})\text{Rh}(\text{MaxPHOS})]\text{BF}_4$ mediante la ruta optimizada descrita en el esquema 13.18, se preparó el complejo $[(\text{NBD})\text{Rh}(\text{MaxPHOS})]\text{BF}_4$ **96** a partir de $[(\text{NBD})\text{Rh}(\text{acac})]$. El complejo **96** resultó ser mucho más inestable que el complejo **40**. Se

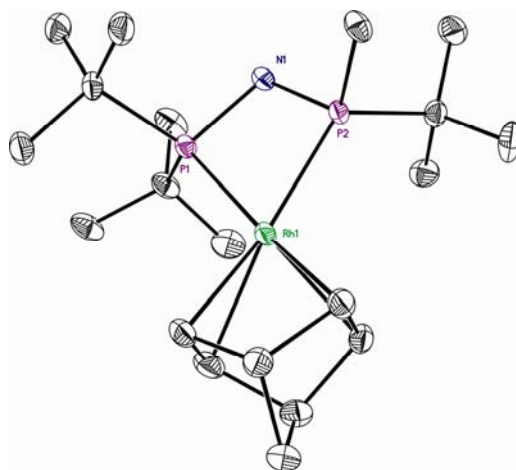
podía observar la degradación del complejo **96** después de 2 horas en contacto con el aire; cambiando éste de un naranja brillante a marrón oscuro.

Esquema 13.19: Preparación del complejo [(MaxPHOS)Rh(NBD)]BF₄.



Se obtuvieron cristales adecuados del complejo **96** para análisis Rayos-X mediante un proceso *layering* añadiendo éter sobre el complejo disuelto en la mínima cantidad de cloruro de metileno.

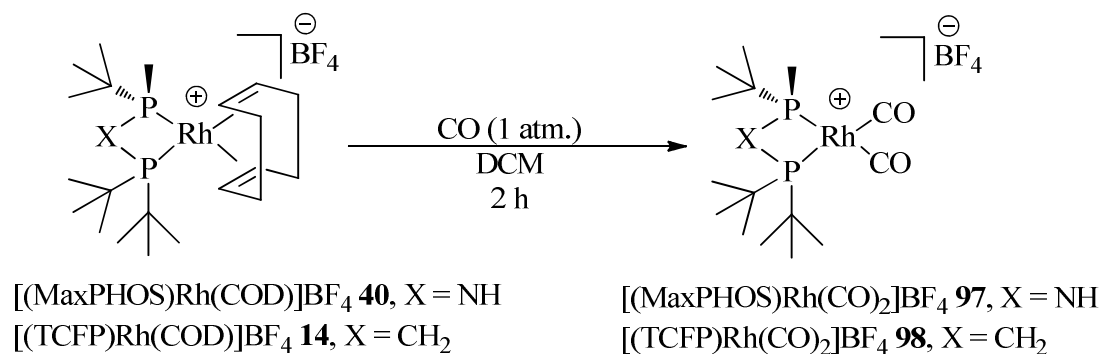
Figura 13.9: Dibujo ORTEP del complejo [(NBD)Rh(MaxPHOS)]BF₄ **96**. Los protones están omitidos por claridad.



13.2.2 Investigación de la naturaleza electrónica del ligando MaxPHOS

Se llevaron a cabo unos estudios iniciales para investigar las propiedades electrónicas del ligando MaxPHOS. Primeramente se estudió las frecuencias “stretching” de carbonilo de los complejos de dicarbonil rodio. A partir de este estudio, se encontró que el ligando era menos rico en electrones que el ligando TCFP.

Tabla 13.4: Desplazamiento del ciclooctadieno e inserción de monóxido de carbono en los complejos de rodio con MaxPHOS y TCFP.



Complex	νCO simétrica (cm-1)	νCO no-simétrica (cm-1)
$[(\text{R-MaxPHOS})\text{Rh}(\text{CO})_2]\text{BF}_4$	2091	2046
$[(\text{TCFP})\text{Rh}(\text{CO})_2]\text{BF}_4$	2085	2040
$[(\text{R,R-MeDuPHOS})\text{Rh}(\text{CO})_2]$	2089	2045
$[(\text{R-BINAP})\text{Rh}(\text{CO})_2]$	2097	2051
$[(\text{S,S-DIOP})\text{Rh}(\text{CO})_2]$	2102	2046

La frecuencia “stretching” del carbonilo fue obtenida justo después de la formación del complejo mediante FT-IR usando una pastilla de KBr.

Otro estudio que se llevó a cabo para investigar las propiedades electrónicas del ligando MaxPHOS involucró la formación de los diselenuros de ambos ligandos MaxPHOS y TCFP. Se examinaron las frecuencias $J(^{31}\text{P}-^{77}\text{Se})$ de los espectros de ^{31}P RMN. Este estudio era

consistente con los resultados obtenidos en los experimentos FT-IR concluyendo que el ligando MaxPHOS era menos rico en electrones que el ligando TCFP.

Esquema 13.20: El compuesto **99** se obtuvo a partir de la sal de fosfonio MaxPHOS·HBF₄.

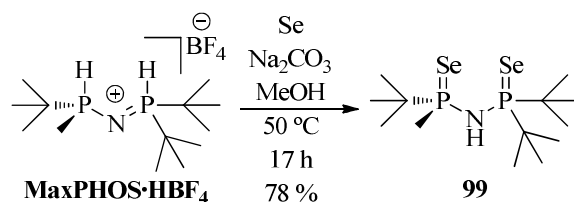
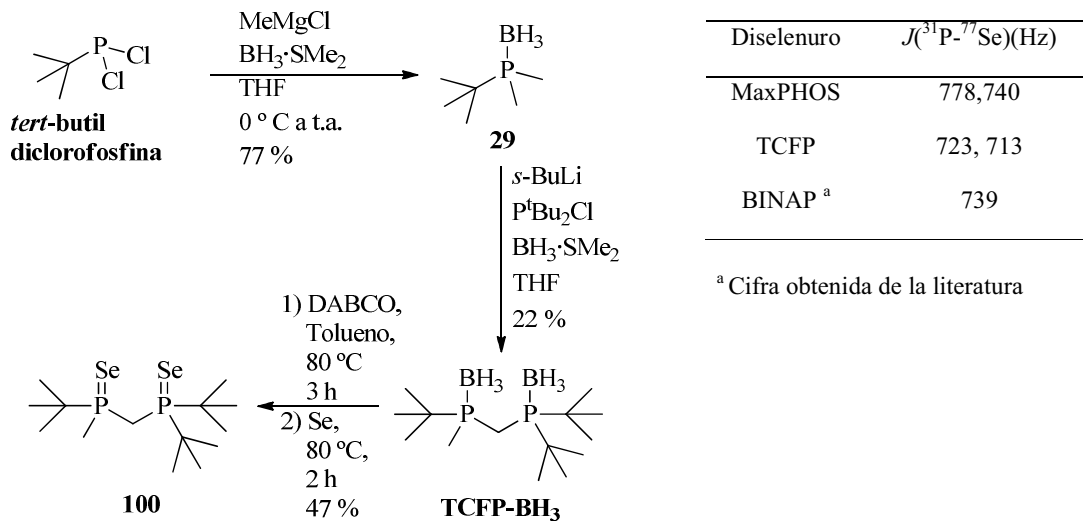
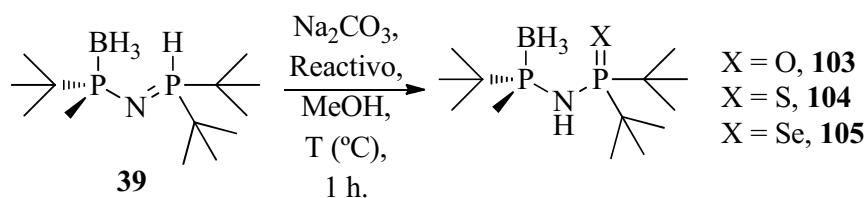


Tabla 13.5: Preparación del diselenuro TCFP.



13.2.3 Derivados del ligando MaxPHOS como ligandos

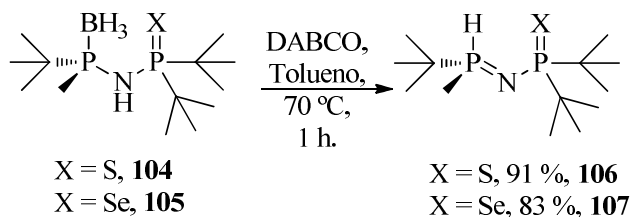
También se investigó la posibilidad de emplear derivados calcogenados del MaxPHOS-BH₃ como ligandos. Se representa el método de inserción del átomo calcógeno en la tabla 13.5.

Tabla 13.5: Introducción de un átomo calcógeno en el MaxPHOS-BH₃.

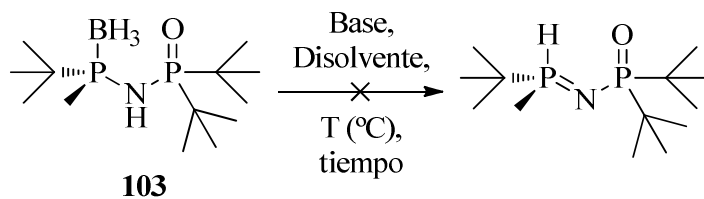
Entrada	Reactivo ^a	T. (°C)	X	Rend. (%) ^b	Producto
1	H ₂ O ₂ ·H ₂ O	r.t.	O	62	103
2	S	50	S	85	104
3	Se	50	Se	85	105^c

^a 3 equivalentes fueron empleados. ^b Después de cromatografía en columna. ^c El otro configuración de **39** fue usado al respecto de lo que está representado. (*S*-(+)-MaxPHOS-BH₃).

Se utilizó DABCO para eliminar la unidad de borano de los ligandos **104** y **105**. Se aislaron las fosfinas **106** y **107** puras después de cromatografía en columna. Mediante ¹H RMN se confirmó que los compuestos existían en su estado tautomérico donde la metil-*tert*-butilfosfina en forma de P(V) y por tanto protegida de la posible oxidación.

Esquema 13.21: Desprotección de borano de los ligandos **104** y **105** usando DABCO.

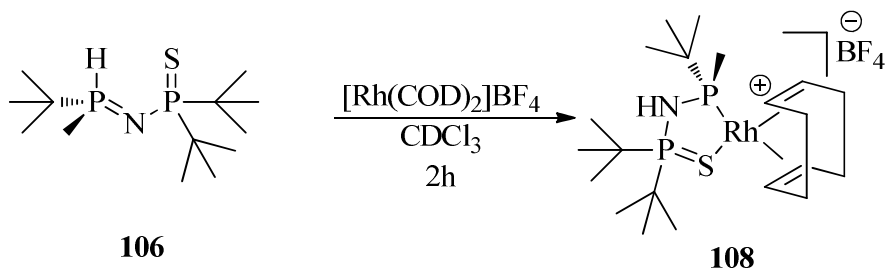
Se empleó DABCO para desproteger la fosfina **103** pero no se pudo aislar el producto desprotegido. Se intentó usar NHEt₂ para desprotegerlo pero solo se obtuvo producto de partida.

Tabla 13.5: Intentos fallidos de intentar eliminar la unidad de borano.

Entrada	Base	Disolvente	T (°C)	Tiempo (h)	Resultado ^a
1	DABCO ^b	Tolueno	70	1	incapaz de aislar
2	NHEt ₂ ^c	THF	60	17	p.p.

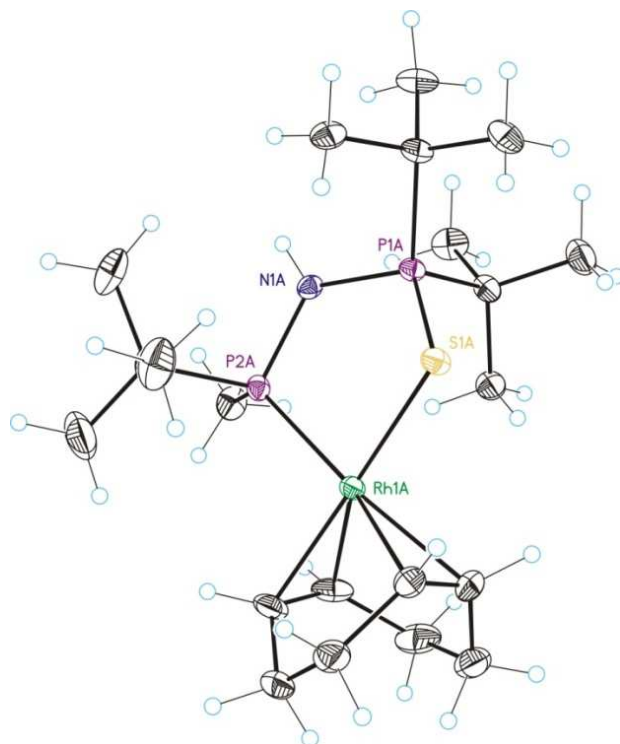
^aDeducido por ¹H RMN. ^b 3 equivalentes empleados. ^c 10 equivalentes empleados.

Se coordinó la fosfina **106** a rodio con éxito.

Esquema 13.22: La fosfina **106** fue coordinado con rodio.

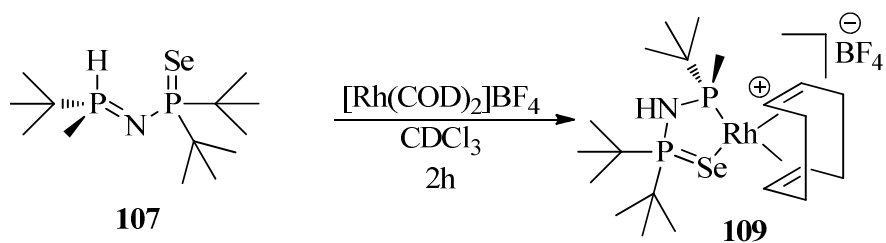
Se obtuvieron cristales adecuados para análisis Rayos-X del complejo de rodio **108** mediante un proceso de *layering*. La información cristalográfica se representa en la figura 13.10.

Figure 13.10: Dibujo ORTEP del complejo de rodio **108**. El contra-ion está omitido por claridad.

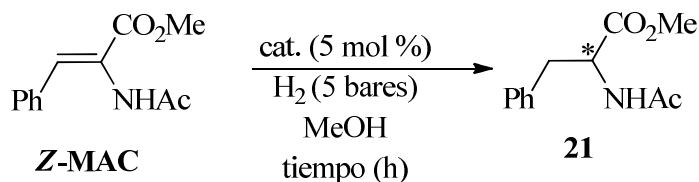


También se coordinó el compuesto selenuro **107** con rodio.

Esquema 13.23: Formación del complejo de rodio **109**.



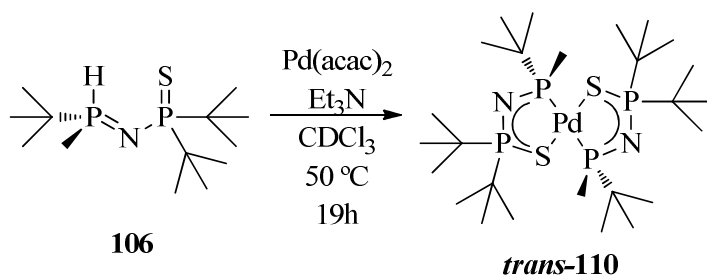
Se emplearon los complejos de rodio **106** y **109** como catalizadores en la hidrogenación asimétrica del sustrato *Z*-MAC. Los resultados presentaron bajos excesos enantioméricos.

Tabla 13.6: Hidrogenaciones del sustrato *Z*-MAC catalizados por los complejos **106** y **109**.

Entrada	cat.	P. (bares H ₂)	t (h)	conversión (%) ¹	ee (%)
1	106	5	24	20	--
2	106	8	74	75	19
3	106	20	18	100	21
4	109	20	18	100	23

¹ Deducido por ¹H RMN. ² Deducido por HPLC quiral.

Se complejó el ligando **106** con paladio utilizando Pd(acac)₂ en la presencia de Et₃N, calentando en metanol. Se formó un complejo neutro compuesto de un núcleo de paladio con dos ligandos a su alrededor presentando simetría C₂. Se obtuvo puro después de cromatografía en columna.

Esquema 13.24: Coordinación del ligando **106** con paladio.

Se protonó el complejo neutro **110** mediante la adición del ácido HBF₄·OEt₂ para formar la sal **111**. Al añadir un protón a un lado del complejo, se rompió su simetría y se formó un complejo con simetría C₁. A partir de la sal **111**, se hicieron cristales adecuados para análisis Rayos-X, el cual confirmó la configuración *trans* de los ligandos alrededor del metal.

Esquema 13.24: Protonación del complejo **110** para formar el complejo catiónico.

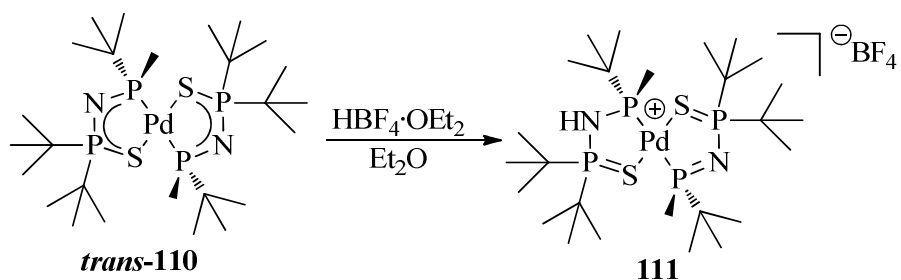
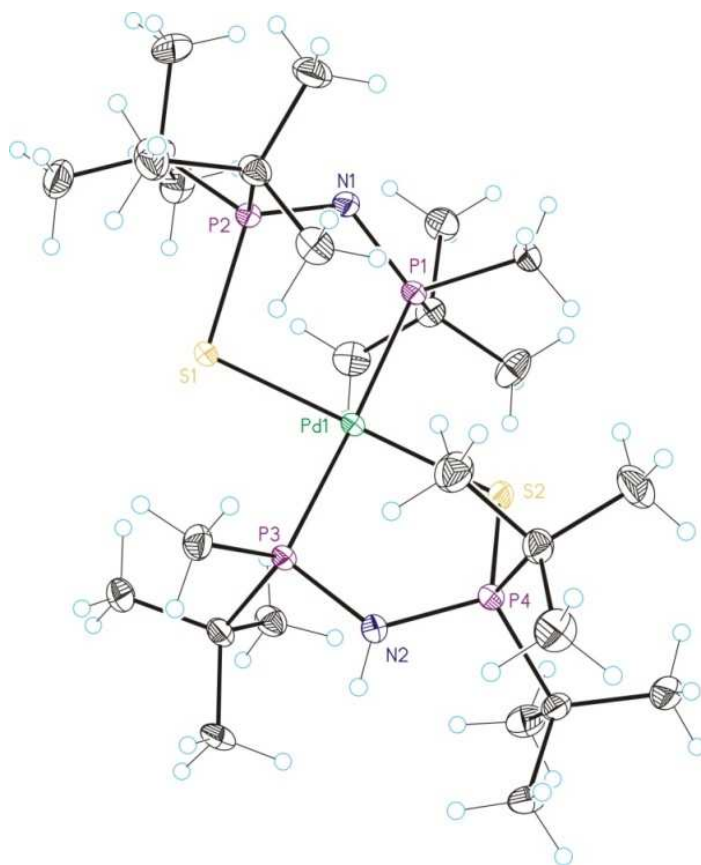
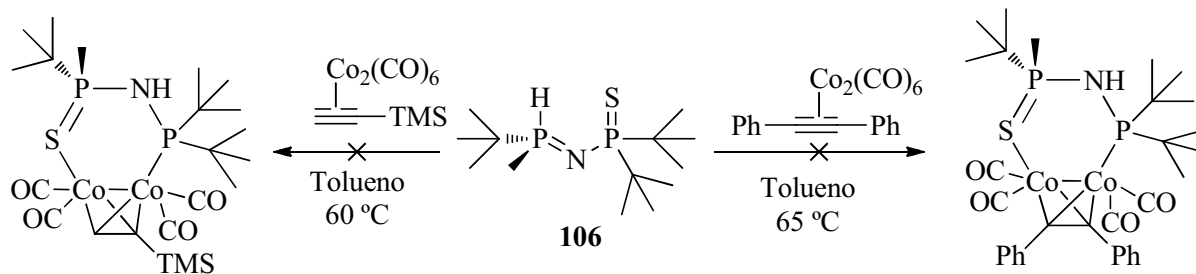


Figura 13.11: Dibujo ORTEP del complejo de paladio **111**..



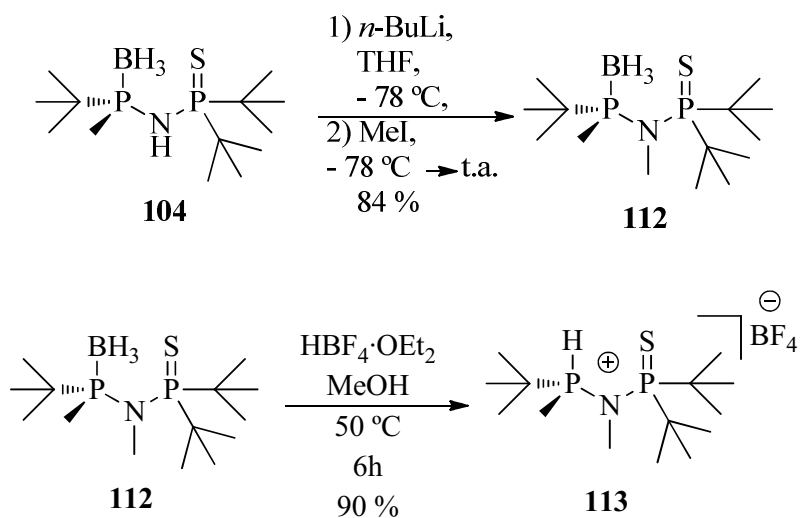
Se intentó coordinar el ligando **106** con un clúster alquino-dicobalto pero no hubo complejación. Se pensó que la existencia de un grupo NH en el ligando **106** impedía la coordinación.

Esquema 13.25: Intentos fallidos de coordinar la fosfina **106** con un clúster dicobalto carbonilo alquino.

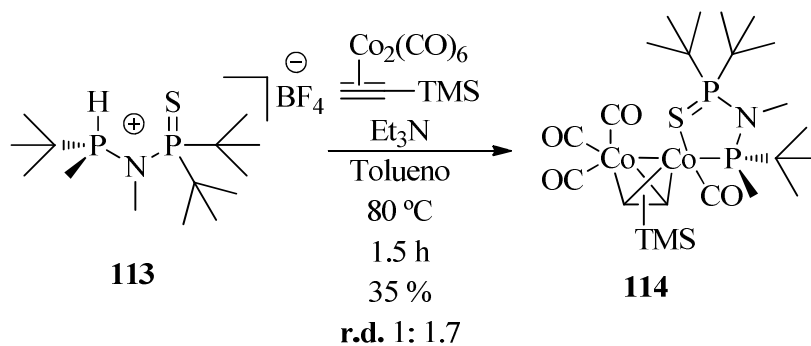


Se decidió preparar el ligando **106** metilado en la posición NH para lograr coordinarlo con el clúster dicobalto. Se metiló la fosfina **104** y se desprotegió con $\text{HBF}_4 \cdot \text{OEt}_2$ para formar la sal de fosfonio **113**.

Esquema 13.26: Metilación de la fosfina **104** en la posición nitrógeno y desprotección de compuesto **112** para formar la sal **113**.

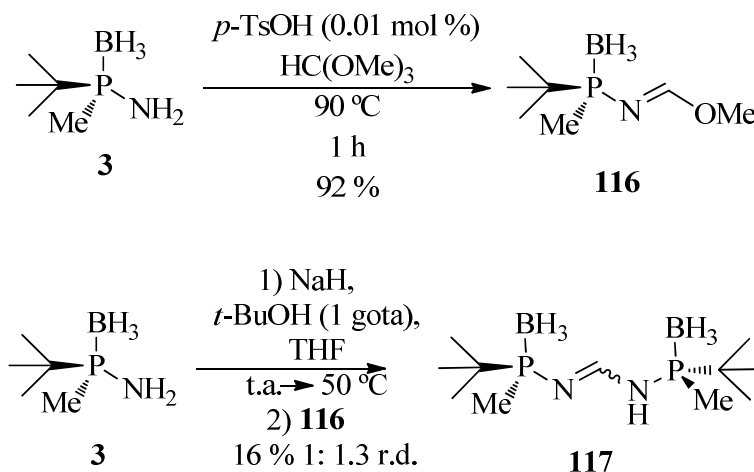


Se consiguió coordinar la fosfina **113** con un clúster dicobalto. El ligando coordinó a través de los átomos azufre y fósforo a un único átomo de cobalto. Se formó como mezcla de diastereoisómeros en una ratio de 1: 1.7. Se decidió que el complejo no era factible o aplicable como catalizador.

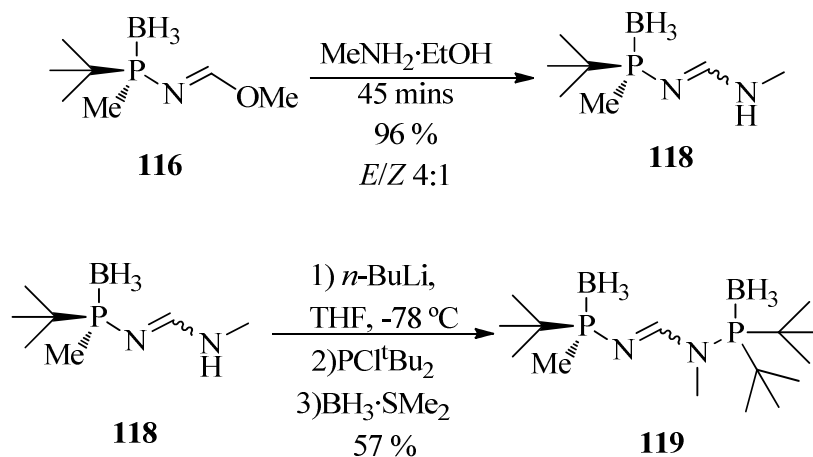
Esquema 13.27: Coordinación de la sal **113** con un clúster alquino-dicobalto.

13.2.4 Hacia la preparación de ligandos de tipo amidina P-esterogénicos

Hubo varios intentos para conseguir ligandos de tipo amidina P-esterogénicos. Se formó un grupo imidato con la aminofosfina **3** para obtener la fosfina **116**. Se usó el compuesto **116** como electrófilo en la siguiente reacción con la aminofosfina **3**. Se logró la preparación de la difosfina **117** con bajo rendimiento como mezcla de diastereoisómeros.

Esquema 13.28: Formación de la imido-fosfina **116** a partir de la aminofosfina **3** y el uso de **116** para formar la difosfina **117**.

Se formó la imidamido-fosfina **118** como mezcla 4:1 de isómeros *cis/trans* mediante la reacción de **116** con metilamina. En la siguiente reacción se formó el anión en la posición NH del compuesto **118** mediante la adición de butil-litio, se añadieron el electrófilo PCl^tBu_2 y $\text{BH}_3 \cdot \text{SMe}_2$ y se consiguió la difosfina **119** después de un tratamiento acuoso y cromatografía en columna.

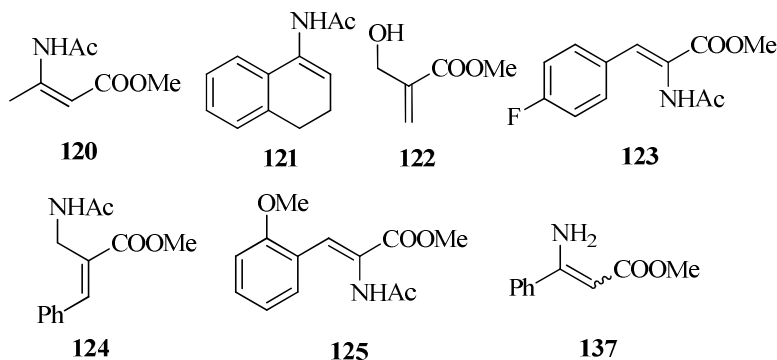
Esquema 13.29: Obtención del compuesto **119**.

La difosfina **119** no demostró aplicación en catálisis asimétrica como ligando ya que no se podía conseguir la reducción del doble enlace ni de la fosfina **119** ni la imidamido-fosfina **118** tras varios intentos empleando Pd/C, LiAlH₄ y NaBH₄.

13.3 El ligando MaxPHOS en la hidrogenación asimétrica**13.3.1 Nueva colección de sustratos para probar con el catalizador MaxPHOS-Rh**

Queríamos examinar más a fondo el potencial del catalizador MaxPHOS-Rh en la reacción de hidrogenación asimétrica así que se prepararon 7 sustratos ya descritos en la literatura.

Figura 13.11: Sustratos preparados para probar en la reacción de hidrogenación asimétrica con MaxPHOS-Rh como catalizador.



Se buscaron las condiciones optimizadas para la hidrogenación de los sustratos preparados con MaxPHOS-Rh como catalizador, se representan los mejores resultados en la tabla 13.7. El sustrato **124** ya había sido hidrogenado antes utilizando MaxPHOS-Rh pero durante este

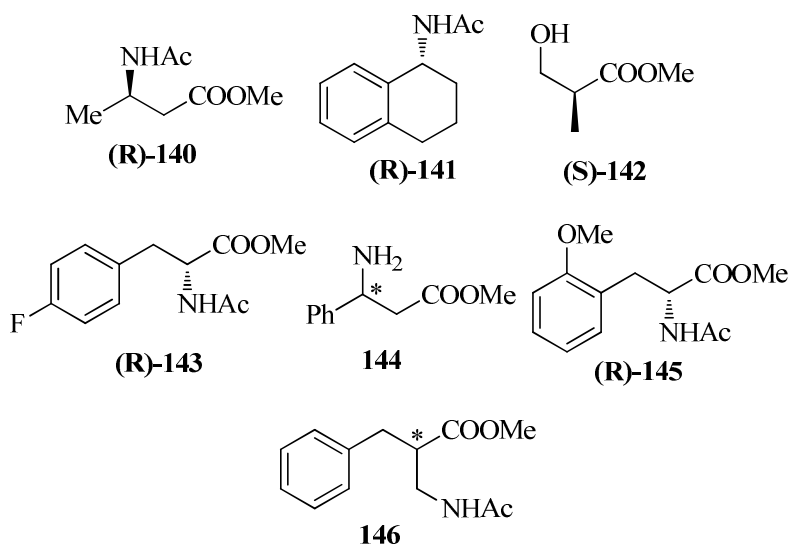
trabajo se intentaba mejorar los excesos enantioméricos obtenidos. No se logró repetir los resultados obtenidos anteriormente: siempre se obtenían mezclas de productos y producto de partida aunque se confirmó la pureza del producto de partida usado por ^1H RMN. Ningún intento con el complejo MaxPHOS-Rh como catalizador consiguió hidrogenar el sustrato **137**, siempre se observó producto de partida por ^1H RMN después de la reacción.

Tabla 13.7: Hidrogenación asimétrica de los distintos sustratos y los mejores resultados al respecto a la enantioselectividad.



Entrada	Sustrato	P. (bares)	dis.	temp. (°C)	t. (h)	conv. (%) ^a	ee (%) ^b	Prod.
1	120	3	THF	t.a.	2	100	96	140
2	121	2	MeOH	0	26	83	83	141
3	122	3	MeOH	0	26	100	87	142
4	123	3	THF	t.a.	2,5	100	99	143
5	124	--	--	--	--	--	--	146^c
6	125	1	MeOH	t.a.	22,5	100	98	145
7	137	--	--	--	--	--	--	144^d

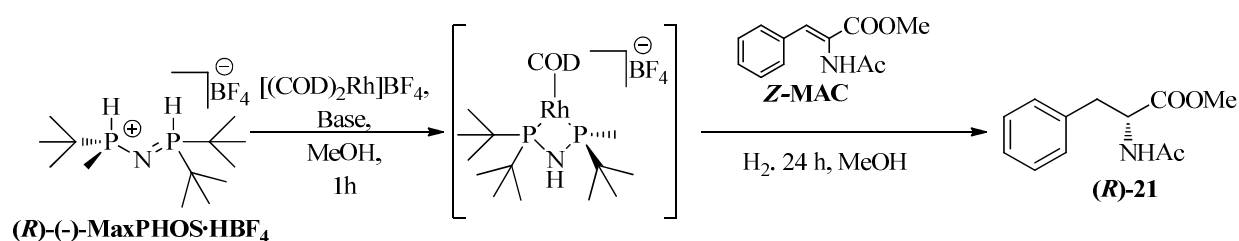
¹ Deducido por ^1H RMN. ² Deducido por HPLC en columna quiral. ³ Los resultados no fueron fiables. ⁴ Siempre daba producto de partida.



13.3.2 Estudios de hidrogenación del sustrato Z-MAC: Utilizando la formación del catalizador *in situ*

Se llevó a cabo un estudio donde se buscaron las mejores condiciones para realizar la hidrogenación del sustrato Z-MAC mediante con la formación del catalizador *in situ* a partir de $[(\text{COD})_2\text{Rh}]\text{BF}_4$. Las mejores condiciones encontradas para realizar esta transformación fueron las de la entrada 13 de la tabla 13.8. A 3 bares de presión de hidrógeno, TBA como base para activar el ligando a coordinar con rodio y 1 mol % carga catalítica se pudo observar un exceso enantiomérico de 99.1 %.

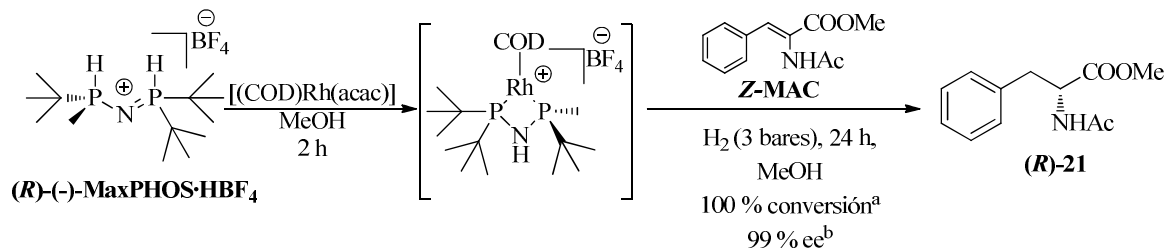
Tabla 13.8: La hidrogenación de Z-MAC con formación del catalizador *in situ*.



Entrada	Base	Eq. ^a	cat. (mol %)	P. (Bares)	ee (%) ^b
1	Et ₃ N	2	1.5	1	97,8
2	Et ₃ N	14	1.5	1	97,3
3	Et ₃ N	2	3	5	91
4	Et ₃ N	14	3	5	98,1
5	Et ₃ N	2	1.5	5	91,7
6	Et ₃ N	14	1.5	5	98,2
7	DBU	2	3	3	83,9
8	DBU	20	3	3	p.p. ^c
9	DIP	2	3	3	99,2
10	DIP	20	3	3	98,8
11	DIP	2	1	3	98,6
12	DIPEA	2	1	3	98,9
13	TBA	2	1	3	99,1

^a Equivalentes de base al respecto del ligando. ^b Determinado por HPLC quiral (Chiralpak AD-H). ^c Solo se recuperó producto de partida. La conversión era 100 % en cada caso confirmado a una certeza de ¹H RMN.

Esquema 13.9: Hidrogenación del sustrato Z-MAC empleando formación del catalizador *in situ*.

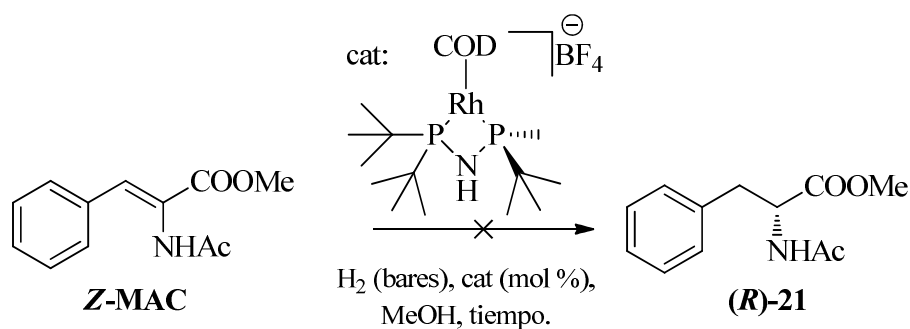


^a 100 % conversión confirmado por ^1H RMN. ^b Determinado por HPLC quiral (Chiralpak AD-H). 1 mol % carga de catalizador.

Mediante la mejora en el proceso de síntesis del catalizador MaxPHOS-Rh **40** como ya ha sido explicado en el esquema 13.18 se llegó a una manera más fácil, limpia y efectiva para llevar a cabo la hidrogenación del sustrato Z-MAC con la formación del catalizador *in situ*. Se eliminó la necesidad de usar una base orgánica y se obtuvo conversión total con un exceso casi perfecto de 99 % ee.

13.3.2 Estudios de la hidrogenación del sustrato Z-MAC: Bajando la carga catalítica

Se evaluó la capacidad de hidrogenación del catalizador MaxPHOS-Rh a valores menores que 1 mol % llevándose a cabo varios ensayos con resultados positivos. MaxPHOS-Rh logró hidrogenar el sustrato Z-MAC con excesos enantioméricos altos. Se observó en los ensayos que a menor carga catalítica, mejor exceso enantiomérico, 99 % ee a 0,01 mol % en lugar de 97 % a 0,1 mol %. Seguramente esto se debía a problemas o diferencias físicas teniendo que ver con la pureza de sustrato, estado del catalizador y estado del disolvente que podrían influir más a baja carga catalítica.

Tabla 13.9: Reducción de la carga catalítica

Entrada	P. (bares)	cat. (mol%)	conc. (g/mL)	t. (h)	conversión (%) ^a	ee (%) ^b
1	3	0,1	0,109	22	100	97
2	5	0,1	0,292	4,8	100	97
3	5	0,01	0,292	72	99	98
4	5	0,01	0,292	43	100	99

^a Conversión confirmado por ¹H RMN. ^b Determinado por HPLC quiral (Chiralpak AD-H). 1 mol % carga de catalizador.

13.3.3 Estudios de hidrogenación del sustrato Z-MAC: Mirando la velocidad de la reacción

Se midió el flujo de hidrógeno entrante en el reactor durante la hidrogenación del sustrato Z-MAC utilizando un aparato especialmente adaptado. Se observó que la reacción tardaba aproximadamente 10 minutos en empezar pero una vez iniciada, su velocidad se incrementaba gradualmente hasta que una vez consumido el sustrato se detenía abruptamente.

Se aplicó el complejo [(NBD)Rh(R-MaxPHOS)]BF₄ **96** también en el mismo proceso. Se observó en este caso la ausencia de un periodo de incubación del catalizador, y que la reacción se iniciaba inmediatamente después del proceso de purga del reactor.

Gráfico 13.1: Flujo de hidrógeno durante la reacción catalizada por el complejo [(R-MaxPHOS)Rh(COD)]BF₄.

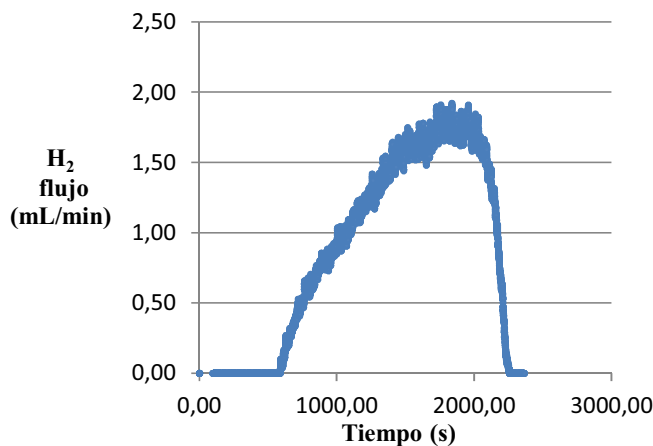
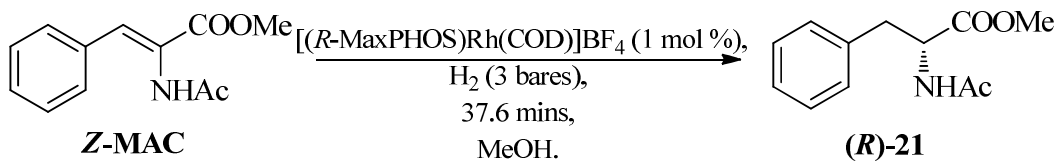
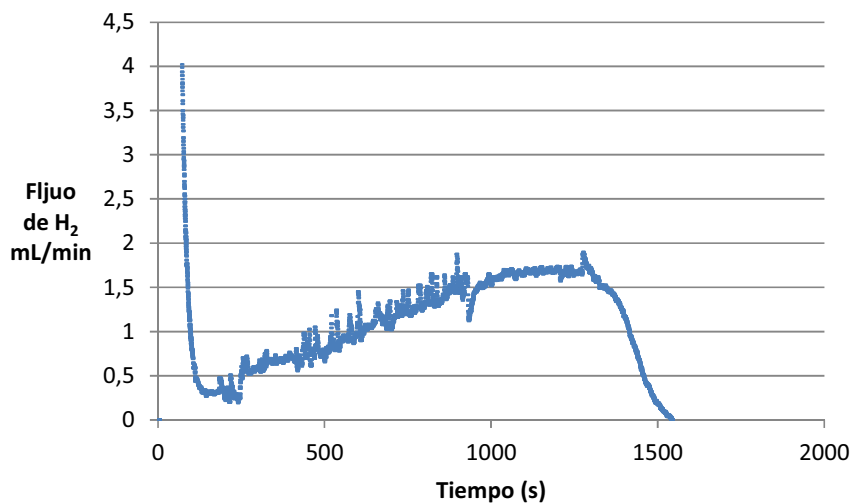
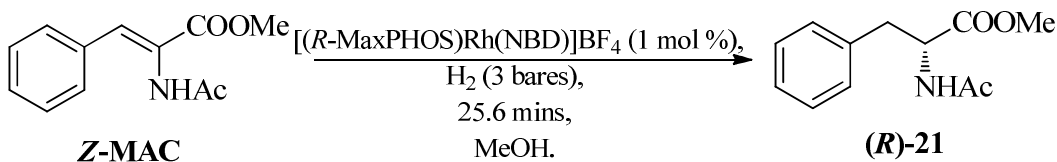


Gráfico 13.2: Flujo de hidrógeno durante la hidrogenación de Z-MAC catalizada por el complejo [(R-MaxPHOS)Rh(NBD)]BF₄.



Se observó que una vez que el catalizador estaba activado la reacción tardaba aproximadamente 25,6 minutos para completarse. Se calculó que esto igualaba a que una molécula de catalizador catalizaba la hidrogenación de casi 4 moléculas de sustrato a producto hidrogenado por minuto, o 0.065 moléculas por segundo. Este dato cuadraba bien con el tiempo que hacía falta para llegar a conversión total en los estudios de baja carga catalítica en la tabla 13.9.

Para concluir, la posibilidad de usar ligandos PNSO en la hidrogenación asimétrica fue explorada más a fondo. Se produjeron resultados prometedores al principio con el complejo **73** pero surgieron problemas en conseguir análogos. La coordinación del ligando MaxPHOS con otros metales más allá de rodio ha sido estudiada así como la actividad del ligando MaxPHOS en otras transformaciones además de la hidrogenación asimétrica como la reacción Pauson-Khand. Se prepararon nuevos ligandos y complejos usando los precursores claves en la preparación del ligando MaxPHOS. Por último se exploró el potencial del ligando MaxPHOS en hidrogenación asimétrica en una nueva colección de sustratos.